Elucidation of the Ammonium Major Facilitator (AMF) Family in Plants

Apriadi Situmorang

Thesis submitted for the degree of Doctor of Philosophy

to the School of Agriculture, Food and Wine,

The University of Adelaide.

November 2018

THE UNIVERSITY of ADELAIDE

Table of content

Abstract

The discovery of the Ammonium Major Facilitator (AMF) family in plants and yeast by overexpression of the soybean transcription factor *GmbHLHm1* in yeast has opened up new insights into the transport of NH_4^+ in eukaryotic systems. Using both yeast and *Xenopus* oocyte expression systems, ScAMF1 and a plant homolog (GmAMF3) were shown to transport NH_4^+ and the toxic ammonium analogue methylammonium (MA). The AMF family is conserved in most plants including *Arabidopsis thaliana* where three homologs exist, these being *AtAMF1* (At2g22730), *AtAMF2* (At5g64500) and *AtAMF3* (At5g65687). All three *AMF* genes are expressed throughout the plant with noticeable expression in senescing shoot tissues. Transient expression in *Nicotiana benthamiana* leaves indicated AtAMF1, AtAMF2, and AtAMF3 proteins are located on the ER, tonoplast and plasma membrane, respectively. Functional testing in an ammonium transport deficient yeast strain (31019b) did not result in activities which rescued growth of yeast cells grown on low ammonium concentrations. However, like GmAMF1;3 and ScAMF1, AtAMF2 was capable of inducing an increased sensitivity to the toxic ammonium analogue methylammonium. These alternative protein locations and activities may reflect a distinct function of each protein in cellular NH_4^+ transport and homeostasis.

A disruption of both the high (Trk1) and low (Trk2) affinity K^+ transport proteins in the yeast strain CY162 (*trk1*Δ; *trk2*Δ) was found to inhibit growth on high concentrations of NH_4^+, a process potentially linked to the efflux of amino acids out of yeast cells. The overexpression of the tonoplast-localised AMF protein, AtAMF2, was shown to rescue CY162 when grown at high NH_4^+ concentrations while continuing to induce a toxic phenotype to high concentrations of MA. The data suggests that AtAMF2 may participate in the release of acid-trapped NH_4^+ from the vacuole into the cytoplasm, a process required to supply nutrients to support cellular growth in NH_4^+ grown but amino acid-starved cells. In contrast, when MA is supplied, vacuole-localised MA^+ is released by AtAMF2 into the cytoplasm inducing a toxicity phenotype. This process was enhanced when cells were supplied with only proline or limited concentrations of amino acids. Collectively these data suggest the tonoplast-localised AtAMF2 is a functional NH_4^+ efflux protein that can support cellular growth when limited by available nitrogen (NH_4^+ and or amino acid) resources.

Individual *amf* T-DNA knockouts in Arabidopsis were identified and used to create multiple *amf* mutations through selected crosses. The *amf1* mutant displayed an increased rate of unidirectional $^{15}NH_4^+$ influx into Arabidopsis roots that was not present in either *amf2* or *amf3*. The growth of mutants with *amf1* background (*amf1*, *amf1amf2* or *amf1amf3*) on low NO_3^- (0.05 mM) and adequate K^+ (3.75 mM) were found to be sensitive to 20 mM MA. In the presence of low or high NO_3^- (0.05 and 7.5 mM, respectively) and low K^+ (<0.1 mM), root growth in the *amf2amf3* mutant was significantly inhibited by 2 mM NH_4^+, a phenotype that could be rescued with the provision of external K^+. These data demonstrated that AtAMF1 might have a dominant role in NH_4^+ toxicity tolerance when supplied low concentrations of NO_3^- while AtAMF2 and AtAMF3 aid in the management of NH_4^+ toxicity in a K^+-dependent manner. Collectively with

experiments in yeast, the *in-planta* experiments confirm the importance of K^+ availability in mitigating NH_4^+ toxicity in Arabidopsis, a process which appears to involve members of the AMF family.

Declaration

I certify that this work contains no material which has been accepted for the award of any other degree or diploma in my name, in any university or other tertiary institution and, to the best of my knowledge and belief, contains no material previously published or written by another person, except where due reference has been made in the text. In addition, I certify that no part of this work will, in the future, be used in a submission in my name, for any other degree or diploma in any university or other tertiary institution without the prior approval of the University of Adelaide and where applicable, any partner institution responsible for the joint-award of this degree.

I give permission for the digital version of my thesis to be made available on the web, via the University's digital research repository, the Library Search and also through web search engines, unless permission has been granted by the University to restrict access for a period of time.

Signed .....

Date 28 November 2018

Acknowledgement

The completion of my PhD and this thesis would have not been possible without the inexhaustible guidance and encouragements of my principal supervisor, Prof. Brent Kaiser, and my co-supervisors, Prof. Steve Tyerman and Dr. Megan Shelden. I would like to express my sincere gratitude and appreciation for all your suggestions, discussions and especially for all the support provided in my most difficult time during my PhD.

I wish to express my gratitude to all of the Plant Energy Biology lab members for their friendship and being supportive especially in my difficult times. Special thanks to Dr. Sunita Ramesh for teaching me how to work properly with yeast and Dr. Stefanie Wege and Dr. Gwen Mayo for sharing your expertise in confocal imaging. Thanks to Yue Wu (Crystal), Yue Qu (Julian), Dr. Jiaen Qiu, Samantha McGaughey, Ali Mafakheri, Dr. Johannes Scharwies, Wendy Sullivan, Dr. Stephanie Watts-Williams, Dr. Bo Xu, Dr. Rebecca Vandeleur, Dr. Jonathan Wignes for all your help and for all other members of Gilliham and Tyerman labs for being wonderful lab mates. I would also like to thank the Kaiser lab members in Sydney, Dr. Zhengyu Wen (Allen), Dr. Julie Dechorgnat, and Dr. Wenjing Li for the friendship, collaborations, and supports.

My sincere thanks to my PhD scholarship sponsor, RISET-Pro (Research and Innovation in Science and Technology Project), Ministry of Research, Technology and Higher Education of the Republic of Indonesia.

Special thanks to my dearest parents, especially to my mom and dad who will always be my greatest supporters of my life and thank you for teaching me “never give up whatever life throws at you”. For my brothers and sisters, thank you for your limitless love. For my in-laws, thank you for accepting me unconditionally in your family. Without all your support, my journey to the completion of my PhD would have not been possible.

A very special thanks to my beautiful and wonderful wife Angela Wika Citra Kusuma for your unconditional love, patience and sacrifice. Thank you for giving me the most adorable children in the world, Ramos Binar Situmorang and Kinandari Tara Situmorang. Thank you for being the cornerstone of our family and making us stand firm to face any challenge in our life. Without your love and supports, my PhD journey will be unthinkable.

I dedicate this thesis to my family, especially my son Ramos Binar Situmorang. Your tough life journey battling Acute Myeloid Leukaemia has become the inspiration of this thesis. You have taught me to pick myself up every time I fall on my knees. Love you forever.

Finally, I wish to thank everyone who supported us when Ramos underwent his chemotherapy treatments at Michael Rice Centre for Haematology and Oncology, Women’s and Children’s Hospital, Adelaide. For the doctors and nurses, thank you for care and you love. For the parents of other patients, thank you for supporting each other in our difficult times.

1. Literature review

1.1 Nitrogen in agriculture

Nitrogen (N), along with phosphorus (P) and potassium (K), is an essential nutrient required for plant growth. Nitrogen has important functions as a structural component of proteins, nucleic acids, pigments, chlorophyll, secondary metabolites and other molecules required by plants to grow. As N uptake and storage is essential, plants have developed various mechanisms including physiological, biochemical and morphological strategies (Garnett et al., 2009) including N root-to-shoot translocation (Giehl et al., 2017) and remobilisation from senescing leave (Masclaux-Daubresse et al., 2010) as well as crosstalk of plant phytohormones (Xu et al., 2012) to assure an adequate availability of N. However, in most agricultural soils, reduced forms of N (i.e. other than N_2) can be limiting. Therefore, in agricultural situations, maintaining adequate N supply for crop production is required involving the application of N-containing fertilizers. In the US, N fertiliser application was approximately 60% of the total fertilisers used in farming systems in 2011 (USDA-ERS, 2013). Furthermore, data from FAO indicates that in 2017, world N fertilizer demand was 113.6 million tonnes (FAO, 2017). Farmers tend to apply excess amounts of fertilizers to ensure maximum yield is met, often exceeding the N requirements for growth and productivity. Unfortunately, most agronomically important crops are low in N-use efficiency. This is a combination of factors based on agronomy, plant genetics, soil microbial competition and soil chemistry. Furthermore, low NUE is often translated into wastage of N fertilizers. Lost N is economically costly to growers and contributes to significant environmental problems globally that includes; excessive use of fossil fuels to generate N fertilisers, degradation of drinking water through N contamination and, pollution of aquatic ecosystems that influence toxic algae blooms causing eutrophication/hypoxia episodes that reduce O_2 concentration in the water required to support aquatic life (Camargo and Alonso, 2006). Therefore, improving NUE of crop plants is essential in order to ensure sustainable agriculture with limited N fertiliser supply. This improvement can be partially achieved by understanding the mechanisms of N uptake, storage and assimilation within plants (Garnett et al., 2009). Selection and use of NUE-improved crops will ultimately reduce N application dosage, and simultaneously decrease N pollution in the environment.

In soil, apart from N_2 gas, N is available to plants in various forms including inorganic N - nitrate (NO_3^-) and ammonium (NH_4^+), as well as organic N forms including, amino acids and nucleic acids. The available concentrations of these N species depends on the physical, chemical and biological condition of the soil, such as accumulation of organic matter, water supply, temperature, pH microbial activity and the presence of alleopathic chemicals (Britto and Kronzucker, 2002). In aerobic soils, NO_3^- is abundant as microbial activity quickly converts most forms of reduced N to NO_3^-, while in anaerobic and cold soils, NH_4^+ becomes more prevalent than NO_3^- (Yamaya and Oaks, 2004; Miller, 2010; Xu et al., 2012). In addition, free amino acid concentrations are generally high at the surface of soils rich in organic matter ranging from 0.1 to 50 mM. This is in contrast to agricultural soils, which have a lower concentration range

between 1 and 100 µM (Jones et al., 2002). In plants, transport systems for NO_3^-, NH_4^+, and amino acids exist including, nitrate (NRTs), ammonium (AMTs) and amino acid transporters, respectively.

1.2 Current understanding of ammonium transport in *Arabidopsis thaliana*

1.2.1 Ammonium transport by AMT protein families

Some plants prefer NH_4^+ rather than NO_3^- as it requires lower energy inputs for uptake and assimilation (Touraine, 2004). For NO_3^-, uptake and assimilation is more energy-dependent where an energy equivalent of 8-12 adenosine triphosphate (ATP) molecules is required per molecule of NO_3^- reduced (Bloom et al., 1992). In contrast, the assimilation of NH_4^+ in roots or shoots only requires an energy equivalent of 2 ATPs (Bloom, 2011). However, NH_4^+ influx into plant cells must be regulated, as elevated concentrations in the cytoplasm are toxic, causing detrimental effects on plant growth and development (Britto and Kronzucker, 2002). Some studies have shown that osmotic balance and cell function disruption are the main reasons for growth inhibition of plants grown at high NH_4^+ concentrations. An experiment by Gerendas et al. (1997) showed that NH_4^+ toxicity relates to disrupted water potential and osmotic balance in plant cells. Additionally, Britto et al. (2001) explained that in NH_4^+ sensitive plants, such as barley, NH_4^+ toxicity is due to the inability of cells to exclude NH_4^+ through plasma membrane regulation, which eventually leads to intracellular toxicity. Therefore, plants have evolved mechanisms (morphological, physiological and / or biochemical) to avoid toxicity including the up-regulation of NH_4^+ uptake during limited supply and down-regulation of NH_4^+ uptake during excess supply (Glass et al., 2002). Better understanding of these mechanisms would be essential for the development of higher NUE in crop plants.

AMT's have been widely known and studied as the main transport proteins of NH_4^+ though NH_3 is known to be transported via some aquaporins (Holm et al., 2005; Loqué et al., 2005; Bertl and Kaldenhoff, 2007; Kirscht et al., 2016). AMT proteins are conserved in bacteria, yeast, plants and animals (named Amt/Mep/AMT/Rh, respectively) showing their importance in living organisms (Marini et al., 1997; Howitt and Udvardi, 2000; Shelden et al., 2001; Mayer et al., 2006; Andrade and Einsle, 2007). In plants, AMTs are the primary transport proteins known to transport NH_4^+. In *Arabidopsis thaliana,* there are six AMTs divided into two families. The first family is comprised of five genes, *AMT1;1-AMT1;5* while the second family only has one gene, *AMT2;1* (Sohlenkamp et al., 2000; Glass et al., 2002; Sohlenkamp et al., 2002; Yuan et al., 2007). All known AMTs are assumed responsible for NH_4^+ transport at low concentrations representing the high affinity transport system –HATS. No AMT has been associated with NH_4^+ transport at high concentrations, which would represent the low affinity transport system – LATS. Although previously it was suggested AtAMT1;2 was a potential LATS transporter (Yuan et al., 2007). The expression of plant AMT genes in various tissues and cellular locations is strongly correlated with N availability, therefore it is assumed that every gene has a distinct function in NH_4^+ transport (Yuan et al., 2007). AMT1;1, AMT1;2, AMT1;3 and AMT1;5 are the main transporters involved in NH_4^+ influx from soil

as they are mostly expressed in root cells including the epidermis, cortex and endodermis (Yuan et al., 2007; Masclaux-Daubresse et al., 2010). Additionally, Gazzarrini et al. (1999) showed *AtAMT1;1* is expressed in all plant organs, while *AtAMT1;2* and *AMT1;3* expression is mainly expressed in the roots. Furthermore, Yuan et al. (2007) in a study utilizing transgenic plants expressing green fluorescence protein (GFP) driven by a native promoter, showed that *AtAMT1;5* is highly expressed in the root tip and root hairs. In contrast, *AMT1;4*, is specifically expressed in pollen, however there is no visible or functional difference between wild type plants and *amt1;4* mutant plants in pollen function (Yuan et al., 2009). In addition, it has been shown that *AMT2;1* is also expressed in roots, however its role in NH_4^+ influx remains unclear as an *amt2;1* mutant shows no phenotypical differences compared to wild type plants (Sohlenkamp et al., 2002; Yuan et al., 2007).

The regulation of NH_4^+ uptake is controlled by the overall N status of the whole plant and often controlled to match the N requirements for normal growth across different growth stages (von Wiren et al., 2001). It includes regulation by concentration of external NH_4^+ and/or the level of N assimilation products. At high NH_4^+ concentrations, plants tend to regulate NH_4^+ influx in order to avoid NH_4^+-induced toxicity. Some studies have shown that NH_4^+ influx is down-regulated when plants are grown in elevated N levels, while influx is up-regulated under low N (Gazzarrini et al., 1999; Glass et al., 2000). Glutamine, as one of the primary N assimilation products, also regulates NH_4^+ uptake possibly as a negative feedback regulator as suggested by Rawat et al. (1999). In this study, there was clear evidence that showed *AtAMT1* transcript levels decreased when exogenous glutamine was applied. Stimulation by light is another regulatory mechanism involved in NH_4^+ uptake. Expression of *AtAMT1;1*, *AtAMT1;2* and *AtAMT1;3* increased 1.5, 1.7 and 3 times respectively, and correlated to ^{15}N influx that increased during the daytime and decreased during the dark (Gazzarrini et al., 1999). Additionally, in a study in *A. thaliana*, N metabolism was altered when chloroplast fructose-1,6-bisphosphatase, an enzyme involved in the Calvin cycle during photosynthesis, was silenced indicating the possible regulation of N by sugars (Sahrawy et al. (2004). Likewise, a study in field pea (*Pisum arvense* L. var. Nieznaniecki) revealed that the application of exogenous supply of sucrose or glucose increased NH_4^+ uptake. Furthermore, addition of 1% of sucrose could maintain expression levels of *AtAMT1* transcripts as well as NH_4^+ influx during the dark period in *A. thaliana* grown on 1 mM NH_4NO_3 (Lejay et al., 2003). This particular regulation may relate to the nitrogen/carbon (N/C) balance and photosynthesis production (sugar) within plants.

Every AMT gene may have a distinct function and they are also predicted to contribute differently in the overall NH_4^+ transport pathway in *A. thaliana*. AtAMT1;1 has been shown to contribute ~30 % of overall NH_4^+ uptake (Kaiser et al., 2002). Similar activities have also been shown for AtAMT1;3, which contributes ~30 % of overall NH_4^+ uptake (Loque et al., 2006). An experiment using double knockout mutants (*dko*) revealed that AtAMT1;1 and AtAMT1;3 have an additive contribution, approximately 60-70 % of net NH_4^+ uptake (Loque et al., 2006). Furthermore, subsequent experiments using a quadruple knockout mutant (*qko*) showed that ~90% of NH_4^+ influx is facilitated by AMT1;1, AMT1;2, AMT1;3 and

AMT1;5 sharing a contribution of ~30%, ~20%, ~30%, and ~10%, respectively (Yuan et al., 2007). The fact that there is still unknown mechanism(s) contributing ~10% of NH_4^+ influx, poses an intriguing question regarding the possibility of unidentified transporters involved in NH_4^+ uptake system in *A. thaliana.*

1.2.2 Ammonium transport by non-AMT protein families

Although AMT protein families were thought to be only transporters responsible for NH_4^+ transport, some recent data have shown that other transport proteins are able to transport NH_4^+. Experiments using the *qko Arabidopsis* mutant line which has lost all four root-expressed AMTs, still showed evidence of NH_4^+ influx through the root tissues (Yuan et al., 2007). Similarly, the yeast triple *mep* mutant that has mutations in all three MEP genes (Δ*mep1-3*), was able to grow on buffered media (pH 6.1) and high concentration of NH_4^+ (>20 mM) (Marini et al., 1997). These studies provide evidence that there is other NH_4^+ transport mechanism(s) unrelated to AMT/Mep proteins that contribute to overall NH_4^+ transport.

Nonselective cation channels (NSCC) have been shown to facilitate NH_4^+ transport in some plant species. However, information regarding the role of NSCC to regulate NH_4^+ transport in Arabidopsis is still limited. Using electrophysiology approaches on the plasma membrane of Arabidopsis root protoplasts, it was shown that NSCC's allow permeation of NH_4^+ (Demidchik and Tester, 2002). Subsequent experiments using protoplasts isolated from wheat roots also showed similar results (Davenport and Tester, 2000), however wheat showed a higher NH_4^+ conductance compared to the conductance observed in Arabidopsis root protoplasts. The difference in conductance among species might determine the unique physiological roles and important functions of the NSCC in regulating ions balance and transport in different species. Additionally, the NSCC may also serve as an alternative nutritional acquisition pathway in symbiotic plants such as legumes. In soybean root nodules, unidentified channels, predicted to be NSCC, showed the ability to facilitate NH_4^+ movement across peribacteroid membrane (Tyerman et al., 1995; Obermeyer and Tyerman, 2005). Unfortunately, the molecular identity of the NSCC permeable to NH_4^+ yet to be uncovered. A candidate for NSCC has been identified as PIP2;1 aquaporin (Byrt et al., 2017) that can show NSCC activity when expressed in Xenopus oocytes, however the NH_4^+ permeability of these aquaporins has yet to be determined.

In animal systems, potassium transporters and channels are also believed to transport NH_4^+ due to their similarity in chemical size (mw) and charge (Martinelle and Häggström, 1993; Weiner and Hamm, 2007). A study by Moroni et al. (1998) showed that root-expressed AtKAT1 is permeable to NH_4^+ and a single amino acid mutation of Threonine (at position 256) to either Aspartic Acid or Glycine (T256D or T256G, respectively) significantly increased the permeability of NH_4^+ through the mutated KAT1 channel (Uozumi et al., 1995). Another study on rye also showed that NH_4^+ is permeable through a voltage-independent K^+ channel located in the plasma membrane of rye roots (White, 1996). Studies in barley clearly demonstrated a competitive interaction between NH_4^+ and K^+ (Hoopen et al., 2010). However, the

contribution of K^+ channels in the overall NH_4^+ transport and uptake in plants is relatively unknown and needs further research.

The main role of aquaporins (AQPs) are to facilitate water transport in and out of cells however, in some cases they can also transport small solutes (Takata et al., 2004) including NH_3 (Niemietz and Tyerman, 2000; Jahn et al., 2004), glycerol, CO_2, urea, H_2O_2, NO, metalloids, and ions (Wu and Beitz, 2007; Yool and Campbell, 2012; Zhao et al., 2016). Heterologous expression in yeast and *Xenopus* oocytes were used for the functional characterisation of plant AQPs in relation to NH_4^+/NH_3 transport ability across the plasma membrane. Tonoplast intrinsic proteins (TIPs) from wheat (TaTIP2;1, TaTIP2;2 and TaTIP2;3) showed the ability to restore growth inhibition of Δ*mep1-3* mutant yeast (31019b) at 2 mM NH_4^+ as a sole N source (Jahn et al., 2004). Additionally, expression of *TaTIP2;1* in *Xenopus* oocytes increased the influx of methylammonium (MA), a toxic analogue of NH_4^+, at pH > 7 (Jahn et al., 2004; Holm et al., 2005). Subsequent experiments by Bertl and Kaldenhoff (2007) using stopped-flow spectrometric studies provided further evidence of the ability of TaTIP2;2 to facilitate NH_3 transport across the plasma membrane of yeast protoplasts. Experiments by Loqué et al. (2005), showed that TIPs isolated from *Arabidopsis thaliana* (AtTIP2;1 and AtTIP2;3) were able to transport MA into the vacuole, hence increase the tolerance of wild type yeast (BY4741) to MA . When *AtTIP2;1* was expressed in *Xenopus* oocytes, a significant increase of MA influx across the plasma membrane was also evident. A recently published crystal structure of AtTIP2;1 revealed a unique side pore which is speculated to deprotonate NH_4^+, thereby increasing NH_3 permeability (Kirscht et al., 2016) adding more evidence of TIPs ability to transport NH_3. Unfortunately, *Arabidopsis* transgenic plants overexpressing *AtTIP2;1*, failed to demonstrate a significant physiological impact or changes on overall NH_3/NH_4^+ transport and regulation *in planta* (Loqué et al., 2005).

1.2.3 Identification of Ammonium Major Facilitator (AMF) families

In 2014, a novel gene was discovered in yeast when a soybean membrane-localised transcription factor *GmbHLHm1* (Chiasson et al., 2014) was overexpressed in the yeast mutant strain 26972c (Δ*mep1-2*). Microarray analysis was conducted by using RNA extracted from the yeast mutant overexpressing *GmbHLHm1* grown under low NH_4^+ conditions (Mazurkiewicz, 2008). The microarray results showed that a yeast gene, YOR378w, was significantly upregulated (~57-fold). Based on homology, YOR378w was classified as a Major Facilitator Superfamily protein (MFS). The uncharacterised YOR378w gene was renamed Ammonium Major Facilitator 1 (AMF1).

Subsequent experiments were carried out by Mazurkiewicz (2013) to functionally characterize this novel protein in relation to NH_4^+ transport and regulation. Yeast mutants 26972c and 31019b were used to investigate the capability of AMF1 to facilitate MA uptake. Overexpression of the yeast AMF1 (*ScAMF1*) caused MA toxicity and a significant increase in the accumulation of 1 mM ^{14}C-MA in both strains of yeast compared to control cells (pYES3-DEST empty vector). However, complementation of ScAMF1 demonstrated limited ability to restore yeast growth at 1 mM NH_4^+. These results indicated a clear ability

of ScAMF1 to mediate MA transport but NH_4^+ influx occurred only at higher concentrations (>1 mM). Additionally, heterologous expression systems and electrophysiology studies using *Xenopus* oocytes consistently showed the ability of ScAMF1 to facilitate NH_4^+ transport across the oocyte plasma membrane. There was a significant increase of ^{14}C-MA uptake in the oocytes injected with *ScAMF1* cRNA compared to water-injected oocytes. Using a two-electrode voltage clamp, a consistent NH_4^+ inducible inward current across the oocyte plasma membrane was detected in the oocytes injected with *ScAMF1*-cRNA while in the water-injected controls the current was not present.

Chiasson et al. (2014) produced a phylogenetic tree showing the amino acid sequence homology of AMF1 families across different plant species including, *Glycine max*, *A. thaliana*, *Medicago truncatula*, *Vitis vinifera*, *Zea mays*, *Oryza sativa*, *Populus trichocarpa*, *Ricinius communis*, *Sorghum bicolor*, *Picea sitchensis*, *Physcomitrella patens*. A high degree of conservation may reflect the importance of the protein in plants, possibly in relation to NH_4^+ transport mechanisms. Subsequent experiments on AMF homologs in soybean (GmAMF3) demonstrated similar features to ScAMF1. In yeast (strain 26972c and 31019b), overexpression of *GmAMF3* significantly increased ^{14}C-MA uptake relative to the empty vector control. Similarly, when *GmAMF3* was expressed in *Xenopus* oocytes, it generated an NH_4^+-dependent inward current (Chiasson et al., 2014).

Even though the previous results have shown that AMF1 proteins possess the characteristics of an NH_4^+ transport protein, the definitive functions of AMF1 and its mode of activity remain unclear. Therefore, further studies are needed to understand whether AMF1 is involved in NH_4^+ uptake into roots or NH_4^+ redistribution within plants.

1.3 Ammonium toxicity

1.3.1 Ammonium toxicity in plants

Despite NH_4^+ being the preferred source of reduced N for many plants especially grown under anaerobic conditions, NH_4^+ uptake must be carefully regulated. Hyperaccumulation of NH_4^+ is toxic and detrimental to most plants. This problematic situation usually happens in areas with intensive agricultural and livestock cultivation where NH_4^+ deposition is relatively high (van der Eerden, 1982; Pearson and Stewart, 1993). NH_4^+ deposition in some parts of Europe was estimated to be as high as 50 kg/ha/year (Pearson and Stewart, 1993). The reasons for NH_4^+ toxicity is still unclear. van der Eerden (1982) proposed that NH_4^+/NH_3 toxicity is due to: (i) inhibitory effects of NH_3 on photosynthetic phosphorylation presumably working as an uncoupler, which consequently reduces carbohydrate production and growth. Gerendás et al. (1997) hypothesized that NH_4^+ toxicity is a combined result of the following effects, including (i) nutrient deficiency due to an impaired uptake of essential metal ions, particularly K^+; (ii) root growth inhibition as a consequence of medium acidification; (iii) disturbance to intercellular pH and osmotic balance; (iv) uncoupling of photophosphorylation due to accumulation of NH_4^+ in leaves and (v) a shift in plant carbohydrate allocation to compensate for the energy demand of NH_4^+ detoxification.

Additionally, Barker (1999) suggested that incorporation of NH_4^+ into amino acids is a pathway for detoxification of accumulating NH_4^+ in leaf tissues.

One hypothesis is that NH_4^+ toxicity is a consequence of the high energetic cost required for cell detoxification by pumping NH_4^+ back out of root cells that eventually leads to growth inhibition (Britto et al., 2001). This hypothesis was based on a comparative study of two cereal plants (rice and barley) known to differ significantly in their tolerance to high NH_4^+. Rice is considered a species with an exceptional tolerance to high NH_4^+ while barley is a susceptible species. Using short-lived ^{13}N radiotracer, Britto et al. (2001) showed that barley roots have a higher NH_4^+ efflux from root cells to the external medium compared to rice roots. The efflux from barley roots reached almost 80% of initial influx. This detoxifying mechanism demands a substantial energy requirement. Based on theoretical calculations for barley roots, Kronzucker et al. (2001) proposed that 3.2 kJ energy is required to pump out one mol of NH_4^+ from the cell, or around 9-18 ions/ATP hydrolyzed. This is consistent with an increased O_2 consumption observed in barley roots subjected to high NH_4^+ and is strongly associated with the magnitude increase of NH_4^+ efflux (Britto et al., 2001). Eventually, growth inhibition is a consequence of the energy demanding process.

Despite extensive studies being carried out to elucidate NH_4^+ tolerance mechanism in Arabidopsis, most results have only revealed partial answers. This is probably a consequence of the complex nature of NH_4^+ toxicity. A review by Li et al. (2014) detailed molecular studies that demonstrated genes important for NH_4^+ sensitivity and tolerance in Arabidopsis. Surprisingly, only three of those genes discussed in the review are related to ion transport, a potassium transporter; TRH1 (Zou et al., 2012) and two NH_4^+ transporters; AMT1 and AMT3 (Lima et al., 2010). Other studies have mainly considered the proceeding consequences of NH_4^+ intrusion and accumulation in cells, such as root growth perturbation and biochemical changes in plants suffering NH_4^+ toxicity (Li et al., 2014). This is in contrast to the proposed hypothesis of Britto et al. (2001), which suggests regulation of NH_4^+ ion through transport proteins across the plasma membrane is the fundamental mechanism in NH_4^+ toxicity tolerance. Therefore, identification and elucidation of novel NH_4^+ transporters located in the plasma membrane and/or tonoplast will help to comprehensively answer the elusive question of NH_4^+ toxicity tolerance.

1.3.2 Ammonium toxicity tolerance mechanisms: efflux and sequestration

A high energy demanding NH_4^+ efflux mechanism is considered as the first step in NH_4^+ toxicity tolerance in most plants (Coskun et al., 2013a). Through this step, plants can fine-tune NH_4^+ homeostasis in the cytoplasm to maintain appropriate concentrations and avoid toxicity. Unfortunately, the gene(s) responsible for this mechanism have yet to be identified. Aquaporins were suggested to facilitate NH_3 efflux in plants (Howitt and Udvardi, 2000; Coskun et al., 2013a) as shown in symbiotic membrane of infected nodules in legumes (Udvardi and Day, 1997; Day et al., 2001). This process is mostly considered as a nutrient exchange step between the plant host and invaded bacteria rather than a toxicity tolerance mechanism. Nevertheless, aquaporins might participate in efflux mechanisms in both symbiotic and non-

symbiotic plants when NH_3 concentrations are elevated. Note that aquaporins (TIP2;1, TIP2;2) have been shown to transport NH_3, not NH_4^+, though some that function as NSCCs may also transport NH_4^+ (Byrt et al., 2017). Since the cytoplasm is slightly alkaline, NH_3 may be sufficiently elevated to efflux via aquaporins to the external more acidic apoplast.

Identification of NH_4^+ transporters in yeast (Mep) and plants (AMT) has led to the identification of related proteins in animals and humans (Rh). In contrast to Mep and AMT which only show influx capability (Marini et al., 1997; Yuan et al., 2007), some Rh and Amt proteins have been identified to facilitate NH_4^+ efflux. Human rhesus-associated RhAG protein and a kidney homologue (RhGK) enhanced resistance of yeast mutant Δ*mep1-3* grown at a toxic concentration of MA (Marini et al., 2000b; Westhoff et al., 2004). Subsequent studies by Mayer et al. (2006) and Marini et al. (2006) also revealed an enhanced tolerance when RhCG-expressing yeast were grown on toxic MA concentration. This enhancement was related to the ability of the Rh protein to pump out the toxic MA from cells.

In plants, vacuolar sequestration is also believed to confer NH_4^+ toxicity. When cells fail to maintain appropriate NH_3/NH_4^+ concentrations in the cytoplasm, storing excess NH_3/NH_4^+ into the vacuole seems to be a crucial step. However, the mode of action, transported species (NH_4^+ or NH_3) and transport proteins responsible for this pathway are still unclear. Coskun et al. (2013a) suggested that NH_3 is the species passively transported into the vacuole facilitated by tonoplast-localized proteins such as aquaporins. Accordingly, a study by Loqué et al. (2005) revealed that overexpression of *AtTIP2;1* and *AtTIP2;3* in yeast increased tolerance to toxic MA concentrations and the detoxifying ability of these tonoplast-localized proteins depended on a functional vacuole. On the other hand, the pathway facilitating NH_4^+ transport out of the vacuole back into the cytoplasm when required for assimilation is yet to be discovered.

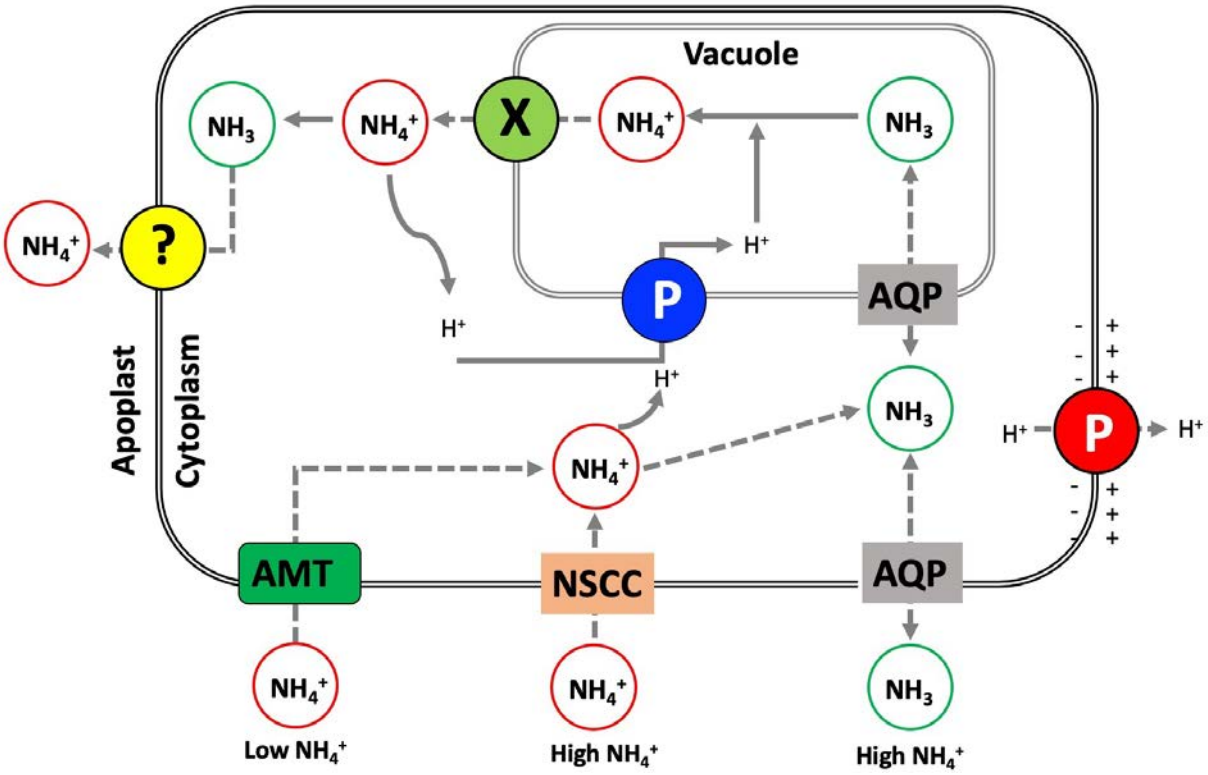

Figure 1.1 Schematic representation of transporters involved in NH_3/NH_4^+ uptake across plant cell membranes. Adapted from from *Plant Science*, 248, Esteban, R., Ariz, I., Cruz, C., and Moran, J.F. Review: Mechanism of ammonium toxicity and the quest for tolerance, Pages 92-101., Copyright (2016), with permission from Elsevier.

Under low/non-toxic NH_4^+ concentrations and adequate K^+ provision, plant cells facilitate NH_4^+ influx through high-affinity AMT transporters. When NH_4+ is present at high concentrations accompanied by low K^+, the AMT transporters are inactivated to avoid hyperaccumulation. However uncontrolled NH_4^+ influx may still occur through AQPs and NSCCs permeable to NH_3/NH_4^+ and contribute to net NH_3/NH_4^+ influx into the cytoplasm. Once inside the cytoplasm, the NH_4^+ is de-protonated to form NH_3. Sequestration of NH_3 into the vacuole is facilitated by tonoplast-localized AQPs. Due to acidic environment of the vacuole, the NH_3 is protonated to form NH_4^+ and acid-trapped inside the vacuole. Release of NH_4^+ from the vacuole back into the cytoplasm is facilitated by unidentified vacuolar NH_4^+ effluxer (X). In cytoplasm the released NH_4^+ is de-protonated to form NH_3. To achieve appropriate NH_3 concentration inside the cytoplasm, excessive NH_3 is pumped out into the apoplast by unidentified plasma membrane NH_3 effluxer (?). Once gets into the apoplast, the NH_3 is protonated into NH_4^+.

(?) : plasma membrane NH_3 effluxer; (X) : vacuolar NH_4^+ effluxer; (P) : plasma membrane proton pump; (P) : vacuolar proton pump; ➖➡ : NH_3/NH_4^+ flux through transport across plasma membrane and tonoplast.

1.3.3 K^+ and NO_3^- are essential for NH_4^+ toxicity alleviation

Interaction between K and N is complicated, yet interesting, as plants require both in relatively large quantities for proper growth and productivity. Both elements intersect in some important mechanisms

including influences of K^+ on regulation NO_3^- and NH_4^+ uptake, and *vice versa* (Lin et al., 2008; Hoopen et al., 2010; Zheng et al., 2016; Coskun et al., 2017). However, excessive concentrations of NH_4^+ under low external K^+ leads to NH_4^+ toxicity (Hoopen et al., 2010; Coskun et al., 2013a). In these conditions, both competition and inhibition effects of NH_4^+ on K^+ transport have been linked to NH_4^+ toxicity. Therefore, adequate K^+ is essential for NH_4^+ toxicity tolerance in plants (Szczerba et al., 2008; Hoopen et al., 2010; Coskun et al., 2017). In NH_4^+-sensitive plants such as barley, increasing external K^+ concentration significantly reduces the apparent energetic cost of NH_4^+ futile cycling (Szczerba et al., 2008). While in rice (NH_4^+-tolerant), additional K^+ improved NH_4^+ acquisition and metabolism leading to improved growth (Balkos et al., 2010). Likewise, root inhibition in Arabidopsis under NH_4^+ stress can be reversed by additional K^+ (Cao et al., 1993; Hirsch et al., 1998; Spalding et al., 1999). However, the mechanism underlying this alleviation remains unclear and may be due to differences in NH_4^+ sensitivity. In barley, reduction of NH_4^+ accumulation following K^+ supply was proposed to prevent disturbance on K^+-dependent metabolic processes and enzymatic reactions (Hoopen et al., 2010). Furthermore, elimination of NH_4^+ from media dramatically increased K^+ uptake in rice and Arabidopsis (Coskun et al., 2013b), and restored growth of Arabidopsis mutant lines defective in K^+ transport, *akt1* and *athak5*, grown under low K^+ (Pyo et al., 2010). In NH_4^+-sensitive plants, reduction of NH_4^+ futile cycling (across the plasma membrane) with additional K^+ is a fundamental mechanism for growth improvement (Szczerba et al., 2008) while in NH_4^+-tolerant species, improvement in growth is related to improved NH_4^+ assimilation and increased enzyme activity associated with elevated K^+ (Balkos et al., 2010).

Co-provision of NO_3^- can alleviate NH_4^+ toxicity in many species. Several mechanisms underlying this have been proposed. Wang et al. (2004) showed that NO_3^- acts as a signal to induce genes participating in NH_4^+ assimilation (GS/GOGAT). Therefore, rapid assimilation of NH_4^+ may lead to the reduction of free-NH_4^+ in the cytosol, thus reducing toxicity. Medium alkalinisation by NO_3^- is also postulated to participate in alleviation of NH_4^+ toxicity (Britto and Kronzucker, 2002; Escobar et al., 2006). Mutation of the *SLAH3* gene (a nitrate efflux channel) increases toxicity of *slah3* mutant plants grown under high NH_4^+ combined with low NO_3^-, or low pH conditions, suggesting that pH regulates function of SLAH3 during a NH_4^+ toxicity event (Zheng et al., 2015). It is commonly believed that NH_4^+ toxicity generally leads to deficiency of organic acids and inorganic cations following NH_4^+ accumulation. Surprisingly, Hachiya et al. (2012) reported that NO_3^- can alleviate NH_4^+ toxicity without lessening NH_4^+ accumulation and reduced depletion of organic acids and inorganic cations. It was suggested that this alleviation is closely associated with physiological processes corresponding to NO_3^-signaling, uptake and reduction. However, more studies need to be carried out to fully elucidate this phenomenon.

1.4 Aims, significance and contribution of the project to the discipline

The aim of this PhD study was to functionally characterize members of the AtAMF family in relation to NH_4^+ regulation in *Arabidopsis thaliana*. Previous heterologous expression studies on AMF homologs

from yeast and soybean (Chiasson et al., 2014) have demonstrated potential function related to NH_4^+ transport mechanisms. However, the definite roles of the proteins *in-planta* are yet to be determined. Here it is hypothesized that AMF is a transport protein involved in NH_4^+ regulation mechanisms distinctive to the well-studied ammonium transporter (AMT/Mep/Rh) families. The specific aims of were:

a. To functionally characterize AMFs in wild type *Arabidopsis thaliana* plants.
b. To investigate the function of AMFs by heterologous expression in yeast.
c. To study the physiological impact of AMF mutations in *amf* mutated lines.

Having a better understanding of AMF functionalities in the model plant *Arabidopsis thaliana* will broaden our insight into how plants regulate NH_4^+ transport. This information can be translated into a more comprehensive knowledge of how AMFs function and are regulated in agriculturally important crops. Furthermore, collectively with previous knowledge on N regulation in plants, additional information from studying AMFs would help to gain better insight in the quest for developing plants with improved NUE.

2. AMF studies in *Arabidopsis thaliana*

2.1 Introduction

The Major Superfamily (MFS) is one of the most diverse and largest groups of secondary active transport proteins conserved in living organisms (Yan, 2013). The transport mechanisms of MFS members include uniport, symport and antiport activities. MFS covers a broad spectrum of solutes, including ions, carbohydrates, lipids, amino acids, peptides, nucleosides and other molecules. The original MFS cluster are classified as (1) drug-resistance proteins, (2) sugar facilitators, (3) facilitators for Krebs cycle intermediates, (4) phosphate ester-phosphate antiporters and (5) a distinct group of oligosaccharide-H^+ symporters (Marger and Saier, 1993). Following the rapid growth of genome sequences, currently there are 76 subfamilies identified in the Transporter Classification Database (http://www.tcdb.org) based on phylogenetic analysis, data on substrate specificity, and the characterisation of transport activity. Unfortunately, nearly half of the subfamilies functions are hypothetical and have yet to be characterized (Yan, 2013). MFS members have been shown to play a vital role in physiological processes, including sugar and nitrate transport in organisms ranging from *Arabidopsis thaliana*, yeast to mammals (Özcan and Johnston, 1999; Büttner, 2007; Wilson-O'Brien et al., 2010).

A novel yeast gene, YOR378W, was identified through the overexpression by a non-yeast soybean transcription factor, *GmbHLHm1* transformed and expressed in a yeast strain defective in NH_4^+ transport (26972c). Microarray results showed a significant up-regulation of *YOR378W* in cells expressing *GmbHLHm1*. Based on the encoded protein sequence of YOR378W, the gene belongs to the MFS super family (Chiasson et al., 2014) and has been named *Saccharomyces cerevisiae* Ammonium Major Facilitator 1 (ScAMF1).

2.1.1 Preliminary functional data of AMF

There is a lack of information or studies that have examined the function of AMF and its potential role in NH_4^+ transport or other ions. AMF1 itself has been classified by sequence comparisons as a spinster-like MFS protein (TC 2.A.1.49) (http://www.tcdb.org). For example, AtAMF2 (At5g64500) shares 29 and 24% similarity with spinster proteins identified in fruit fly (*Drosophila melanogaster*) and zebra fish (*Danio rerio*), respectively. Furthermore, Nakano et al. (2001) showed that spinster proteins are essential in neuron cell development as well as glial cell migration along nervous systems (Yuva-Aydemir et al., 2011). The spinster protein is predicted as a lysosomal sugar carrier in *D. melanogaster* (Dermaut et al., 2005), while in *D. rerio* it plays important roles in the signalling mechanisms involving a bioactive lipid mediator, sphingosine 1-phosphate (Osborne et al., 2008). Moreover, a loss of spinster proteins leads to perturbed carbohydrate mobilization (Dermaut et al., 2005) and carbohydrate accumulation (Rong et al., 2011) in *D. melanogaster* mutants. These data suggest that spinster proteins including its plant homologs,

the AMFs, are potentially related to a putative efflux mechanism of carbohydrates, however no experimental measurements have ever been conducted to verify this.

In yeast, ScAMF1 shares limited similarity to members of the DHA2 family of H^+/drug antiporters (ATR1: YML116W, 38.7%identity; ATR2: YMR279c,36.5% identity) involved in boron efflux and tolerance (Kaya et al., 2009; Bozdag et al., 2011). However, Chiasson et al. (2014) demonstrated an NH_4^+ transport capability of ScAMF1, following functional characterization studies in yeast and *Xenopus* oocytes. Overexpression of *ScAMF1* in a yeast mutant strain 26972c (mep1-1 *mep2*∆ MEP3) and 31019b (∆*mep1-3*) increased cells sensitivity to methylamine (MA). Correspondingly, heterologous expression of *ScAMF1* in *Xenopus* oocytes also increased ^{14}C-MA uptake into oocytes. Subcellular localisation using GFP-tagged protein revealed that ScAMF1 is located on the plasma membrane. These data clearly showed the ability of AMF to facilitate NH_4^+ influx into the cells through the plasma membrane. Subsequent experiments showed that ScAMF1 was likely to participate in low affinity NH_4^+ transport (Chiasson et al., 2014).

Several AMF homologs have been identification in plants. In soybean, AMF expression in yeast and *Xenopus* oocytes also demonstrated similar transport properties to that of ScAMF1. However, these preliminary studies have not completely explained the definite function of AMF and how it contributes to global NH_4^+ transport in organisms. The fact that AMF proteins are conserved in most plants might indicate that AMF proteins have important roles in plant physiology. Therefore, more studies using both genetic and physiological means are essential to help fully elucidate AMF function.

2.1.2 Utilization of *Arabidopsis thaliana* for functional studies *in planta*

Since the completion of the *Arabidopsis thaliana* genome sequence, it has been a fundamental tool for genetic and physiological studies in plants. Data discovered from experiments using *Arabidopsis thaliana* have provided an enormous quantity of data that is allowing for an improved understanding of plant function and a mechanism to translate discovery to other plant species such as crop plants.

2.2 Materials and methods

2.2.1 Plant material and growth conditions

Arabidopsis thaliana Columbia-0 ecotype (Wild type) was utilised to study AtAMFs in this chapter. For plant growth in soil, a combination of cocopeat: vermiculite (4:1) was used. Three to five seeds were directly sown in soil media and then thinned to select the best seedling after two weeks. Plants were also grown in an aerated hydroponic system. The base nutrient solution contained: 1 mM $MgSO_4.7H_2O$, 1 mM KH_2PO_4, 0.05 mM H_3BO_3, 0.005 mM $MnSO_4.H_2O$, 0.001 mM $ZnSO_4.7H_2O$, 0.001 $CuSO_4.5H_2O$, 0.0007 mM $Na_2MoO_4.2H_2O$, 0.1 mM Fe-Na-EDTA, 0.25 mM K_2SO_4, 0.25 mM $CaCl_2.2H_2O$. In most situations, the nitrogen concentration was adjusted to 1 mM NH_4NO_3 unless otherwise indicated. Plants were tested for their response to nitrogen provision and starvation. With these experiments 2 mM NH_4Cl was used as the sole nitrogen source after a period of nitrogen starvation. All nutrient solutions were buffered with 0.05% MES (~ 2.5 mM) (Kagenishi et al., 2016) and pH adjusted with NaOH to 5.7 - 5.9. Prior to seedling transplantation into the hydroponic system, seeds were previously vernalised for 48 h at 4^{o}C in the dark and then single seeds sown directly onto holed-microtube lids filled with ½ strength base nutrient solution solidified with 0.7 % w/v agar. The lids were arranged on a holed-pizza tray and grown on nutrient solution for two weeks before transplantation. Plants were initially grown on short day (8 h light/16 h dark) at 22^{o}C/18^{o}C (light/dark) with light intensity of 110-120 µmol m^{-2} s^{-1} Photosynthetically Active Radiation (PAR) at rosette level. When required, light conditions were changed to a long day setting (16 h light/8 h dark) to induce flowering.

2.2.2 RNA extraction and cDNA synthesis

Tissue samples were harvested and immediately frozen with liquid N_2 and kept at -80^{o}C until analysed. The samples were then ground frozen to fine power using 2010 Geno/Grinder pre-cooled with liquid nitrogen for RNA extraction. Total RNA was extracted from ~100 mg frozen tissues using Spectrum™ Plant Total RNA Kit (Sigma-Aldrich) following manufacturer's instructions. The extracted RNA was treated with DNase following TURBO DNA-free™ Kit protocols to remove residual genomic DNA prior to cDNA synthesis. Approximately 1 µg DNase treated-total RNA was used for cDNA synthesis following SuperScript™ III First-Strand Synthesis System (Invitrogen) protocol using oligo$(DT)_{20}$ primer and half of the recommended enzyme added per reaction. The cDNA was diluted 10-fold with sterile water and then stored at -20^{o}C until required.

2.2.3 Quantitative PCR analysis

KAPA SYBR ® FAST qPCR Master Mix (2X) Kit was used to perform qPCR analysis using a QuantStudio 12K Flex Real-Time PCR System. The primer pairs (Table 2.1) used for qPCR experiments were designed with Geneious software (Biomatter Inc.) and tested for efficiency. *Arabidopsis thaliana TUB4* was chosen as a housekeeping gene for expression normalisation. qPCR reactions were run in 20 µl reactions consisting of 5 µl of diluted RNA, 10 µl master mix and 200 nM of each primer.

2.2.4 Tissue specific localisation of AtAMF

Investigation of tissue specific localisation of *AtAMF* homologs in Arabidopsis were carried out by developing transgenic plants harbouring an AMF native promoter fused with a GUS/GFP reporter. A ~1 kb portion of genomic DNA sequence upstream of the start codon of each *AtAMF* was cloned and inserted into the promoter-less binary vector pKGWFS7 (Supplemental Figure S2.1). The sequenced constructs were then transformed into wild type *Arabidopsis thaliana* Col-0 plants using the floral dip method (Clough and Bent, 1998). Transformed seeds were selected on media containing 50 μg/ml kanamycin. The resistant seedlings were transplanted into soil and grown to maturity for seed collection. These seeds were then used for further genomic analysis.

GUS histochemical staining was conducted following that of Kim et al. (2006). During harvesting, tissue samples were kept on ice in a cold acetone-H_20 (9:1, v/v) solution followed by 20 min incubation at room temperature. The samples were rinsed with staining buffer three times on ice. The staining buffer consisted of 50 m*M* sodium phosphate buffer (pH 7.0), 0.2% Triton X-100, 2 m*M* potassium ferrocyanide, and 2 m*M* potassium ferricyanide. The samples were then incubated in staining solution (staining buffer supplemented with 1 mM X-Gluc) and vacuum infiltrated for 15 min, followed by overnight incubation at 37˚C. After overnight incubation, the samples were washed with 70% ethanol repeatedly until samples turned colourless. Stained tissues were analysed, and images taken using a Nikon SMZ25 stereo microscope at Adelaide Microscopy, Waite campus.

2.2.5 Tissue culture

Tissue culture techniques were used in experiments that require intact plants with antibiotic resistance and tissue specific expression. Media for tissue culture grown plants was based on MS media with modifications. The media contained 2.5 mM KCl, 2 mM $CaCl_2$, 1.5 mM $MgSO_4.7H_2O$, 1.25 mM KH_2PO_4, 0.1 mM Na_2-EDTA, 0.1 mM $FeSO_4.7H_2O$, supplemented with micronutrients and vitamins (Table 2.2), 1% (w/v) sucrose, 0.8% agar (w/v), buffered with 0.05% MES and pH adjusted with NaOH to 5.7-5.9. For antibiotic resistance screening and control treatment, plants were supplied 1 mM NH_4NO_3 in the modified MS media.

Prior to germination, seeds were surface sterilized as follows: first, the seeds were washed with 20% (v/v) bleach solution containing 0.1% Tween 20 (v/v) for 5 min with vigorous shaking. After carefully discarding the bleach solution, seeds were rapidly washed (30 s) with vigorous shaking) in 70% ethanol (twice) and 100% ethanol (once). Next, the seeds were rinsed with sterile H_2O (5-6 times) to remove any residual bleach. The water was replaced with ~1 ml sterile 0.1% agar (w/v) to disperse the seeds. The seeds were then carefully placed into the media using 200 μl large orifice pipette tips. The seeds were vernalised at 4˚C for 48 hr before proceeding to germination in a growth chamber (environmental conditions explained in section 2.2.1).

2.2.6 Cloning of *AtAMFs*

The coding sequence of three Arabidopsis *AMF* homologs were amplified from previously generated cDNA using high fidelity DNA polymerase (NEB Phusion® High Fidelity Polymerase) with the following PCR conditions: 30 s initial denaturation at 98˚C, 35 cycles of denaturation at 98˚C, annealing at 70˚C for 30 s, and 45 s elongation at 72˚C, followed by final extension at 72˚C for 5 min. Based on the TAIR database (https://www.arabidopsis.org), primer pairs were designed for *at2g22730*, *at5g64500*, and *at5g65687* representing *AtAMF1*, *AtAMF2* and *AtAMF3*, respectively (Table 2.1). The 5'-end of each forward primer was modified to contain CACC sequence which is a requirement for cloning into entry vector pENTR™/D-TOPO™. The entry vector was transformed into TOP10 competent cells and screened on selective media containing 50 μg/ml kanamycin. The resistant colonies were propagated on selective liquid media followed by plasmid extractions using FavorPrep™ Plasmid Extraction Mini Kit (FAPDE 300, FavorGen). The accuracy of cloned sequences was reviewed by sequencing purified plasmid DNA at Australian Genome Research Facility (AGRF), Adelaide.

2.2.7 Sub-cloning of *AtAMFs* into pUBN-GFP-DEST expression vector using Gateway© System

The entry vectors harbouring the correct sequences of the *AtAMFs* (pENTR-*AtAMFs*) were recombined with the expression vector pUBN-GFP-DEST (Grefen et al., 2010) using the LR clonase™ II enzyme. The expression vector contains ubiquitin10 (UBQ10) promoter driving a N-terminal GFP fusion to a target protein (Supplemental Figure S2.2). A final LR reaction was transformed into TOP10 competent cells and screened on selective media containing 50 μg/ml spectinomycin. Following transformation, multiple colonies were picked and grown on liquid selective media, followed by plasmid isolation using FavorPrep™ Plasmid Extraction Mini Kit (FAPDE 300, FavorGen). Sequencing analysis was performed on the isolated plasmid to ensure no mutation occurred to the sequences. A heat shock protocol (Weigel and Glazebrook, 2006) was used to transform the expression vectors, organelle markers and p19 plasmid (Supplemental Table 2.3) into *Agrobacterium* AGL1.

2.2.8 Subcellular localisation in *Nicotiana benthamiana* leaves

A soil mixture consisting of cocopeat: vermiculite: perlite (4:1:1) was used to grow *Nicotiana benthamiana* plants. Seeds were directly sown into soil. Two-week-old seedlings were transplanted into a new pot and grown for another 3-4 weeks in a growth chamber under a 16-h day/night cycle at 23˚C and 50% air humidity. Five - six week old plants were infiltrated following the methods described by Arpat et al. (2012). Two days before infiltration, starter cultures of *Agrobacterium* harbouring expression vectors and p19 plasmid were initially grown overnight at 28˚C with 200 rpm shaking in 2 ml 2YT media (Table 2.4) supplemented with appropriate antibiotics (20 μg/ml rifampicin + 50 μg/ml spectinomycin for pUBN-GFP-AtAMFs and pUBC-CBL1-RFP, and 20 μg/ml rifampicin + 50 μg/ml kanamycin for p19 and pER-rk-CD3-959). 200 μl of the initial starter culture was transferred into 5 ml fresh 2YT media and grown overnight at 28˚C with 200 rpm shaking. The culture was centrifuged at 4000 x g for 12 min at room

temperature to collect a cell pellet. Supernatant was discarded, and the cell pellet resuspended in 2 ml acetosyringone (AS) media (Table 2.4), followed by centrifugation at 4000 x g for 7 min. After removing the supernatant, the pellet was resuspended again with 2 ml AS media and OD_{600} was measured. The concentration of infiltration culture mix was adjusted to have OD_{600} ~0.3 for the expression vectors and organelle markers and ~0.1 for p19. A 1 ml infiltration culture sample was infiltrated using syringe on the abaxial side of a leaf. The infiltrated leaves were allowed to grow for two-three days prior to image analysis using confocal microscopy (Nikon A1R laser scanning confocal, Adelaide Microscopy Waite Facility).

2.3 Results

2.3.1 Identification of AMF homologs in plants

A database search based on AMF protein similarities showed that AMF homologs are present in most genome sequenced plants. The database search also identified a large number of uncharacterized *AMF* genes. Based on these data alignments, a phylogenetic tree was developed to highlight evolutionary change and similarities amongst plant AMFs (Figure 2.1). In most dicot plants, including *Arabidopsis*, soybean, *Medicago, Brassica,* and *Vitis*, there were multiple AMF homologs identified with high amino acid similarities that were clustered into six clades. In *Arabidopsis*, there are three AMF homologs that can be identified by sequence analysis: *AtAMF1* (*At2g22730*), *AtAMF2* (*At5g64500*) and *AtAMF3* (*At5g65687*) with predicted amino acid lengths of 536, 484 and 492, respectively. Furthermore, each AMF has 56.5 - 57.4% protein similarity to each other. Interestingly, each of the AtAMFs belong to a specific clade suggesting conserved functional roles within the family. In contrast, most monocots examined including barley, sorghum, *Setaria*, and *Brachypodium*, rice and its relatives only have one *AMF* gene homolog. Furthermore, the monocot branch consists of three clades which strongly correlate to Poaceae evolution. Maize, and close relatives, *Sorghum bicolor* and *Setaria italica*, are in the same clade. Similarly, related species, wheat, barley and *Brachypodium*, are grouped together. Rice and relatives belong in the same clade. Monocot plants that have multiple *AMF* homologs are *Triticum aestivum* and maize. There are three homologs identified in the hexaploid, *Triticum aestivum*. These multiple homologs may have evolved due to genome multiplication during *T. aestivum* evolutionary development. The three genes, (*TRIAE_CS42_2AL_TGACv1_093684_AA0285140*, *TRIAE_CS42_2BL_TGACv1_129681_AA0392390*, and *TRIAE_CS42_2DL_TGACv1_158329_AA0515760*) are located on the long-arm of chromosome 2 of each chromosome set A, B and D respectively, with 86.6 - 94.2% similarity to each other. Accordingly, its diploid ancestor, *Triticum urartu*, has only one AMF homolog (*TRIUR3_31027*). *T. urartu* is the ancestor of chromosome set A in *T. aestivum*, hence, it is not surprising that this homolog has 88.1% similarity with *TRIAE_CS42_2AL_TGACv1_093684_AA0285140*. Unexpectedly, even though maize is a diploid plant, it has only two *AMF* homologs that are located on separate chromosomes. The *ZmAMF1* (*Zm00001d002964*) is located on chromosome 2 while *ZmAMF2* (*Zm00001d025894*) is located in chromosome 10. Both genes have 93.7% similarity to each other.

2.3.2 Structural characteristic and conserved sequences

The prediction of trans-membrane spanning helices was conducted using Trans-Membrane Hidden Markov Models (TMHMM) with Geneious software. The results showed that AtAMF1, AtAMF2 and AtAMF3 are predicted to have 10, 9 and 11 trans-membrane spanning domains, respectively (Figure 2.2 and Supplemental Figure S2.3). It also predicted that AtAMF2 has a longer extracellular N-termini (90 amino acid residues) compared to the N-termini of AtAMF1 and AtAMF, with 43 and 22 amino acid residues, respectively. Additionally, the C-terminus end of AtAMF1 and AtAMF2 is predicted

to be cytoplasmic whereas the C-terminus of AtAMF3 is predicted to be extracellular (Figure 2.2). However, trans-membrane prediction using Phobius algorithm showed that AtAMF1, AtAMF2 and AtAMF3 are predicted to have 12, 11 and 10 trans-membrane spanning domains (Supplemental Figure S2.4).

Several conserved amino acid residues were observed among the AtAMF family protein sequences. The second transmembrane domain of AtAMF1 and AtAMF3 has a highly conserved region compared to the first transmembrane of AtAMF2. Similar conservation was also observed in the third and fourth transmembrane of AtAMF1 and AtAMF3 and the second and the third transmembrane of AtAMF2, respectively (Figure 2.2).

2.3.3 AtAMF expression across different plant tissues

Understanding the expression patterns of *AtAMFs* in different tissues will ultimately help to uncover their function and role in plant growth. Therefore, expression analysis was carried out on hydroponically grown wild type *Arabidopsis thaliana* Col-0 plants grown under 'control conditions' where an adequate and balanced nitrogen regime was provided (1 mM NH_4NO_3). The plants were grown for six weeks under a short-day regime (16 h night, 8 h day) and then transferred into a long day photoperiod (8 h night, 16 h day) to initiate flowering. The results revealed that *AtAMFs* were expressed in all of the plant tissues sampled (Figure 2.3). In general, *AtAMF2* is expressed at the highest level, followed by *AtAMF3* and *AtAMF1*. In contrast to the high-affinity ammonium transporters (*AtAMT),* the *AtAMFs* showed higher expression in shoot tissues compared to the roots. This discrepancy might indicate a distinct role of AtAMFs compared to AtAMTs. Furthermore, the highest expression of *AtAMF2* and *AtAMF3* appeared in senescing leaves, while *AtAMF1* showed highest expression in young leaf tissues. Both *AtAMF2* and *AtAMF3* also displayed considerable expression in stem tissues. Interestingly, expression of *AtAMF2* showed a similar pattern to that of *AtAMF3*. This might suggest a functional redundancy between these genes. On the other hand, *AtAMF1* expression showed a considerably distinct pattern compared to the other two genes. All genes showed a low expression pattern in reproductive organs including flowers and siliques.

2.3.4 Diurnal regulation of AtAMFs

Earlier studies have demonstrated a diurnal regulation pattern of *AtAMTs* expression (Gazzarrini et al., 1999). Therefore, we were intrigued to investigate whether the *AtAMFs* have similar regulation to light/ dark cycles. Shoot tissue samples were collected from soil grown plants at different time points following light/ dark cycle under long day period (16 h light/8 h dark). We identified that *AtAMFs* were responsive to a light/ dark cycle and diurnally regulated similar to the *AtAMTs*. All *AtAMFs* expression reached their peak after midday around 3 PM and then came back down before the dark cycle started (Figure 2.4).

2.3.5 Expression changes in response to N-starvation and resupply

Information on how gene expression changes in response to nitrogen-based treatments is crucial to properly understand the relationship between *AMF* genes and the nitrogen transport and assimilatory pathways in plants. In particular, changes in gene expression following N-starvation and/or resupply will help to accurately reveal the function of the gene of interest. All *AtAMFs* were responsive to both N-starvation as well as resupply of NH_4^+ when supplied as the sole N source. Both *AtAMF1* and *AtAMF2* were up-regulated mostly in leaf tissues in response to N starvation and resupply (Figure 2.5). Following three days of N-starvation, *AtAMF1* and *AtAMF2* were up-regulated in leaf tissues while *AtAMF3* did not show a significant up-regulation in the same tissues. However, *AtAMF3* showed an apparent up-regulation 1 h after N resupply in both root and leaf tissues. Surprisingly, all genes remained up-regulated following the resupply of 2 mM NH_4Cl. Both *AtAMF1* and *AtAMF2* showed up-regulation (24 h) after resupply which then gradually decreased by 48 h. The induction by *AtAMF3* peaked in the first 6 h then gradually reduced 24 - 48 h after resupply. Interestingly, *AtAMF3* responded to resupply in both shoot and root tissues, while *AtAMF1* and *AtAMF2* showed a response predominantly in shoot but not root tissues.

2.3.6 Cloning of *AtAMFs*

Based on database search on TAIR (https://www.arabidopsis.org), three *AMF* homologs exist in *Arabidopsis thaliana*, *At2g22730*, *At5g64500*, *At5g65687* representing *AtAMF1*, *AtAMF2* and *AtAMF3*, respectively. *At2g22730* is predicted to have up to seven splice variants (*At2g22730.1-7*) (http://www.arabidopsis.org/servlets/TairObject?type=locus&name=At2g22730). For each gene, individual sets of primers were designed based on online sequence data (Table 2.1). *AtAMF2* and *AtAMF3* were readily amplified in a single PCR reaction from 7-day-old seedlings grown on modified MS plate. However, the same reaction failed to amplify *AtAMF1*, possibly due to a low expression level and or cDNA copy number in the reaction. Therefore, amplification of *AtAMF1* involved two PCR reactions, where 1 µl PCR product from the first reaction was used as template for the second PCR reaction. This experiment successfully amplified *AtAMF1* sequence from the enriched template library. Each sequence was cloned into the entry vector pENTR-D-TOPO and amplified plasmids sequenced. The sequencing results indicated that both *AtAMF2* and *AtAMF3* sequences matched the online reference sequence. Unexpectedly, sequencing results indicated the attempt to amplify the reference sequence *At2g22730.1* (1533 bp) failed. A re-evaluation of the annotated reference sequence and predicted splice variants allowed new PCR primers to be synthesised. The splice variant *At2g22730.2* (1611 bp) and a second unidentified splice variant, hereafter named *At2g22730.8* (1677 bp) were amplified from the cDNA templates. In comparison to *At2g22730.1*, both *At2g22730.2* and *At2g22730.8* have 15 bp and 63 bp additional exons at +382 and +741, respectively, whereas another 66 bp of additional exon at +1182 is only present in *At2g22730.8* (Figure 2.6). The clones *At2g22730.2* (1611 bp) and *At2g22730.*8 (1677 bp) were named *AtAMF1.1* and *AtAMF1.2* respectively and used in the following experiments.

2.3.7 Localisation of *AtAMF*s expression in specific tissues

The native promoter sequence of each *AtAMF* (~1 kb upstream the start codon) was inserted into the promoter-less vector pKGWFS7 harbouring GUS/GFP reporter genes (Supplemental Figure S2.1) and transformed into *Arabidopsis thaliana* (Col) using *Agrobacterium*-mediated transfection following floral dip protocols (Clough and Bent, 1998). Following seedling selection on media containing kanamycin, surviving plants were grown to maturity for seed collection. In general, tissue specific localisation of each *AtAMF* was distinct. In young seedlings (10-day old plate grown plants with sufficient nitrogen), *AtAMF1* was found strongly localised to the vascular bundles in both roots and shoots (Figure 2.7.B, C, E, F) but also in guard cells of the first primary leaves (Figure 2.7.C and D). In contrast, *AtAMF2* was localised strongly in the root cap just after the root primordia region (Figure 2.8.F). There was a low level of signal in vascular tissues opposing secondary roots (Figure 2.8.D and E). AtAMF3 showed low promoter activity with signal appearing in roots as part of the region where vascular bundles reside (Figure 2.9.D).

2.3.8 Subcellular localisation of AtAMFs

Previous findings showed a basic level of tissue specific localisation for the three *AtAMFs*. However, the data was not sufficient to help understand the potential function of each of these proteins. Therefore, a transient protein expression was used to help identify the default intercellular localisation of each AMF. To do this, the *Nicotiana benthamiana* transient expression system was employed where the coding sequence of each *AtAMF* was subcloned into the N-terminal in-frame expression vector pUBN-GFP (Grefen et al., 2010). The expression vector contains the ubiquitin-10 (*UBQ10*) promoter driving the transcriptional expression of the hybrid N-terminal GFP fusion mRNA (Supplemental Figure S2.2). The pUBN-GFP (AMF) constructs were transformed into *Agrobacterium tumefaciens* AGL1, and then infiltrated into the abaxial side of tobacco leaves. After a short incubation period, GFP signal was detected in the endoplasmic reticulum (ER) for both AtAMF1.1 and AtAMF1.2. AtAMF2 signal was localised to the tonoplast while the AtAMF3 was localised at the plasma membrane. To strengthen these findings, each expression vector was co-expressed with secondary expression vectors containing various organelle markers (Supplemental Table 2.3). Both pUBN-GFP-AtAMF1.1 and pUBN-GFP-AtAMF1.2 were co-expressed with pUBC-CBL1-RFP, an expression vector containing CBL1, a plasma membrane marker fused with RFP (Yue Wu, unpublished), and pER-rk-CD3-959, an expression vector containing the HDEL sequence to act as a ER marker fused with mCherry (Nelson et al., 2007). The pUBN-GFP-AtAMF2 and pUBN-GFP-AtAMF3 were co-expressed with pUBC-CBL1-RFP and pB7-H2B-RFP (Wege et al., 2016), an expression vector containing the nuclear *H2B* marker fused with RFP.

Figure 2.10 shows the localisation of AtAMF1.1 to the ER. Signals detected from GFP-AtAMF1.1 and HDEL-mCherry displayed overlapping ER signatures. On the other hand, there was a distinct subcellular localisation of GFP-AtAMF1.1 from CBL-RFP where CBL-RFP showed a clear subcellular localisation to the plasma membrane (Supplemental Figure S2.5). Comparable results were observed in GFP-AtAMF1.2 subcellular localisation. Signals overlapping in the ER were detected between AtAMF1.2

and HDEL-mCherry (Figure 2.11). Additionally, Supplemental Figure S2.6 shows localisation of GFP-AtAMF1.2 to the ER while CBL1-RFP was localised in the plasma membrane.

AtAMF2 localisation on the tonoplast of the epidermal cells is evident based on the co-expression of GFP-AtAMF2 and H2B-RFP (Figure 2.12). One particular feature observed in GFP-AtAMF2 is the presence of loop-like GFP signals around the nucleus (N). Accordingly, RFP signal clearly identifies the nucleus inside the cells. Another character that signifies the tonoplast localisation is presentation of two membranes with a significant gap between each other. In contrast, when GFP-AtAMF2 was co-expressed with CBL1-RFP, GFP signal was absent around the nucleus and not overlapping with RFP signal on the plasma membrane (Supplemental Figure S2.7). Collectively, these data suggest AtAMF2 localisation to the tonoplast.

Localisation of AtAMF3 is detected in the plasma membrane. Figure 2.13 shows overlapping signals for GFP-AtAMF3 and CBL1-RFP in the epidermal cells. Additionally, Supplemental Figure S2.8 shows the absent of GFP signal around the nucleus that distinctively discriminate plasma membrane from tonoplast. Altogether, these data exhibit the localisation of AtAMF3 in the plasma membrane.

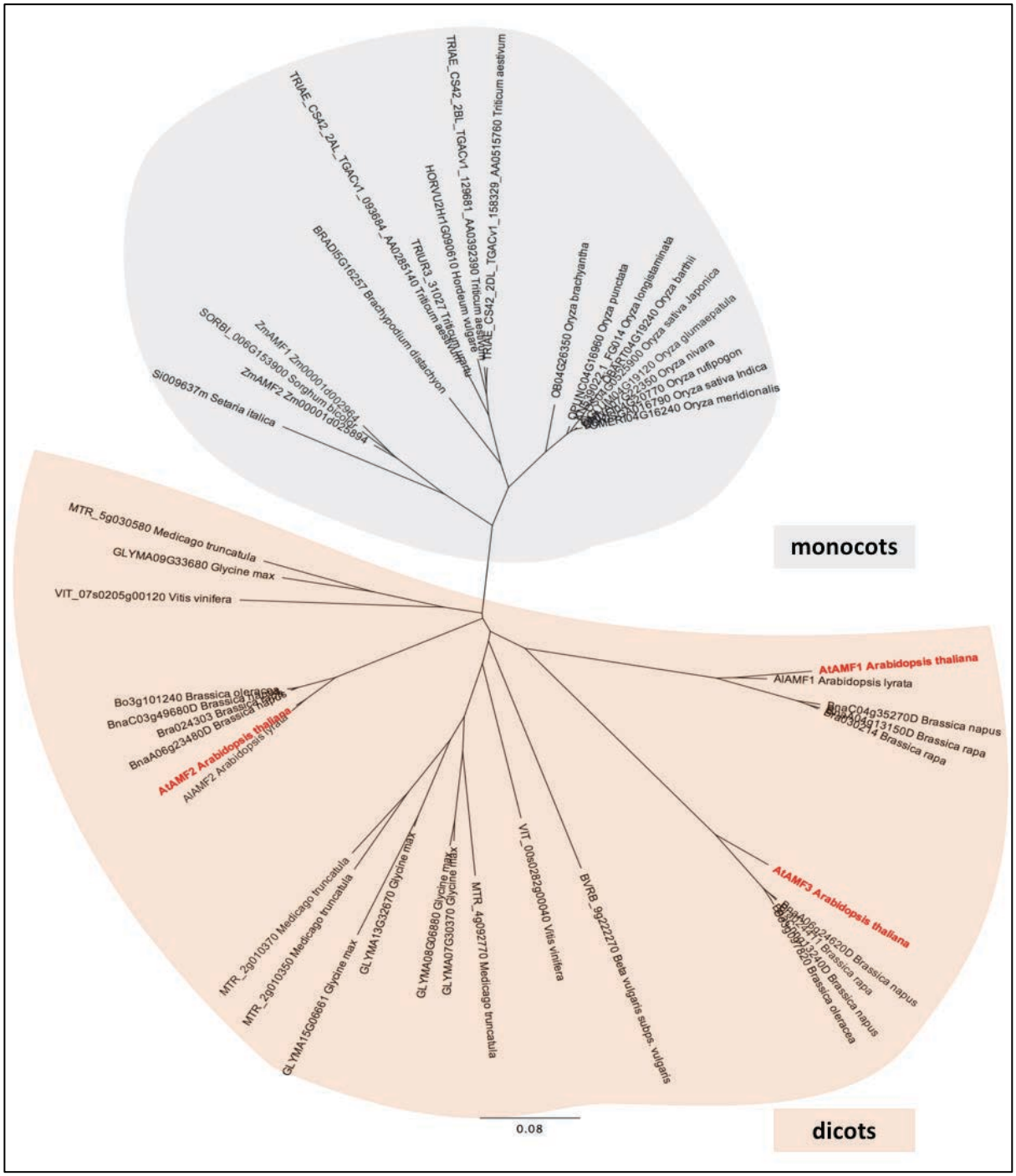

Figure 2.1. AMF is conserved among plants.

Analysis of AMF protein sequence homology in plants. The tree was generated using Geneious 6.1.7 software with global alignment and neighbour-joining methods. The branch length is proportional to the number of amino acid substitutions per site.

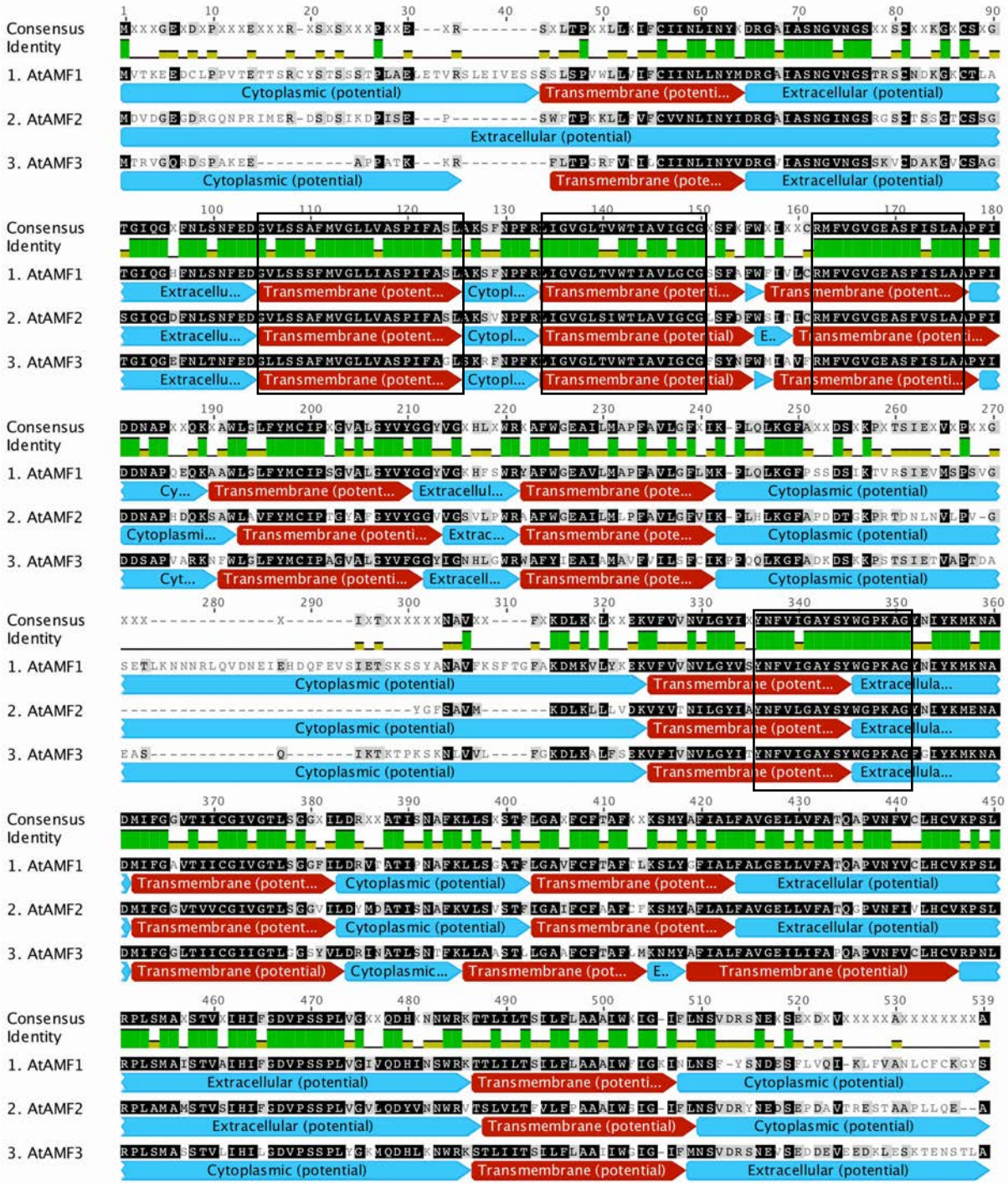

Figure 2.2. Transmembrane prediction and amino acid sequence alignment of AtAMF1, AtAMF2 and AtAMF3.

Membrane topology prediction of AtAMF1, AtAMF2 and AtAMF3 based on Transmembrane Hidden Markov models (TMHMM) using Geneiuos software. Conserved regions are highlighted with orange boxes.

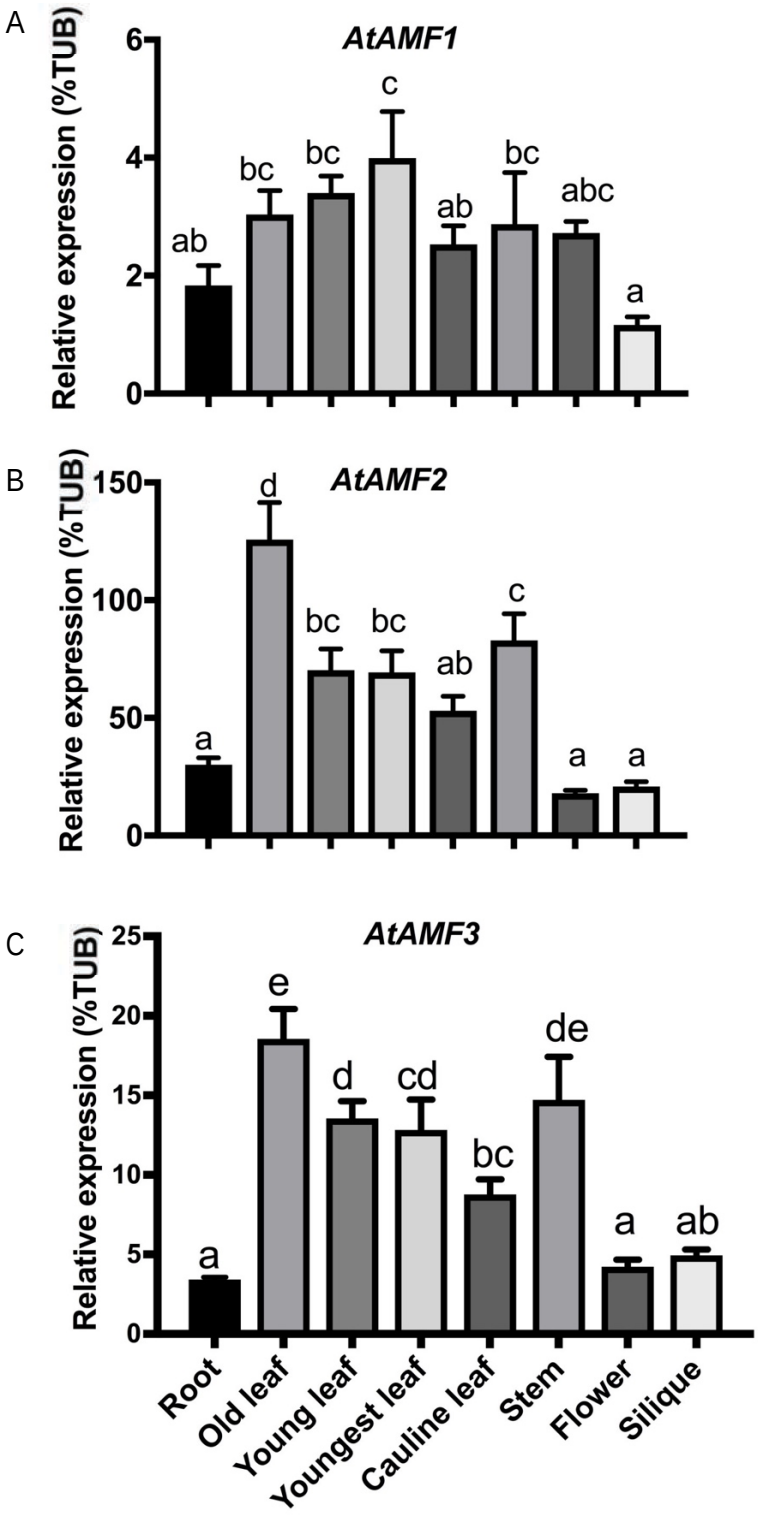

Figure 2.3. Gene expression of *AtAMF1* (A), *AtAMF2* (B) and *AtAMF3* (C) in different tissues of eight-week-old Arabidopsis plants.

Data values represent the means of 4 biological replicates ± SEM. Different letters indicate significant differences among means at P<0.05 and uncorrected Fisher's LSD post-test. *AtTUB4* was used as a housekeeping gene. Old leaf: >50% of leaf senescence; Young leaf: 10-50% leaf senescence; Youngest leaf: <10% leaf senescence.

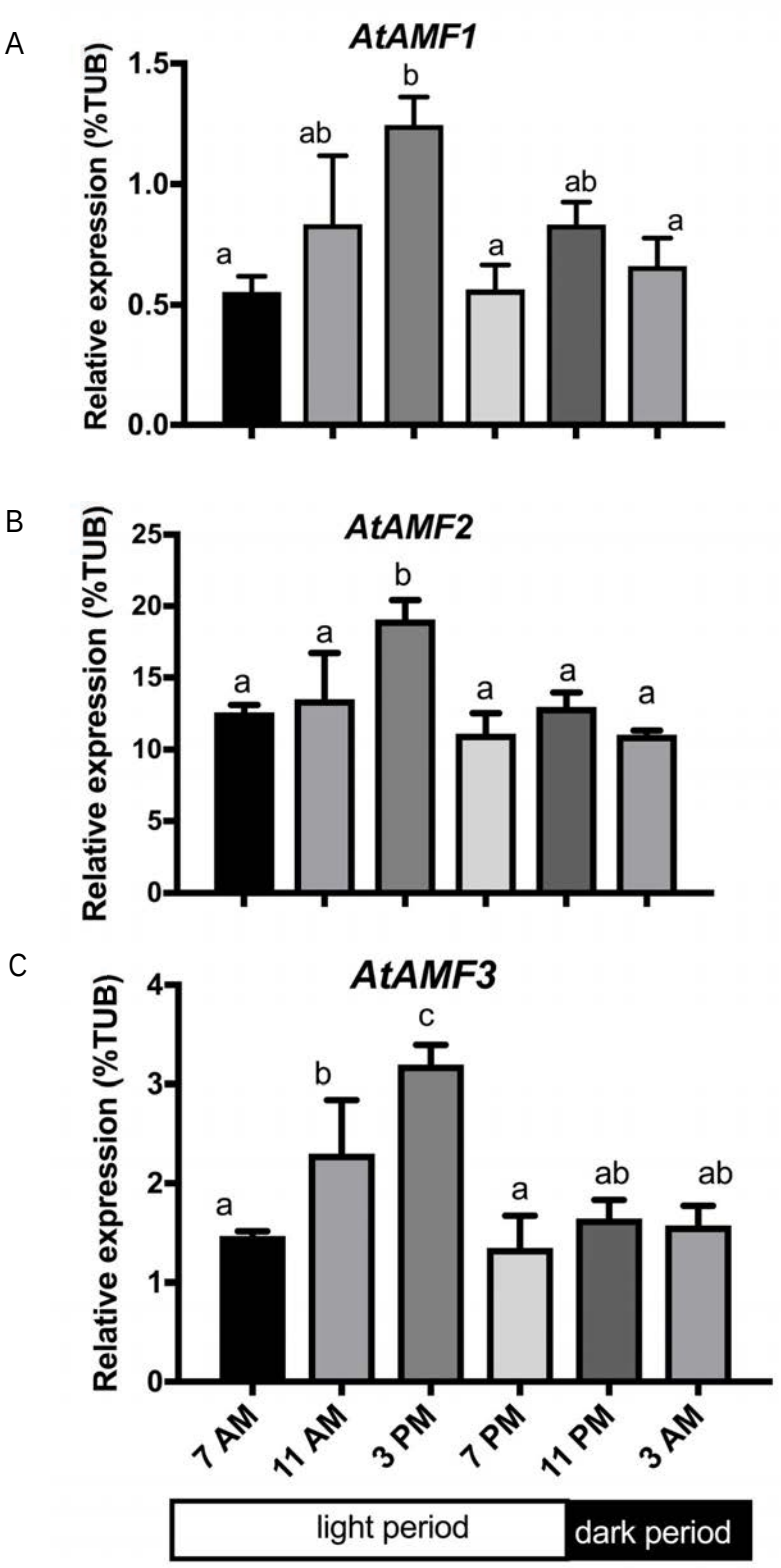

Figure 2.4. Gene expression of *AtAMF1* (A), *AtAMF2* (B) and *AtAMF3* (C) in six-week-old Arabidopsis shoots show diurnal regulation.

Plants were grown on soil for six weeks prior to tissue collections. Data values represent the means of 4 biological replicates ± SEM. Different letters indicate significant differences among means at $P<0.05$ and uncorrected Fisher's LSD post-test. *AtTUB4* was used as a housekeeping gene.

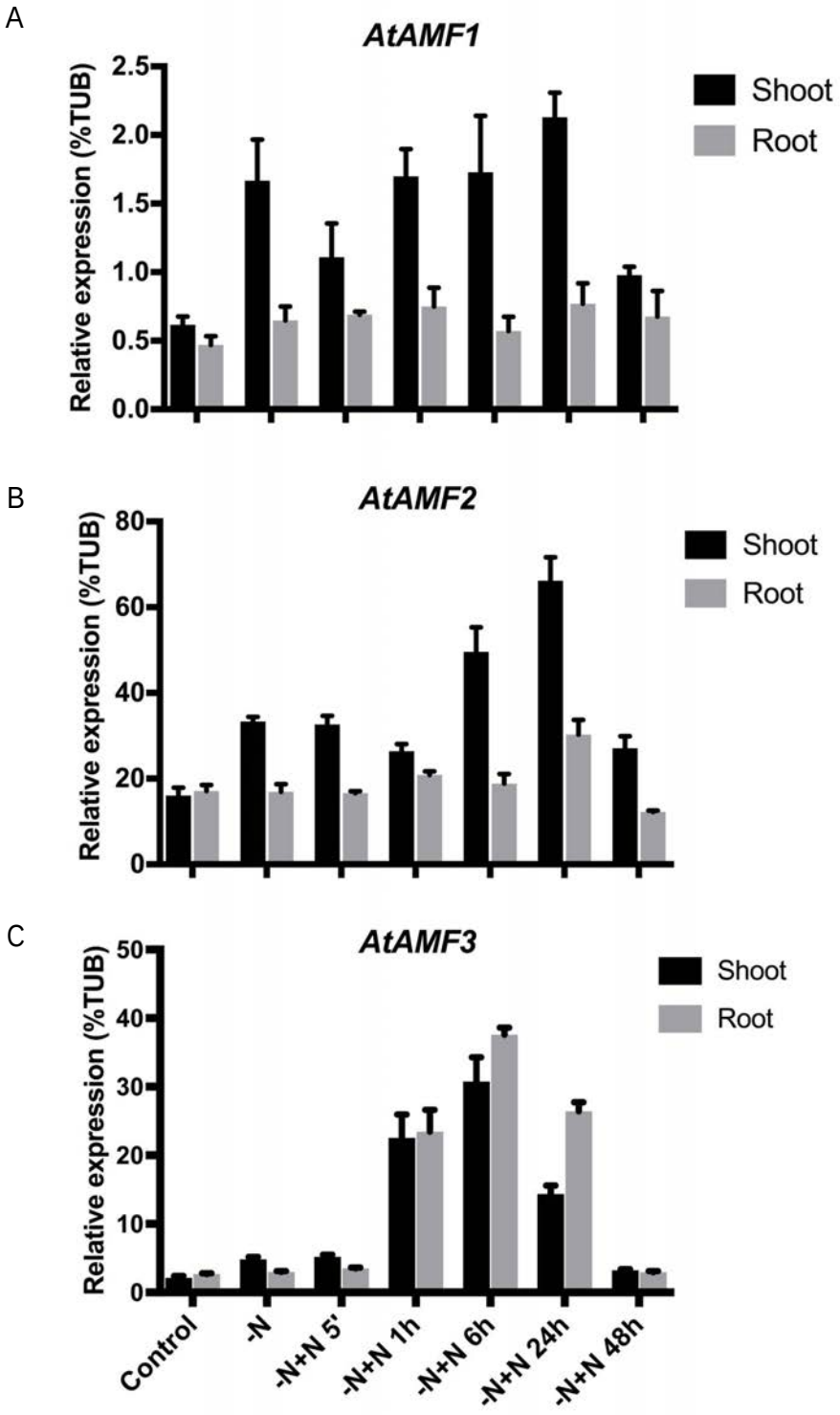

Figure 2.5. Relative expression of *AtAMF1* (A), *AtAMF2* (B) and *AtAMF3* (C) in six-week-old Arabidopsis plants in response to N-starvation and resupply.

Plants were hydroponically grown under short day conditions for six weeks prior to three-day N-starvation treatment. Resupply treatment with 2 mM NH_4Cl was initiated following the starvation. Root and shoot samples were harvested in various time points. RNA was extracted individually from plants grown under identical condition. Data values represent the means of 4 biological replicates ± SEM. *AtTUB4* was used as a housekeeping gene.

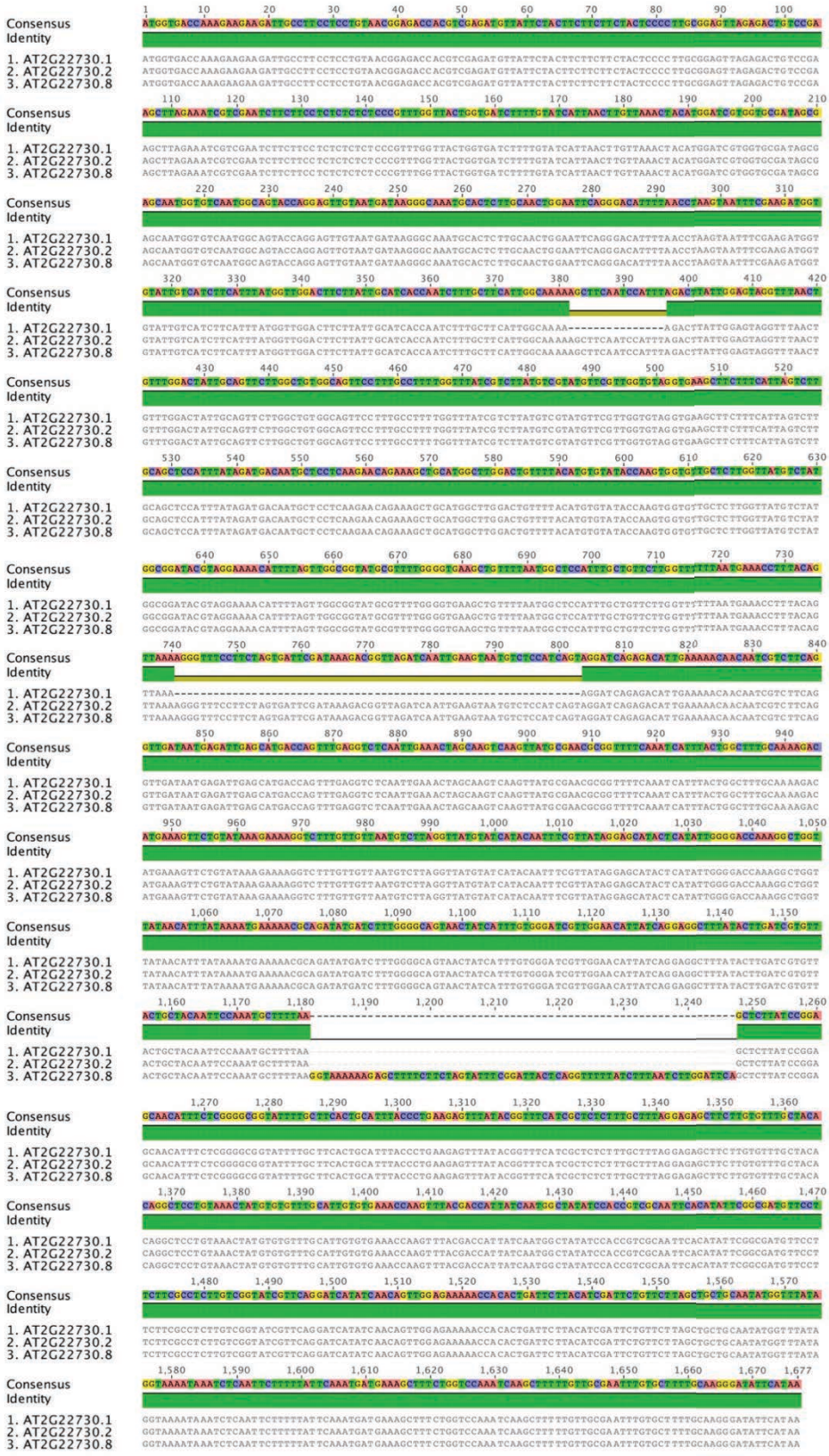

Figure 2.6. Nucleotide sequence alignment of cloned *AtAMF1* splice variants

There are multiple splice variants predicted originating from the *AtAMF1* locus. Comparison overview of reference sequence *At2g22730.1* with the cloned splice variants *At2g22730.2* (*AtAMF1.1*) and *At2g22730.8* (*AtAMF1.2*). Green blocks indicate consensus identitiy while joining dashes indicate discrepancy in nucleotide alignment between the clones to the reference sequence.

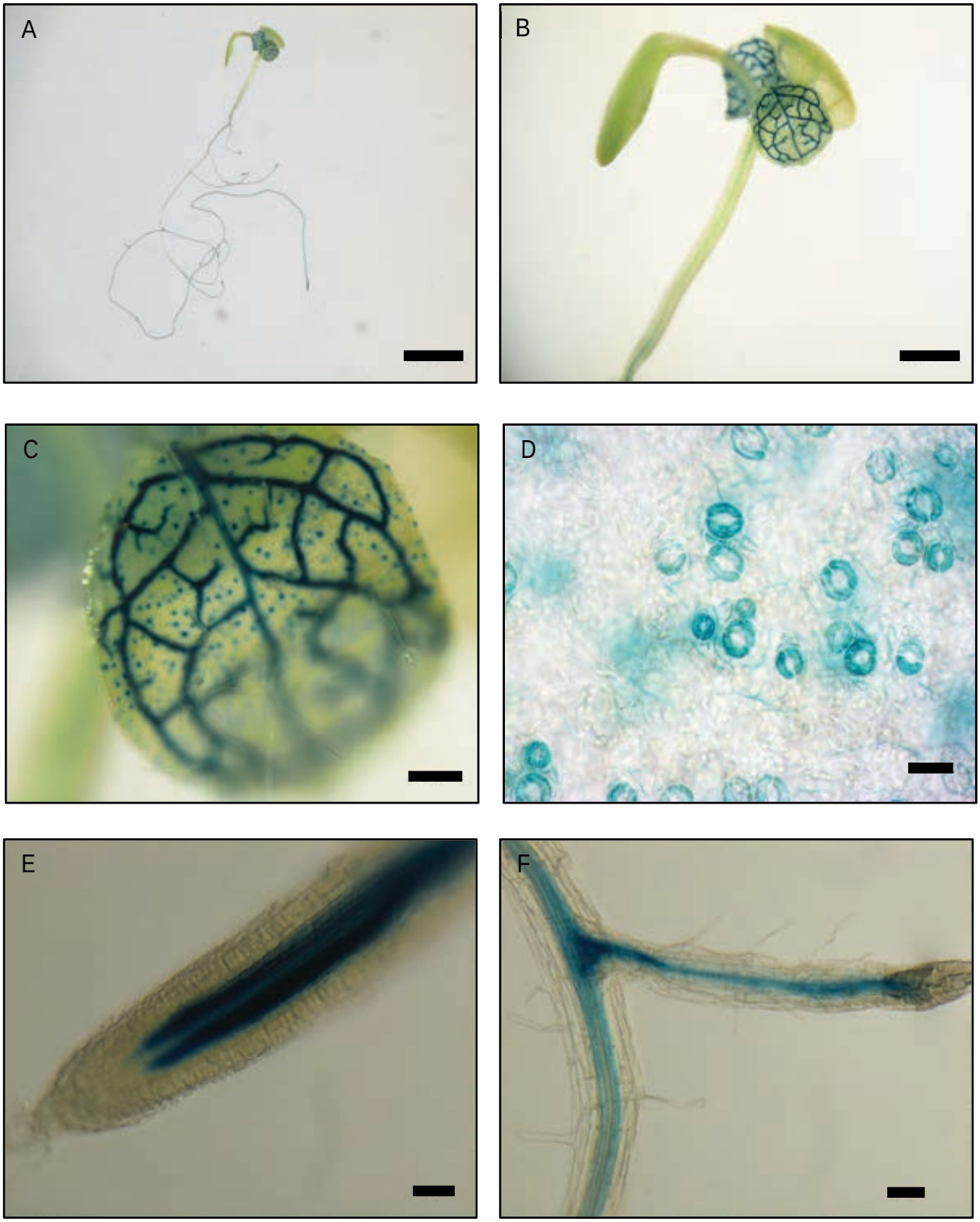

Figure 2.7. GUS expression of *AtAMF1* is expressed in guard cells and in vascular tissues of 10-day-old Arabidopsis seedlings.

Seeds of transgenic plants were grown on agar plates with 1 mM NH_4NO_3 for 10 d under short days prior to GUS staining. A. Overview of GUS expression in a whole seedling. Scale bar = 2 mm. B and C, GUS expression in vascular tissues and guard cells in leaves. D, GUS expression in guard cells. E and F, GUS expression in the vascular tissues of roots. Scale bar = 2 mm (A); 0.5 mm (B); 0.1 mm (C); 25 μm (D-F)

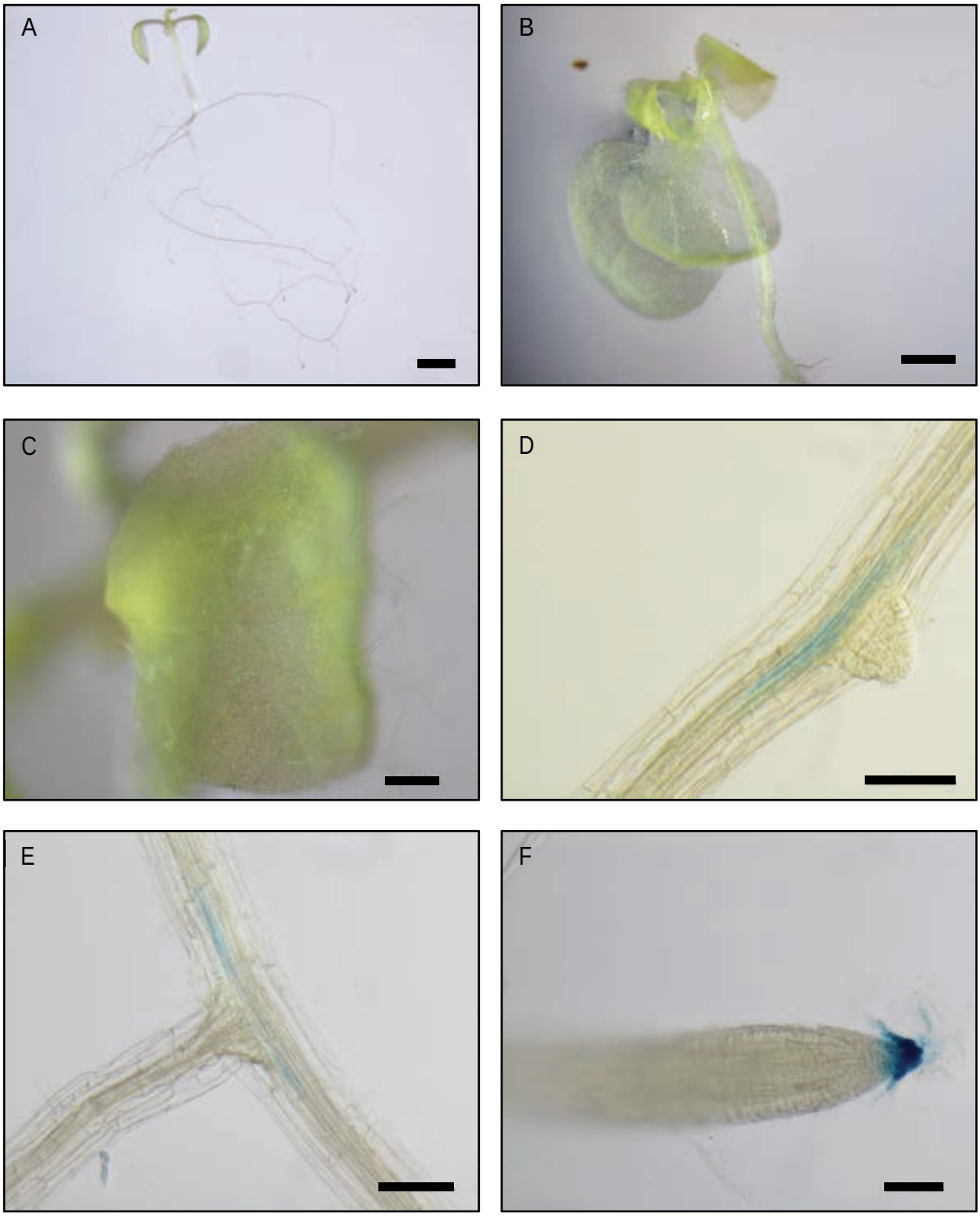

Figure 2.8. *AtAMF2* is expressed in the root cap and pericycle cells under root primordia and lateral roots of 10-day-old Arabidopsis seedlings.

Seeds of transgenic plants were grown on agar plates with 1 mM NH_4NO_3 for 10 d under short days prior to GUS staining. A, Overview of GUS expression in a whole seedling. B and C, GUS expression is absent in leaf tissues. D, GUS expression appeared with vascular tissues next to root primordia. E, GUS expression in vascular tissues in root branches and F, GUS expression in the root tip localised to the root cap. Scale bar = 1 mm (A); 0.5 mm (B); 0.1 mm (C); 50 μm (D-F)

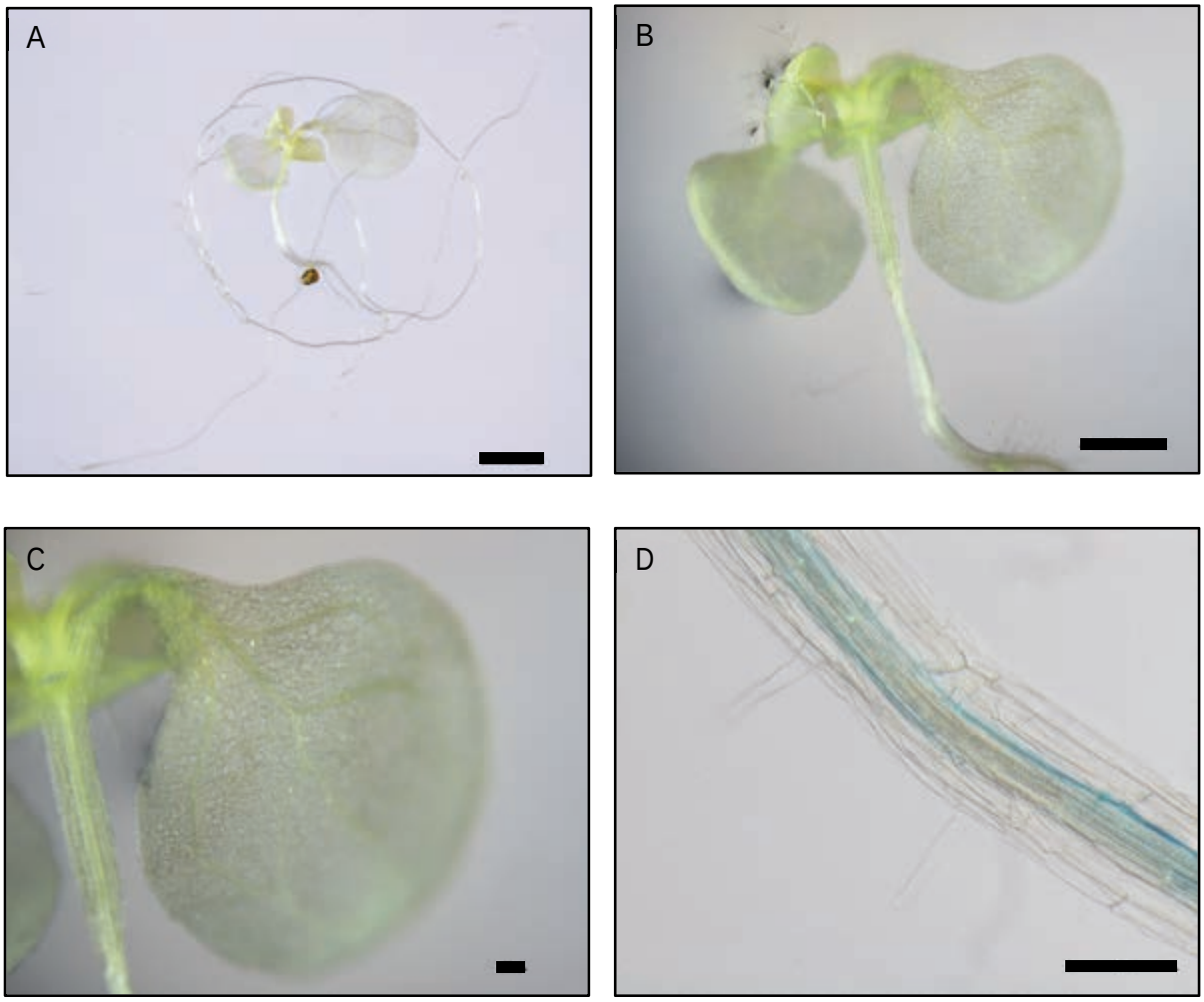

Figure 2.9. *AtAMF3* is expression in vascular tissues of 10-day-old Arabidopsis seedlings. Seeds of transgenic plants were grown on agar plates with 1 mM NH_4NO_3 for 10 d under short days prior to GUS staining. A, Overview of GUS expression in a whole seedling. B and C, GUS expression is absent in leaf tissues. D, GUS expression is localised to the vascular bundle in root tissues. Scale bar = 1 mm (A); 0.5 mm (B); 0.1 mm (C); 50 μm. (D)

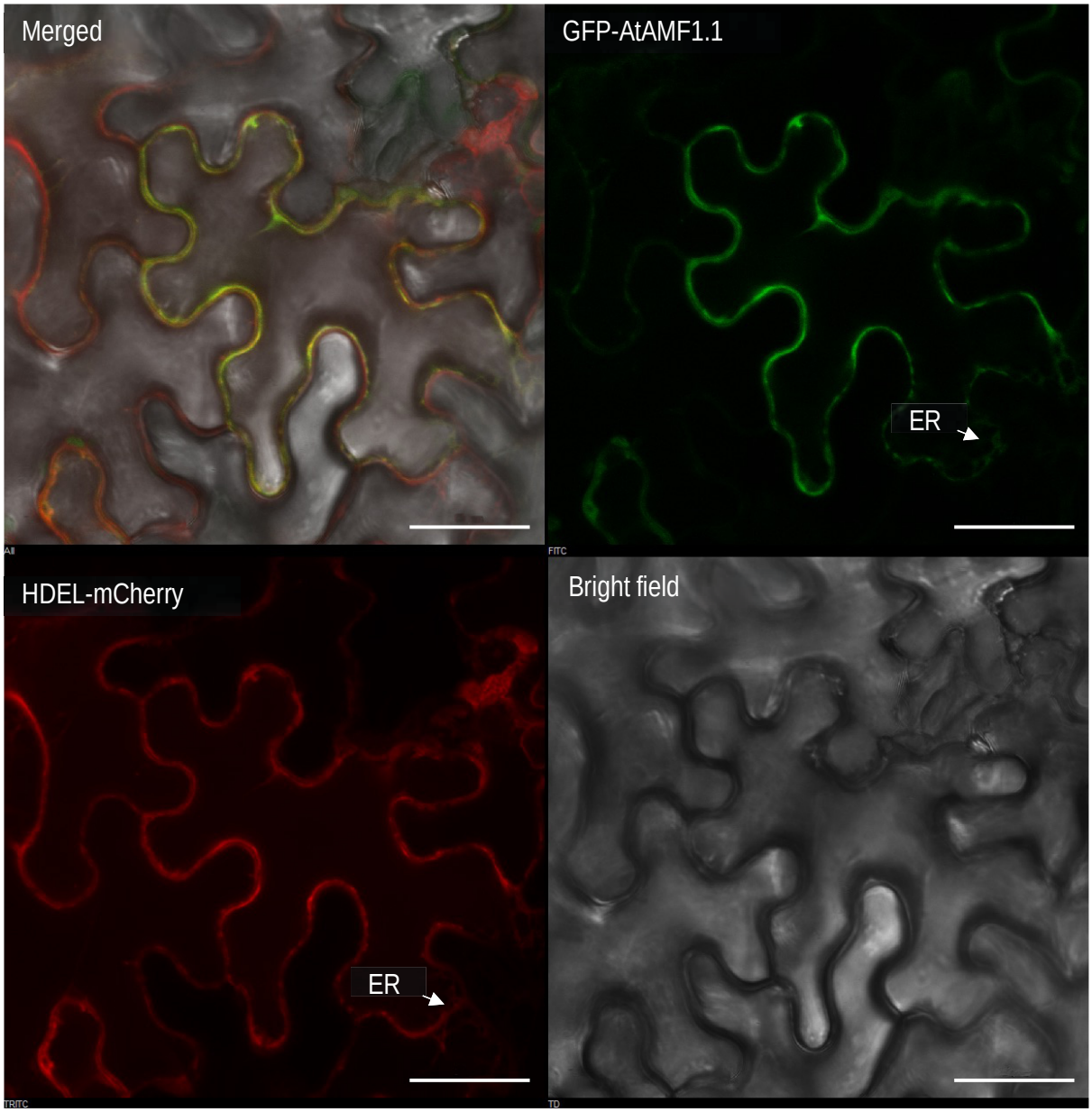

Figure 2.10. Subcellular localisation of GFP-AtAMF1.1 in the Endoplasmic reticulum (ER) transiently expressed in *Nicotiana benthamiana* leaf cells.

GFP-AtAMF1.1 was co-expressed with an ER marker, HDEL-mCherry. Scale bars = 25 μm

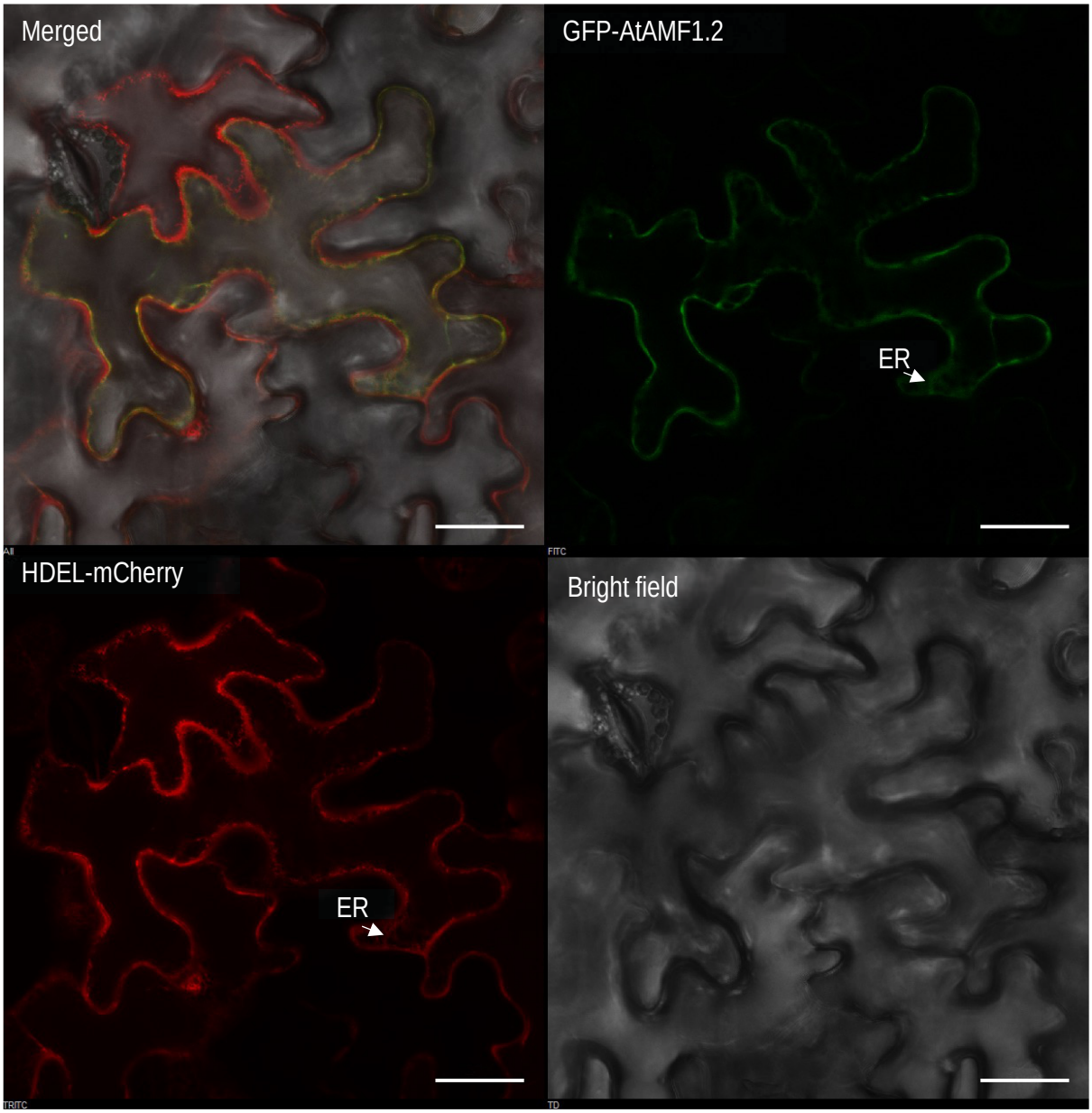

Figure 2.11. Subcellular localisation of GFP-AtAMF1.2 in Endoplasmic reticulum (ER) transiently expressed in *Nicotiana benthamiana* leaf cells.

GFP-AtAMF1.2 was co-expressed with an ER marker, HDEL-mCherry. Scale bars = 25 μm.

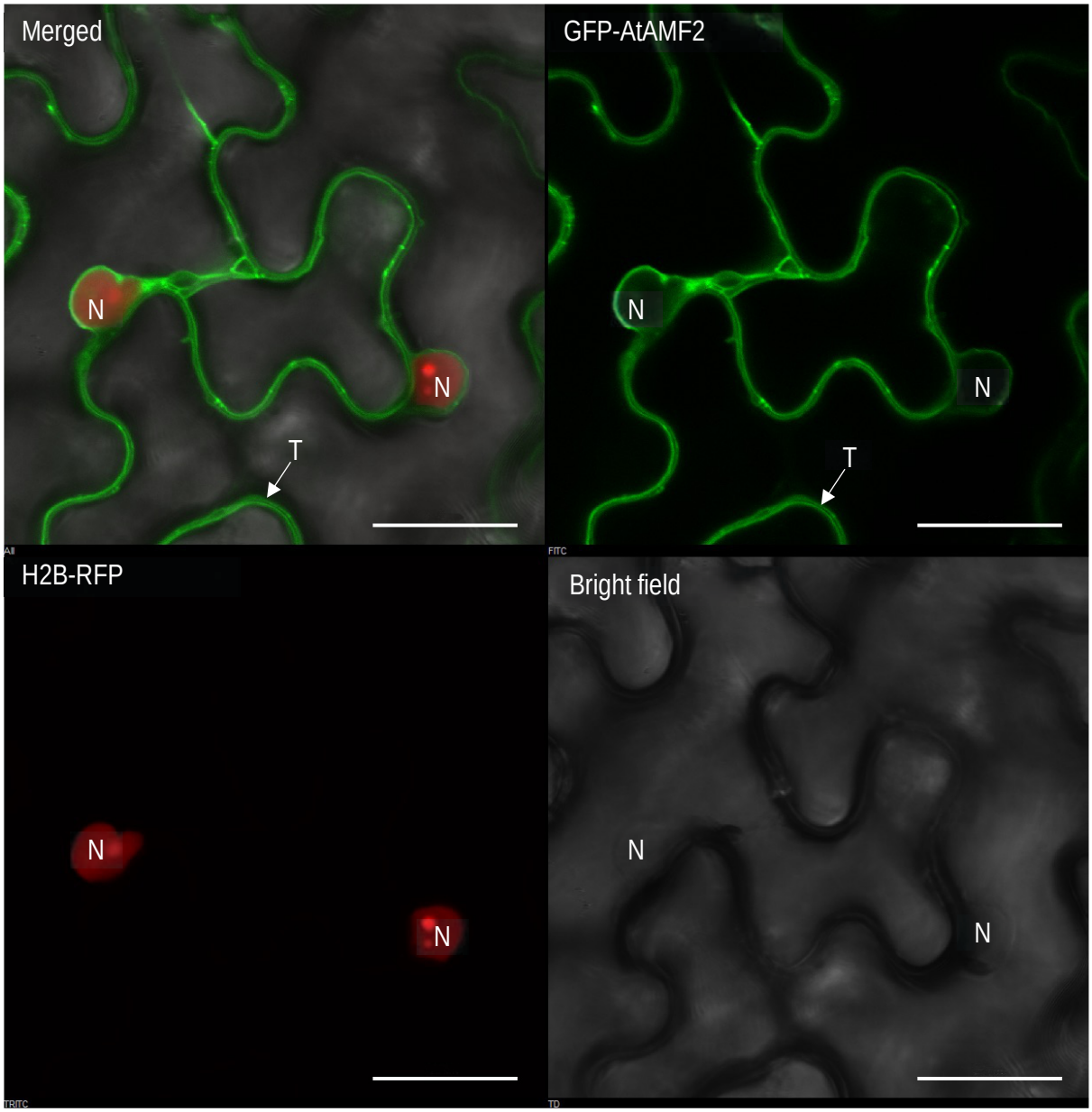

Figure 2.12. Subcellular localisation of GFP-AtAMF2 in the tonoplast transiently expressed in *Nicotiana benthamiana* leaf cells.

GFP-AtAMF2 was co-expressed with a nuclear marker, H2B-RFP. Distinctive loop-like GFP signal around nucleus appears on GFP-AtAMF2. Location of nucleus (N) is clearly identifiable from RFP signal. T = tonoplast. Scare bars = 25 μm.

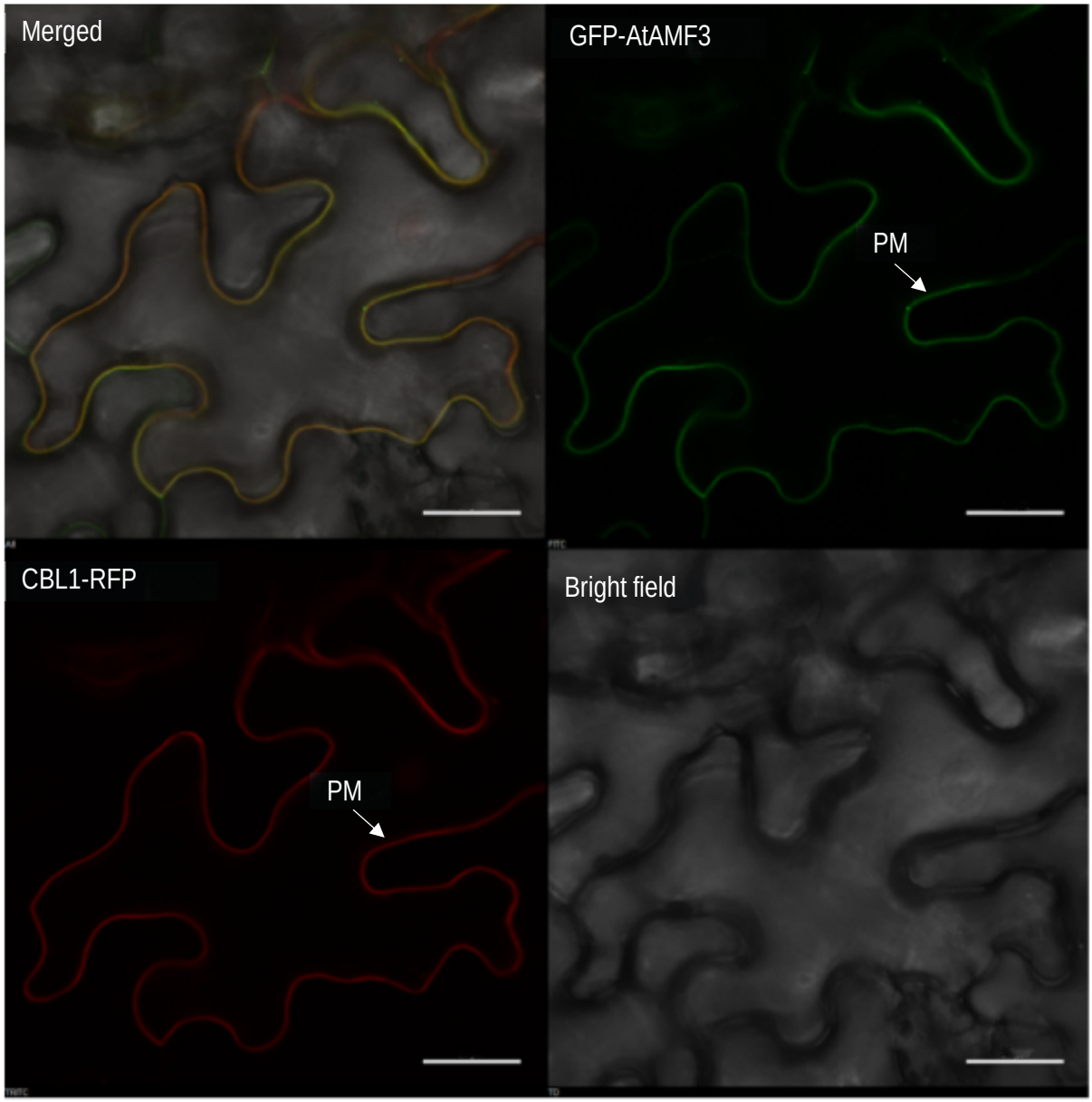

Figure 2.13. Subcellular localisation of GFP-AtAMF3 in the plasma membrane (PM) transiently expressed in *Nicotiana benthamiana* leaf cells.

Co-expression of GFP-AtAMF2 and CBL1-RFP (a plasma membrane marker). Evident overlapping is evidently observed in the plasma membrane of epidermal cells. Scare bars = 25 μm.

2.4 Discussion

Identification of the low affinity NH_4^+ transport protein ScAMF1, has led to new research on the regulation of NH_4^+ transport in various organisms. To the best of our knowledge, ScAMF1 and the soybean homolog GmAMF1 are the only AMF proteins empirically shown to be involved in low affinity NH_4^+ transport. Interestingly, protein amino acid sequence analysis revealed that AMF is conserved broadly amongst plants across both monocots and dicots, reflecting an important role in plant growth and development. Based on phylogenetic analysis of multiple AMF proteins, most dicotyledonous plants have multiple AMF homologs, this is contrary to monocots, that mostly have one AMF homolog except for maize (two) and wheat (three) (Figure 2.1). Additionally, all of the AMF homologs from monocot plants are closely related as they are clustered together in similar clades, whereas dicot plants display multiple clades. This might indicate a diverse physiological function of AMF in different plant classes. Unfortunately, empirical functional studies of AMF plant homologs are still very limited.

2.4.1 *AtAMFs* show a distinct expression pattern from *AtAMTs*

Using both yeast and *Xenopus* oocyte heterologous expression systems, ScAMF1 and a plant homolog (GmAMF3) were shown to transport NH_4^+ (Chiasson et al., 2014). However, the physiological implications of the protein *in planta* are still unknown. Therefore, *Arabidopsis thaliana* was used to study the gene(s) *in planta*. This study investigated the expression patterns of the three AMF homologs that exist in *Arabidopsis thaliana*: *AtAMF1*, *AtAM2* and *AtAMF3*. All three genes are expressed across various parts of the plant with increased expression in senescing shoot tissues (Figure 2.3). This expression profile is in contrast to the well-studied NH_4^+ transporters (*AtAMT1* and *AtAMT2*), which are highly expressed in root tissues and widely known for their role in NH_4^+ uptake from soil and redistribution to the shoots (Gazzarrini et al., 1999; Loque et al., 2006; Yuan et al., 2007). In contrast, it would appear AtAMFs may have a more defined role in senescing shoot tissues, although their role in daily management of NH_4^+ transport cannot be ignored as they are broadly expressed across most tissues. This discrepancy suggests a distinct function between AtAMFs and AtAMTs in relation to NH_4^+ regulation. Although *AtAMFs* and *AtAMTs* are different in an organ-dependent expression profiles, both gene families display responses to light and dark cycles, suggesting a link to photoperiodic control of nitrogen and carbon metabolism. *AtAMTs* have been shown to be up-regulated following a light cycle and down-regulated during a dark cycle in root tissues (Gazzarrini et al., 1999). Interestingly, *AtAMF* expression profiles in shoot tissues also displayed a day/night regulated expression profile. All three *AMF* genes reached a peak in expression after midday, followed by a down-regulation before the dark cycle started (Figure 2.4). This suggests a synchronized response to light availability and the potential coordination of NH_4^+ transport. Additionally, NH_4^+ resupply following a N-starvation period triggered up-regulation of all *AtAMFs* in shoot tissues while only *AtAMF3* responded to NH_4^+ resupply in root tissues (Figure 2.5). This may indicate a distinct function of AtAMF3 in relation to NH_4^+ transport and homeostasis in shoot and root tissues, while AtAMF1 and AtAMF2 suggest NH_4^+ transport processes to manage internal NH_4^+.

2.4.2 Promoter activity in GUS lines do not correspond with qPCR results

Results generated from the analysis of AtAMF promoter::GUS fusion lines, indicated that promoter activity for each *AtAMF* did not correspond to the expression profiles obtained using qPCR. qPCR experiments demonstrated that *AtAMF2* was expressed at the highest level followed by *AtAMF3*, while the *AtAMF1* showed the lowest level in most tissue analysed (Figure 2.3). However, the GUS lines displayed contrasting results where *proAtAMF2::GUS* was only expressed in the root tip and within pericycle cells located under emerging lateral root nodes (Figure 2.8). In contrast, *proAtAMF1::GUS* displayed significant GUS signal around the pericycle and in guard cells (Figure 2.7). Low levels of AtAMF3 promoter activity was limited to vascular bundles in root samples (Figure 2.9). The identities of the GUS lines were confirmed with PCR using specific primers flanking promoter and the backbone plasmid (data not shown). It is possible the promoter sequences (~1 kb) that were cloned and inserted in the expression vector were not adequate in size to properly drive gene expressions due to some missing motifs or other essential transcription elements. Further analysis of more extensive promoter fragments will be required to better understand tissue and cellular expression profiles.

The qPCR results of the three *AMF* genes reported in this thesis demonstrated corresponding expression patterns compared to the online database (Klepikova Atlas), which is based on a high resolution RNA sequencing profiles (Klepikova et al., 2016). Based on the absolute expression level, the RNA sequencing data revealed that *AtAMF1* (Figure S2.9.A) is expressed at the lowest level, followed by *AtAMF3* (Figure S2.9.C) and *AtAMF2* has the highest expression level within the family members (Figure S2.9.B). Similar to our findings, the expression of the *AtAMF* family members are evident in the senescing leaves compared to other tissue samples (Figure S2.9.A-C). At this point, compared to the tissue specific expression using native promoter::GUS lines, the expression data profiles (qPCR and online database) are more informative in regards to the elucidation of the potential function of the AtAMF family members, particularly in NH_4^+ transport in senescing leaves.

2.4.3 Proposed functions of AtAMFs

AtAMF proteins display distinct features on structural characteristics (Figure 2.2), tissue specific expressions (Figure 2.7-9) and subcellular localizations (Figure 2.10-13). These diversities may relate to their functionalities in NH_4^+ homeostasis.

Studies in both attached and detached leaves have shown that free NH_4^+ accumulates during senescence as the consequences of nucleic acid, amino acid, protein and chlorophyll degradation (Mattsson and Schjoerring, 2003). Accumulated NH_4^+ in the cytoplasm must be remobilized and/or stored to maintain NH_4^+ homeostasis and avoid potential cytoplasmic toxicity. This could be facilitated by pumping out NH_4^+ via an efflux mechanism (Coskun et al., 2013a) as well as storing excess NH_4^+ into the vacuole (Wood et al., 2006; Zhou et al., 2015). Unfortunately, despite an exhaustive number of studies, the identity of genes involved in the mechanisms are still elusive. AtAMFs may be involved in these NH_4^+ homeostatic mechanisms to some extent. Interestingly, this study identified the subcellular localisation of

AtAMF2 to the tonoplast, which reflects its potential function for NH_4^+ sequestration or release (Figure 2.12). Recently, Zhou et al. (2015) proposed an unknown tonoplast-localised NH_4^+ transporter responsible for facilitating NH_4^+ influx into the vacuole during NH_4^+ toxicity event. This unknown transporter is predicted to be phosphorylated by CAP1 (a tonoplast-localized receptor-like kinase) which is essential for root growth during NH_4^+ stress. Intriguingly, AtAMF2 demonstrates expression and localisation profiles that resemble the unknown protein, although it is unclear on the direction of transport that AtAMF2. Another compelling line of evidence that supports AtAMF2's role in NH_4^+ homeostasis is its specific localisation in the cells under lateral primordia and the root tip (Figure 2.8.F). Excess NH_4^+ has been widely documented to inhibit both primary and lateral root growth (Cao et al., 1993; Li et al., 2010; Zou et al., 2012; Liu et al., 2013; Li et al., 2014). Moreover, previous studies in *Arabidopsis* have demonstrated the importance of the root tip as a potential sensor to detect exogenous NH_4^+ concentrations (Li et al., 2010; Bai et al., 2014). For example, direct contact between the root tip and NH_4^+ has been shown to inhibit root elongation (Li et al., 2010; Zou et al., 2012). Similarly, Zou et al. (2013) demonstrated an increased activity of *GSA1* in the root tips in response to prolonged NH_4^+ exposure. Reduced cell expansion is proposed to be the underlying mechanism in NH_4^+-mediated root inhibition (Li et al., 2010; Liu et al., 2013). Therefore, root tip-localised and root primordia localised genes, including *AtAMF2*, may play important roles in a NH_4^+ tolerance mechanism, particularly in pathways related to root growth mechanisms. Li et al. (2010) suggested that root growth inhibition is associated with energetic-costly efflux in the elongation zone. As AtAMF2 is localised on the tonoplast it could have a diverse role in either NH_4^+ sequestration into the vacuole or its potential release from the vacuole for efflux out of the cell.

AtAMF3 was found expressed around the vascular bundles and speculatively in pericycle cells. This is an exciting finding for an NH_4^+ transporter to be localised around the vascular bundle. Current thought about NH_4^+ regulation is based on the assumption that most (if not all) NH_4^+ is assimilated in the root and then translocated as amino acids following assimilation by the GS/GOGAT pathway (Lea and Miflin, 2011). However, studies by Schjoerring et al. (2002) have demonstrated that significant concentrations of NH_4^+ is detected in the xylem sap and in leaf apoplastic solutions, suggesting NH_4^+ translocation to shoot indeed takes place via the xylem. Unfortunately, molecular mechanisms underlying this process is not well understood. A schematic model by Yuan et al. (2007) suggests that NH_4^+ loading from the soil into the xylem occurs by both symplastic and apoplastic pathways coordinated by the AtAMT families. AtAMT1;1, AtAMT1;3 and AtAMF1;5 are responsible for the symplastic pathway, whereas AtAMF1;2 is proposed to facilitate NH_4^+ movement into the cortex and endodermis following the apoplast pathway. However, this model does not demonstrate how NH_4^+ loading from the pericycle into the xylem occurs and the molecular mechanisms involved. Therefore, identification of NH_4^+ transporters expressed in the pericycle is crucial to help complete the model. This yet to be identified protein(s) must be able to facilitate bidirectional flux (influx and efflux) of NH_4^+ in pericycle cells. The influx mechanism is essential for passing NH_4^+ from the endodermis into the pericycle cells while the efflux mechanism is fundamental

for NH_4^+ loading into xylem from the pericycle cells. A recently published paper by Giehl et al. (2017) demonstrated the function of AtAMT2;1 to facilitate NH_4^+ loading into the xylem. However, there is limited evidence to support the essential bidirectional capability of the AtAMT2;1 and it is still an open question whether the protein is capable of efflux activity. Therefore, the efflux from the pericycle into the xylem could be facilitated by other unidentified proteins. AtAMF3 seems to fit the profile of the unidentified protein(s) based on the following data: 1) Tissue expression in pericycle cells (Figure 2.9.D); 2) Subcellular localisation in the plasma membrane (Figure 2.13) and 3) Responsiveness to NH_4^+ resupply (Figure 2.5). This protein may be involved in the efflux mechanism to facilitate NH_4^+ loading into the xylem possibly in coordination with AtAMT2.1. However, this hypothesis still needs extensive research, particularly to exhibit the efflux mechanism capability of AtAMF3.

Based on limited data available, AtAMF1 involvement in NH_4^+ regulation is far from clear, especially due to its subcellular localisation in the ER (Figure 2.10 and Figure 2.11). However, this finding needs further research to investigate whether its localisation in the ER happens due to protein misfolding following fusion with GFP. It has been reported that positioning of reporter proteins such as GFP (N or C terminally tagged) plays a vital role for proper protein folding (Snapp, 2005). Furthermore, reports show that terminally misfolded proteins are retained in the ER (Nehls et al., 2000) and will be degraded following ER associated protein degradation (Bagola et al., 2011). However, its tissue specific localisation in guard cells and around vascular tissues (e.g. pericycle cells) may indicate the potential involvement in NH_4^+ transport. Its function in pericycle cells maybe similar to AtAMF3, predicted to participate in xylem loading. Furthermore, it was fascinating to find out that *AtAMF1* is expressed in guard cells. Studies have shown that NH_4^+ stress is detrimental on chloroplast function in guard cells (Li et al., 2012). Similarly, Kumar et al. (1986) have demonstrated the effect of NH_4Cl, a photophosphorylation uncoupling agent, on stomatal movement. The presence of 10 mM NH_4Cl at pH 8.0 significantly inhibited stomatal opening. Therefore, based on this limited information it is possible that AtAMF1 is responsible for guard cell chloroplast NH_4^+ homeostasis as well as for NH_4^+ transport.

2.5 Supplementary materials of Chapter 2

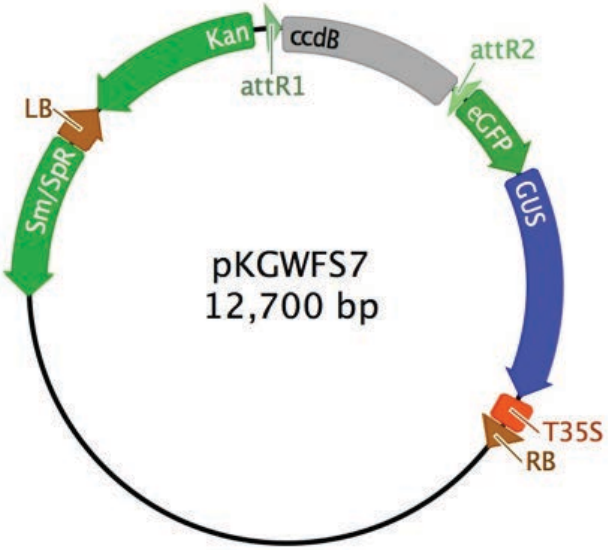

Supplemental Figure S2.1. Schematic representation of pKGWFS7 vector used for tissue specific localisation.

This vector is used for promoter activity analysis with GFP/GUS reporter genes.

LB: left border; Kan: kanamycin resistance gene; eGFP: green fluorescent protein gene; GUS: blue-colouring β-glucuronidase gene; T35S: cauliflower mosaic virus 35S terminator; and RB: right border.

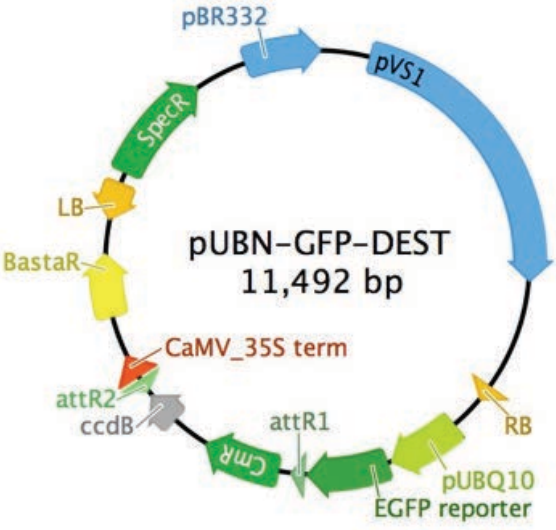

Supplemental Figure S2.2. Schematic representation of pUBN-GFP-DEST vector used for subcellular localisation.

LB: left border; SpecR: spectinomycin resistance gene, BastaR: basta resistance gene; EGFP: green fluorescent protein gene; pUBQ10: ubiquitin-10 promoter; CaMV_35S term: cauliflower mosaic virus 35S terminator; and RB: right border.

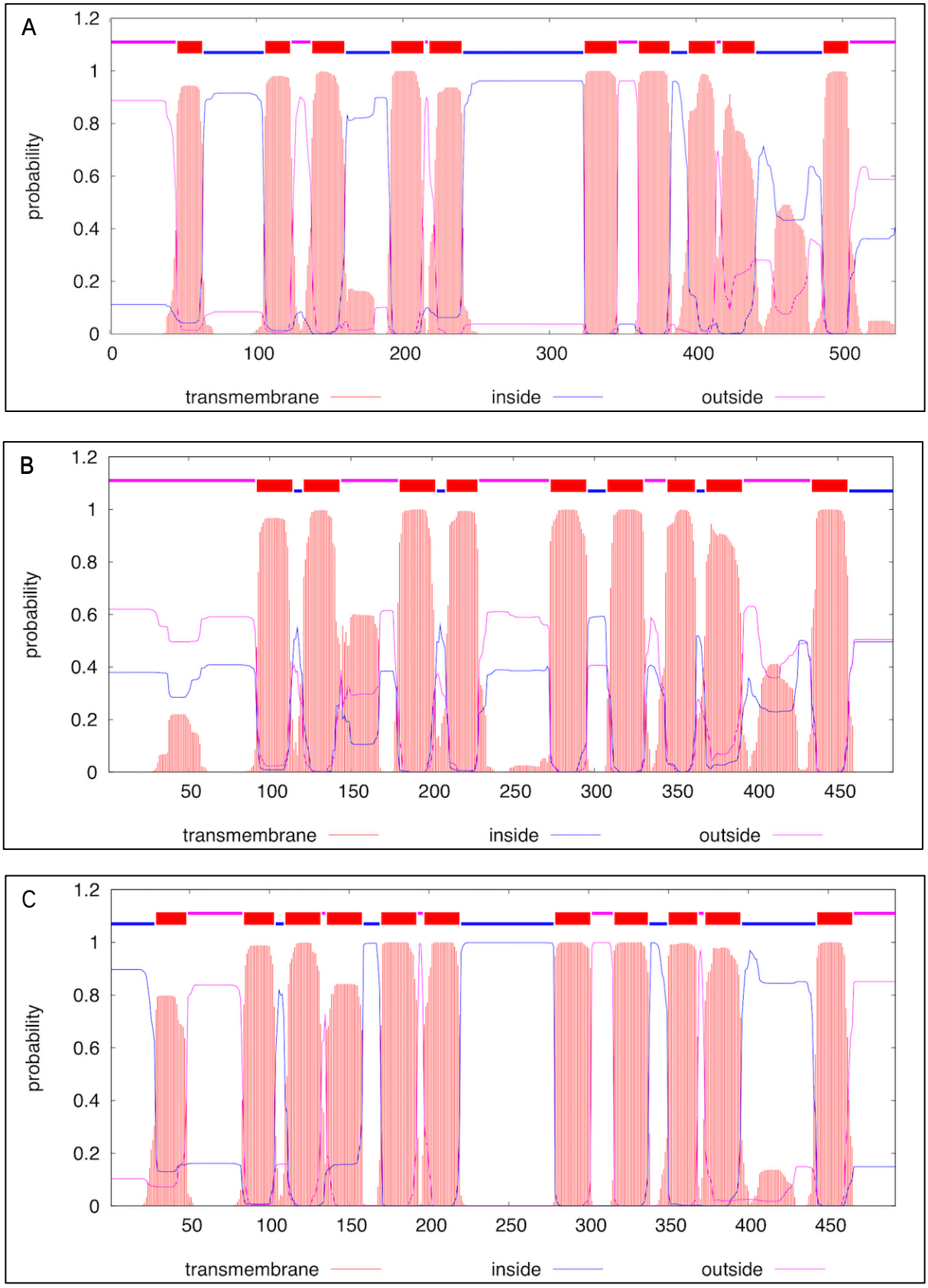

Supplemental Figure S2.3. Transmembrane helices prediction based on Transmembrane Hidden Markov models (TMHMM).

Visualisation of transmembrane helices arrangement of AtAMF1 (A), AtAMF2 (B) and AtAMF3 (C) was developed by online software TMHMM Server v. 2.0 (http://www.cbs.dtu.dk/services/TMHMM/).

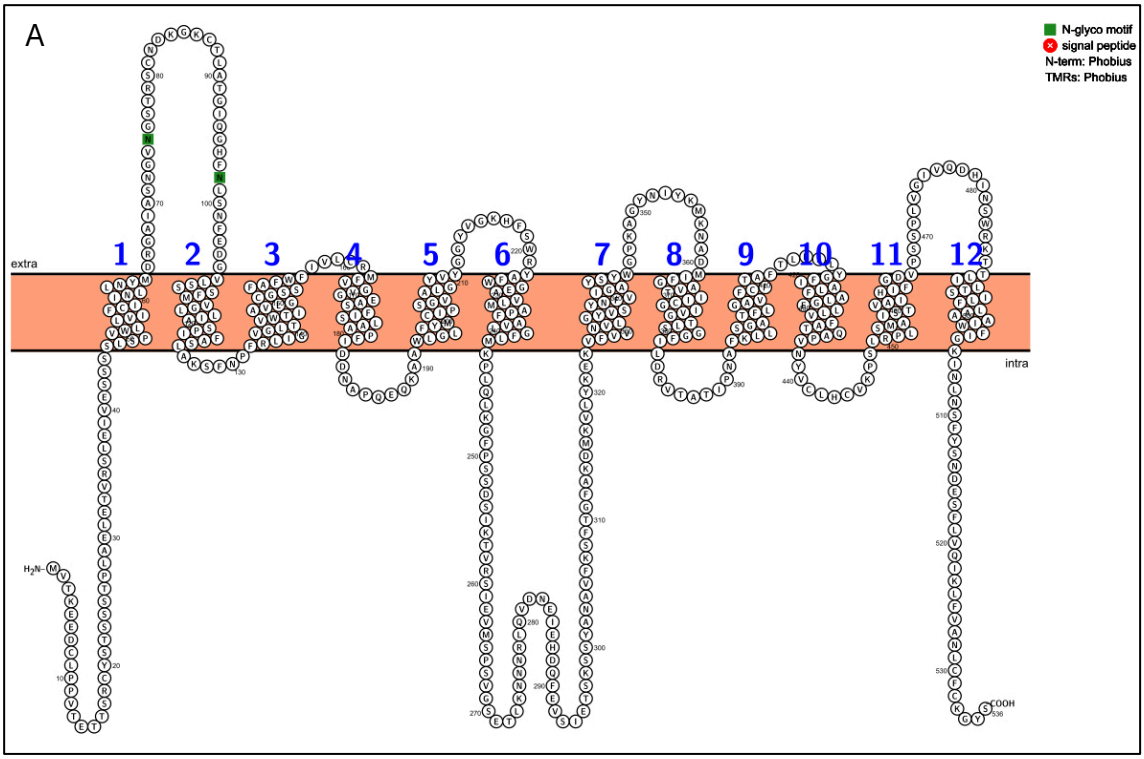
A
N-glyco motif
signal peptide
N-term: Phobius
TMRs: Phobius
extra
intra
1
2
3
4
5
6
7
8
9
10
11
12
H2N-
COOH

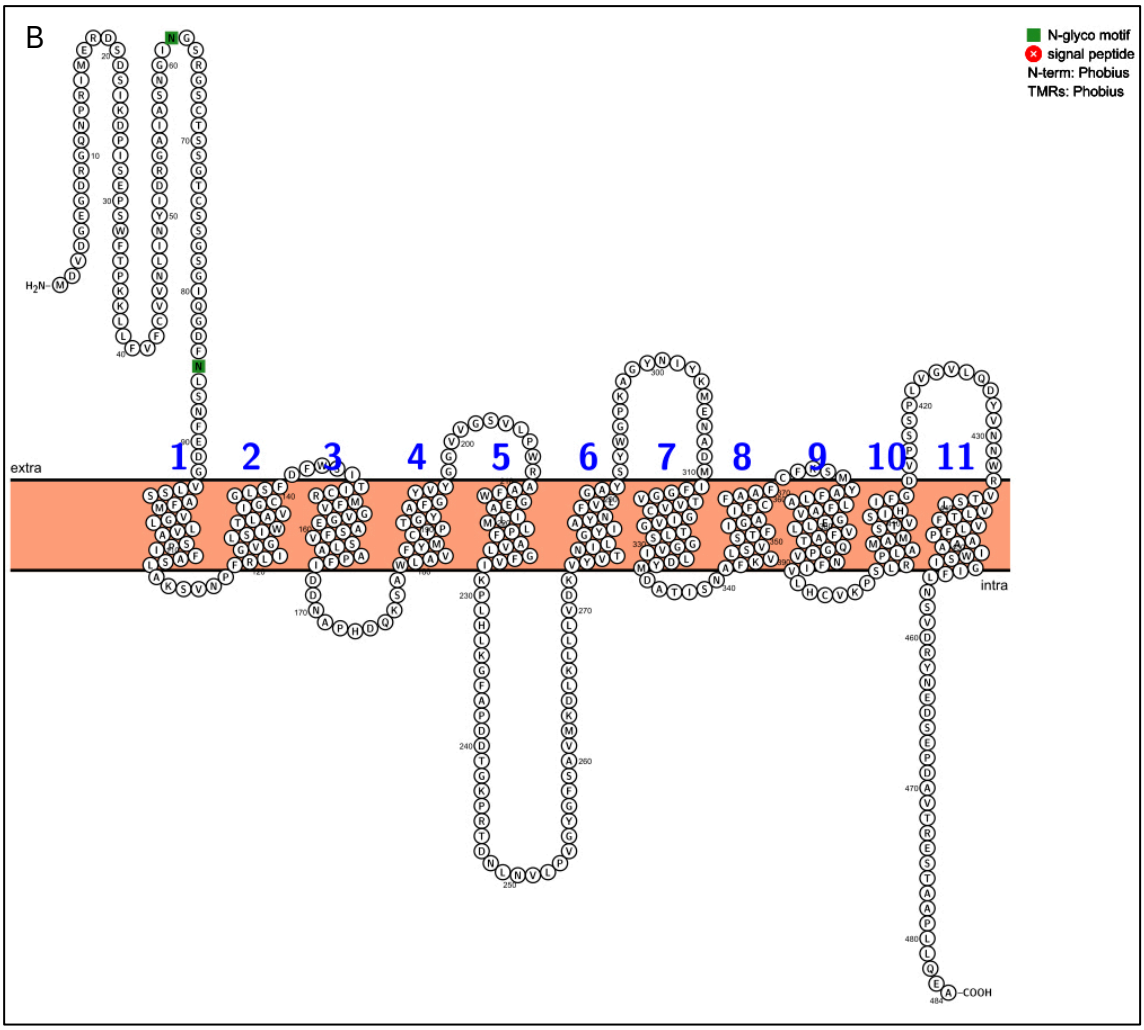
B
N-glyco motif
signal peptide
N-term: Phobius
TMRs: Phobius
extra
intra
1
2
3
4
5
6
7
8
9
10
11
H2N-
COOH

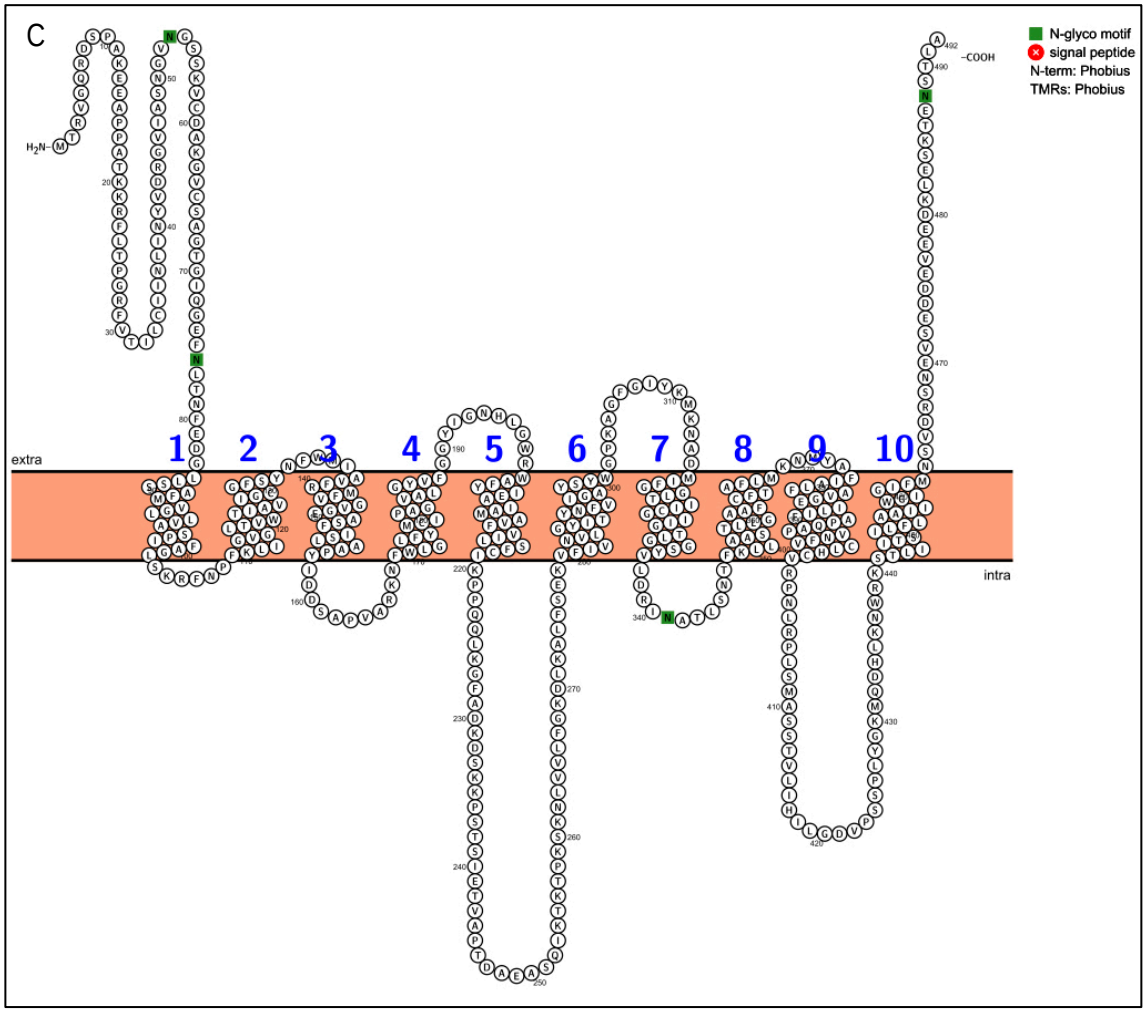

Supplemental Figure S2.4. Transmembrane prediction of AtAMF1 (A), AtAMF2 (B) and AtAMF3 (C) using Phobius algorithm.

Membrane topology prediction was generated by Protter software (http://wlab.ethz.ch/protter/start/).

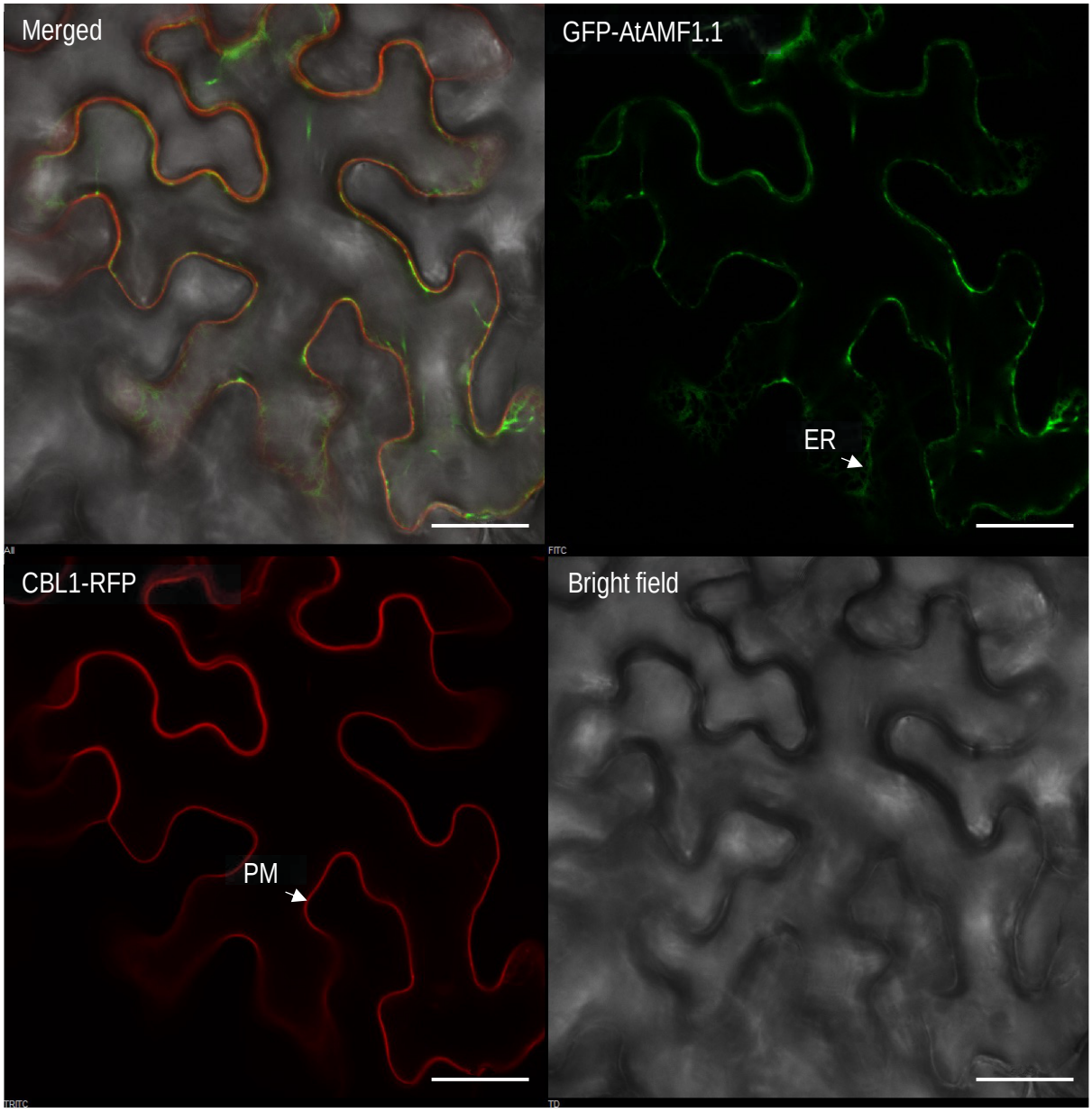

Supplemental Figure S2.5. Co-expression of GFP-AtAMF1.1 and CBL1-RFP (a plasma membrane marker).

ER = endoplasmic reticulum; PM = plasma membrane. Scale bars = 25 μm

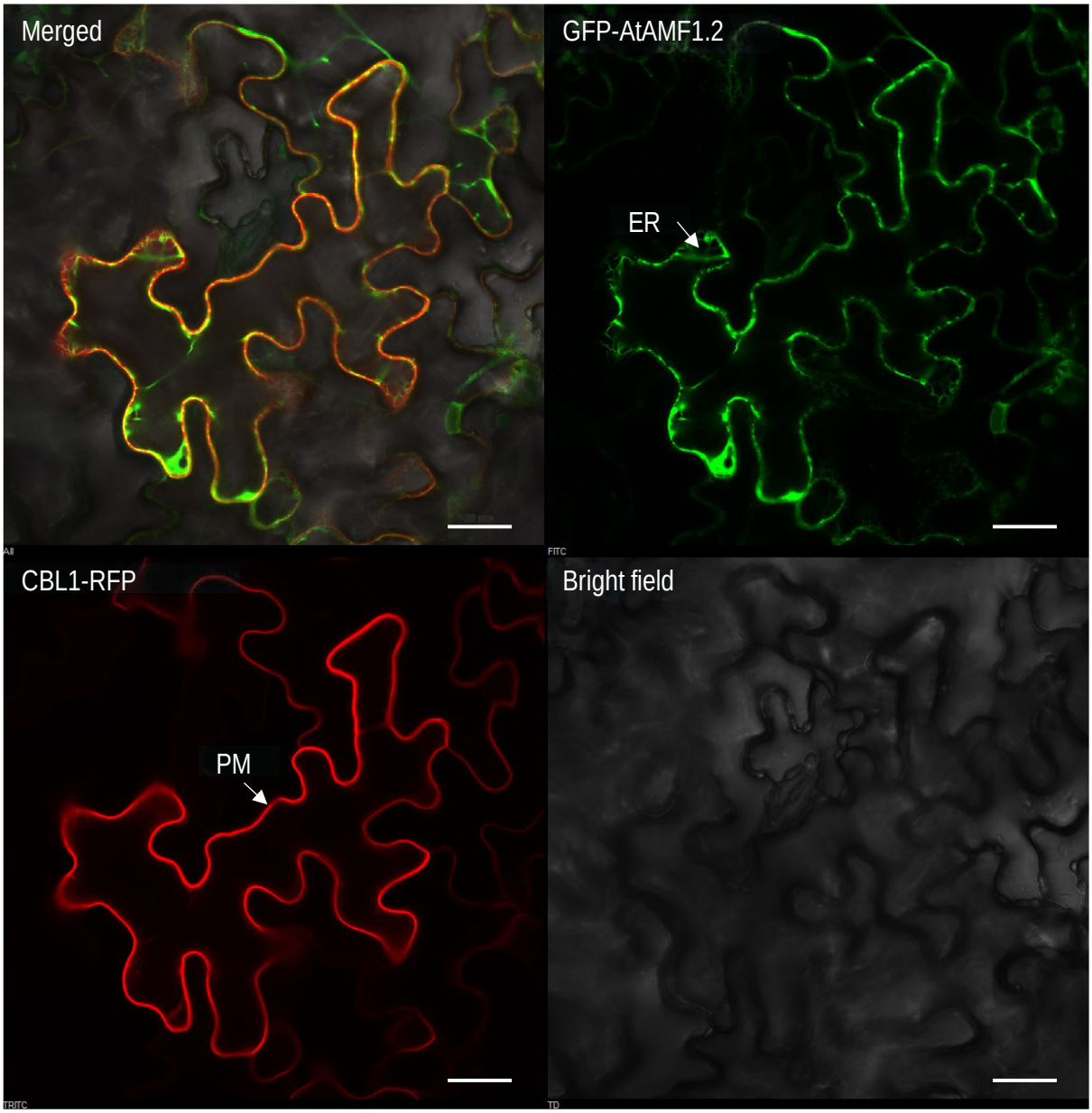

Supplemental Figure S2.6. Co-expression of GFP-AtAMF1.2 and CBL1-RFP (a plasma membrane marker).

ER = endoplasmic reticulum; PM = plasma membrane. Scale bars = 25 μm

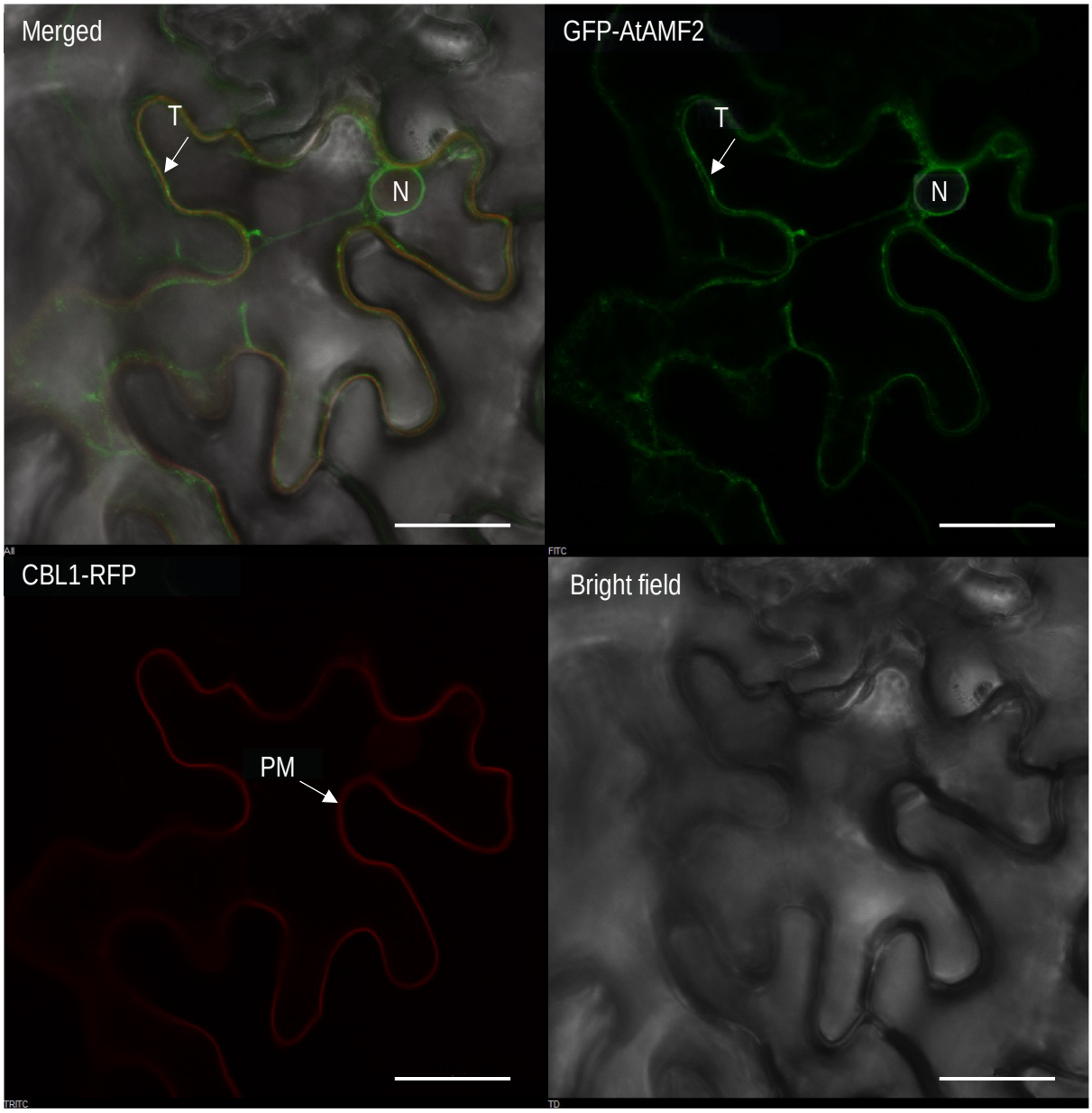

Supplemental Figure S2.7. Co-expression of GFP-AtAMF2 and CBL1-RFP (a plasma membrane marker).

N = nucleus; PM = plasma membrane; T = tonoplast. Scare bars = 25 μm.

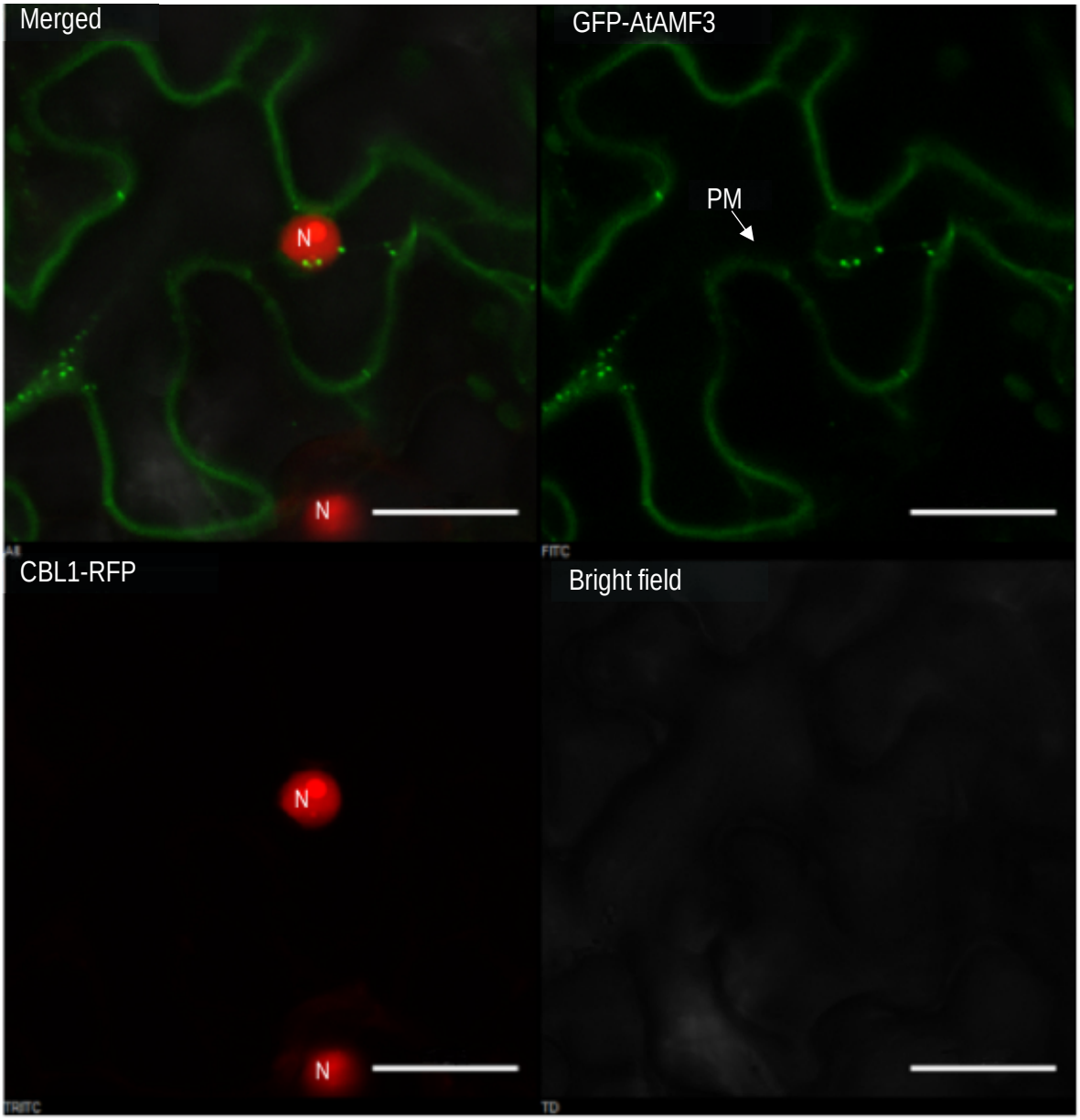

Supplemental Figure S2.8. Co-expression of GFP-AtAMF3 and H2B-RFP (a nuclear marker).
GFP signal is evident in plasma membrane (PM) and absent around the nucleus (N) which is clearly identifiable from RFP signal. Scare bars = 25 μm.

A

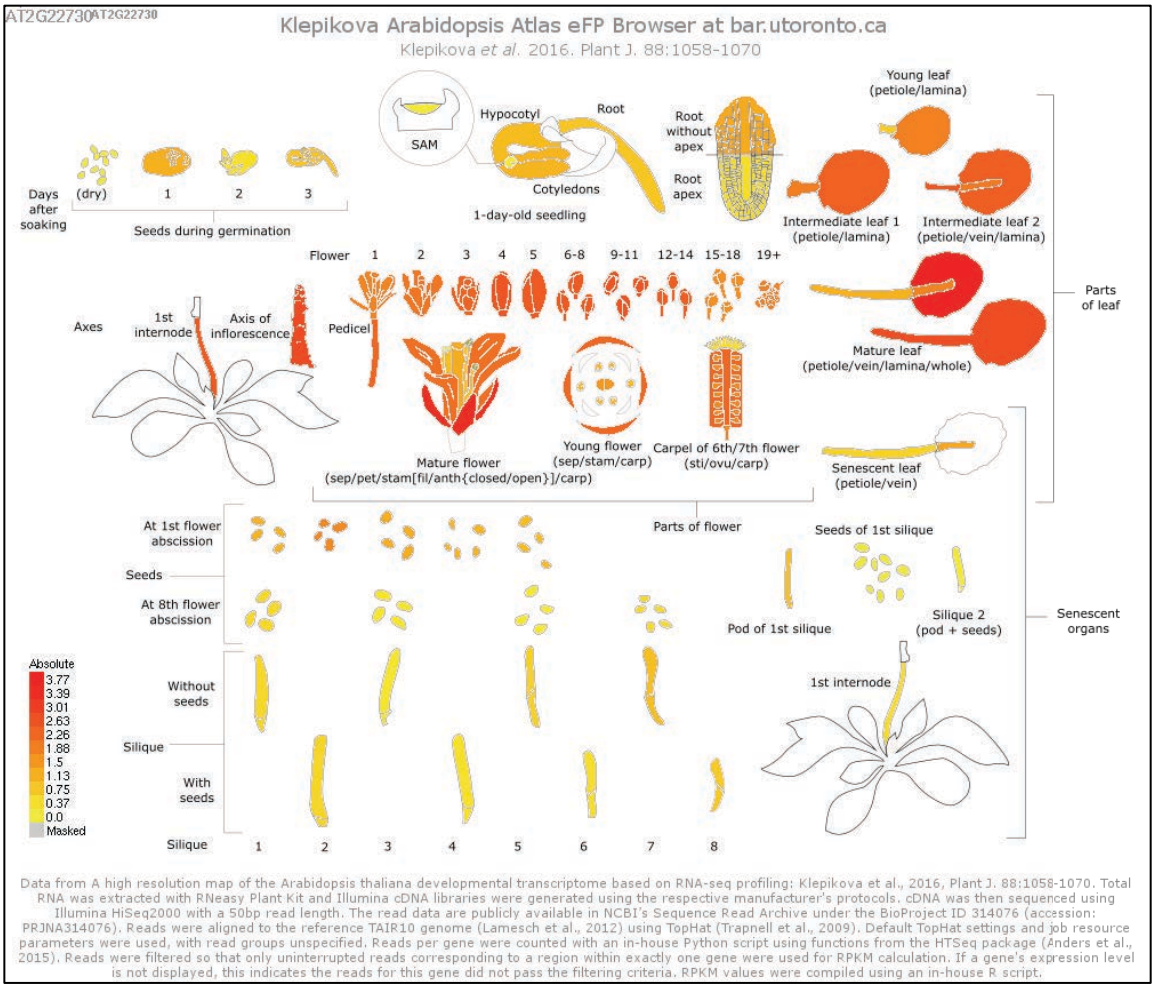

Data from A high resolution map of the Arabidopsis thaliana developmental transcriptome based on RNA-seq profiling: Klepikova et al., 2016, Plant J. 88:1058-1070. Total RNA was extracted with RNeasy Plant Kit and Illumina cDNA libraries were generated using the respective manufacturer's protocols. cDNA was then sequenced using Illumina HiSeq2000 with a 50bp read length. The read data are publicly available in NCBI's Sequence Read Archive under the BioProject ID 314076 (accession: PRJNA314076). Reads were aligned to the reference TAIR10 genome (Lamesch et al., 2012) using TopHat (Trapnell et al., 2009). Default TopHat settings and job resource parameters were used, with read groups unspecified. Reads per gene were counted with an in-house Python script using functions from the HTSeq package (Anders et al., 2015). Reads were filtered so that only uninterrupted reads corresponding to a region within exactly one gene were used for RPKM calculation. If a gene's expression level is not displayed, this indicates the reads for this gene did not pass the filtering criteria. RPKM values were compiled using an in-house R script.

B

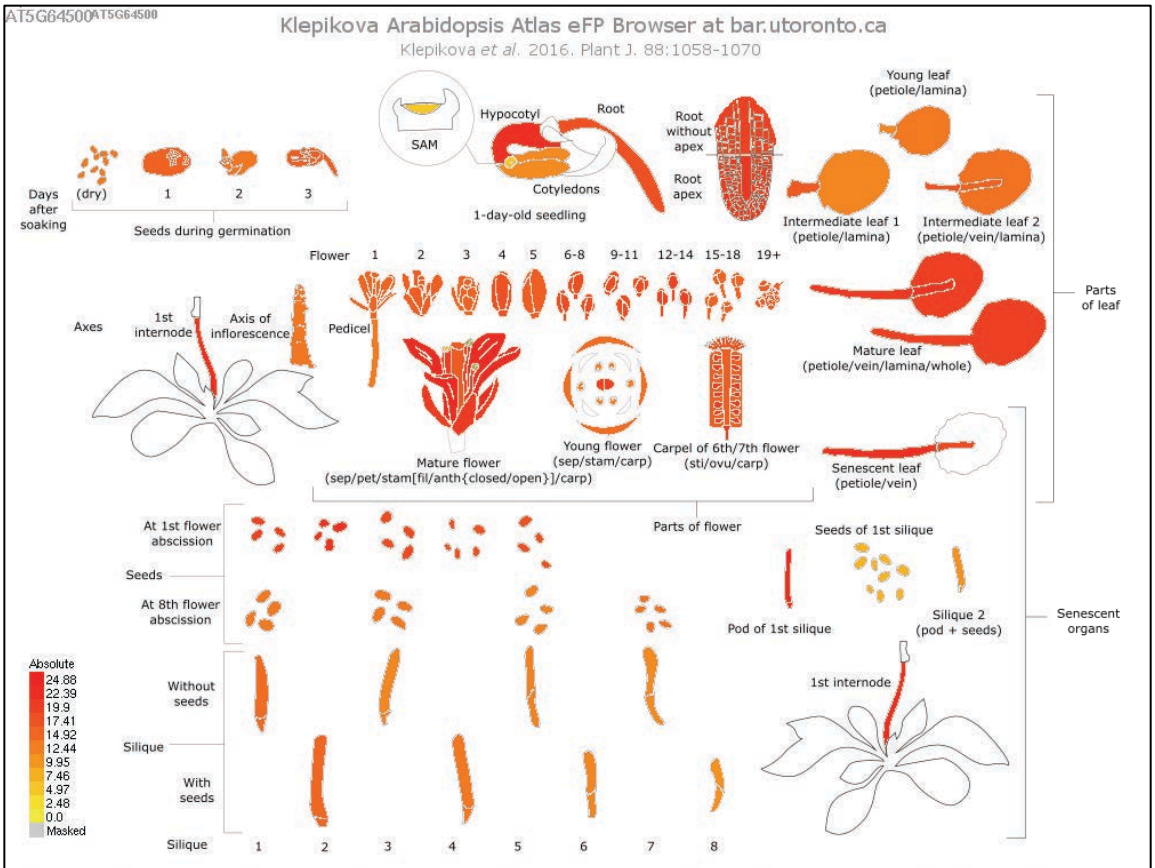

Data from A high resolution map of the Arabidopsis thaliana developmental transcriptome based on RNA-seq profiling: Klepikova et al., 2016, Plant J. 88:1058-1070. Total RNA was extracted with RNeasy Plant Kit and Illumina cDNA libraries were generated using the respective manufacturer's protocols. cDNA was then sequenced using Illumina HiSeq2000 with a 50bp read length. The read data are publicly available in NCBI's Sequence Read Archive under the BioProject ID 314076 (accession: PRJNA314076). Reads were aligned to the reference TAIR10 genome (Lamesch et al., 2012) using TopHat (Trapnell et al., 2009). Default TopHat settings and job resource parameters were used, with read groups unspecified. Reads per gene were counted with an in-house Python script using functions from the HTSeq package (Anders et al., 2015). Reads were filtered so that only uninterrupted reads corresponding to a region within exactly one gene were used for RPKM calculation. If a gene's expression level is not displayed, this indicates the reads for this gene did not pass the filtering criteria. RPKM values were compiled using an in-house R script.

C

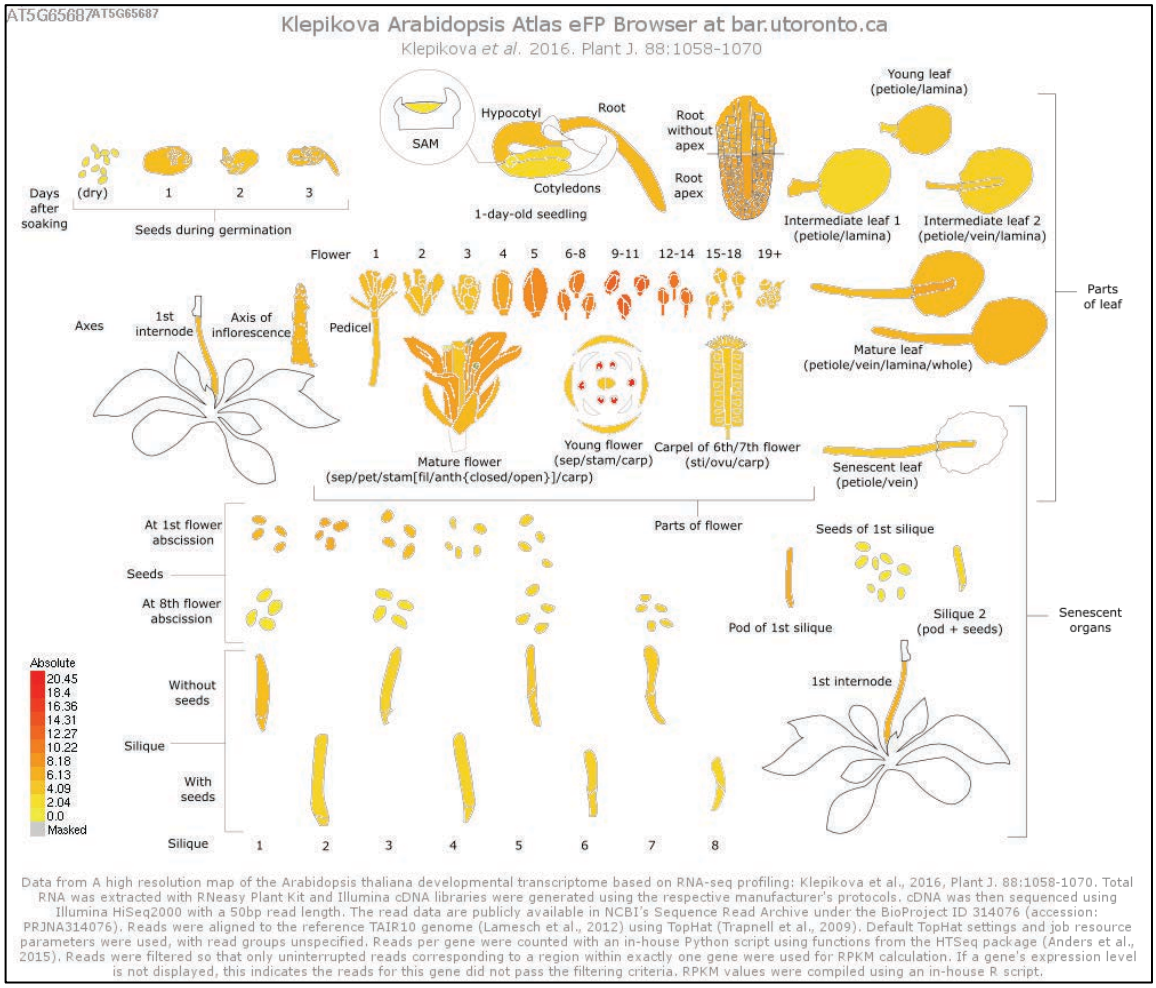

Figure S2.9. General expression profile of the *AtAMF* family based on the Klevikova Atlas.

The figure was created online in TAIR website by querying the corresponding locus identifier: A. *at2g22730* (AtAMF1); B. *at5g65400* (AtAMF2); and C. *at5g65687* (AtAMF3).

Colour key at bottom left represents the absolute expression of the gene and must be used only to compare the expression of the same gene in different tissue samples.

Supplemental Table 2.1. Primer pairs used for qPCR and cloning experiments

Primer name	Primer sequence (5'-3')	Purpose
at2g22730_qpcr_F1	CTTCTTCTACTCCCCTTGCGG	qPCR of AtAMF1
at2g22730_qpcr_R1	GCCATTGACACCATTGCTCG	
at5g64500_qpcr_F1	CTGGACTCTCGCTGTGATTGG	qPCR AtAMF2
at5g64500_qpcr_R1	GCAAGCCACGCTGATTTCTG	
At565687_Fw_qpcr	TACTCGGCGCAGCGTTTTGTT	qPCR AtAMF3
At565687_Rv_qpcr	CGGAGCCTGTGGTGCAAAGAT	
TUB4-F	TTTCTCAGTGTTTCCTTCTCC	AtTUB4 (housekeeping gene)
TUB4-R	CCTCATTGTCCAAAACCATAC	
AtAMF1-F	CACCATGGTGACCAAAGAAGAA	Cloning of AtAMF1
AtAMF1-R	TTATGAATATCCCTTGCAAAAGCAC	
AtAMF2-F	CACCATGGATGTTGACGGAGAA	Cloning of AtAMF2
AtAMF2-R	TCATGCTTCCTGGAGAAGAGGC	
AtAMF3-F	CACCATGACGAGAGTTGGCCA	Cloning of AtAMF3
AtAMF3-R	TTAGGCGAGAGTAGAGTTCTCTGTTTTGCT	

Supplemental Table 2. 2. Micronutrients and vitamin stocks for tissue culture media

Micronutrients	(μM)	Vitamins	(mg/L)
MnSO4.H2O	100	Glycine	2
ZnSO4.7H2O	30	Myo-inositol	100
H3BO3	100	Nicotinic acid	0.5
KI	5	Pyridoxine-HCl	0.5
NaMoO4.2H20	1	Thiamine-HCl	0.1
CuSO4.5H2O	0.1		
CoCl2.6H2O	0.1		

Supplemental Table 2.3. Expression vectors used for transient expression on tobacco leaves

Plasmid name	Type	Purpose	Reference
pENTR/D-TOPO	Entry vector	To clone target genes	
pUBN-GFP-DEST	Destination vector	To fuse target gene with GFP reporter protein	Grefen et al. (2010)
pUBN-GFP-AtAMF1.1	Expression vector	To express AtAMF1.1 tagged with GFP reporter protein	
pUBN-GFP-AtAMF1.2	Expression vector	To express AtAMF1.2 tagged with GFP reporter protein	
pUBN-GFP-AtAMF2	Expression vector	To express AtAMF2 tagged with GFP reporter protein	
pUBN-GFP-AtAMF3	Expression vector	To express AtAMF3 tagged with GFP reporter protein	
pER-rk-CD3-959	Expression vector	Endoplasmic reticulum marker with mCherry reporter gene	Nelson et al. (2007)
pUBC-CBL1-RFP	Expression vector	Plasma membrane marker with RFP reporter gene	Yue Wu, unpublished
pB7-H2B-RFP	Expression vector	Nucleus marker with RFP reporter gene	(Wege et al., 2016)
p19		Anti-silencing	

Supplemental Table 2.4. Media for transient expression on tobacco leaves

2YT media	AS media
16 g/l bactotryptone	10 mM $MgCl_2$
10 g/l yeast extract	10 mM MES-KOH pH 5.6
5 g/l NaCl	150 uM Acetosyringone (in DMSO, store in -20^{o}C)
Water to 1000ml	
Mixtures are autoclaved for sterilisation	

3. Heterologous expression of AMF proteins in *Saccharomyces cerevisiae*

3.1 Introduction

3.1.1 Yeast as a tool for studying plant protein function

Saccharomyces cerevisiae (yeast) has been widely utilised in functional studies of expressed genes. Aside from its versatility, yeast cells offer benefits including simple and inexpensive culture conditions, tractable genetics and a fully sequenced and annotated genome. More importantly, it shares similarity of basic cellular machinery and signal transducing pathways with higher eukaryotes, including plants (Ton and Rao, 2004). As an eukaryotic organism, yeast has intercellular compartmentation that ensures expressed plant proteins are highly likely to be processed through appropriate machinery and undergo any necessary modifications such as protein glycosylation in the endoplasmic reticulum (ER) or Golgi (Scheiner-Bobis, 2018). The ease of molecular and genetic manipulation in yeast (Kingsman et al., 1985), the availability of knockout mutants and the growing number of online databases providing comprehensive transcriptomes, proteomes or phenome data, make yeast a preferred system for functional studies (Ton and Rao, 2004) even with genes with very limited information. Several discoveries have been made on plant transporters through heterologous expression in yeast, including the identification of novel NH_4^+ transport proteins, the AMFs (Chiasson et al., 2014) and other important genes identified from plants and mammalian systems (Frommer and Ninnemann, 1995). Functionalities of target genes are confirmed following complementation studies in mutant yeast strains. If the appropriate mutants are not available, specific mutations can be introduced via gene disruption methods (Rothstein, 1983). However, some modifications might be needed for the heterologously expressed protein to complement the loss of function in a specific yeast mutant. For example, removal of the C-terminal domain of *Arabidopsis thaliana* AHA2 is essential for full complementation of the *pma1* yeast mutant (Regenberg et al., 1995).

3.1.2 Functional studies of ammonium transporters in yeast

There are three ammonium transporters in yeast, namely Mep1, Mep2 and Mep3. These proteins belong to an evolutionary conserved protein family that includes plant AMTs and the mammalian rhesus (Rh) blood group polypeptides of erythrocytes (Marini et al., 2000a). The availability of yeast strains defective in NH_4^+ transport, including 26972c (*mep1-1 mep2-1*) and 31019b (*mep1Δ mep2Δ mep3Δ*) have enabled identification of various NH_4^+ transporters across organisms including bacteria, plants and mammals. These strains are useful particularly for characterisation of ammonium transporters localised to the plasma membrane. Both yeast strains have also helped to clarify the definitive function of GmSAT1, which was initially characterized as an ammonium transporter (Kaiser et al., 1998) but later recharacterized by Marini et al. (2000a) where they showed GmSAT1 could facilitate NH_4^+ influx in 26972c

yeast strain based on an interaction with MEP3. Further studies revealed that GmSAT1 behaves as a novel membrane localized transcription factor (now called GmbHLHm1), which is important for nodule growth and NH_4^+ transport in soybean. Interestingly, overexpression of GmbHLHm1 in the 26972c yeast strain significantly upregulated ScAMF1, a low affinity NH_4^+ transporter and modified the expression of Mep3 (Chiasson et al., 2014). A wild type yeast strain, BY4741 has also been utilized to confirm functionalities of AtTIP2;1 and AtTIP2;3 in relation to NH_3 sequestration into the vacuole resulting in an increased tolerance to methylammonium (MA), a toxic analogue of NH_4^+ (Loqué et al., 2005). Unfortunately, yeast mutant's sensitive to high ammonium have yet to be discovered. Such a mutant will be beneficial especially for the functional characterization of genes responsible for ammonium toxicity tolerance either by NH_4^+ efflux or internal NH_4^+ sequestration.

3.1.3 Ammonium toxicity in yeast

As hyperaccumulation of NH_4^+ inside the cytoplasm is detrimental for yeast cells, the ion influx must be finely regulated to achieve appropriate concentrations. The Mep protein family is mainly responsible for regulation of NH_4^+/MA^+ in yeast (Marini et al., 1997). Dysfunctionalities of these proteins increase tolerance to MA in the yeast mutant 31019b (*mep1-3Δ*). Additionally, overexpression of tonoplast-localized proteins permeable to NH_3, e.g. AtTIP2;1 and AtTIP2;3, has also been shown to improve MA tolerance in wild type strain BY4741 (Loqué et al., 2005). Furthermore, Hess et al. (2006) have demonstrated that NH_4^+ toxicity in yeast is more evident at low K^+ availability and also revealed that amino acid excretion is one of the NH_4^+ tolerance mechanisms used by yeast cells. Accordingly, a recent report by Ariz et al. (2018) consistently confirmed the detection of higher concentrations of amino acids in the external medium of yeast grown at high NH_4^+ and low K^+ concentrations. These data suggest that amino acid extrusion through SPS amino acid transporters (Hess et al., 2006) is a consequence of NH_4^+ toxicity particularly at low K^+ and potentially leads to an amino acid deficiency by yeast cells.

The aim of this study was to functionally characterize the AtAMF family (AtAMF1, AtAMF2, and AtAMF3) by using heterologous expression in yeast. Based on the studies described previously, similar experiments were conducted in various yeast strains to investigate the ability of AtAMF proteins to transport NH_4^+ as well as their potential roles in NH_4^+ toxicity tolerance mechanisms. MA tolerant mutant 31019b was utilized to study the functionalities of AtAMF proteins in facilitating NH_4^+/MA^+ influx. Wild type strain BY4741 was used in MA toxicity experiments to examine the potential roles of the AtAMFs in NH_4^+/MA^+ tolerance mechanisms. A yeast strain, CY162 (*trk1Δ*; *trk2Δ*) defective in two main K^+ transporters (TRK1 and TRK2), was used in experiments focusing on the implication of K^+ availability on NH_4^+ toxicity in yeast.

3.2 Material and methods

3.2.1 Yeast strains and plasmids

Multiple strains were used in this chapter depending on the purpose of each experiment as detailed in Supplemental Table S3.1. Expression vector pDR196 (Rentsch et al., 1995) (Figure S3.1) was used in most experiments including for GFP-AtAMF2 subcellular localization. For subcellular localization of C-terminally tagged AtAMF2 (AtAMF2-GFP), pAG426GPD-ccdB-EGFP (Alberti et al., 2007) was utilised. Both pDR196 and pAG426GPD-ccdB-EGFP carry a functional *URA3* gene, responsible for the complementation of uracil auxotrophy.

3.2.2 Growth media

In most experiments, yeast nitrogen base media without amino acid and ammonium sulfate (Sigma) supplemented with drop-out mix without uracil (SD AA-ura) was used unless otherwise indicated. The concentrations of NH_4^+ and MA were adjusted with either $(NH_4)_2SO_4$, NH_4Cl or CH_3NH_3Cl (MA-Cl), respectively. Medium M (Ramos and Wiame, 1979) and asparagine-phosphate (AP) media (Rodríguez-Navarro and Ramos, 1984) were utilized in some experiments using yeast strain 31019b and CY162, respectively. Addition of 100 mM KCl is necessary to culture the CY162 yeast strain. For the BY471 strain, essential amino acids: histidine (76 mg/l), leucine (380 mg/l) and methionine (76 mg/l) were added into the SD-ura media for culturing and growth assays. Media used in this chapter is detailed in Supplemental Table S3.2.

3.2.3 Gene cloning in expression vectors

Cloning protocols as detailed in Chapter 2.2.6, were used to clone *AtAMF1-3* and *AtTIP2.1-3* genes into yeast expression vectors. Specific primers pairs (Supplemental Table S3.3) were designed to include distinct sequences corresponding to multiple cloning sites (MCS) of the backbone vector *pDR196*. Restriction sites *Spe*I-*Xho*I and *Eco*RI-*Xho*I were included in the 5' and 3' end of the cloning primer pairs of AtAMF and AtTIP2 gene families, respectively. *AtAMF* gene sequences were amplified using high fidelity DNA polymerase (NEB Phusion® High Fidelity Polymerase) with entry vector pENTR-AtAMFs previously generated (Chapter 2.2.6) as DNA templates. Using the same strategy, *AtTIP2* sequences were amplified from previously generated entry vector *pENTR-AtTIP2;1-3* (Scharwies, 2017). Cloning into *pDR196* was carried out using restriction-ligation cloning protocol. Vector DNA *pDR196* was linearized with appropriate restriction enzymes and purified and then ligated with T4 DNA ligase to the digested and purified transporter cDNA.

3.2.4 Yeast transformation protocol

Introduction of the expression vector into yeast cells was carried using lithium acetate/single-stranded DNA/PEG method (Gietz, 2014) with modification. Starter cultures were grown overnight in YPD media (1% (w/v) Bacto yeast extract, 2% (w/v) Bacto peptone and 2% (w/v) D-glucose) at 28°C with 200

rpm rotation prior to transformation procedure. Approximately 2 ml of overnight culture was transferred into 30 ml of YPD media to obtain an OD_{600} = ~ 0.2-0.3. The inoculated culture was grown for approximately 3-4 hours to reach an OD_{600} = ~ 0.5-0.6 at 28°C with 200 rpm rotation. Cells were collected by centrifugation at 3000 *x g* for 5 minutes, rinsed twice with sterile water and resuspended with 1 ml of 0.1 M lithium acetate. The resuspended cells were collected by spinning at maximum speed for 15 s and supernatant removed. The cells were resuspended in 500 μl 0.1 M lithium acetate and 50 μl aliquot was distributed into sterile 1.5 ml microtubes. The 50 μl aliquot was centrifuged to remove the lithium acetate by aspiration. The remaining pellet was overlaid with the following reagents in order: i) 240 μl 50% PEG, ii) 36 μl 1 M lithium acetate, iii) 5 μl single-stranded DNA carrier (10 mg/ml), iv) plasmid DNA 2-3 μl in a final volume of 50 μl. The mixture was vigorously vortexed and then incubated at 28°C for 30 min. Following the incubation, the mixture was subjected to heat shock at 42°C for 25 min. Cells were collected by centrifugation at 6000 rpm for 15 s, supernatant removed, and resuspended with 500 μl sterile water. 100-150 μl resuspended cells were plated onto selective media SD AA-ura and incubated at 28°C for 2-3 d. Multiple single colonies were re-streaked onto fresh SD AA-ura media to confirm successful transformation. For transformation and transformant selection of CY162 strain, additional KCl (final concentration 100 mM) was added to the YPD and SD AA-ura media.

3.2.5 Growth assay

Selected transformants were grown overnight in SD AA-ura (with 100 mM KCl for CY162 strain). A small portion from the overnight culture was transferred into 10 ml of fresh SD AA-ura media to obtain an OD_{600} = ~ 0.2-0.3 and grown for 3-4 hours to reach OD_{600} = ~ 0.5-0.6 at 28°C with 200 rpm rotation. Cells were collected by centrifugation at 5000 rpm for 5 min and rinsed twice with sterile water. The cells were resuspended with sterile water to OD_{600} = ~ 1.0 and then subjected to 1 in 10 serial dilutions. Aliquots (5 μl) of each dilution was spotted onto media and incubated at 28°C for 5-10 days.

3.2.6 Yeast staining and confocal imaging

Vacuole staining was conducted using the protocol described by Vida and Emr (1995) with modifications. Yeast transformants harboring expression vectors were grown overnight in 4 ml selective media SD AA-ura (containing 100 mM KCl for the CY162 background) to maintain selection pressure. The cells were pelleted by centrifugation at 5000 rpm for 5 min and supernatant removed. The cells were then resuspended in 500 μl YPD containing 8 μM FM4-64 in 2 ml microtubes to improve the efficiency of FM4-64 staining. The microtubes were then wrapped with aluminum foil and incubated at 30°C for 30 min. Residual dye was removed by rinsing the cells twice with 1 ml SD AA-ura. The stained cells were resuspended in 1 ml SD AA-ura and transferred into 50 ml falcon tubes with 4 ml SD AA-ura (5 ml total volume) and incubated at 30°C for 90-120 min with 200 rpm rotation. The cells were collected by 5000 rpm centrifugation for 5 min, supernatant removed, and cells resuspended in 1 ml SD AA-ura.

Prior to visualization using confocal microscopy, an agar pad was pre-made on a microscope slide following a protocol previously described by Sundin et al. (2004) with modifications. The pad contained SD AA-ura and 1% agarose. 30 μl of molten agar was carefully spotted on one microscope slide fitted with masking tape on each side. Another microscope slide was carefully aligned on top of the agar with a gentle pressure on each side. The microscope slide sandwich was carefully placed on top of a flat ice-cold surface covered with Kim wipes to protect the slide. After 2-3 min, the slide sandwich was contained in new Kim wipes and stored in a clean container for analysis.

For imaging, 15 μl of previously stained cells was spotted onto the agar pad of one of the microscope slide sandwiches and covered with microscope slide. Image analysis was carried out using Nikon A1R laser scanning confocal microscope (Adelaide Microscopy Waite Facility).

Subcellular localisation of ZmAMF1 in *Nicotiana benthamiana* leaves was conducted with the same protocol as previously described in Chapter 2.2.8.

3.3 Results

3.3.1 AtAMFs are not involved in high affinity transport system of NH_4^+

To investigate the involvement of AtAMF1.1, AtAMF1.2, AtAMF2 and AtAMF3 in high affinity ammonium transport, we utilised the *Δmep (1,2,3)* triple knockout mutant, 31019b. Growth analysis was carried out to study the ability of the AtAMFs to rescue growth on SD-ura media under low NH_4^+ (1-5 mM) concentrations when supplied as the sole N source. Figure 3.1 shows that there was no significant difference among the yeast strains overexpressing the four AtAMF genes compared to the one overexpressing empty vector pDR196. Additionally, growing yeast under a range of pH levels (5.5-6.5) also failed to significantly support yeast growth on low NH_4^+ (Supplemental Figure S3.2). These results indicated that AtAMFs are not able to complement the growth recovery of 31019b cells at low concentrations of NH_4^+.

3.3.2 Overexpression of AtAMF2 increases toxicity under high MA at pH 6.5 while AtAMF3 slightly improves growth at pH 7.0

To gain further insight of the functionality of AtAMFs, subsequent experiments were conducted utilising high concentrations of the toxic analog methylammonium (MA). 31019b transformants were grown on SD-ura media containing high MA (100 mM) at different pH (5.5 - 7.0) supplemented with 2% (w/v) glucose and 0.1% (w/v) proline as sole N source. Figure 3.2 shows that only yeast cells overexpressing AtAMF2 exhibited a typical 'death phenotype' at 100 mM MA at pH 6.5. At pH 5.5, there was no impact of methylammonium on AtAMF1 and AtAMF3, while at pH 7.0, all cells became sensitive to 100 mM methylammonium. This result indicated that the ability of AtAMF2 to facilitate MA transport into the cells might be pH dependent. To confirm this finding, subsequent experiments were conducted using either SD-ura or M media. These experiments revealed comparable outcomes, in which yeast cells overexpressing AtAMF2 displayed arrested growth at 100 mM MA at pH 6.5 (Figure 3.3). Surprisingly, 31019b cells overexpressing AtAMF2 and grown on medium M demonstrated an improved growth compared to that on SD-ura (Figure 3.3). SD-ura and medium M have different K^+ concentrations of 7.3 and ~160 mM, respectively. This difference in K^+ concentration might contribute to the contrasting growth. To investigate this hypothesis, cells were grown on SD-ura containing 0.1% (w/v) proline as the sole N source at pH 6.5 and supplemented with 100 mM MA with increasing concentrations of KCl (0, 10, 20, 50 and 100 mM KCl). As external [KCl] increased, yeast overexpressing AtAMF2 gradually grew better overcoming the MA induced toxicity (Supplemental Figure S3.3). In these media, Cl^- concentration was increased as well, however, due to the nature of the strain, it was suggested that the improved growth is related to increased availability of K^+ not Cl^-. These findings corroborate other studies suggesting an essential role of K^+ to help overcome NH_4^+ toxicity events in yeast and plants (Kronzucker et al., 2003; Hess et al., 2006; Barreto et al., 2012). Additionally, we observed a slight growth improvement of yeast cells overexpressing AtAMF3 grown on media containing toxic MA only at pH 7.0 (Figure 3.2). This data suggests that the protein might be involved in NH_4^+ efflux mechanisms possibly the uncharged NH_3.

3.3.3 Overexpression of AtAMF2 rescues CY162 strain growth

It was intriguing that the additional K^+ helped to improve growth of 31019b yeast grown at high MA concentrations. To get a better understanding of the relationship between K^+ and NH_4^+/MA^+, AtAMF members were expressed in the yeast strain CY162 (*trk1Δ, trk2Δ*), which is defective in high-affinity (TRK1) (Gaber et al., 1988) and low-affinity (TRK2) K^+ transport at the plasma membrane (Ko et al., 1990). Transformants were grown on SD AA-ura supplemented with 5 g/l $(NH_4)_2SO_4$ (75.6 mM NH_4^+) in the absence or presence of 100 mM KCl at pH 5.5. All media contained a basal K^+ concentration of 7.3 mM. Yeast overexpressing AtAMF2 were able to grow without additional K^+ while the empty vector control and other AMF1 homologs (AMF1;1, AMF1;2, AMF3) failed to grow (Figure 3.4). All strains were rescued with 100 mM K^+. Accordingly, at pH 5.5 increasing the KCl concentration in the media improved yeast growth (Supplemental Figure S3.4).

Further experiments were carried out to investigate whether AtAMF2 functions in a pH dependent manner as previously suggested in 31019b. Transformants were grown on SD AA-ura supplemented with 5 g/l $(NH_4)_2SO_4$ at pH 5.5 and 6.5. AtAMF2 was able to rescue CY162 at pH 5.5 but at pH 6.5, all yeast transformants were able to grow regardless of external K^+ concentrations (Figure 3.5). This indicates that growth pressure on CY162 is diminished at higher pH. Sensitivity of CY162 (*trk1Δ, trk2Δ*) mutants to low pH has been documented previously (Ko and Gaber, 1991). Accordingly, Navarrete et al. (2010) demonstrated that at 5-10 mM K^+ and pH 5.8, both the wild type strain BY4741 and its double mutant derivative BYT12 (*trk1Δ::loxP, trk2Δ::loxP*) did not show a significant growth difference. It is possible that at higher pH, K^+ is more readily available in the media which enables *trk1Δ, trk2*Δ mutant cells to grow. Another suggestion is that at higher pH, unidentified yeast proteins might facilitate K^+ influx, therefore increasing K^+ availability to the cells as proposed by Ko and Gaber (1991).

3.3.4 AtAMF2 failed to rescue CY162 growth at low K^+ concentration

Previous results demonstrated the ability of AtAMF2 to rescue growth of CY162 strain (Figure 3.4). To confirm whether the AtAMF2 is a functional K^+ transporter, transformed CY162 cells were plated onto modified AP media which contain arginine as an alternative N source and controlled K^+ concentrations. In contrast to SD media which contain 7.3 mM K^+, basal AP media is a K^+-free media, therefore specified concentration is the final concentration in the media. Unexpectedly, all transformants, including CY162 yeast cells overexpressing AtAMF2 failed to grow on AP media at low K^+ concentration (0-0.1 mM K^+). On the other hand, all transformations including the empty vector control could grow on media containing K^+ between 1 and 4 mM (Supplemental Figure S3.5). These data suggested all AtAMF family members, AtAMF1, AtAMF2, and AtAMF3 are unlikely transporting K^+ at low concentrations.

3.3.5 CY162 is an ammonium sensitive strain

Overexpression of AtAMF2 in CY162 cells allowed growth on SD AA-ura media supplemented with 5 g/l $(NH_4)_2SO_4$. In contrast, the low K^+ media failed to rescue cells containing AtAMF1;1, AtAMF1;2 and

AtAMF3 (Figure 3.4). This complementation could be overcome when plated on AP media containing 10 mM arginine and K^+ at concentrations greater than 1 mM K^+ (Supplemental Figure S3.5). To help clarify these results, CY162 transformants were plated onto SD AA-ura media in the presence or absence of 5 g/l $(NH_4)_2SO_4$. Yeast cells expressing AtAMF1.1, AtAMF1.2 and AtAMF3 were able to grow on SD AA-ura media without NH_4^+ (0 mM) but failed to grow on media containing ~ 75.6 mM NH_4^+ (Figure 3.6). These findings show that the CY162 strain is sensitive to high NH_4^+. However, when AtAMF2 was expressed in CY162, the cells were able to grow on high NH_4^+. Subsequent experiments have shown that overexpression of AtAMF2 enabled CY162 yeast to grow on toxic levels of NH_4^+ of up to 140 mM (Supplemental Figure S3.6). The other AMFs were unable to grow above 60 mM NH_4^+. The ability of AtAMF2 to rescue growth at high NH_4^+ suggests that AtAMF2 may facilitate some level of NH_4^+ tolerance either through NH_4^+ efflux or a process involving AtAMF2-mediated internal sequestration.

3.3.6 AtAMF2 displays strong localization in the tonoplast of BY4741 strain

The observations using the 31019b strain indicated that AtAMF2 may be localised to the plasma membrane when expressed in yeast, where transport activities would allow MA uptake, eventually leading to MA accumulation poor growth and cell death. This is in contrast to observations using plant-based transient expressions systems that showed localisation at the tonoplast (Chapter 2.3.7). To verify this discrepancy, the membrane localisation of AtAMF2 in yeast cells was determined using a GFP tag added to N-terminus of AtAMF2. In transformed CY162 cells, we identified GFP signal targeted to the tonoplast, there was no signal at the plasma membrane but some signal detected in other organelles, potentially the ER and or Golgi (Figure 3.7.A). However, when AtAMF2 was expressed in BY4741, the localisation at the tonoplast was clearly defined and no signal was detected at the plasma membrane. Furthermore, the GFP signal overlapped with the red signal created by the vacuole specific dye, FM4-64 (Figure 3.7.B). A C-terminal tagged AtAMF2 (AtAMF2-GFP) was developed but the level of expression was poor relative to the N-terminal tag (Supplemental Figure S3.7).

3.3.7 GFP-AtAMF2 partially complement CY162 growth at high NH_4^+

Growth assays at high NH_4^+ were conducted to investigate the functionality of the GFP-AtAMF2 construct to alleviate NH_4^+ toxicity conditions in CY162. Yeast cultures were grown on SD AA-ura media supplemented with 40 mM $(NH_4)_2SO_4$ (80 mM NH_4^+). The GFP-AtAMF2 construct when transformed into CY162 showed reduced activity and only partially rescued yeast growth at elevated NH_4^+ concentrations (80 mM) (Supplemental Figure S3.8). The yeast overexpressing GFP-AtAMF2 demonstrated less growth compared to yeast overexpressing non-tagged AtAMF2. This lack of performance of GFP-AtAMF2 is possibly due to a disruption in AMF2 activity with the fusion of a N-terminal GFP tag and or the mis-localisation of the protein.

3.3.8 ZmAMF1 and ZmAMF2 also rescue CY162 growth at high NH_4^+

AMF proteins are broadly conserved amongst most plants including both dicots and monocots. In collaboration with Wenjing Li (University of Sydeny), we focused on characterising the functional activity of two AMF homologs from maize, ZmAMF1 and ZmAMF2. Both ZmAMF1 and ZmAMF2 were able to rescue CY162 yeast growth on yeast media containing elevated (80 mM) concentrations of NH_4^+ (Figure 3.8). These data suggest that both maize and Arabidopsis AMF proteins possess similar activities when expressed independently in the yeast strain CY162. Both most likely have a role in plants which mediate ammonium transport and potentially ammonium toxicities.

3.3.9 ZmAMF1 is localized in the tonoplast of *Nicotiana benthamiana*

As both AtAMF2 and ZmAMF1 display comparable functionalities in yeast we tested whether in plants ZmAMF1 also shares a similar subcellular localisation as AtAMF2. Transient expression of *ZmAMF1* clearly showed that the encoded GFP-tagged protein was localised at the tonoplast of *Nicotiana benthamiana* leaf cells (Supplemental Figure S3.11). The tonoplast localisation is clearly identifiable by the presence of loop-like signals around the nucleus (N). Accordingly, a significant gap between two adjacent GFP-emitting membranes as well as membrane invagination also denote strong tonoplast features. Further experiments are required to investigate ZmAMF1 subcellular localisation in yeast cells which was not conducted in this study due to time constraints.

3.3.10 AtTIP2 family members display diverse functionalities to rescue CY162 growth at high NH_4^+

As the AtTIP2 family has been widely known to enhance high ammonium tolerance, all of the AtTIP2 family members (AtTIP2;1-3) were expressed in CY162 strain. Interestingly, overexpression of AtTIP2 members in CY162 displayed diverse activities in alleviating NH_4^+ toxicity (Figure 3.8). AtTIP2;3 displayed the strongest efficiency to rescue CY162, followed by AtTIP2;1. In contrast, overexpression of AtTIP2;2 completely failed to rescue growth of CY162 at 80 mM NH_4^+. These findings indicate the functionalities of AtTIP2 might be dependent on the K^+ concentrations available to the cells and whether disruptions in K^+ transport influence NH_4^+ sensitivity.

3.3.11 AtAMF2 and ZmAMF1 increase MA sensitivity in CY162 yeast strain

Previous data showed that AtAMF2 and ZmAMF1 possess a comparable function in rescuing yeast grown at high NH_4^+ (Figure 3.8). To support this finding, all transformant cells (transformed with empty vector pDR196, AtAMF2, ZmAMF1 or AtTIP2;3) were grown on media containing proline as a sole amino acid in the presence of 50-100 mM MA. In these conditions, all transformants grew poorly (Supplemental Figure S3.9). A subsequent experiment was conducted, where cells were grown on Low Amino-N (LAN) media and a complete amino acid supplement without uracil (SD AA-ura) in the presence or absence of 100 mM MA (Figure 3.9.A-C). Results from this experiment demonstrated that overexpression of AtAMF2 and ZmAMF1 increased yeast sensitivity to toxic MA conditions at both pH 5.5 and 6.5 (Figure 3.9).

Interestingly, the MA toxicity phenotype was significantly alleviated on SD AA-ura (Figure 3.9.C) compared to the growth on just 0.1% proline (Figure 3.9.A) or the LAN media (Figure 3.9.B). These data indicate that sufficient amino acids supply is essential in supporting tolerance to MA toxicity.

3.3.12 AtAMF2 and ZmAMF1 overcome NH_4^+ toxicity in CY162 when supplied with proline as a sole amino acid.

Subsequent experiments were carried out to investigate how the CY162 cells response to high NH_4^+ in the presence of proline as a sole amino acid. Contrary to the previous observations on cells grown on MA, overexpression of AtAMF2 and ZmAMF1 enabled the cells to grow on media containing 100 mM NH_4^+ supplied with 0.1% proline as sole amino acid source at pH 5.5 (Figure 3.10). Surprisingly, cells overexpressing AtTIP2.3 failed to grow at pH 5.5, however all transformants grew well at pH 6.5. Indeed, the ability of the CY162 cells to grow well at pH 6.5 has been shown before (Figure 3.5).

3.3.13 AtAMF2 plays different roles in NH_4^+ tolerance mechanisms compared to AtTIP2

All AtTIP2 family members (Scharwies, 2017) and AtAMF2 have been shown to localise in the tonoplast (Chapter 2. Figure 2.12 and Figure 3.7). However, both protein classes demonstrated distinct functionalities in regard to NH_4^+/MA toxicity alleviation mechanisms. The AtTIP2 family members have been shown to facilitate NH_3 sequestration into the vacuole (Loqué et al., 2005) as proposed in Figure 3.12.A and C. On the other hand, AtAMF2 is suggested to facilitate the NH_4^+ release from the vacuole for further assimilation as pictured in Figure 3.12.D. This hypothesis was clearly confirmed in Figure 3.10 where overexpression of AtAMF2 and ZmAMF1 in CY162 rescued the cells growth at 100 mM NH_4^+ supplied with 0.1% proline as sole amino acid. Accordingly, when supplied with MA, overexpression of AtAMF2 induced toxicity phenotype due to the release of MA from the vacuole into the cytoplasm (Figure 3.9, Figure 3.12.B and Figure 3.12.E).

To confirm these findings, wild type yeast strain BY4741 was transformed with AtAMF2 and all AtTIP2 members. The ability of AtTIP2;1 and AtTIP2;3 to rescue the wild type yeast strain BY4741 grown on toxic concentrations of MA ($\geq$ 100 mM) (Loqué et al., 2005) was confirmed as shown in Figure 3.11. It was concluded that AtTIP2;1 and AtTIP2;3 were involved in a NH_4^+/MA tolerance mechanism involving a possible NH_3 vacuolar-sequestration pathway. Additionally, it was also revealed that overexpression of AtTIP2;2 enhanced MA tolerance in the BY4741 (Figure 3.11) potentially by the same NH_3 vacuolar-sequestration pathway. On the other hand, overexpression of AtAMF2 induced toxicity phenotype in the wild type strain BY4741, most evidently on LAN media at pH 5.5 (Figure 3.11.A) where the cells failed to grow. In contrast, the cells transformed with empty vector pDR196 displayed mild toxicity phenotype while, as expected, cells overexpressing AtTIP2;1-3 grew well (Figure 3.11.A). Previously, Cohen and Engelberg (2007) have reported that BY4741 grew poorly in minimal media such as SD-ura supplemented with a drop-out amino acid mix, while increasing amino acid concentrations improves the strain's growth. To differentiate between poor growth and MA toxicity, subsequent experiments were carried out on SD-

ura media containing 2 g/l histidine, 4 g/l leucine, 2 g/l methionine, supplemented with 1 g/l proline (high amino N/HAN), in the absence or presence of 100 mM MA. The AtAMF2-induced toxicity phenotype was slightly alleviated when the cells were grown on HAN at pH 5.5 whereas the cells transformed with pDR196 empty vector overcame the MA toxicity (Figure 3.11.B). This finding confirmed that the toxicity phenotype on cells overexpressing AtAMF2 was due MA toxicity rather than a poor growth of the cells. Interestingly, in the following experiments where cells were grown on media containing complete amino acids without uracil (SD AA-ura), the toxicity phenotype was completely overcome (Supplemental Figure S3.10). Additionally, at pH 6.5, all transformed BY4741 cells including AtAMF2 and the empty vector control grew in the presence of MA on LAN, HAN (Figure 3.11.A and B, respectively) and SD AA-ura (Supplemental Figure S3.10) media, suggesting a pH dependent insensitivity to MA in the BY4741 strain. This sensitivity is negatively influenced at more alkaline pH (6.5) when amino N is provided.

3.3.14 Adequate amino acid concentrations overcome MA toxicity

Previous studies have demonstrated that NH_4^+ toxicity in yeast only occurs when supplied with low concentrations of K^+, and that amino acid excretion is most-likely an outcome to help detoxify excess NH_4^+ (Hess et al., 2006; Ariz et al., 2018). Additionally, this process might lead to N or amino acid starvation in the yeast cells which eventually promotes growth arrest or death. Therefore, we propose that supplementation of amino acids is crucial under toxic NH_4^+/MA conditions. Experiments using different concentration of amino acid supplies in both CY162 strain (Figure 3.9) and BY4741 (Figure 3.11 and Supplemental Figure S3.10) clearly confirmed the hypothesis. Under toxic concentrations of MA, cell growth of both strains grown on media containing complete amino acids without uracil (SD AA-ura) was significantly improved. Collectively, these data suggest that MA sensitivity in general is linked to the amino acid status of the yeast cells, where elevated amino acids can overcome general MA sensitivities.

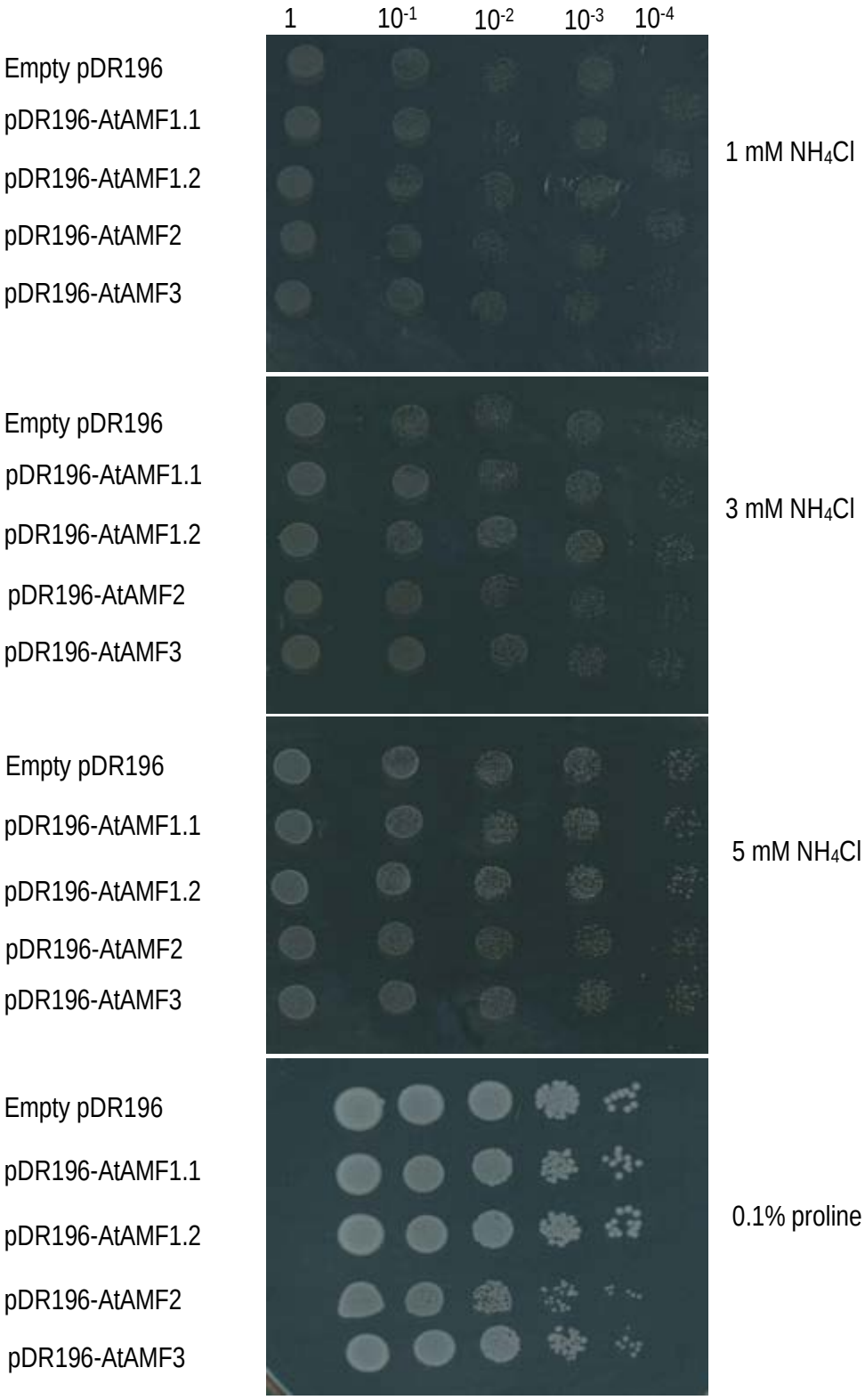

Figure 3.1. Overexpression of the AtAMFs failed to support significant growth of the 31019b yeast strain when grown on SD-ura media containing low concentrations of NH_4Cl.

Transformed 31019b (*mep1-3Δ*) cells transformed with AtAMF members did not show a significant growth improvement compared to the cells transformed with empty vector pDR196 on SD-ura media (pH 6.1) containing low 1 mM NH_4^+ as a sole N source. Cells were grown at 28˚C for 6 days.

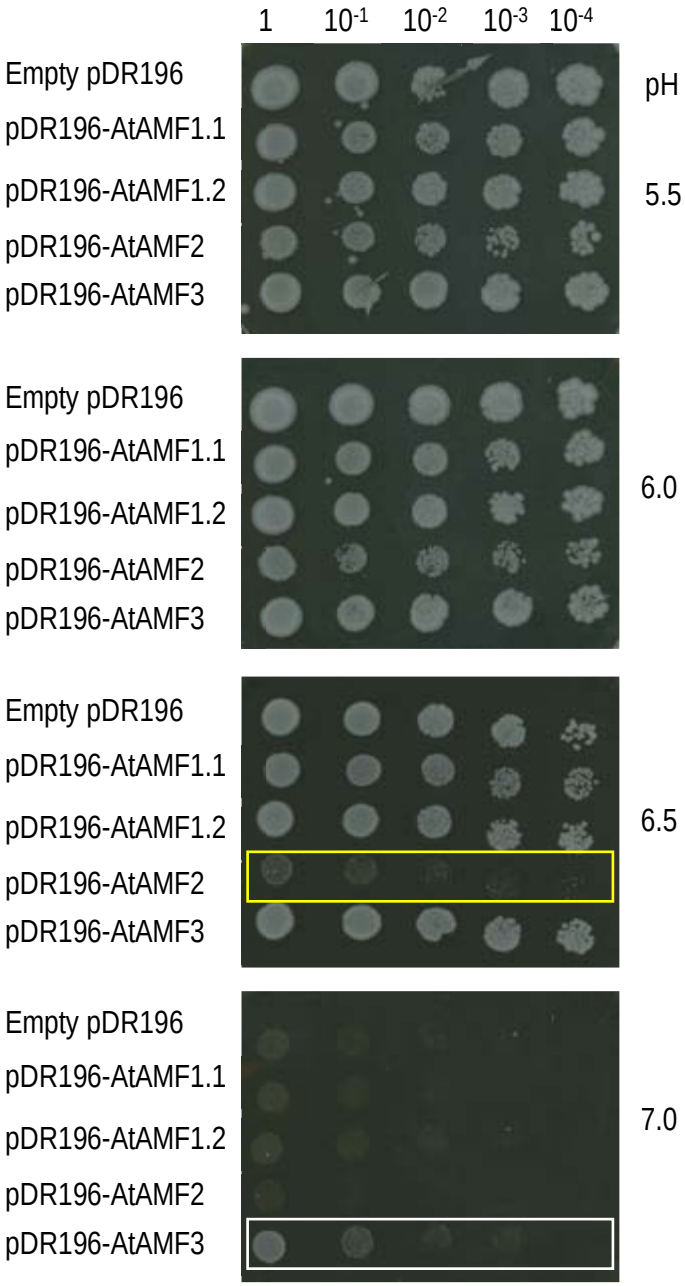

Figure 3.2. Yeast strain 31019b overexpressing AtAMF2 shows a toxicity phenotype at pH 6.5 while overexpression AtAMF3 slightly improves growth at pH 7.0 under toxic [MA].

Transformed 31019b cells were grown on SD-ura media supplemented with 0.1% (w/v) proline, 2% (w/v) glucose 100 mM MA buffered at pH 5.5, 6.0, 6.5 and 7.0 with 50 mM MES-Tris. Cells were grown at 28˚C for 10 d. Yellow outlined box identifies AMF2 inhibiting growth of 31019b at pH 6.5. White outlined box identifies a slight growth improvement facilitated by AMF3.

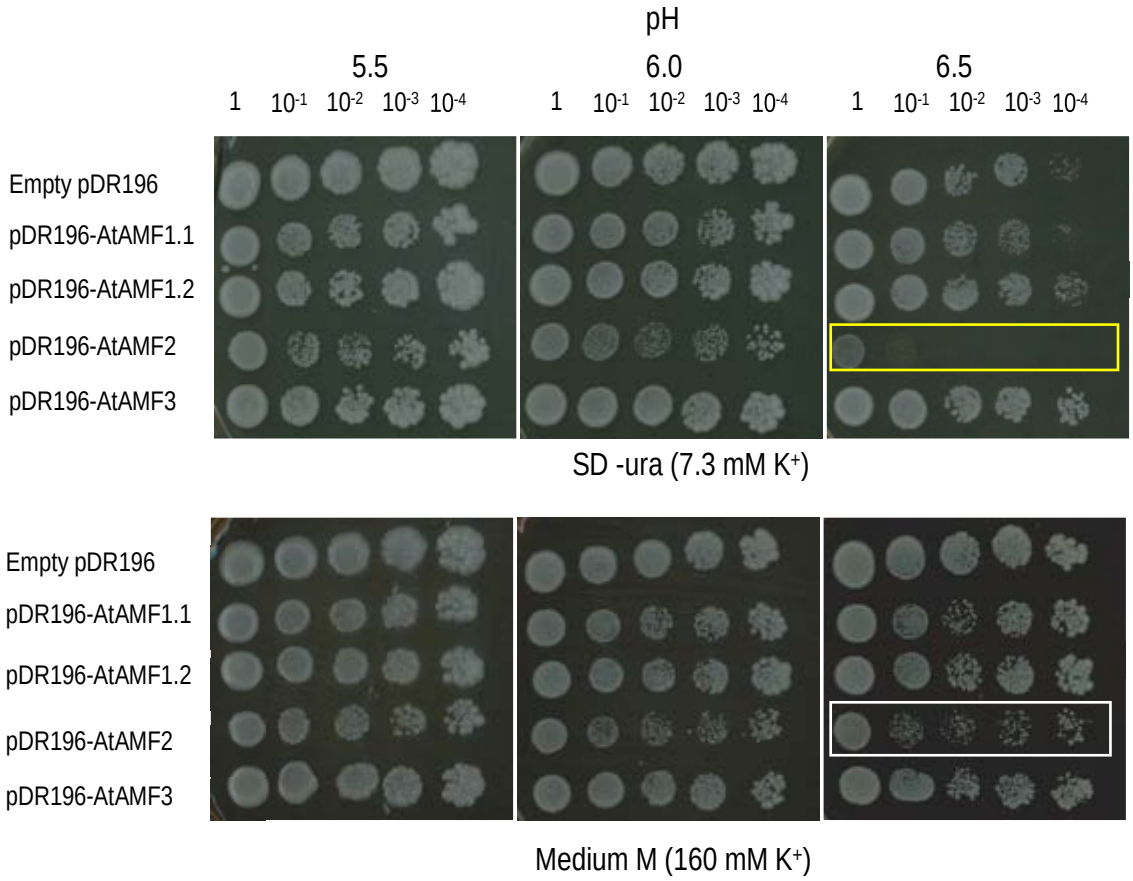

Figure 3.3. AtAMF2-induced MA toxicity is overcome with media containing high **[**K^+**]**.

Transformed 31019b cells were grown on SD-ura or Medium M differentiated by K^+ concentrations of 7.3 mM K^+ and 160 mM K^+, respectively. SD-ura and Medium M were supplemented with 0.1% (w/v) proline, 2% (w/v) glucose and 100 mM MA buffered with 50 mM MES-Tris to pH 5.5, 6.0 and 6.5. Cells were grown at 28˚C for 10 d. Yellow and white outlined boxes identify AtAMF2 inhibiting growth of 31019b on SD-ura and Medium M, respectively, at pH 6.5.

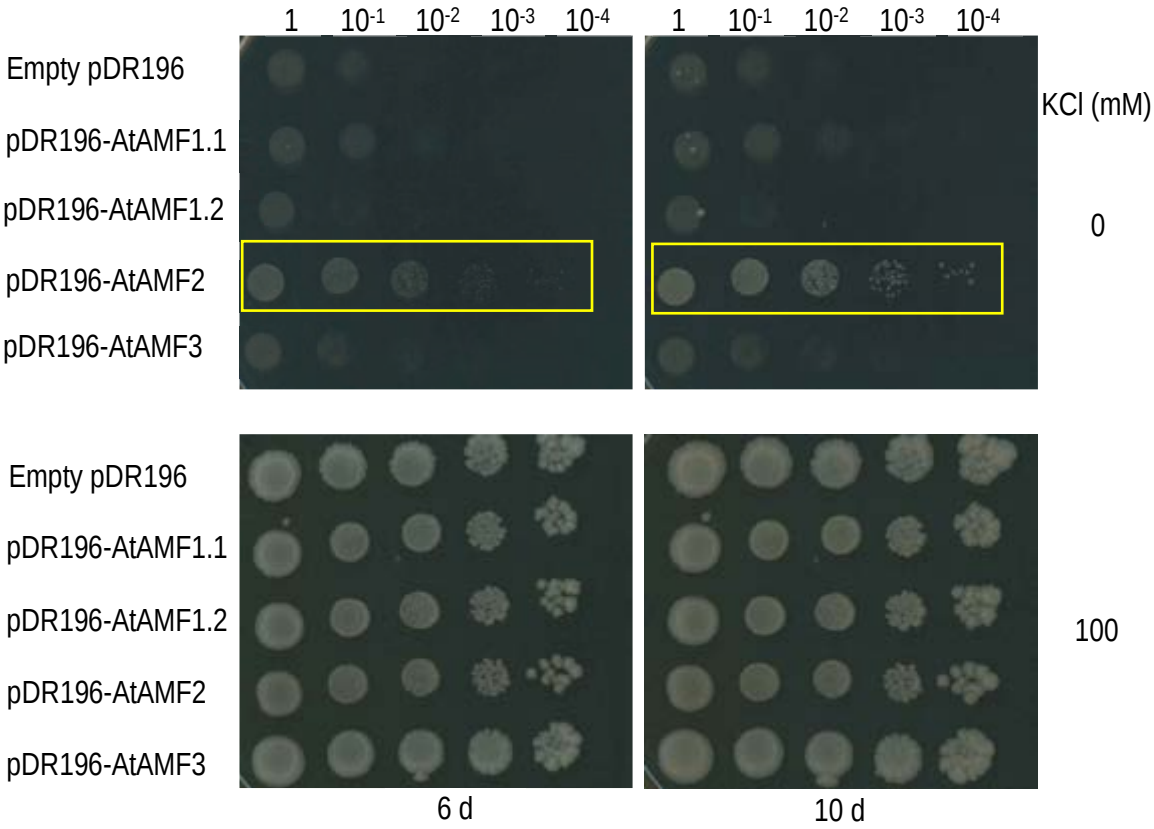

Figure 3.4. AtAMF2 rescues growth of the potassium transport mutant CY162 on high ammonium and low K^+ concentration.

Transformed CY162 cells were grown on SD-ura media supplemented with 5 g/l $(NH_4)_2SO_4$ (~75.6 mM NH_4^+) ± 100 mM KCl. Basal [K^+] concentration is 7.3 mM. Media pH was 5.5. Cells were grown at 28˚C for 6-10 d. Yellow box identifies AtAMF2 containing cells growing at low K^+ and high NH_4^+.

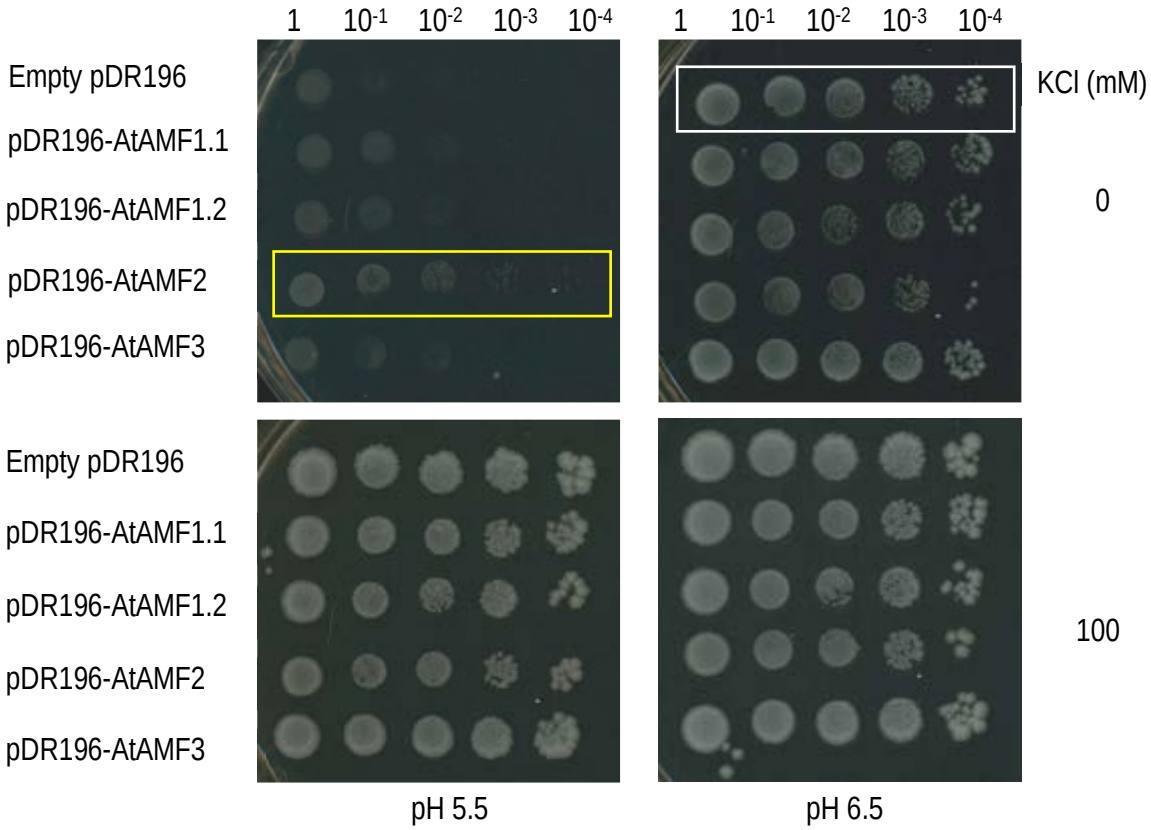

Figure 3.5. CY162 growth improves on SD AA-ura media at elevated pH.

Transformed CY162 cells were grown on SD AA-ura media supplemented 5 g/l $(NH_4)_2SO_4$ and buffered with 50 mM MES-Tris to pH 5.5 or 6.5. Cells were grown at 28˚C for 6 d. At pH 5.5 AtAMF2 (yellow box) begins to complement growth a low K^+. At pH 6.5 all cells grow at low K^+. White outlined box indicates recovery of empty vector control when grown on SD AA-ura (pH 6.5) without additional K^+ (basal concentration of the media is 7.3 mM).

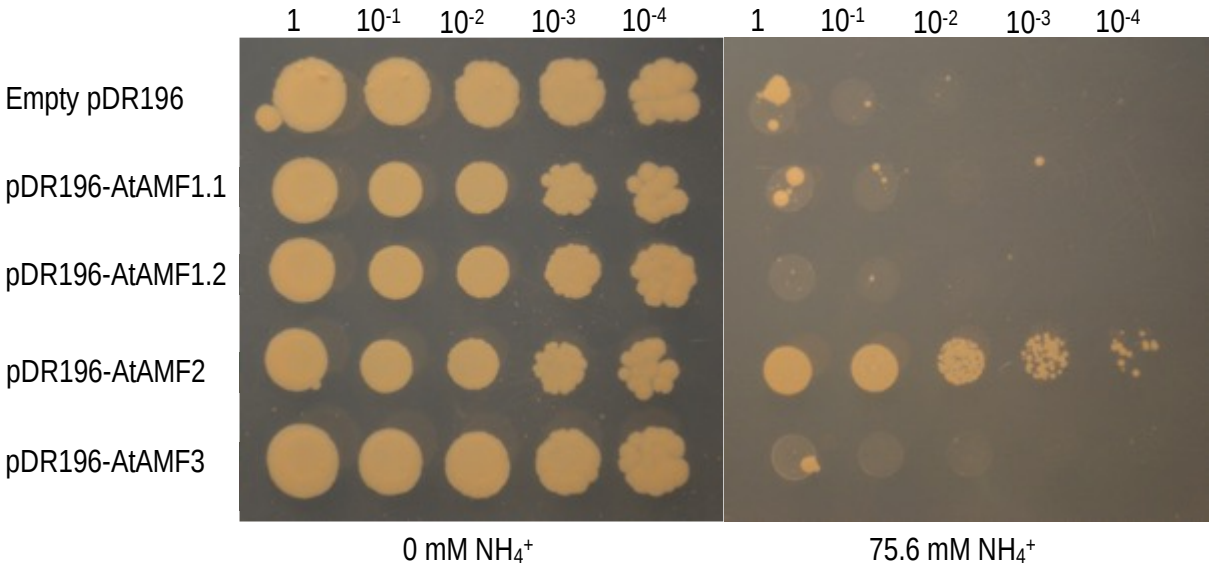

Figure 3.6. CY162 cells expressing AtAMF genes grown on media with and without NH_4^+. Transformed CY162 cells were grown on SD AA-ura in the absence or presence of 5 g/l $(NH_4)_2SO_4$ at pH 5.5. SD AA-ura has a default 7.3 mM K^+ concentration. Cells were grown at 28˚C for 6 d.

A. CY162

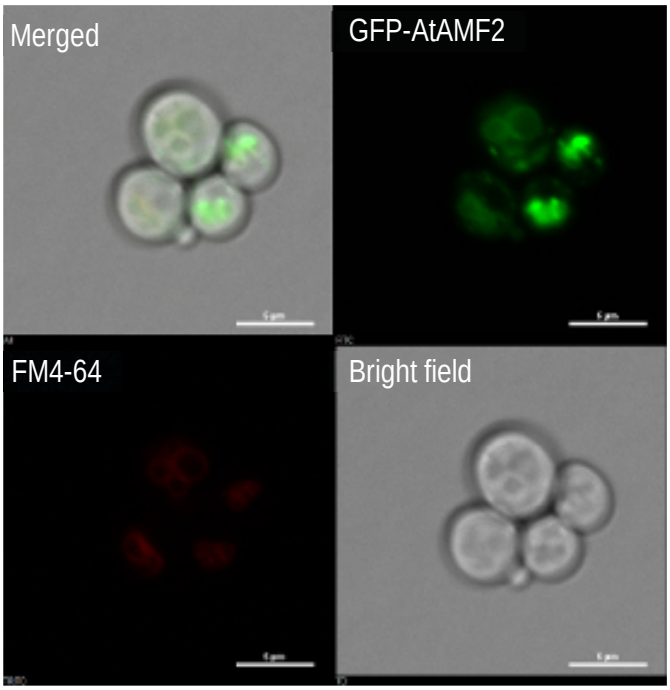

B. BY4741

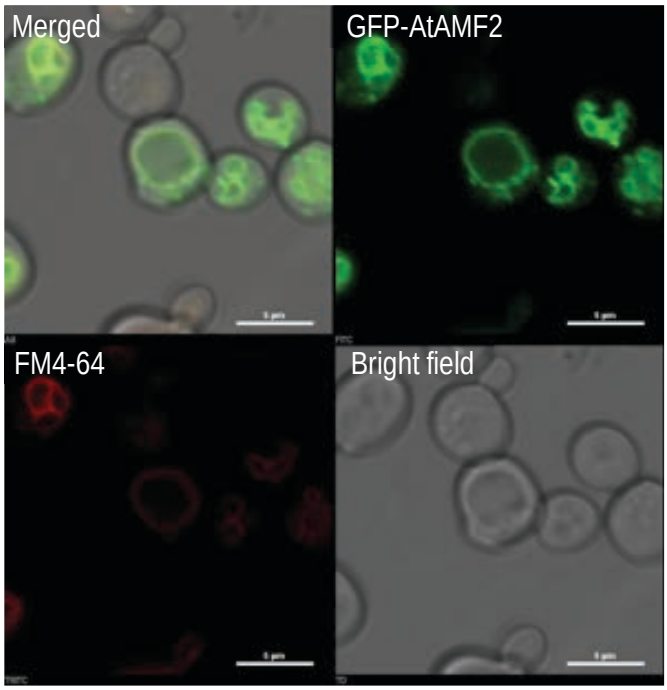

Figure 3.7. AtAMF2 is localised in the tonoplast of CY162 (A) and BY4741 (B) yeast cells.
Both yeast strains were transformed with pDR196 containing a N-terminal GFP fusion to AtAMF2, activated by the PMA promoter. Prior to analysis, cells were grown in SD AA-ura supplemented with 5 g/l $(NH_4)_2SO_4$. In BY4741 strain, N-terminal tagged GFP-AtAMF2 displays strong localisation at the tonoplast with secondary signal possibly in the ER and or cytoplasm (A) while in CY162, AtAMF2 localisation is more diffuse across the tonoplast and the ER (B). Scale bare = 5 μm.

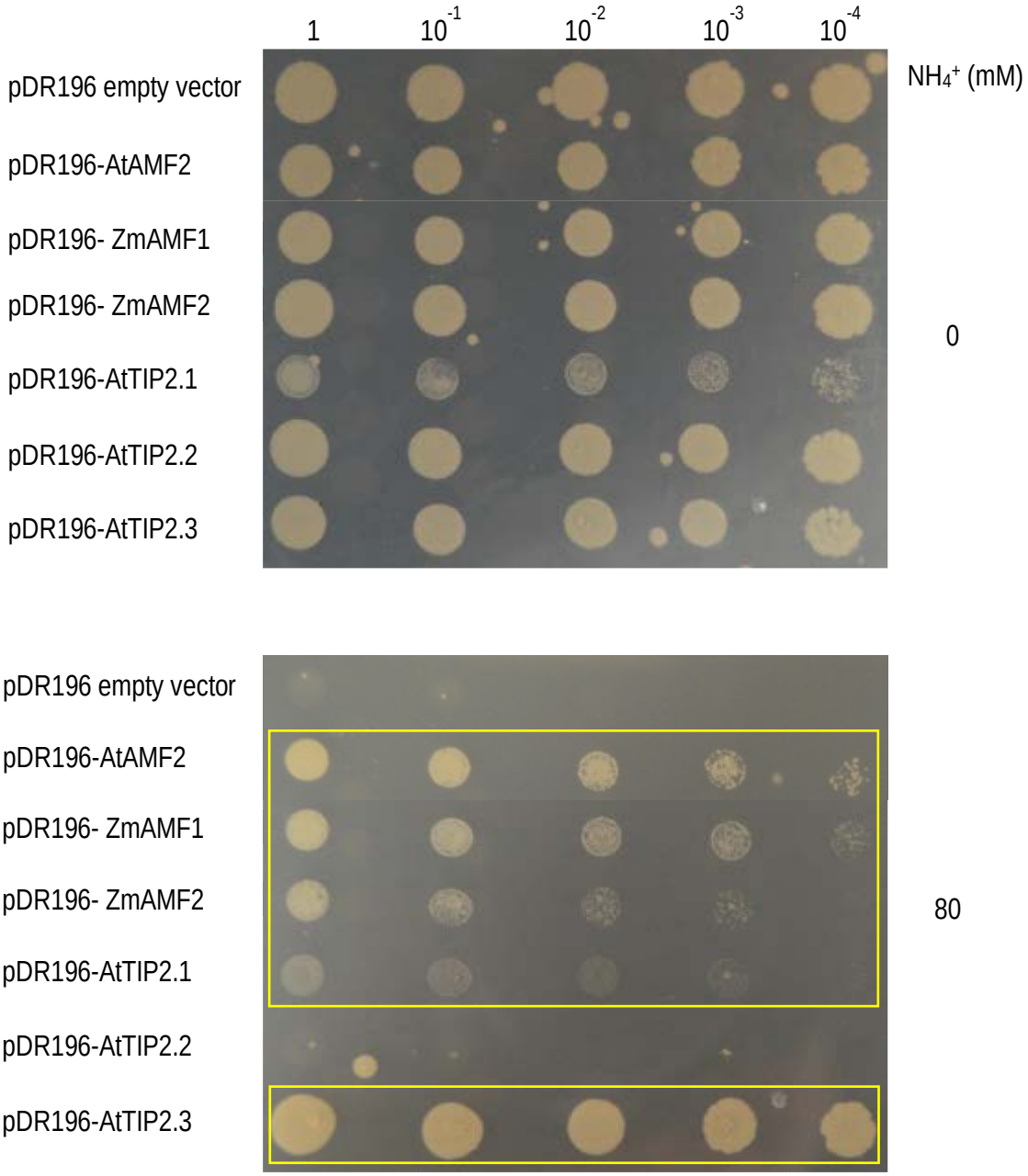

Figure 3.8. Overexpression of ZmAMF1, ZmAMF2, AtTIP2;1 and AtTIP2;3 in CY162 with low or high NH_4^+.

Transformed CY162 cells were grown on SD AA -ura in the absence or presence of 80 mM NH_4^+. Cells were grown at 28°C for 6 d. Yellow boxes highlight rescue of CY162 by AMF2, ZmAMF1, ZmAMF2 AtTIP2;1 and AtTIP2;3 on 80 mM NH_4^+.

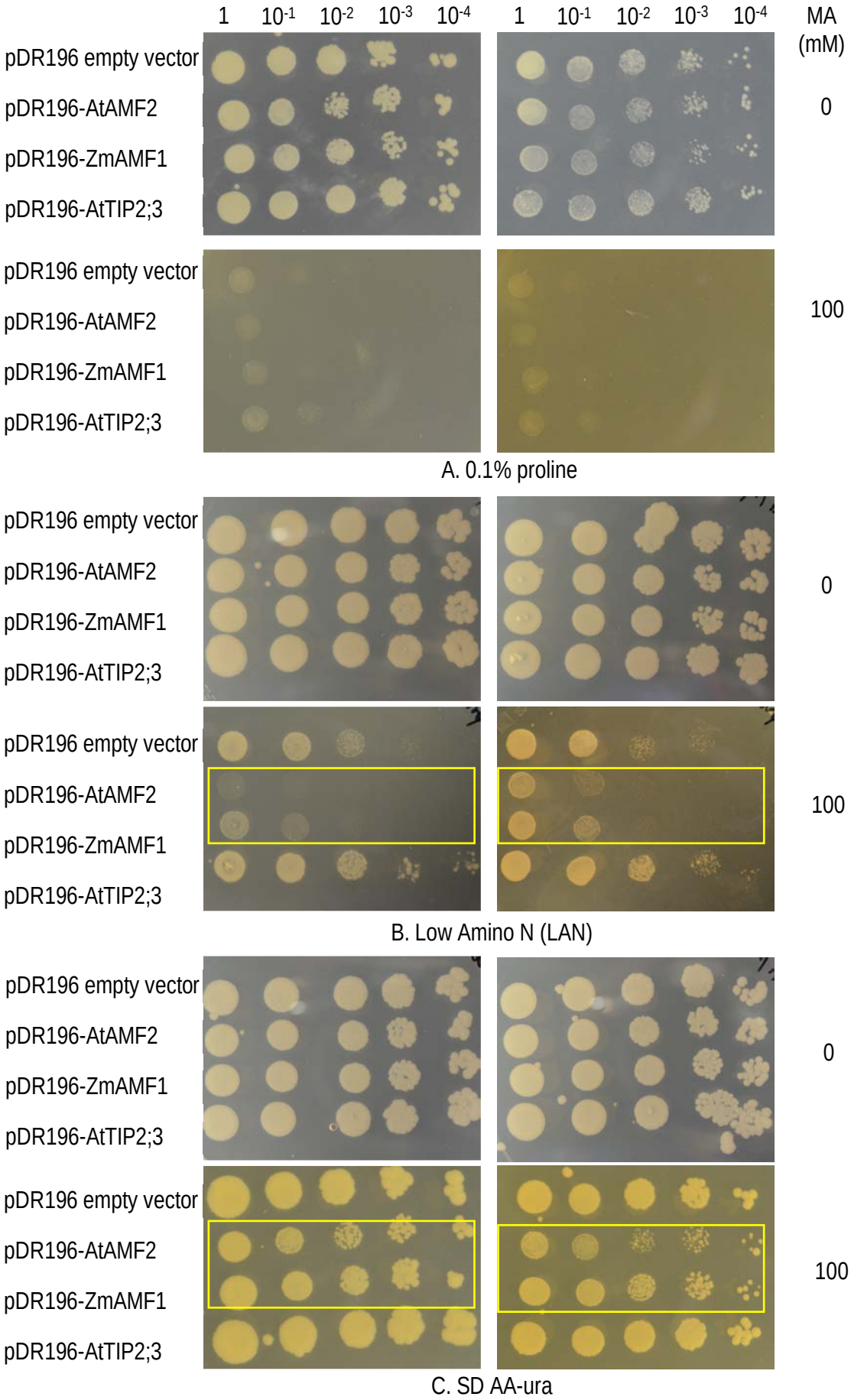

Figure 3.9. Overexpression of AtAMF2 and ZmAMF1 increases MA sensitivity in CY162 strain.

Transformed CY162 cells were grown on media containing different concentration of amino acids (A-C) in the presence or absence of 100 mM MA at pH 5.5 and 6.5. The media were buffered with 50 mM MES-Tris. A. 0.1% (1 g/l) proline as sole amino acid source. B. 76 mg/l histidine, 380 mg/l leucine, 76 mg/l methionine and 1 g/l proline (Low Amino N). C. 1 g/l yeast synthetic drop-out media supplement without uracil (SD AA-ura). Cells were grown at 28°C for 5 d. Yellow outlined boxes show MA toxicity at both pH 5.5 and 6.5.

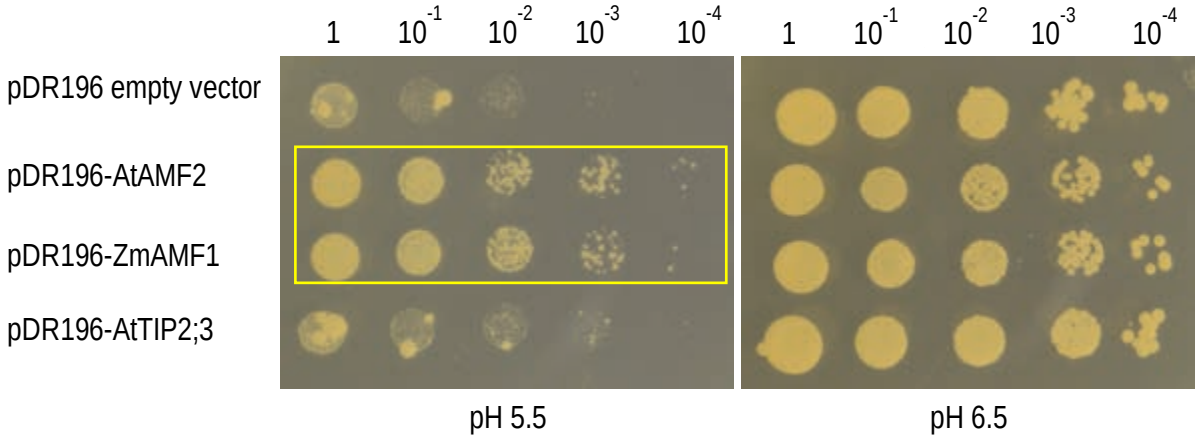

Figure 3.10. Overexpression of AtAMF2 and ZmAMF1 overcomes ammonium toxicity in CY162 with proline as the sole amino acid.

Transformed CY162 cells were grown on SD-ura supplemented with 100 mM NH_4Cl and 0.1% proline (w/v) as the sole amino acid. Media was buffered with 50 mM MES-Tris and pH adjusted to 5.5 and 6.5. Yellow outlined box indicates a growth improvement by AtAMF2 and ZmAMF1 overexpression.

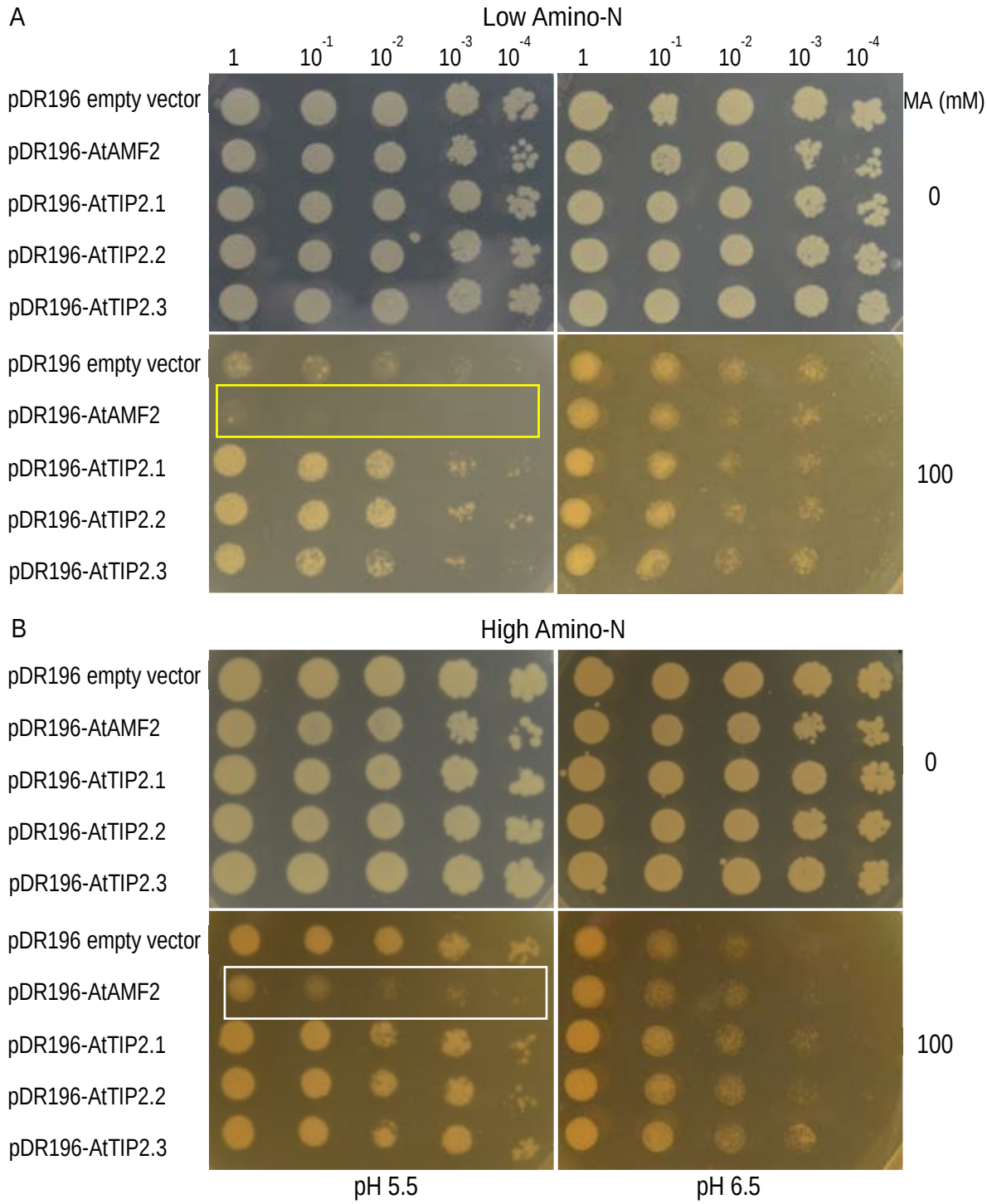

Figure 3.11. AtAMF2 displays increased sensitivity to MA when grown with both high and low amino-N media.

Transformed BY4741 cells were grown on SD-ura supplemented with either Low Amino-N (LAN) media containing 76 mg/l histidine, 380 mg/l leucine, 76 mg/l methionine and 1 g/l proline or High Amino-N (HAN) media containing 2 g/l histidine, 4 g/l leucine, 2 g/l methionine and 1 g/l proline. Media was buffered with 50 mM MES-Tris. Cells were grown at 28˚C for 5 d. Yellow outlined box highlights AtAMF2 induced MA sensitivity on LAN media. White outlined box indicates an improved MA tolerance on HAN media.

A

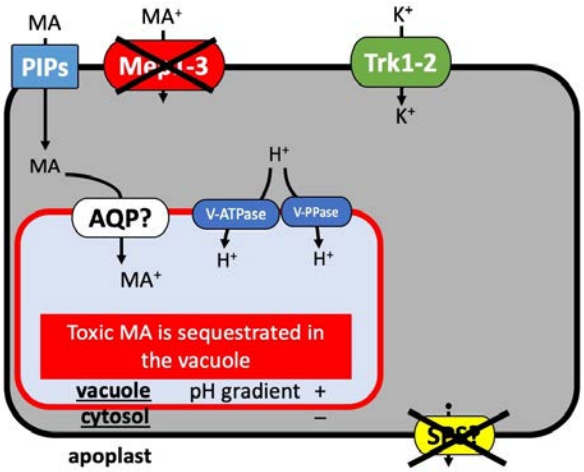

MA-tolerant yeast cells (31019b) grown on media with proline as the sole amino acid source. Yeast cells without tonoplast-localised AMF shows tolerance to toxic [MA] due to MA sequestration in the vacuole.

B

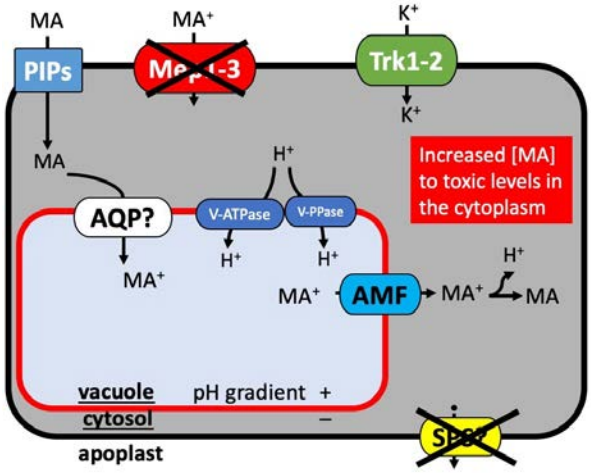

MA-tolerant yeast cells (31019b) grown on media with proline as sole amino acid source. Yeast cells with tonoplast-localised AMF becomes sensitive to toxic [MA] due to AMF facilitates efflux of acid-trapped MA from the vacuole into the cytoplasm.

C

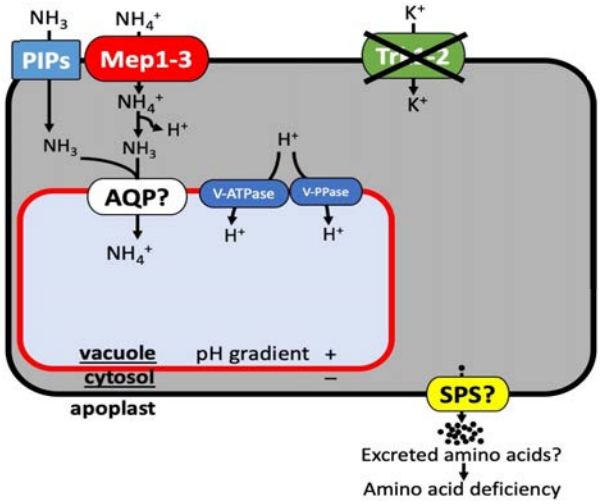

NH_4^+-sensitive yeast cells (CY162) without tonoplast-localised AMF suffer N-starvation and fail to grow on media containing a toxic concentration of NH_4^+.

D

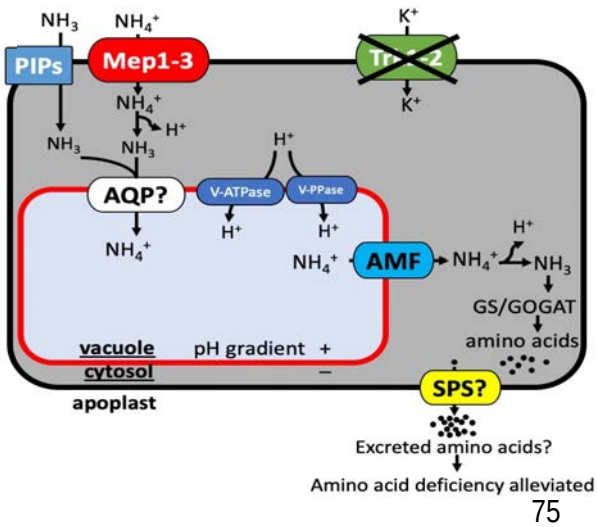

Tonoplast-localised AMF in CY162 enables yeast cells to grow on media containing toxic concentration of NH_4^+. AMF slowly releases NH_4^+ from the vacuole back into the cytoplasm which undergoes assimilation to produce amino acids essential for yeast growth.

E

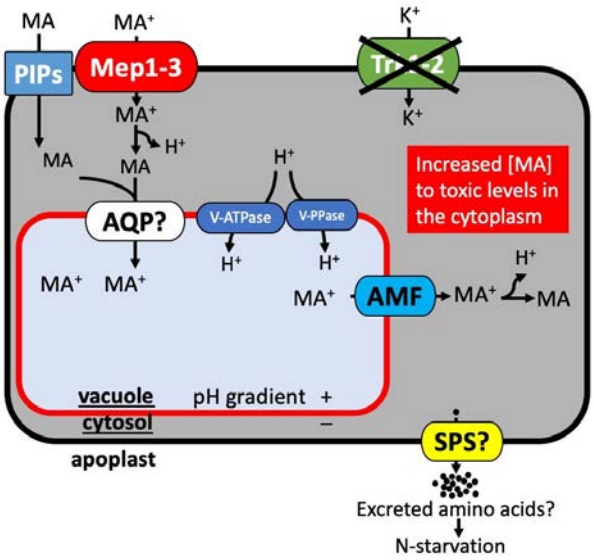

Tonoplast-localised AMF in CY162 strain induces toxicity on media containing toxic concentration of MA. AMF releases MA^+ from the vacuole back into the cytoplasm, inducing a toxicity phenotype.

Figure 3.12. Proposed model of tonoplast-localised AMF transporters facilitating NH_4^+/MA^+ efflux in yeast strain 31019b (A and B) and CY162 (C-E).

In 31019b yeast strain (A and B), the plasma membrane localized aquaporins (PIPs) facilitate the uncontrolled uncharged MA/NH_3 fluxes into the cytoplasm. The elevated MA/NH_3 concentration in the cytosol may trigger TIP-facilitated MA/NH_3 sequestration into the vacuole by the tonoplast localized yeast aquaporin (AQP?), possibly by AQY3 (Patel, 2013) (A). Alternatively, in yeast, MA/NH_3 is thought to diffuse into the vacuole (Wood et al., 2006; Cueto-Rojas et al., 2017). Due to the acidic environment inside the vacuole, MA is protonated into MA^+ and acid-trapped inside the vacuole. The release of MA from the vacuole into the cytosol through AMF activity would increase toxic MA concentrations leading to a toxicity phenotype (B). Furthermore, at low cytosolic K^+ (either due to low external K^+ concentrations or from disrupted K^+ transport mechanisms (i.e. CY162 (C-E)) and high NH_4^+, yeast cells promote amino acid excretion leading to amino acid-deficient cells (C). In such conditions, SPS is suggested as an amino acid effluxer induced by ammonium stress (Hess et al., 2006). Uncontrolled NH_4^+ influx mediated by Mep undergoes disassociation to produce NH_3 in the cytosol accompanied by NH_3 flux through PIPs, follow the same sequestration pathway as described earlier. Tonoplast localized AMF transporters facilitate the release of NH_4^+ into the cytosol which is assimilated allowing cell growth (D). On the other hand, when MA is supplied, the release of toxic MA from the vacuole, elevates MA concentration in the cytoplasm and induces toxicity phenotype (E).

3.4 Discussion

3.4.1 K^+ plays vital roles in NH_4^+ tolerance mechanisms in yeast

NH_4^+ is an essential macronutrient for all living organisms including yeast. If provided at an appropriate level and balanced with other cations, it is a beneficial N source for yeast growth. Studies by Hess et al. (2006) on wild type S288C revealed that NH_4^+ toxicity can occur in yeast only when K^+ is limited. Similarly, Ariz et al. (2018) reported the same phenomenon also happen to another wild type strain Σ1278b. Furthermore, Barreto et al. (2012) revealed that even short-term K^+ starvation substantially changed the expression levels of over one thousand yeast genes and activated an oxidative stress response as well as the retrograde pathway.

Data generated from this thesis confirms the vital role of K^+ as yeast cells experience NH_4^+/MA^+ toxicity. Overexpression of AtAMF2 in the MA-resistant yeast strain, 31019b, led to a lethal phenotype (Figure 3.2). However, overexpression of the other homologs (AtAMF1;1, AtAMF1;2 and AtAMF3), failed to induce a lethal phenotype probably because the other proteins are localised in different organelles (Chapter 2. Figure 2.10-13). Furthermore, AtAMF2-induced lethality could be reversed by increasing the concentration of K^+ in the media. Retarded growth was observed on SD-ura media containing ~ 7.3 mM K^+ (a default concentration), whereas in Medium M, containing ~ 160 mM K^+, growth improved (Figure 3.3), even in the presence of toxic levels of MA (i.e. 100 mM). Similarly, growth of 31019b cells overexpressing AtAMF2 improved when grown on SD-ura containing 0.1% proline supplemented with elevated K^+ concentrations (Supplemental Figure S3.3). Previous studies have demonstrated that at low K^+, yeast cells fail to control NH_4^+ influx properly due to an unregulated NH_4^+ influx pathway possibly mediated through the K^+ transporter, Trk1 (Hess et al., 2006; Barreto et al., 2012). As K^+ produces a competitive inhibition on NH_4^+ uptake in yeast (Peña et al., 1987), any increment of K^+ concentration will reduce uncontrolled NH_4^+ influx and diminish toxic conditions, eventually improving yeast growth.

In yeast, Trk1 and Trk2 are important K^+ transporters involved in both high and low-affinity K^+ transport, respectively (Ko and Gaber, 1991). Deletion of both proteins (*trk1Δ, trk2Δ*) in CY162, significantly impairs the high affinity K^+ transport systems, making cells unable to grow on low K^+ media. CY162 has since been widely used to identify and characterise both K^+ and Na^+ transporters from plants (Schachtman and Schroeder, 1994; Rubio et al., 1999). On this basis, we used CY162 to test if AtAMF1-3 facilitated K^+ transport. The original selection of CY162 was based on a growth phenotype on plates by which cells failed to grow on SD AA-ura media containing 75.6 mM NH_4^+ and 7.3 mM K^+, which could be rescued with the addition of 100 mM K^+ (Ko and Gaber, 1991). When overexpressed, only AtAMF2 allowed CY162 cells to grow on standard SD AA-ura media at pH 5.5, while yeast cells transformed with the empty vector control and the other AtAMF homologs (AtAMF1 and AtAMF2) failed to grow. AtAMF2 could rescue yeast growth further on SD AA-ura media containing higher NH_4^+ concentrations (up to 140 mM) when external K^+ concentrations were kept at 7.3 mM (Supplemental Figure S3.6). However, when the NH_4^+ was completely removed from the media (0 mM NH_4^+), CY162 strain would grow normally with

or without AtAMF2 (Figure 3.6 and Supplemental Figure S3.6). These data suggest that CY162 is sensitive to high NH_4^+ and that additional K^+ provision could reverse NH_4^+ toxicity (Figure 3.4 and Supplemental Figure S3.4). Previous claims by Barreto et al. (2012) and Hess et al. (2006) suggested that unregulated NH_4^+ flows through Trk1. However, based observations presented in this thesis, CY162 is still sensitive to high NH_4^+ regardless of the dysfunctionality of *trk1*. Therefore, it is hypothesized that the primary cause of NH_4^+ toxicity in CY162 is its inability to supply K^+ into the cytoplasm with the loss of *trk1* and *trk2*. The flow of NH_4^+ into CY162 most likely involves Mep proteins as well as from the mass flow of NH_3 through the plasma membrane aquaporins (PIPs) into the cytoplasm. How the accumulated NH_3/NH_4^+ is managed in the cytoplasm may reflect on the role of AtAMF2.

3.4.2 Tonoplast localised transport proteins are important for NH_4^+ management

The vacuole occupies significant portions of cell volume, ~ 20% in yeast (Hecht et al., 2014) and ~ 90% in plants (Zhang et al., 2014). Although the main function of the yeast vacuole is known for macromolecule degradation, it also plays a crucial role in cytosolic pH homeostasis, metabolite and ion storage as well in molecule detoxification (Klionsky et al., 1990). These complex functions are regulated by approximately ~ 200 vacuolar-targeted proteins for which 27% are believed to be transport proteins (Li and Kane, 2009).

NH_4^+/MA^+ vacuolar sequestration is one of the essential pathways responsible for NH_4^+ detoxification mechanisms. Only limited studies have been undertaken to understand the mechanism of ammonium sequestration in the vacuole at the molecular level. There have been few suggestions regarding transport proteins responsible for NH_4^+/MA^+ sequestration. Bai et al. (2014) proposed the presence of an unknown protein(s) localised in the tonoplast which facilitates NH_4^+ sequestration by CAP1 phosphorylation. Furthermore, Coskun et al. (2013a) suggested that various protein classes localised in the tonoplast, including TIPs, (tonoplast-intrinsic proteins), AMTs (ammonium transporters), Kirs (K^+ inward rectifiers), and NSCCs (nonselective cation channels) are responsible for NH_3/NH_4^+ transport across (in and out) the tonoplast. However, only AtTIP2;1 and AtTIP2;3 have been shown to facilitate MA transport into the vacuole (Loqué et al., 2005). Based on experiments conducted in this thesis, it was demonstrated that AtTIP2;2 was functional and most-likely facilitated MA vacuolar sequestration, a phenotype typified by the rescue of yeast growth when grown on toxic MA concentrations (Figure 3.11.A). AtTIP2 families have been shown to promote $NH_3/NH_4^+/MA$ influx across the tonoplast, the transport protein(s) responsible for NH_3/NH_4^+ efflux from the vacuole into the cytoplasm remain unknown (Esteban et al., 2016). This is particularly relevant in light of the substantive quantities of reactive N being processed within vacuoles.

3.4.3 AtAMF2 and ZmAMF1 are responsible for NH_4^+/MA^+ efflux from the vacuole

The majority of ammonium transport proteins have been characterised using the high-affinity ammonium transport deficient yeast strain 31019b. Using 31019b, a large number of *AMT* genes have

been expressed and confirmed as putative plasma membrane transporters that facilitate NH_4^+/MA^+ influx into the cell. Previously, the activities of both GmAMF3 and ScAMF1 suggested AMF proteins have a modified role in facilitating MA influx into yeast cells but are capable of both MA^+ and NH_4^+ transport when expressed in *Xenopus laevis* oocytes (Chiasson et al., 2014). An interesting feature of the yeast ammonium transport mutant, 31019b is that it can tolerate high concentrations (0.1 M) of methylammonium when grown at pH levels below 6.5 but is susceptible to MA at more alkaline pH ranges (>6.5). At pH 6.5, AtAMF2 expression increased the sensitivity of 31019b cells to high concentrations of MA (Figure 3.2), while AtAMF1 and AtAMF3 failed to elicit a similar response. The increased sensitivity to MA by AtAMF2 occurred even though AtAMF2 was found localised to the tonoplast (Figure 3.7). In *Nicotiana benthamiana*, AtAMF2 is also found targeted to the tonoplast of leaf epidermal cells (Chapter 2. Figure 2.12). The tonoplast location suggests AtAMF2 is not directly responsible for the elevated MA transport across the plasma membrane into yeast cells and must have a transport role elsewhere in the cell that influences MA sensitivity.

The partial management of NH_4^+ and MA^+ concentrations inside yeast and plant cells have been suggested to involve the activity of aquaporin (AQP) transport proteins. In yeast cells grown in alkaline media, plasma membrane aquaporins (PIPs) are thought to facilitate the transport of uncharged MA and NH_3 across the plasma membrane. Once in the cytosol, both are thought sequestered to the vacuole by tonoplast-localised aquaporins (AQPs/TIPs) following established concentration gradients. In yeast, these transport pathways are assumed to help alleviate MA toxicity but also help store excess NH_3 in the vacuole as NH_4^+ through a vacuolar acid trapping mechanism, as illustrated in Figure 3.12.A. In the context of the AtAMF2 activity presented in this thesis and its location on the tonoplast, it would appear AMF2 activity may act to counter this default storage mechanism (Figure 3.2). Overall, the data suggests both MA^+ and NH_4^+ may be released from the vacuole back into the cytoplasm. This results in either a MA induced cytosolic toxicity (Figure 3.12.B) or a process which helps to compensate N demands with excessive amino acid excretions from the cell when exposed to toxic concentrations of NH_4^+.

In experiments using CY162, it was shown that CY162 was NH_4^+ sensitive (Figure 3.6). Contrary to the observations in 31019b, overexpression of AtAMF2 increased cell tolerance to high external NH_4^+ concentrations (up to 140 mM) (Supplemental Figure S3.6). Previous studies (Hess et al., 2006; Ariz et al., 2018) have also demonstrated that amino acid extrusion from yeast cells is a detoxifying mechanism under toxic NH_4^+ concentrations and low K^+ availability. This mechanism potentially leads to amino acid deficiency in the yeast cells (Figure 3.12.C). However, when either AtAMF2 or ZmAMF1 were overexpressed in the CY162 cells, the cells became tolerant to extreme NH_4^+ concentrations even with proline being supplied as a sole amino acid (Figure 3.10). In contrast, CY162 cells overexpressing AtTIP2;3 which is involved in sequestering NH_3 into the vacuole, the cells remained sensitive to high NH_4^+ concentrations (Figure 3.10). I believe this difference is due to a limitation of essential amino acids required to support growth. I propose that AtAMF2 and ZmAMF1 retrieve NH_4^+ from the vacuole and

transport it into the cytoplasm to be assimilated. This mechanism would provide amino acids to support growth (Figure 3.12.D). In contrast, cells overexpressing AtTIP2;3 failed to grow due to the absence of an NH_4^+ supply from the vacuole (Figure 3.12.C). Accordingly, when the cells are grown at high concentrations of MA^+, the presence of the tonoplast-localised AMF also releases the toxic NH_4^+ analogue from the vacuole into the cytoplasm inducing a toxicity phenotype (Figure 3.9 and Figure 3.12.E).

Subsequent experiments with AtAMF2 and AtTIP2 members in the wild type strain BY4741, confirmed these hypotheses. When all three Mep transporters are active, MA^+ transport across the plasma membrane into the cytoplasm occurs resulting in a MA-induced toxicity phenotype. Interestingly, cells overexpressing AtAMF2 displayed a more severe toxicity phenotype compared to empty vector control while cells overexpressing AtTIP2 proteins continued to grow well (Figure 3.11.A). These data confirm that AtAMF2 facilitates a retrieval of MA from the vacuole into the cytoplasm inducing a cytosolic toxicity phenotype similar to that observed in the other yeast strains 31019b and CY162. Additionally, these findings clearly demonstrate that AtAMF2 and AtTIP2 members are functionally distinct in relation to NH_4^+/MA^+ transport.

The presence of NH_4^+- efflux proteins in the tonoplast has been postulated previously (Esteban et al., 2016). TIP families (e.g AtTIP2;1 and AtTIP2;3) have been suggested to participate in NH_4^+- efflux (Martinoia et al., 2007; Coskun et al., 2013a). However, this seems unlikely as the TIP2 family was characterized for its ability to transport uncharged NH_3, whereas in the vacuole, charged NH_4^+ will dominate due to the lower pH in the vacuole. The results reported here have demonstrated that tonoplast-localised AMF proteins might be the “real player” for the efflux of NH_4^+ and MA out of the vacuole.

3.4.4 Adequate amino acid levels are essential for NH_4^+/MA toxicity tolerance

Provision of adequate essential amino acids are vital for NH_4^+ tolerance mechanisms in yeast. Studies by Santos et al. (2012) have shown that NH_4^+-induced cell death was enhanced when essential amino acid availability is limited. Accordingly, Hess et al. (2006) and Ariz et al. (2018) have demonstrated that yeast excrete amino acids during NH_4^+ toxicity events as a detoxification mechanism. Therefore, growing yeast at high NH_4^+ and limited essential amino acids might lead to a N-starved state, arrested growth and eventual death. Accordingly, adding proline as a sole amino acid with high concentrations of MA significantly diminished the ability of CY162 to grow even when overexpressing AtTIP2;3 (Figure 3.9.A and Supplemental Figure S3.9). On the other hand, Figure 3.9.C and Supplemental Figure S3.10 show that supplying a complete set of essential amino acids without uracil (SD AA-ura) clearly reversed the adverse effects of MA^+ toxicity in CY162 and BY4741 respectively, including yeast cells with an enhanced sensitivity through AtAMF2 overexpression. These results suggest that when yeast cells become N-starved following amino acid excretion, provision of only proline is insufficient to promote sufficient N metabolism in yeast cells. In this scenario, overexpression of AtTIP2;3 in CY162 sequesters NH_3/MA into the vacuole but the cells ability to support cell growth is undermined by a potential deficiency in cytosolic amino acids levels.

3.4.5 Tonoplast-localised AMF proteins may play crucial roles for N recycling

AMF proteins share ~ 25-30% similarities with spinster (Spin) proteins found in animal cells and both protein classes are classified in the Major Superfamily Facilitators (MFS). Interestingly, similar to subcellular localisation of AtAMF2 and ZmAMF1, Spin from *Drosophila*, zebrafish and mammalian (Young et al., 2002; Dermaut et al., 2005; Rong et al., 2011) homologs are targeted to lysosomes, which are practically equivalent to plant or fungal vacuoles. Both lysosomes and vacuoles are known for their vital roles in biological material degradation that promote nutrient recycling and having a low internal pH. The recycled products include amino acids, monosaccharaides, and possibly NH_4^+. The presence of lysosomal efflux transporters (including Spin) are essential for exporting degraded products to avoid accumulation as mutations in these transporters lead to lysosomal storage diseases (Dermaut et al., 2005). Additionally, starvation was reported to induce Spin activities as abnormal lysosome function and morphology of *spin* mutants became more evident in nutrition-starved cells (Rong et al., 2011).

Compelling resemblances between AMF and Spin proteins strengthen the hypothesis that tonoplast-localised AMF proteins are crucial in nutrient recycling, particularly for NH_4^+. Efflux capability of MFS members have been reported previously, such as lysosomal amino acid transporter (LAAT1) with specific substrates glycine, alanine, proline and GABA (Boll et al., 2004) and Atg22, a vacuolar leucine effluxer (Yang et al., 2006). However, there is no evidence of an NH_4^+ efflux transport system. Therefore, based on the findings reported here, it is proposed that tonoplast-localised AMF proteins are vacuolar NH_4^+ efflux proteins required for NH_4^+ recycling following substrate degradation in the vacuole. It was also observed here that expression of AtAMF2 was up-regulated during N starvation and in senescing leaves (Figure 2.2 and 2.4 in Chapter 2. AMF studies in *Arabidopsis thaliana*).

3.4.6 Tonoplast-localized AMF proteins facilitate NH_4^+ efflux, but the mechanism is unclear

The exact transport mechanism of AMF proteins is yet to be defined. Based on the limited evidence available, it is suggested that AMF tonoplast-localised proteins function as uniport transporters. The acidic environment in the vacuole is maintained through vacuolar H^+-ATPase (V-ATPase) and vacuolar H^+-translocating inorganic pyrophosphatase (V-PPase) activities, which preserve high H^+ (proton) gradients across the tonoplast and acidify the vacuole. When a tonoplast-localised AMF protein facilitates NH_4^+ transport into the cytosol, it would also remove one proton equivalent from the vacuole. Then V-ATPase or V-PPase pumps another proton back into the vacuole to balance the proton gradient (Figure 3.12.B, D and E).

It is also intriguing to postulate that NH_4^+ efflux, alternatively, could happen following cation-coupled transport such as NH_4^+/H^+ or NH_4^+/K^+ antiport mechanisms. An antiporter family of DHA2 proteins of the Major Facilitator Superfamily (MFS) have been characterised as putative drug/H^+ antiporters in yeast (Dias and Sá-Correia, 2013). However, as the H^+ gradient between cytosol (pH ~7.0-7.5) and the vacuole (pH ~ 5.0-5.5) is large (1:100 based on pH), it is very unlikely that tonoplast-localised AMF

proteins operate as a NH_4^+/H^+ antiporter unless the NH_4^+ gradient is significant (vacuole to cytosol) to drive H^+ import against a concentration gradient. It is proposed that a vacuole of plant cells contains ~200 mM NH_4^+ while in the cytosol, NH_4^+concentration is ~1.5 mM (Coskun et al., 2013a). If the tonoplast-localised AMF was acting as an antiporter, it is likely to be an NH_4^+/K^+ antiporter. Kronzucker et al. (2003) demonstrated that the cytosolic K^+ concentration is flexible and the dynamic interaction between NH_4^+ and K^+ fluxes through plant cell membranes. Despite that NH_4^+ toxicity is enhanced at low [K^+], however the plasticity of the cytoplasmic K^+ concentration and the flexibility vacuolar K^+ concentration (Kronzucker et al., 2003) could make it possible for this mechanism to happen.

3.4.7 Functional activities of AtAMF1 and AtAMF3 in yeast remain unclear

Heterologous expression of AtAMF1 and AtAMF3 in various yeast strains did not give a clear understanding in regard to their potential functions in NH_4^+ transport. AtAMF1 failed to display any phenotype in all yeast strains overexpressing the protein. Similarly, the plasma membrane-localised AtAMF3 only exhibited limited capabilities to alleviate MA toxicity at pH 7.0 in 31019b (Figure 3.2), which indicated a potential role in facilitating MA efflux through the plasma membrane. This finding is in contrast to the other plasma membrane localised AMF homologs, ScAMF1 and GmAMF3, where both proteins were shown to facilitate MA influx (Chiasson et al., 2014). Therefore, further experiments in other expression systems (e.g. *Xenopus* oocytes or Sf9 cells) need to be carried out. Unfortunately, it was impossible to follow up these further investigations due to time constraints.

3.5 Supplementary materials of Chapter 3

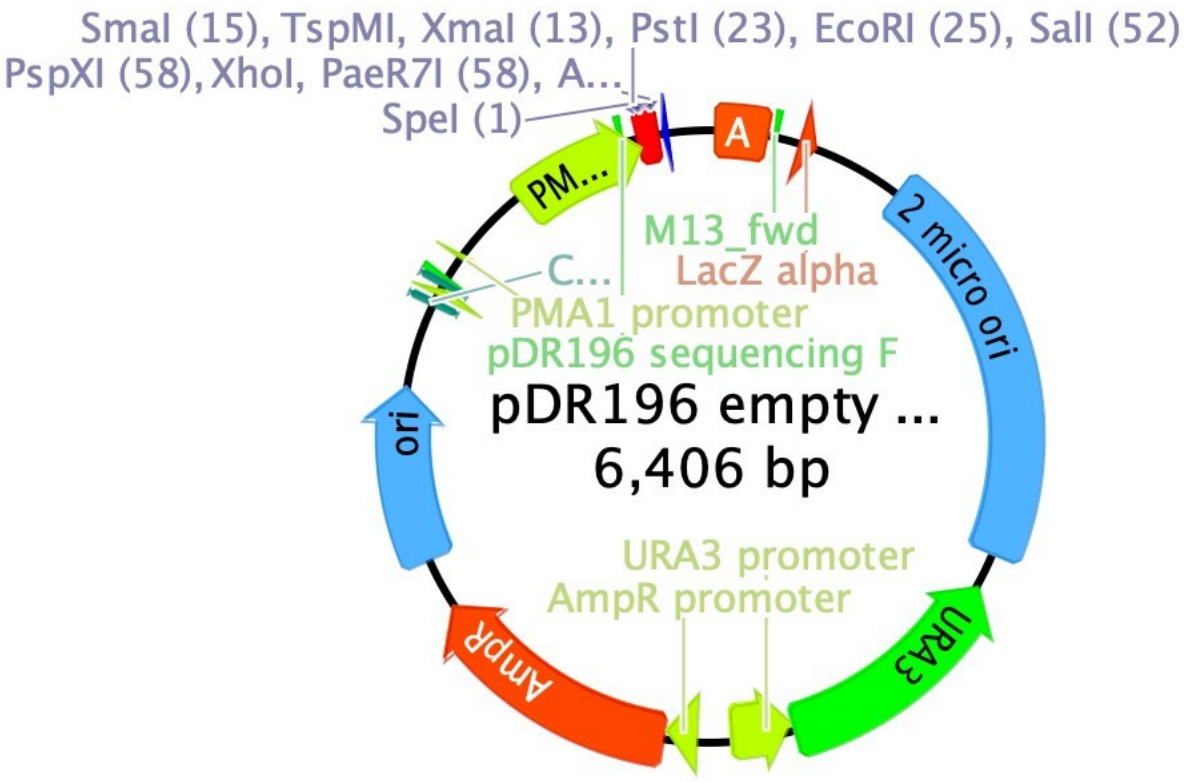

Supplemental Figure S3.1. Vector map of yeast expression vector pDR196.

Supplemental Figure S3.2. AtAMFs failed to rescue growth of 31019b on media containing 1 mM NH_4Cl at different pH levels.

Transformed 31019b (*mep1-3Δ*) cells failed to grow on SD-ura media containing 1 mM NH_4^+ as sole N source at pH 5.5, 6.0 and 6.5. Cells were grown at 28˚C for 6 d.

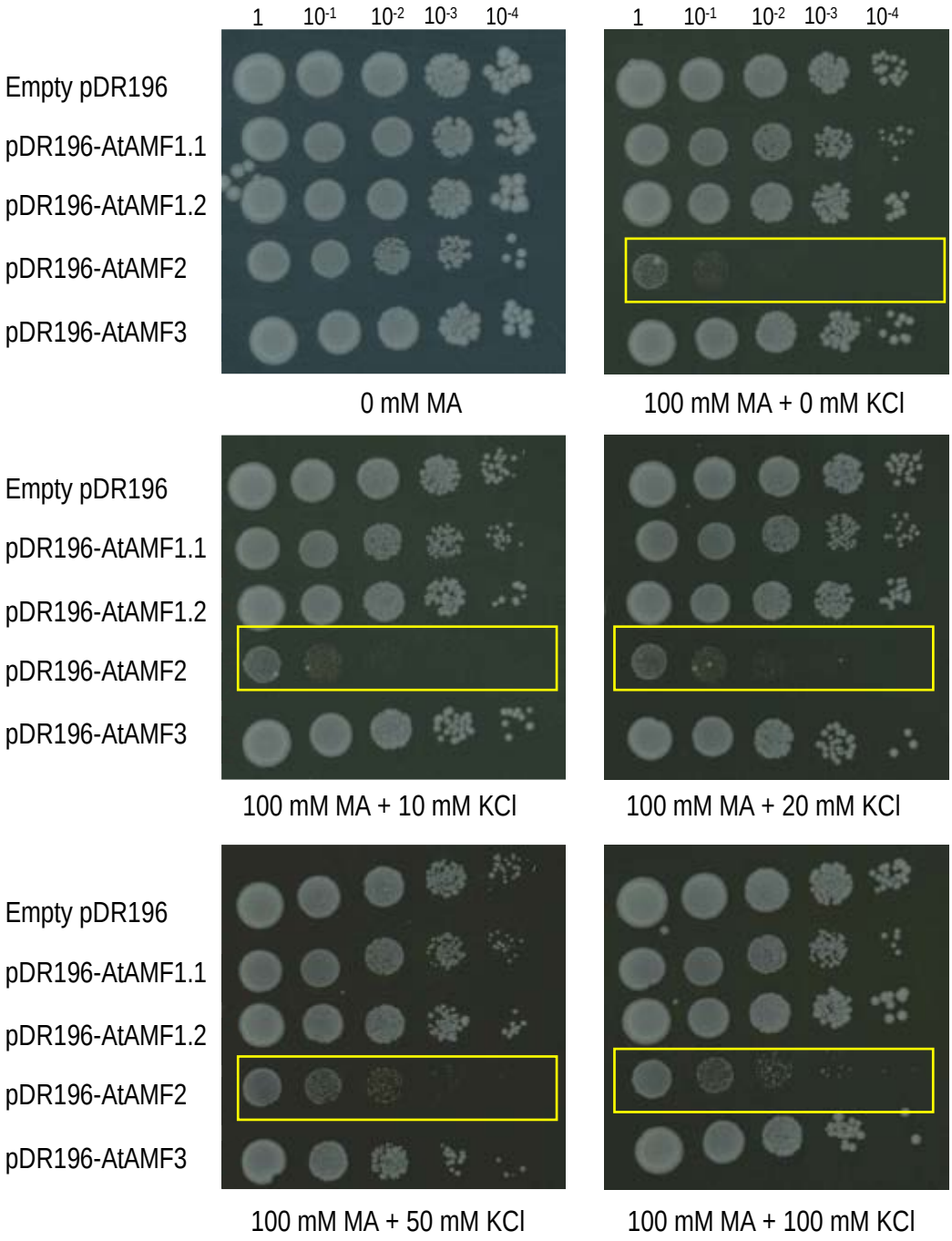

Supplemental Figure S3.3. Increased KCl concentrations overcomes MA toxicity in AtAMF2 transformed 31019b cells.

Transformed 31019b cells were grown on SD-ura media supplemented with 0.1% (w/v) proline, 2% (w/v) glucose, 100 mM MA and supplemented with increasing KCl (0, 10, 20, 50 and 100 mM) buffered at pH 6.5 with 50 mM MES-Tris. Basal [K^+] in SD-ura is 7.3 mM. Cells were grown at 28˚C for 10 d. Yellow outline boxes identify AtAMF2 inhibition growth on 31019b at different [K^+].

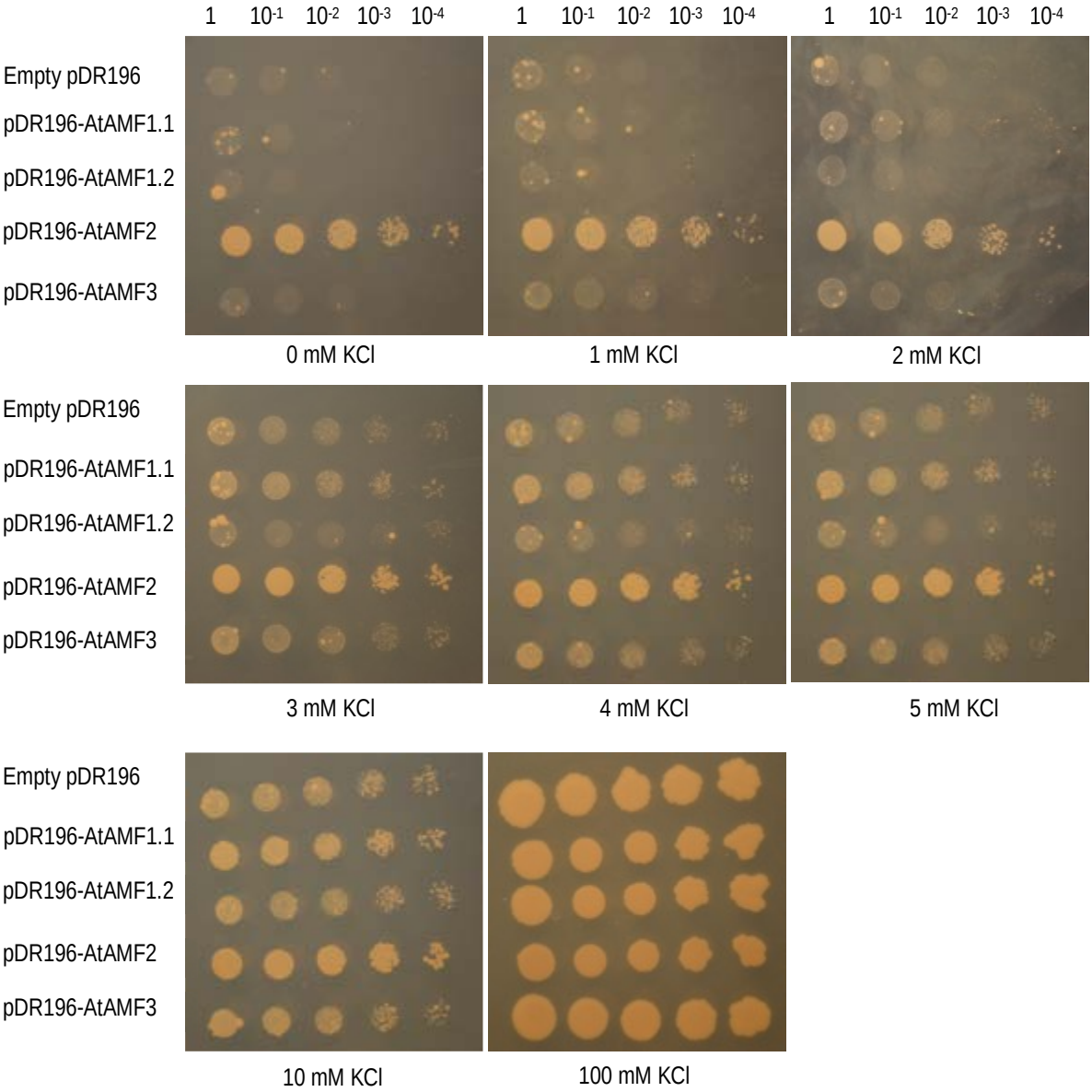

Supplemental Figure S3.4. CY162 growth improves with added KCl.

Transformed CY162 cells were grown on SD AA-ura media supplemented with 5 g/l $(NH_4)_2SO_4$ and increasing KCl of 1, 2, 3, 4, 5, 10, and 100 mM, pH 5.5. Basal [K^+] concentration is 7.3 mM. Cells were grown at 28˚C for 6 d. Empty vector controls can complement CY162 at external K^+ concentrations > 12 mM final K^+.

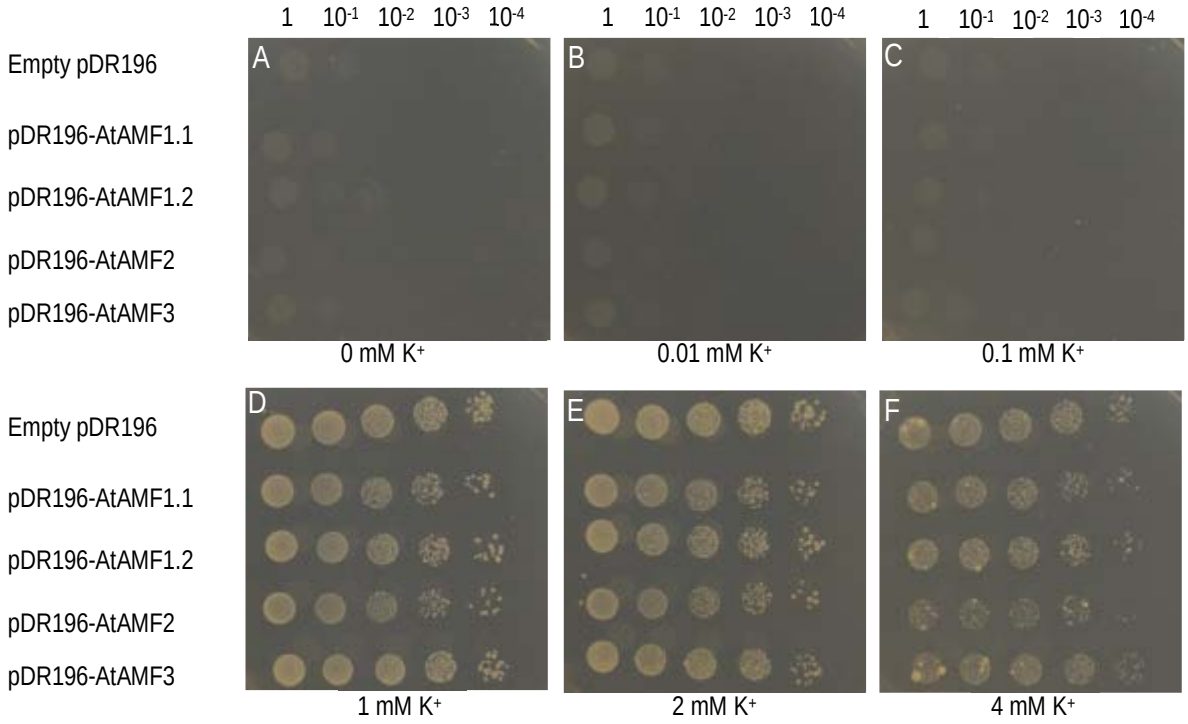

Supplemental Figure S3.5. Growth of CY162 overexpressing AtAMFs on K^+-dependent AP media with arginine as sole N source.

Arginine-phosphate (AP) media was used to grow CY162 cells at controlled K^+ concentrations (0-4 mM KCl). AP media contained 10 mM arginine, 2% glucose and was buffered at pH 6.1. AtAMFs failed to rescue growth on low (≤0.1 mM) K^+ but all cell lines regardless of construct grew at ≥ 1 mM K^+ (D-F). Cells were grown at 28˚C for 6 d.

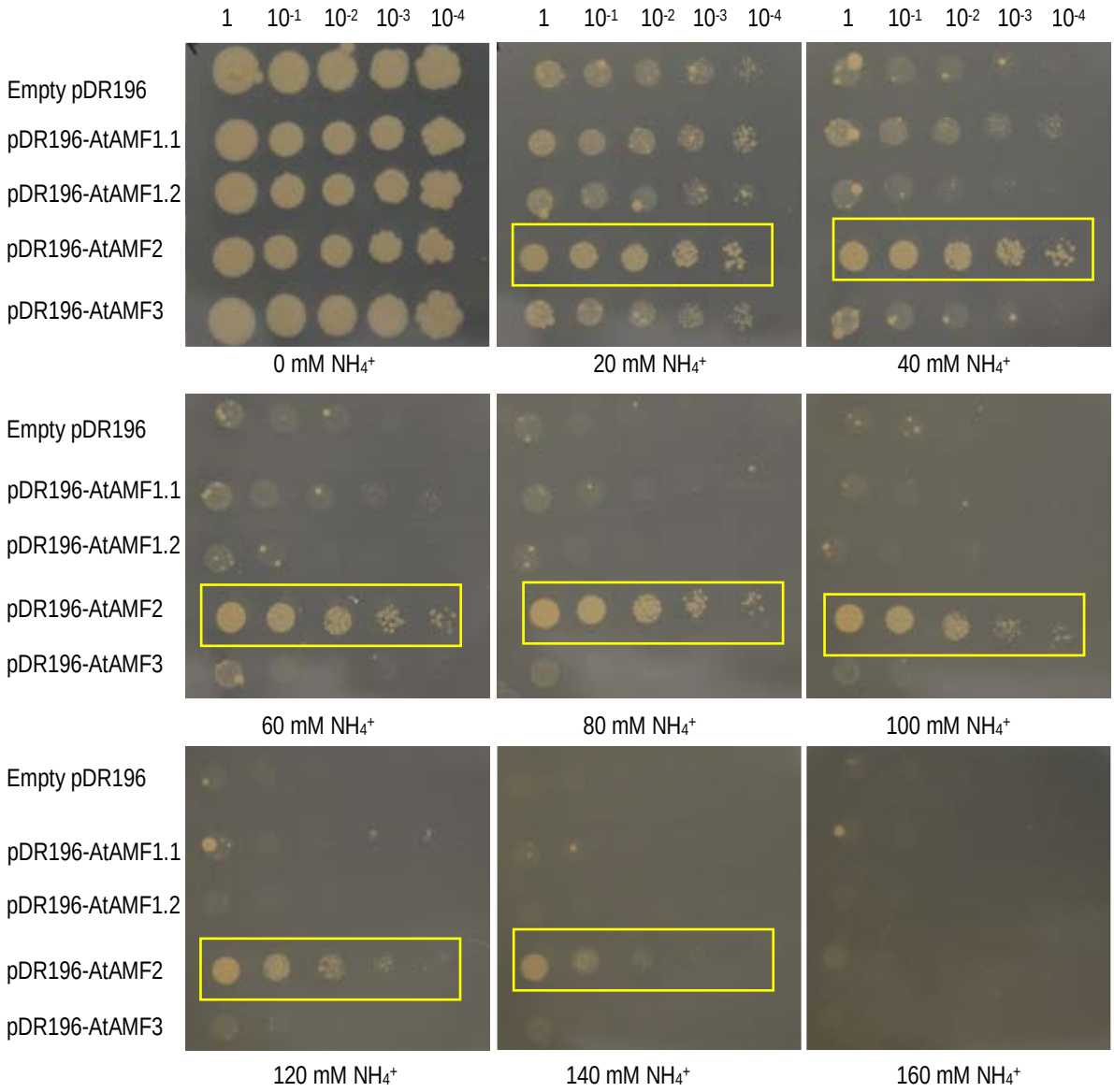

Supplemental Figure S3.6. Overexpression of AtAMF2 enables NH_4^+ tolerance in CY162. Transformed CY162 cells were grown SD AA-ura supplemented with increasing concentrations of $(NH_4)_2SO_4$. This media contain 7.3 mM K^+ and was buffered at pH 5.5 with 50 mM Tris-MES. Cells were grown at 28˚C for 6 d. Yellow boxes highlight AtAMF2 induced tolerance of CY162 to high concentrations of ammonium.

A. CY162

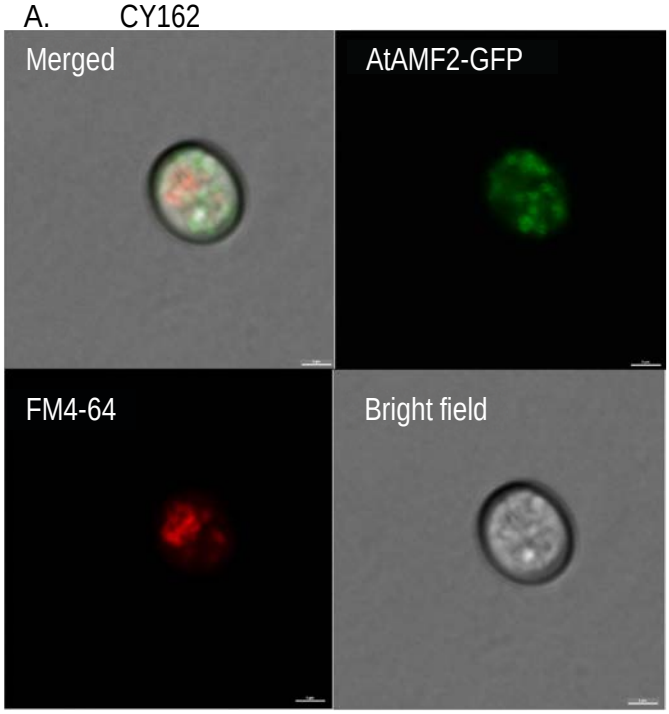

B. BY4741

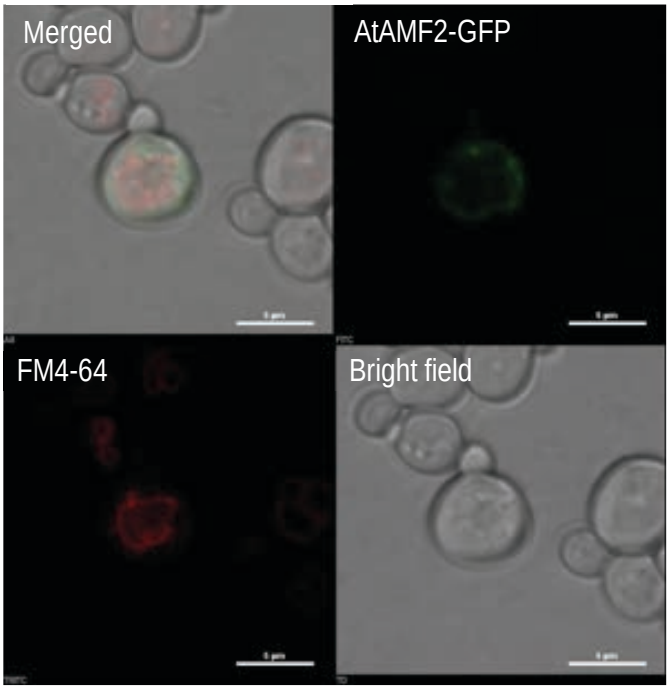

Supplemental Figure S3.7. AtAMF2-GFP fails to demonstrate evident localisation in tonoplast of BY4741 (A) and CY162 (B) cells.

GAP promoter driven AtAMF2-GFP displays localisation in cytoplasm and does not overlap with red signals which denote vacuoles specifically stained by FM4-64.

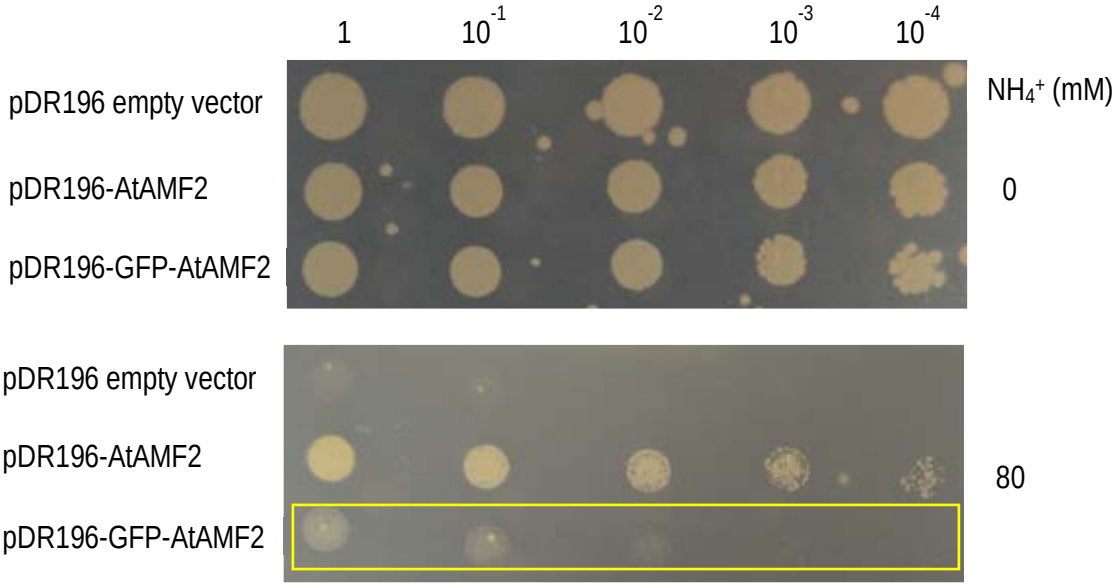

Supplemental Figure S3.8. Overexpression of GFP-AtAMF2 partially complements growth of CY162 at high NH_4^+.

Transformed CY162 cells were grown on SD AA-ura in the absence or presence of 80 mM NH_4^+. Cells were grown at 28°C for 6 d. Yellow box highlights partial rescue of GFP-AtAMF2 on CY162 strain at 80 mM NH_4^+.

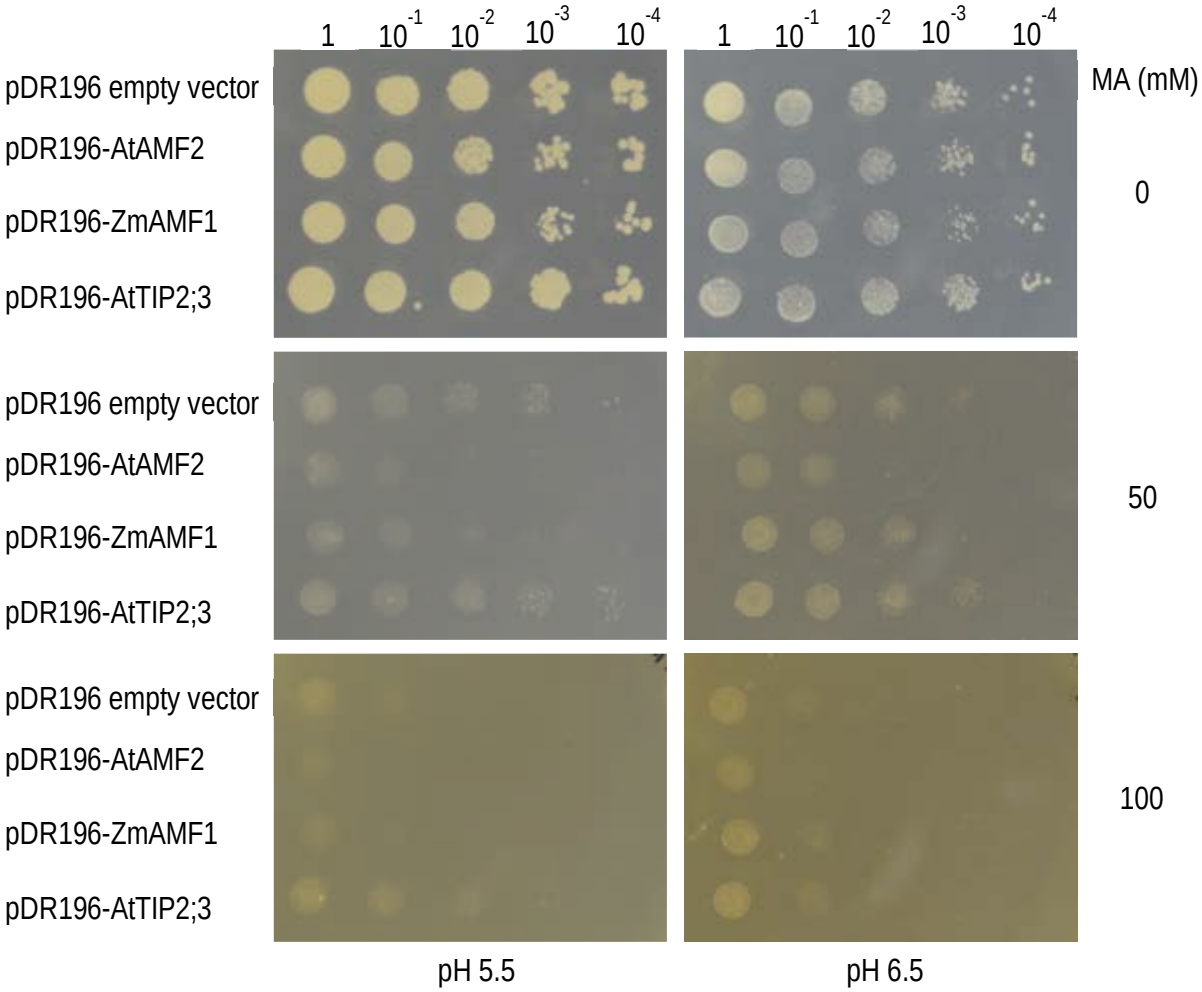

Supplemental Figure S3.9. MA sensitivity of CY162 strain increases at low external amino acid concentrations.

Transformed CY162 cells were grown SD-ura media supplemented with 0.1% proline (w/v) in the absence or presence of 50 and 100 mM MA. Media was buffered with 50 mM MES-Tris and pH adjusted to 5.5 and 6.5.

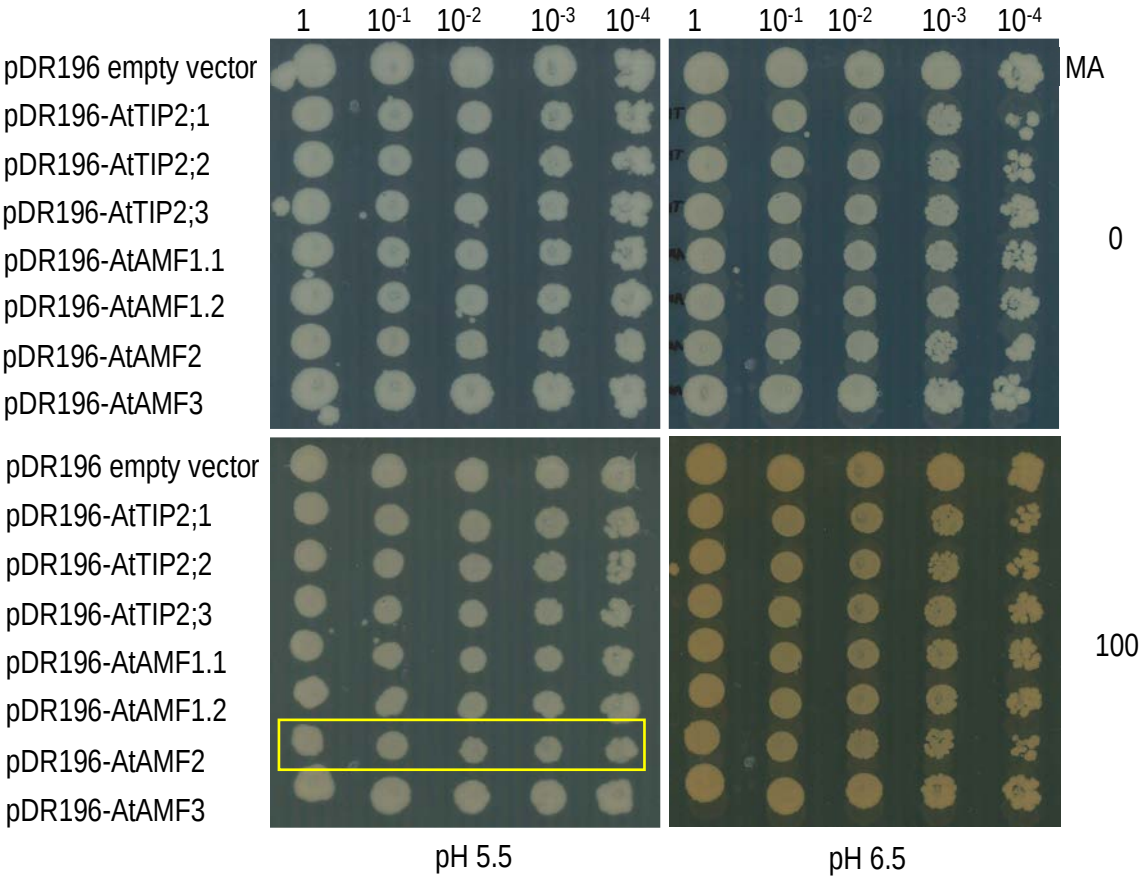

Supplemental Figure S3.10. All transformant of BY4741 were able to grow at toxic MA with adequate amino acids.

Transformed BY4741 cells were grown on SD AA-ura media with ± 100 mM MA. pH was adjusted with 50 mM MES-Tris. Cells were grown at 28°C for 6 d. A full complement of amino acids in SD AA-ura overcomes the AMF2-induced MA sensitivity (highlighted by yellow outlined box).

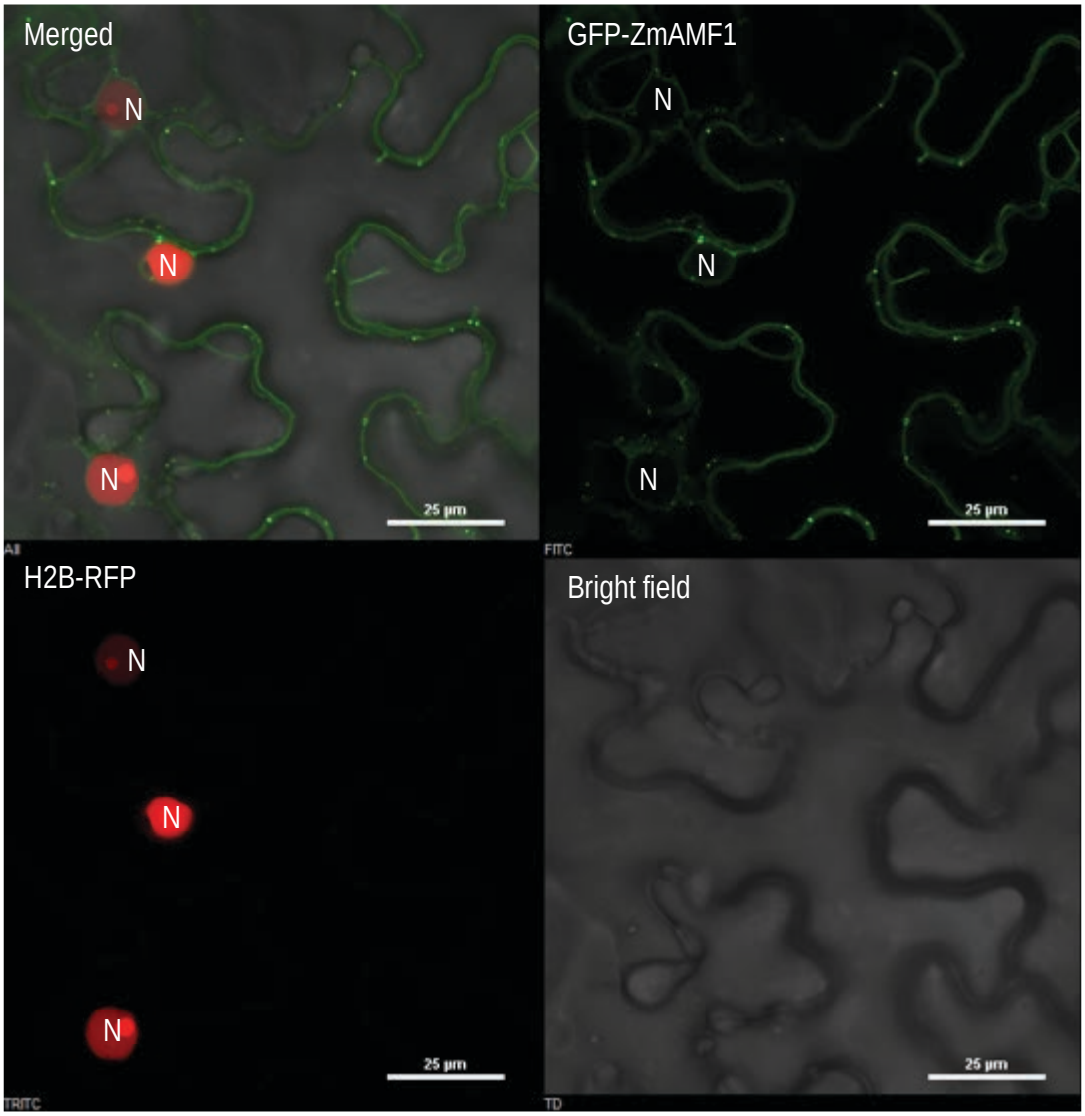

Supplemental Figure S3.11. Subcellular localisation of GFP-ZmAMF1 in transiently expressed *Nicotiana benthamiana* leaf cells

Confocal microscopy images were taken two days after infiltration into leaf tissues of *Nicotiana benthamiana* using *Agrobacterium tumefaciens* transformation. GFP-ZmAMF1 was co-expressed with a nuclear marker, H2B-RFP. RFP signals clearly identify nucleus (N). Scale bar = 25 µm.

Supplemental Table S3.1. List of yeast strains and their features

Yeast strain	Genotype	Special feature	Experiment purpose
31019b	MATa *ura3*, *mep1*Δ, *mep2* Δ::*leu2*, *mep3*Δ::KanMX2	Fail to grow with low NH_4^+ as sole nitrogen source	To investigate the ability of AtAMFs to facilitate NH_4^+ transport
CY162	MATa, *ura3–52*, *his3Δ200*, *his44–15*, *trk1*Δ, *trk2*Δ::pCK64	Fail to grow under low K condition	To investigate the ability of AtAMFs to facilitate K^+ transport
BY4741	MATa *his3Δ1 leu2Δ0 met15Δ0 ura3Δ0*	Wild type	To investigate the ability of AtAMFs to facilitate MA transport

Supplemental Table S3.2 Media used for yeast experiments

Media	Compositions	N level
SD-ura	Basal component: 1.7 g/l Yeast Nitrogen Base (YNB) without amino acid and $(NH_4)_2SO_4$ (Difco: DF0335-15-9) Nitrogen source: depending on experiments.	N is unavailable
SD AA-ura	Basal component: Basal component: 1.7 g/l Yeast Nitrogen Base (YNB) without amino acid and $(NH_4)_2SO_4$ (Difco: DF0335-15-9) Nitrogen sources: 1.92 g/l Yeast synthetic drop-out media supplement without uracil (Sigma: Y1501)	Complete amino acids available
Medium M	Based on Ramos and Wiame (1997). Supplemental Table S3.2.1 details all compositions	0.1% proline available
Arginine-phosphate (AP) media	Based on Rodrigues-Navarro and Ramos (1984). Supplemental Table S3.2.2 details all compositions	10 mM arginine available
Low Amino N (LAN)	Basal component: Basal component: 1.7 g/l Yeast Nitrogen Base (YNB) without amino acid and $(NH_4)_2SO_4$ (Difco: DF0335-15-9) Nitrogen sources: 76 mg/l histidine, 380 mg/l leucine, 76 mg/l methionine and 1 g/l proline	0.1% proline available with limited concentrations of histidine, leucine and methionine
High Amino N (HAN)	Basal component: Basal component: 1.7 g/l Yeast Nitrogen Base (YNB) without amino acid and $(NH_4)_2SO_4$ (Difco: DF0335-15-9) Nitrogen sources: 2 g/l histidine, 4 g/l leucine, 2 g/l methionine and 1 g/l proline	0.1% proline available with high concentration of histidine, leucine and methionine

Supplemental Table S3.2.1 Medium M compositions

Solution I (basal solution)	Mass or volume per litre
$MgSO_4.7H_2O$	0.7 g
KH_2PO_4	1 g
$CaCl_2.2H_2O$	0.4 g
NaCl	0.5 g
K_2SO_4	1 g
Citric acid.H_2O	10.5 g
10 M KOH	16 ml
pH: 6.1 with 10 M KOH	

Solution II (trace metal solution): 1000X stock	Mass per litre
H_3BO_3	10 mg
$CuSO_4.5H_2O$	1 mg
KI	2 mg
$Na_2MoO_4.2H_2O$	4 mg
$ZnSO_4.7H_2O$	14 mg
Citric acid.H_2O	10 mg
$MnSO_4.H_2O$	400 mg
$FeCl_3.H_2O$	5 g

Solution III (vitamin solution): 100X stock	Mass per litre
D-biotin	250 ug
Thiamine-HCl	100 mg
Inositol	1 g
Calcium-D-pantothenate (D-pantothenic acid hemicalcium salt)	200 mg
Pyridoxine-HCl	100 mg

Solution II and III must be autoclaved prior to use. Solution I must be made fresh each time. To make 1 l final solution, 1 ml solution II and 10 ml solution III are added into solution I together with 20 g glucose (2% w/v). Concentration of NH_4^+ or MA are adjusted accordingly.

Supplemental Table S3.2.2 Arginine-phosphate (AP) media compositions

	Components	Final concentration
Carbon	Glucose	2%
Nitrogen source	L-arginine	10 mM
Phosphate	phosphoric acid	8 mM
Magnesium	MgSO4.7H2O	2 mM
Calcium	CaCl2 (anhydrous)	0.2 mM

Vitamins	Mass per litre
Biotin	20 ug
Calcium pantothenate	2 mg
Folic acid	2 ug
Inositol	10 mg
Niacin (nicotinic acid)	400 ug
p-Aminobenzoic	200 ug
Pyridoxine-HCl	400 ug
Riboflavin	200 ug
Thiamine-HCl	400 ug

Trace elements	Mass per litre
Boric acid	500 ug
Copper sulphate	40 ug
Potassium Iodide	100 ug
Ferric chloride	200 ug
Manganese sulphate	400 ug
Sodium molybdate	200 ug
Zinc sulphate	400 ug

Supplemental Table S3.3. Primer pairs for cloning into yeast expression vector

Primer name	Primer sequence (5'-3')	Purpose
pDR196-AMF1-SpeI-F	CCTCAACTAGTATGGTGACCAAAGAAGAA	To clone AtAMF1.1 and AtAMF1.2
pDR196-AMF1-XhoI-R	CAATACTCGAGTTATGAATATCCCTTGCA	
pDR196-AMF2-SpeI-F	CACGAACTAGTATGGATGTTGACGGAGAA	To clone AtAMF2
pDR196-AMF2-XhoI-R	ATATACTCGAGTCATGCTTCCTGGAGAAG	
pDR196-AMF3-SpeI-F	CAACGACTAGTATGACGAGAGTTGGCCAG	To clone AtAMF3
pDR196-AMF3-XhoI-R	CGAAGCTCGAGTTAGGCGAGAGTAGAGTT	
pDR196-AtTIP21-EcoRI-F	TAATAGAATTCATGGCTGGAGTTGCCTTT	To clone AtTIP2.1
pDR196-AtTIP21-XhoI-R	ACCTACTCGAGTTAGAAATCAGCAGAAGCA	
pDR196-AtTIP22-EcoRI-F	TCCTAGAATTCATGGTGAAGATTGAGATAGGA	To clone AtTIP2.2
pDR196-AtTIP22-XhoI-R	ATATACTCGAGTCAAGGGTAGCTTTCTGTGGT	
pDR196-AtTIP23-EcoRI-F	AGTTAGAATTCATGGTGAAGATCGAAGTTGG	To clone AtTIP2.3
pDR196-AtTIP23-XhoI-R	ATATACTCGAGTTACACTCGGATCTCACGG	
pDR196-GFP-SpeI-F	ATTTACTAGTATGGTGAGCAAGGGCGAG	To clone GFP-AtAMFs (combined with reverse primer of each cloning primer pair)
AtAMF2-F	CACCATGGATGTTGACGGAGAA	To clone AtAMF2 without stop codon
AtAMF2-R-no stop	TGCTTCCTGGAGAAGAGGCG	

4. Phenotypic analysis of *Arabidopsis thaliana amf* mutant lines

4.1 Introduction

4.1.1 Arabidopsis mutant lines for functional studies

Arabidopsis thaliana has been utilised as a model plant for more than 50 years. Features of Arabidopsis include, a small sequenced and annotated genome, high-level omic resources available online, high seed productivity yet short seed reproduction time, ease of crossing and an uncomplicated process for mutagenesis and mutant screening. Collectively these attributes have made Arabidopsis a fundamental research tool for gene functional characterization studies in plants (Provart Nicholas et al., 2015). Before whole genome sequence data of Arabidopsis became available, most gene characterization studies were conducted using forward genetic approaches. This required the generation of large, randomly mutagenized populations of plants and their individual screening for desired phenotypes, followed by fine mapping of the genes responsible for the phenotype and sequencing the genomic region for the target gene. Identified mutants were then subject to complementation assays to confirm the observed phenotype (Alonso and Ecker, 2006).

Following the completion of the Arabidopsis whole genome sequencing project, thousands of new genes have been identified and the available information has enabled researchers to characterize their respective genes of interest using a directed reverse genetic approach. Accordingly, identification and functional characterization of ammonium transporters (AMTs) in Arabidopsis was accelerated by the availability of T-DNA mutants. By utilising the *amt1;1* mutant, Kaiser et al. (2002) revealed a reduction of between 30 and 40% NH_4^+ uptake in the mutant plants compared to WT plants. Similarly, disruption of both AtAMT1;1 and AtAMT1;3, further reduced the NH_4^+ uptake capability of a double knockout (*dko*) mutant *amt1;1amt1;3* up to 60-70%, suggesting an additive contribution of the proteins (Loque et al., 2006). Furthermore, combination of single mutant lines to generate plants harbouring multiple mutations e.g. quadruple knockout (*qko*) has led to a deeper understanding of the organization of the transporters involved in NH_4^+ uptake pathway in Arabidopsis (Yuan et al., 2007). These studies have demonstrated the benefits of T-DNA mutant lines in functional studies of ammonium transport proteins.

Aside from beneficial features of the mutants, gene redundancy in the Arabidopsis genome must be taken into consideration when considering observed results with Arabidopsis T-DNA mutants. Often, closely related genes are functionally redundant, thus generation of mutants with multiple mutations and or combinations are necessary to develop noticeable phenotypes. Furthermore, understanding how different family members of genes interact is crucial to help interpret results generated from experiments using single and multiple mutations (Mani et al., 2008). For example, individual mutations of K^+ transporters HAK5 and AKT1 displayed visibly indistinguishable phenotypes compared to WT plants grown at 100 μM K^+. On the other hand, the double mutant *athak5 akt1* failed to germinate when grown

under similar conditions (Pyo et al., 2010). Nevertheless, it is feasible to employ *Arabidopsis* mutants for studying genes with limited information, including the Ammonium Major Facilitator (AMF) family. The aim of this chapter was to functionally characterize the AMF proteins using *amf* mutant lines by applying similar strategies used in previous AtAMT studies.

4.2 Materials and Methods

T-DNA knockout mutant lines were used to characterize the functionalities of the AMF family. Mutant lines SAIL_692_G04, SAIL_164_G06 and SAIL_569_G01 represent the target genes AtAMF1, AtAMF2 and AtAMF3, respectively, and wild type (WT) Columbia-0 (Col-0) was used as a control. All seed stocks were obtained from Nottingham Arabidopsis Stock Centre (NASC). All mutants were backcrossed to WT (Col-0) two times prior to the development of double knockout (*dko*) mutants.

4.2.1 Mutant development and genotyping

PCR-based screening on both genomic DNA and cDNA was utilised to confirm homozygosity of the backcrossed mutants. DNA was extracted following the method described by Edwards et al. (1991). RNA was isolated from 7-day-old seedlings grown under control condition at 1 mM NH_4NO_3. cDNA was generated as previously described in Chapter 2.2.2. Gene specific primer pairs and a combination of gene specific primers and left border (LB) T-DNA specific primers were used to amplify the gene sequence and the T-DNA insertion, respectively. Additionally, cloning primer pairs were used to amplify transcripts of each target gene. Primer pairs for genotyping are detailed in Supplemental Table 4.1.

Following confirmation of homozygous *sko* mutants (*amf1*, *amf2* and *amf3*, respectively), development of double knockout (*dko*) mutants were carried out by crossing each *sko* line to each other to generate *dko amf1amf2*, *amf1amf3* and *amf2amf3*. Homozygosity confirmation was confirmed using the same strategies as was done for *sko* mutant lines.

4.2.2 Preliminary physiological phenotyping of *sko amf* mutant lines

Investigation of *amf* dysfunctionalities impacting on the *sko* mutant lines was conducted. Plants were grown for six weeks in an aerated hydroponic system at 1 mM NH_4NO_3 (growing solution) prior to measurement of parameters. Composition of hydroponic media is detailed in Supplemental Table 4.2. Prior to $^{15}NH_4^+$ uptake experiments, net assimilation rate, stomatal conductance and transpiration rate were recorded using an infrared gas analyser (LCi Ultra Compact Photosynthesis System-ADC). Then, the same plants were used for short-term (5 min) $^{15}NH_4^+$ uptake experiments in which the 1 mM NH_4NO_3 was replaced with 0.5 mM $(^{15}NH_4)_2SO_4$ (flux solution). After 10 min incubation in growing solution, the plants were transferred into the flux solution for 5 min, followed by a 10 min rinse in a fresh growing solution. Afterwards, the root tissues were dried and separated from the shoot tissues and immediately oven-dried at 60^{o}C for two weeks. Dried samples were finely ground and ~ 3 mg powder was used for ^{15}N determination using isotope ratio mass spectrometry (Hydra 20-20, SerCon Ltd, Crewe, UK).

4.2.3 Hypocotyl growth at high NH_4^+ and MA

For hypocotyl growth, basal media was identical as previously described in Chapter 2.2.5 with modified N supply (the basal media contain 3.75 mM K^+). Surface sterilised seeds were directly germinated on solid media containing either 1 mM NH_4NO_3 (control), 20 mM NH_4Cl or 20 mM MA (as a

chloride salt). Plates were vernalised in the dark at 4˚C for two days and then put under light at 110-120 μmol m^{-2} s^{-1} Photosynthetically Active Radiation for 6 h to induce germination. The plates were then completely covered with aluminium foil and grown vertically in a growth chamber at 22˚C for 7 d.

4.2.4 MA toxicity experiments at low NO_3^- concentration

Identical media composition, seed sterilisation and germination protocols as described in the Materials and Methods section of Chapter 2 were used for the MA toxicity experiments with modified N treatments (the basal media contain 3.75 mM K^+). In these particular experiments, NH_4NO_3 was replaced with 0.05 mM KNO_3 (low NO_3^-). This concentration was chosen based on preliminary experiments (data not shown) and corresponding to a previous report using a similar formulation (Zheng et al., 2015). Depending on the experiments, low NO_3^- media was supplemented with 0, 5, 20 mM MA or 20 mM NH_4Cl. Identical media was used for root growth and split-media experiments.

The split-media experiments were conducted following the method of Li et al. (2011) with modification. Briefly, plastic strips (3 mm wide) were made using a 3D printer to fit a standard 10 x 10 cm square petri dish (Sarstedt). To avoid media contamination, one lukewarm media solution was poured at a time. Once the first solution was solidified, the second solution was poured. The strips were removed after both media were completely solidified. 5-day-old seedlings germinated on 1 mM NH_4NO_3 were carefully transplanted onto the split-media, where only shoot or root tissues had direct contact with each of the different media.

4.2.5 NH_4^+ toxicity experiments at low K^+ concentration

For experiments with low K^+ concentration, *in-vitro* media was made according to Hirsch et al. (1998) with added vitamins detailed in Supplemental Table 4.3. KCl was added to adjust the K^+ concentration in the media. To make NH_4-free media, $NH_4H_2PO_4$ was replaced with H_3PO_4 to maintain PO_4^- concentration in the media.

4.3 Results

4.3.1 Development of homozygous single and double knockout *amf* mutants

Homozygous knockout lines of SAIL_692_G04 (*amf1*), SAIL_164_G06 (*amf2*) and SAIL_569_G01 (*amf3*) were confirmed using PCR amplification of the target gene and the flanking T-DNA sequences (Figure 4.1.A and B) using isolated genomic DNA templates. A disruption in transcript expression was confirmed using RT-PCR on tissue specific cDNA templates (Figure 4.1.C). Based on the T-DNA amplified sequence and database searches (http://signal.salk.edu/tdnaprimers.2.html), schematic representations of the predicted T-DNA insertion location were generated with each AMF family member (Figure 4.1. D-F). Following the development of the homozygous single knockout (*sko*) mutant lines, double knockout (*dko*) mutant lines were generated by crossing each of *sko* to each other to generate *amf1amf2*, *amf1amf3* and *amf2amf3* combination. Each *sko* was first backcrossed to Col-0 WT twice prior to the development of the *dko* lines. The homozygosity of each *dko* combination was confirmed by PCR amplification of genomic DNA (Figure 4.2). An attempt to develop triple knockout mutant lines (*tko*) was initiated by crossing homozygous *dko amf2amf3* to both *amf1amf2* and *amf1amf3*. However, due to time constraints and difficulty in identifying a homozygous line, only heterozygous *tko* lines were obtained.

4.3.2 Preliminary physiological phenotyping on homozygous *sko*

To identify phenotypic changes due to the AMF mutations, preliminary growth experiments were conducted on each of the homozygous *sko* mutant lines. The results demonstrated that final shoot dry weights of *amf2* and *amf3* were found to be 25% smaller (significant at $p < 0.05$) than the WT (Figure 4.3.A). Additionally, all *sko amf* mutants had significant ($p < 0.05$) reduction (20-30%) of root dry weights relative to the WT (Figure 4.3.B). Interestingly, the *amf1* mutant showed a significant ($p < 0.05$) increase in constitutive $^{15}NH_4$ uptake into root tissues while *amf2* and *amf3* were comparable to the WT controls (Figure 4.3C). Furthermore, net assimilation, stomatal conductance and transpiration rates of the same plants used for the uptake experiments, were found to be similar to the WT controls (Supplemental Figure S4.1.A-C). Similarly, $^{15}NH_4$ transfer to shoot tissues of the *sko* mutant lines was minimal and did not show a significant difference compared to the WT (Supplemental Figure S4.1.D).

4.3.3 MA toxicity impact is more severe at low NO_3^- concentration

In light of the *amf1* mutants showing higher rates of $^{15}NH_4^+$ uptake into root tissues, further experiments were conducted utilising methylammonium (MA) as a proxy for NH_4^+ transport. As previously shown by Yuan et al. (2007), exposure to MA in Arabidopsis lines with active NH_4^+ transport pathways result in inhibited root growth relative to those where NH_4^+ transport pathways are disrupted. A recent study has shown that MA impacts hypocotyl growth providing an alternative screen for both NH_4^+ transport and sensitivity to toxic concentrations of both NH_4^+ and MA (Straub et al., 2017). WT and *amf* mutant lines (*sko* and *dko*) were germinated in the dark on control (1 mM NH_4NO_3) and treatment (20 mM NH_4Cl or 20 mM MA) media to test for inhibitory effects of high NH_4Cl or MA on hypocotyl growth. At 20 mM NH_4Cl,

only the *dko, amf2amf3,* showed a reduction (17%) in hypocotyl growth ($p < 0.05$) (Figure 4.4). When supplied 20 mM MA, hypocotyl length was more affected (Figure 4.4, Supplemental Figure S4.2). In WT plants, there was a reduction of 30%, while the mutant plants had a reduction ranging between 37- 47% relative to the control. Compared to the WT, all mutant plants, except for *amf2*, showed significant ($p < 0.05$) hypocotyl length reduction, with the *dko* mutant lines exhibiting a more severe reduction (Figure 4.4). These data show that exposure of MA resulted in a stronger inhibitory effect on hypocotyl growth compared to that of NH_4Cl. Additionally, visual observations revealed that root tissues of the MA-treated plants (Supplemental Figure S4.2.C) were shorter than the plants grown on the control media (Supplemental Figure S4.2.A) as well as that on NH_4Cl (Supplemental Figure S4.2.B).

Subsequent experiments were then carried out to test the inhibitory effect of NH_4^+ and MA on root growth across the *amf* mutant lines. A previous study had shown that elevated NO_3^- can alleviate NH_4^+ toxicities in plants (Hachiya et al., 2012). A preliminary experiment was first conducted with WT plants to test the ratio of NO_3^- to NH_4^+/MA to initiate root growth inhibition. These experiments (data not shown) indicated that 0.05 mM NO_3^- was a concentration where WT plants were able to grow without NH_4^+ but where NH_4Cl (20 mM) significantly inhibited root growth. A similar concentration was used in another report investigating NH_4^+ toxicity effect on the *slah3* mutant (Zheng et al., 2015). Plants were then grown on 0.05 mM NO_3^- with either 5 or 20 mM MA and root growth measured after 7 d. MA had a inhibitory effect on root growth on *amf1* and the *dko* mutant lines *amf1amf2* and *amf1amf3* grown at 5 or 20 mM MA for seven days Figure 4.5.B. This phenotype was less noticeable on 20 mM NH_4Cl (Supplemental Figure S4.3). At 5 mM, *amf1* plants had a primary root growth reduction of 45% and 80% at 20 mM MA compared to the WT with 30% and 65% reduction at 5 and 20 mM MA relative to the control (0 mM MA), respectively. Furthermore, *dko* mutants with *amf* backgrounds (*amf1amf2* and *amf1amf3*) showed greater primary root growth reduction of 60% and 85% at 5 and 20 mM MA relative to control conditions, respectively. The *dko amf2amf3* mutant only had a 35% and 75% primary root growth reduction at the same concentrations of MA. These data indicate that AMF1 might have a dominant role compared to AMF2 and AMF3 in NH_4^+/MA toxicity tolerance in Arabidopsis when grown under low NO_3^- concentrations.

As NH_4^+ toxicity can occur from exposure to either root (Britto and Kronzucker, 2002) or shoot tissues (Nielsen and Schjoerring, 1998; Britto Dev et al., 2002; Li et al., 2011), a subsequent set of experiments were carried out using a split-medium assay to localise NH_4^+ exposure to either root or shoot tissues. The results demonstrated that direct contact of root tissues to MA caused more significant growth inhibition compared to direct contact of MA to shoot tissues, and the effect of MA exposure to root tissues was visibly noticeable (Supplemental Figure S4.4.C and D). The mutants *amf1*, *amf1amf2* and *amf1amf3* failed to show root growth three days following exposure to high MA (Supplemental Figure S4.4.A). These results were similar to previous findings that suggest a role of AMF1 in managing NH_4^+ toxicity possibly linked to the control of net NH_4^+ root uptake (Figure 4.3.C).

4.3.4 *amf2amf3* mutant displays hyper-sensitivity to NH_4^+ at low K^+ concentration

As previously discussed, root growth of the *amf dko* mutants containing crosses with *amf1* was inhibited when grown in the presence of 5 mM MA, low NO_3^- concentrations and adequate K^+ (3.75 mM). This response was also tested in a series of experiments using NH_4^+ (2 mM) and across a range of increasing K^+ concentrations (10, 100 and 1000 μM) in the presence of adequate NO_3^- (7.5 mM) in order to test the relationship between K^+ and NH_4^+ toxicity. At 1 mM K^+, visual plant growth between the *amf dko* and the WT control were similar in the presence (Figure 4.6.A) or the absence of 2 mM NH_4^+ (Figure S4.5). When the K^+ concentration was reduced to 100 or 10 μM, only the *dko* mutant, *amf2amf3* showed a visibly poor growth phenotype (Figure 4.6.A). Primary root growth (%) was reduced by 55% and 45% (Figure 4.6.B) and whole plant biomass reduced by 87% and 80% at 10 μM and 100 μM K^+, respectively relative to growth on 1 mM K^+ (Figure 4.6.C). In a number of lines there were significant changes in growth rate and fresh weight, but these changes were relatively small and often not consistent across the two K^+ concentrations (Fig 4.6B, C). When 5 mM MA was added to the media, the *dko* mutant *amf2amf3* displayed a further biomass reduction but across all K^+ concentrations tested (10 μM, 100 μM and 1 mM K^+) (Figure 4.7). Together these data confirm that the *amf2amf3* mutant would appear to be hyper-sensitive to both NH_4^+ and MA, with MA sensitivity overriding the impact of elevated K^+.

In order to understand whether the growth inhibition was caused by a delay in germination, a subsequent experiment was conducted in which seeds were germinated for four days on NH_4^+-free media containing 1 mM K^+ prior to their transfer to low K^+ (10 μM) media with or without 2 mM NH_4^+. Figure 4.8 shows that only *amf2amf3* plants displayed significant biomass reductions when transferred to 2 mM NH_4^+ and 10 μM K^+. These findings indicated that the growth inhibition suffered by *amf2amf3* mutant was caused by a hyper-sensitivity response to NH_4^+ and not by poor germination on the selection media.

A series of subsequent experiments were conducted to examine the effect of low K^+ when plants were grown with adequate (7.5 mM) or low (0.05) NO_3^- in the presence of 2 mM NH_4^+. Results from these experiments consistently showed that *amf2amf3* was hyper-sensitive to NH_4^+ under a low K^+ diet. However, when grown with adequate NO_3^- levels, primary root growth of the *amf2amf3* mutant also progressively reduced overtime (Supplemental Figure S4.7.A). NH_4^+ treatments also impacted the development of lateral root numbers in *amf1amf2*, *amf1amf3* and *amf2amf3* (Supplemental Figure S4.7.B). Similarly, under low NO_3^-, *amf2amf3* showed a reduction in primary root growth (Supplemental Figure S4.7.C) and a significant reduction in lateral root numbers. It was also observed that lateral root number of *amf2amf3* plants grown under low NO_3^- conditions was higher (almost double) compared to the number under adequate NO_3^- provision (Supplemental Figure S4.7.D). Collectively the response of the roots would suggest both AMF2 and AMF3 have a role in root structural architecture in Arabidopsis. Further studies are required to understand this particular trait.

A. Gene sequence amplification

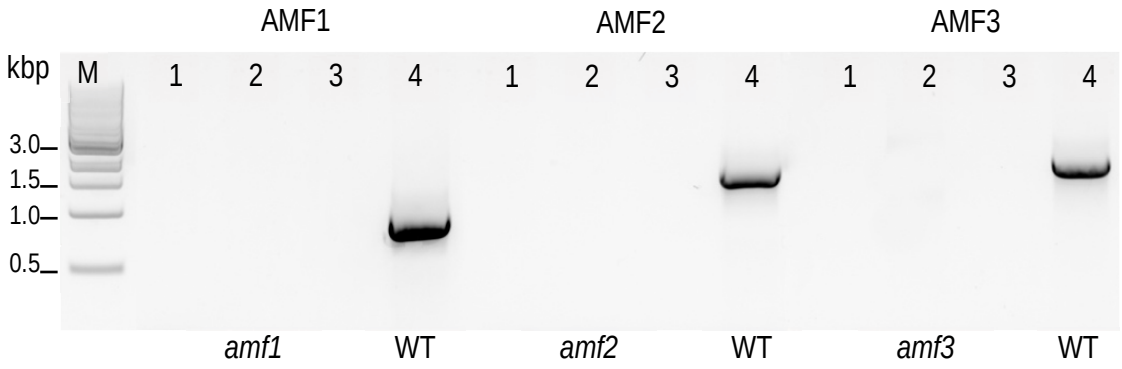

B. T-DNA sequence amplification

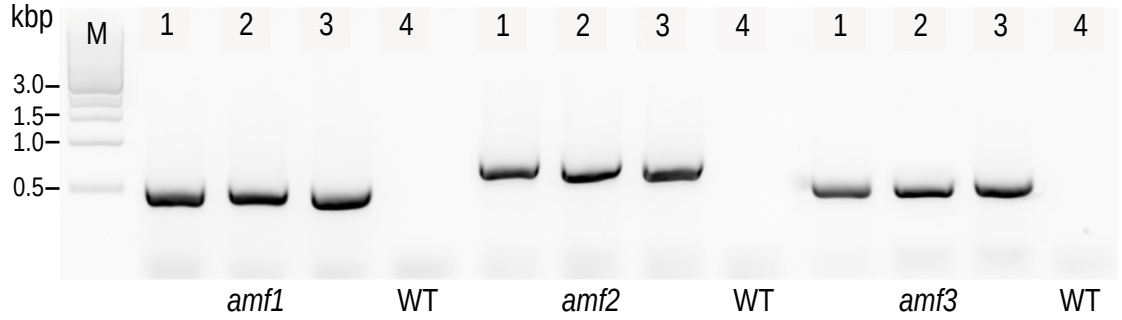

C. Transcript amplification

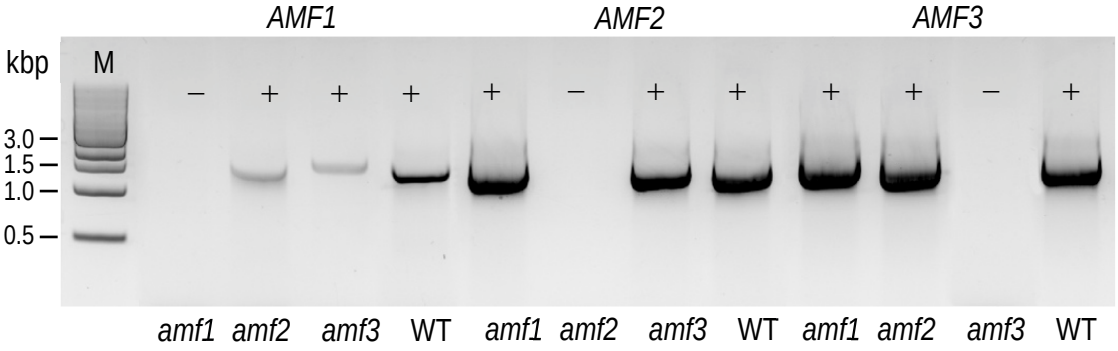

D SAIL_692_G04/*amf1*

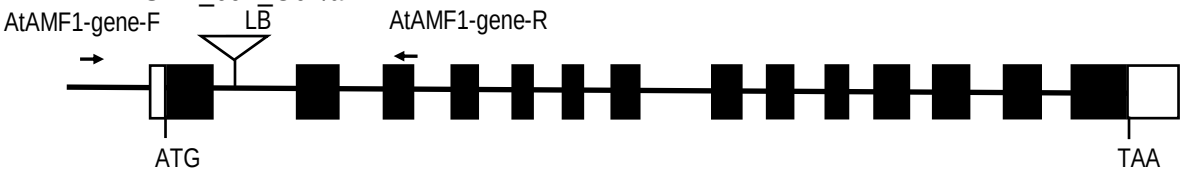

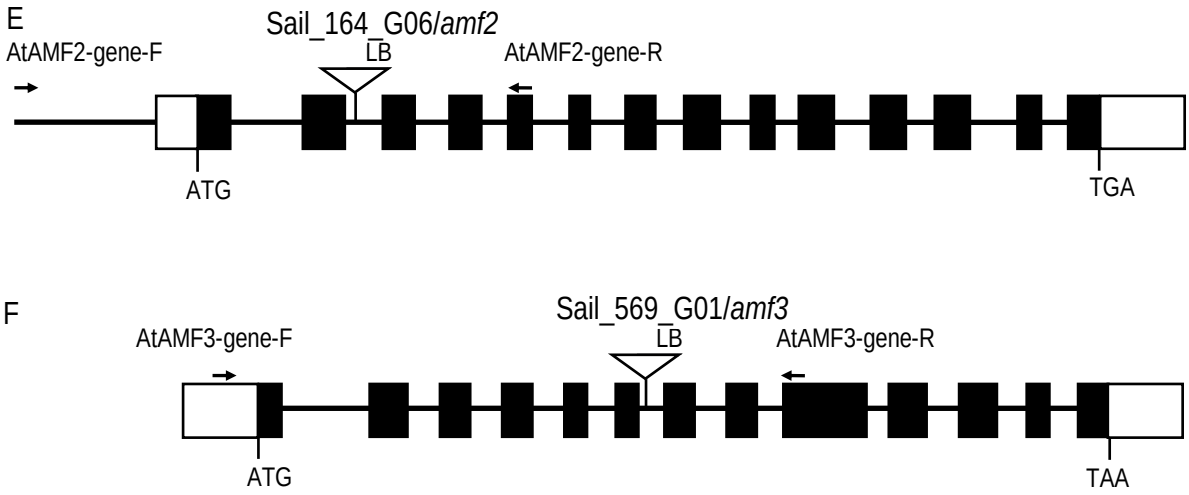

Figure 4.1. Genotypic selection of single knock out *amf* mutant lines.

AMF and *T-DNA* DNA sequence (A and B, respectively) was amplified by PCR using genomic DNA template from three randomly selected mutant plants (1-3). Genomic DNA from WT plants was used as a positive control for *AMF* sequence amplification (4). RNA isolated from 7-day old whole seedlings grown on 1 mM NH_4NO_3 containing media to generate cDNA template used for transcript amplification (C). (+) and (-) identify successful amplification or unsuccessful amplification of transcript, respectively.

Schematic representation of predicted T-DNA insertion location of mutant lines representing *amf1* (D), *amf2* (E) and *amf3* (F). M identifies 1 kb DNA ladder marker; LB identifies left border sequence; ∇ identifies predicted T-DNA insertion site; $\rightarrow$ identifies forward primer; $\leftarrow$ identifies reverse primer.

A

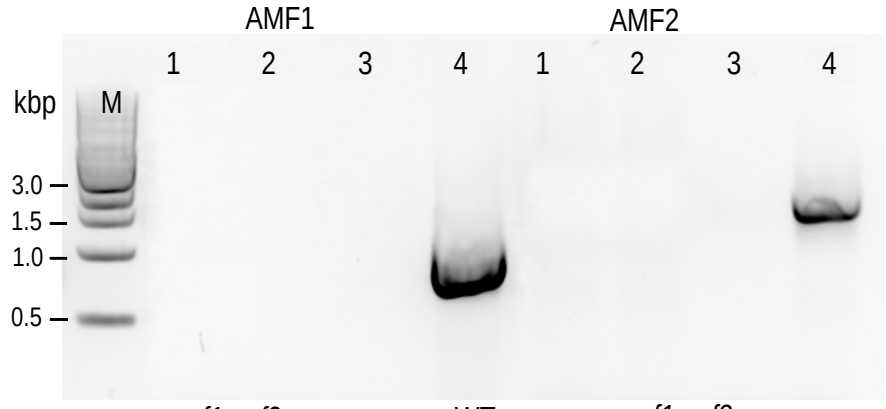

Gene sequence amplification of *amf1amf3* mutant plants

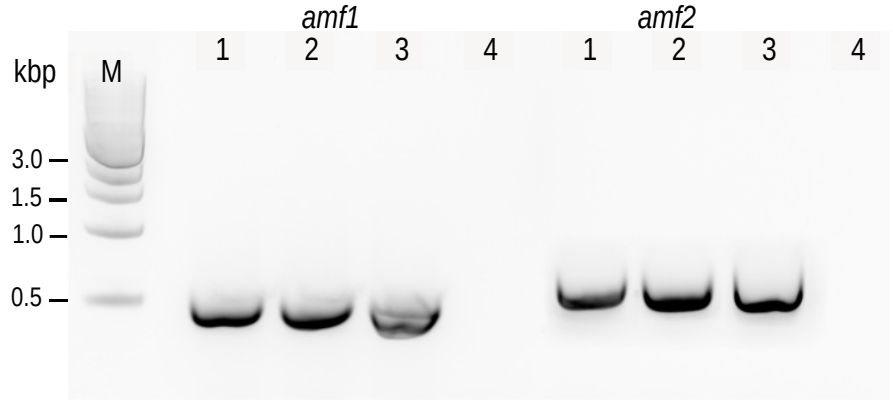

T-DNA sequence amplification of *amf1amf3* mutant plants

B

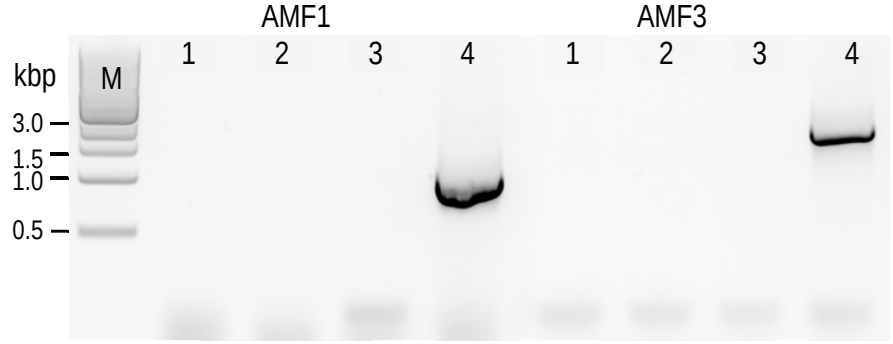

Gene sequence amplification of *amf1amf3* mutant plants

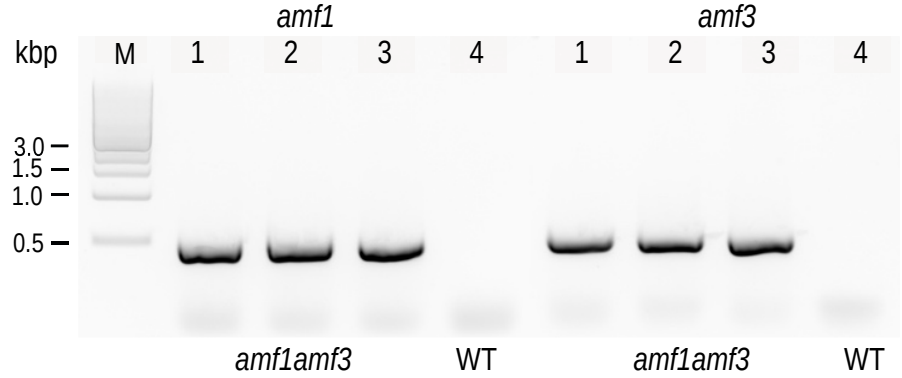

T-DNA sequence amplification of *amf1amf3* mutant plants

C

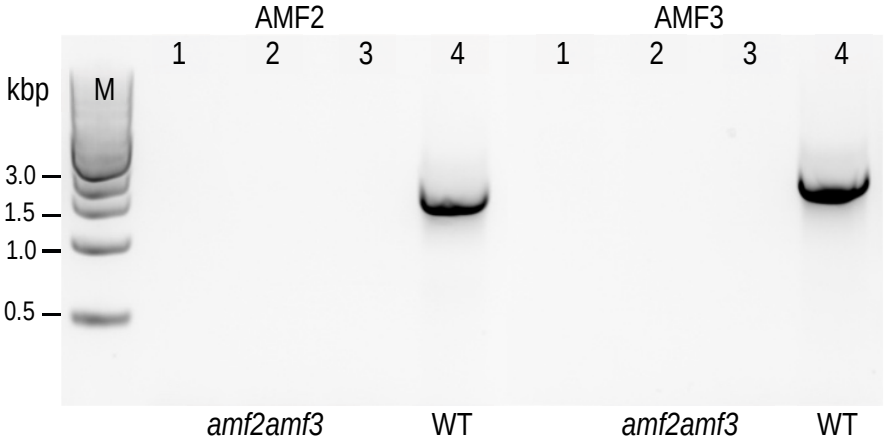

Gene sequence amplification of *amf2amf3* mutant plants

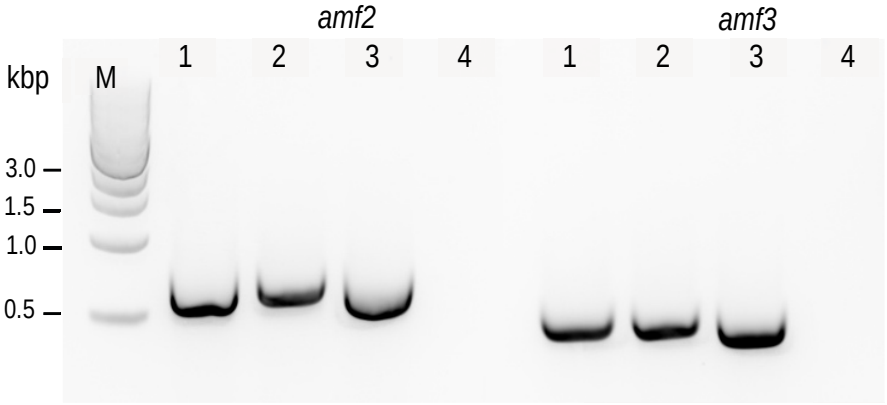

T-DNA sequence amplification of *amf2amf3* mutant plants

Figure 4.2. Genotypic selection of double knock-out *amf* mutant lines

AMF and *T-DNA* DNA sequence was amplified by PCR using genomic DNA template from three randomly selected mutant plants (1-3) of *amf1amf2* (A), *amf1amf3* (B) and *amf2amf3* (C). Genomic DNA from WT plants was used as a control for gene sequence amplification (4). M identifies 1 kb DNA ladder marker.

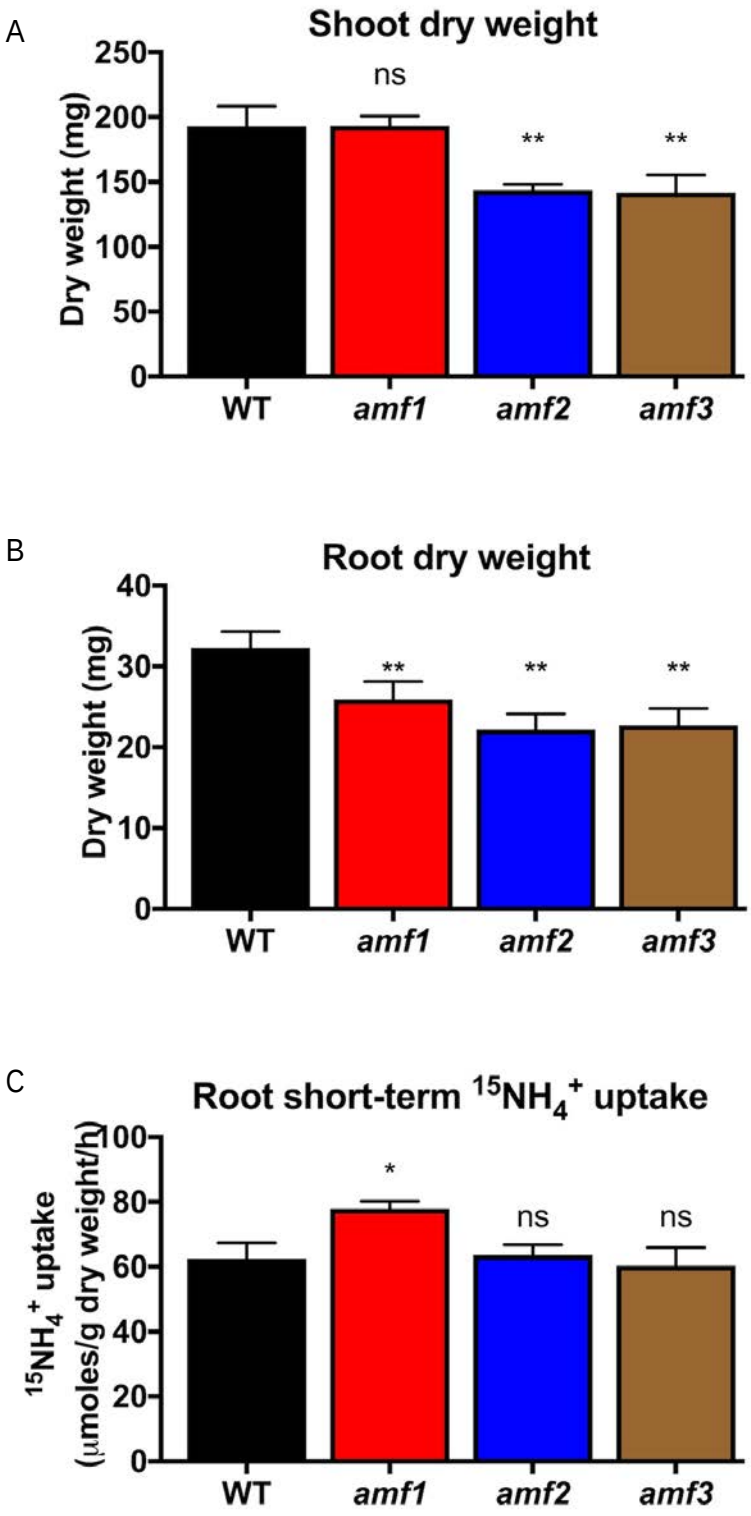

Figure 4.3. Phenotypical analysis on WT and *sko amf* mutants grown under normal conditions. Short-term (5 min) constitutive $^{15}NH_4^+$ uptake experiments were conducted on 6-week-old plants grown hydroponically at 1 mM NH_4NO_3. Following the uptake experiments, shoot and root tissues were separated and dried to obtain shoot (A) and root (B) dry weight data. ~ 3 mg of dried root samples was then used to measure the amount of $^{15}NH_4^+$ uptake (C). Data represents the mean ± SEM (n = 6 biological replicates). Asterix indicates significant difference compared to WT, * P<0.05; ** P<0.005; and uncorrected Fisher's LSD post-test; ns = not significant.

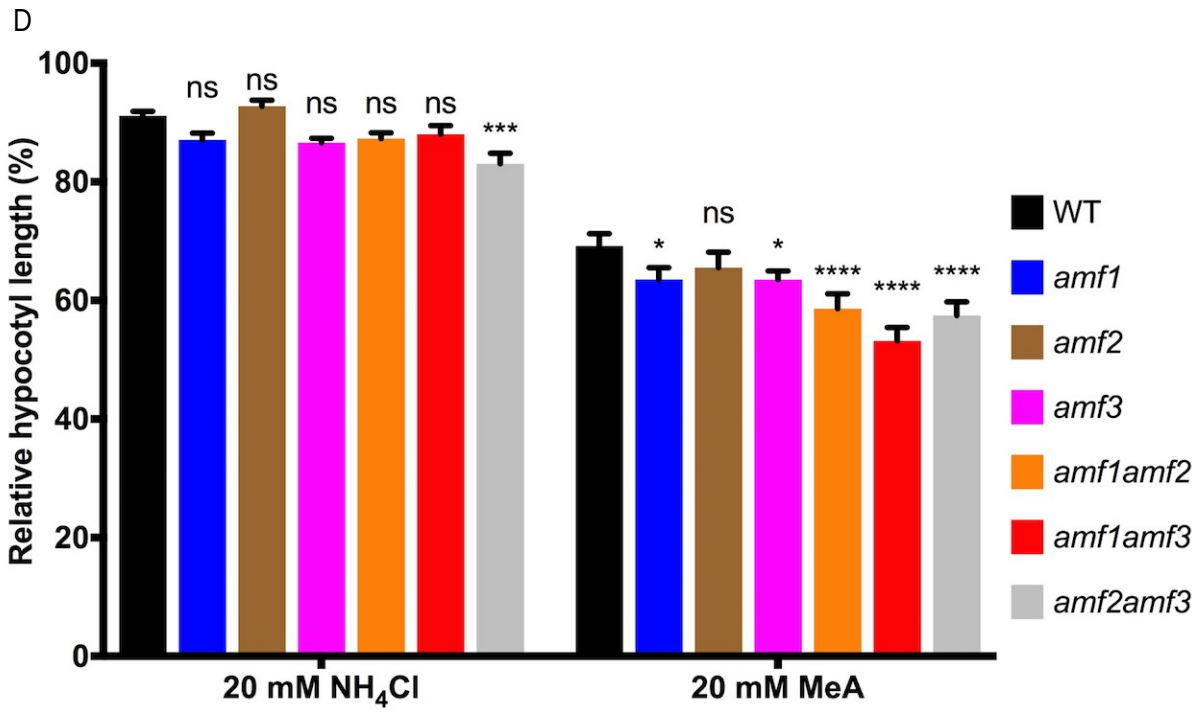

Figure 4.4. Exposure to high MA reduced hypocotyl length.

WT and *amf* mutant lines were grown for 7 d in the dark on media containing adequate K^+ (3.75 mM) supplemented with either 1 mM NH_4NO_3 (control), 20 mM NH_4Cl or 20 mM MA (treatments). Bars represent relative hypocotyl length (%) of WT and *amf* mutant seedlings grown under treatment conditions relative to the control media. Data values represent the mean ± SEM (n= 40-44 biological replicates). Asterix indicates significant difference compared to WT, * P<0.05; *** P<0.001; **** P<0.0001 and uncorrected Fisher's LSD post-test; ns = not significant.

A

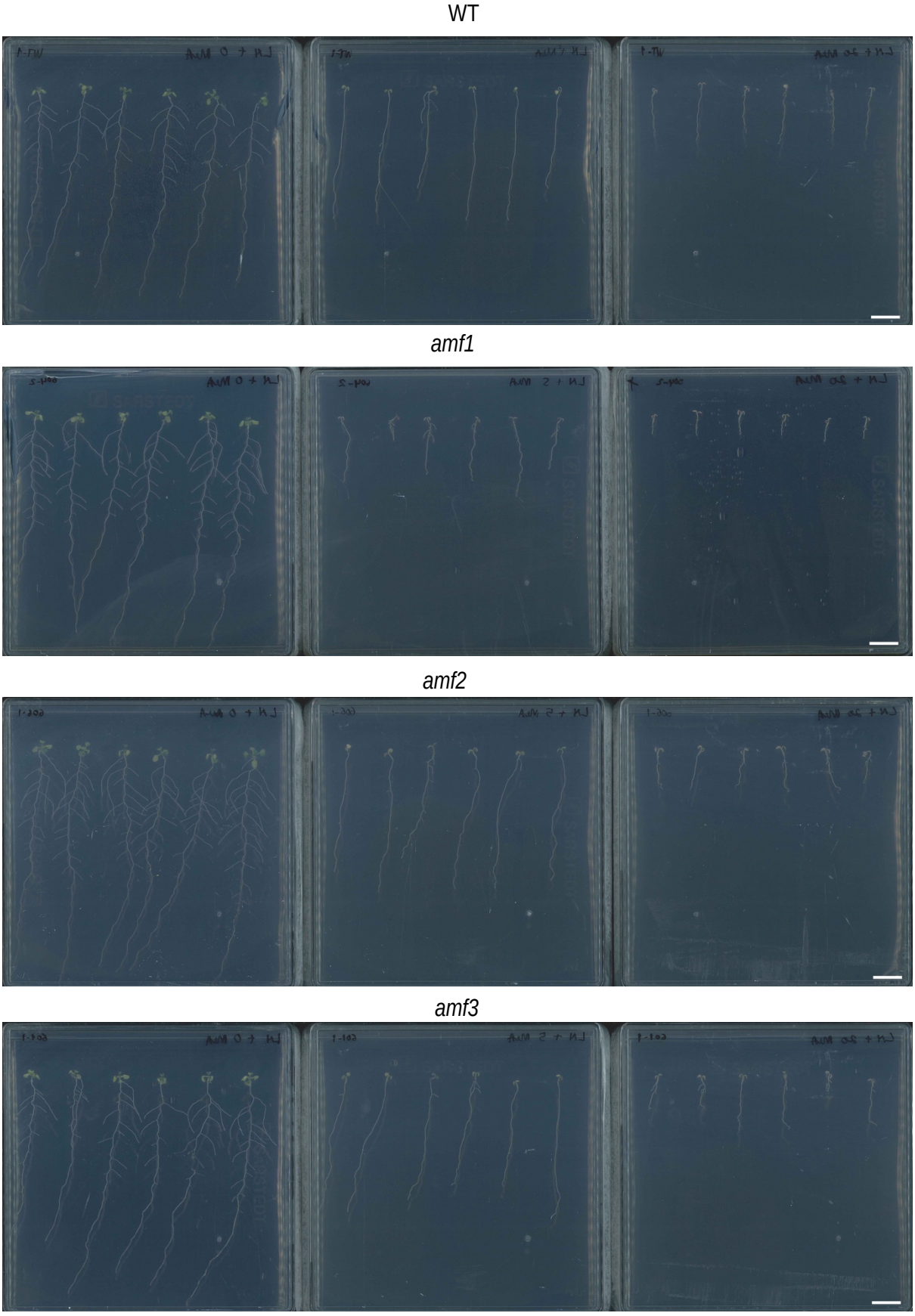

amf1amf2

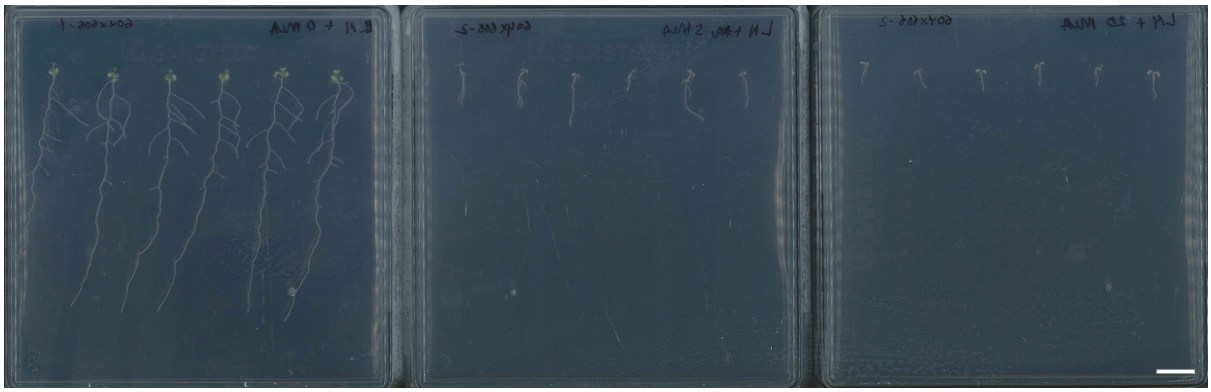

amf1amf3

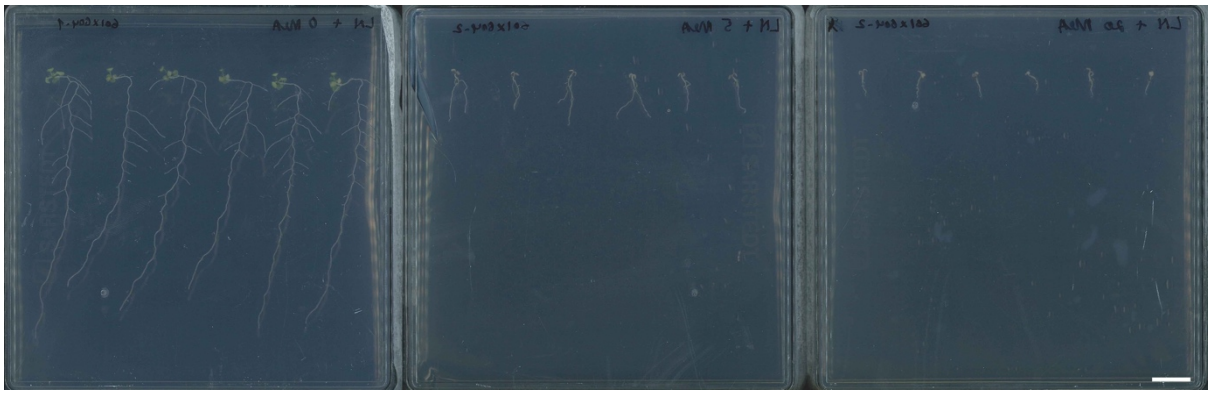

amf2amf3

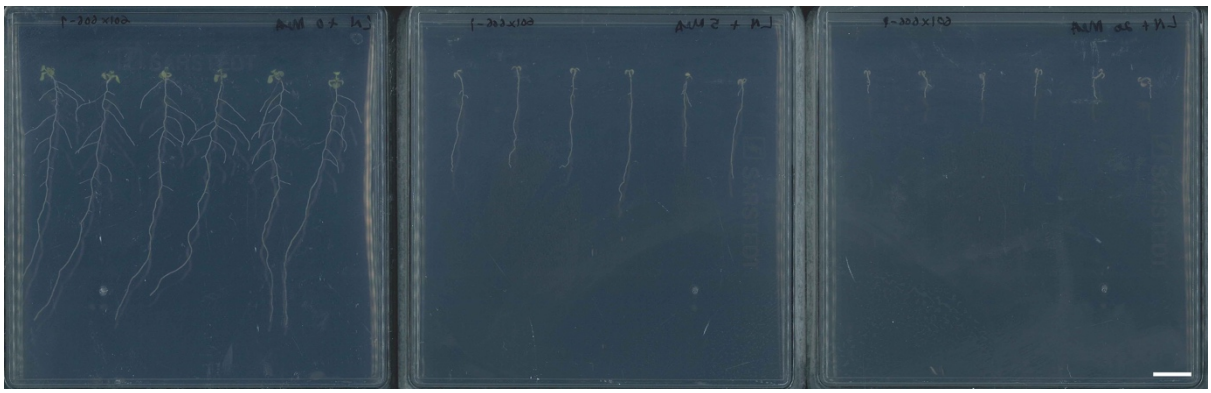

0 5 20

MA (mM)

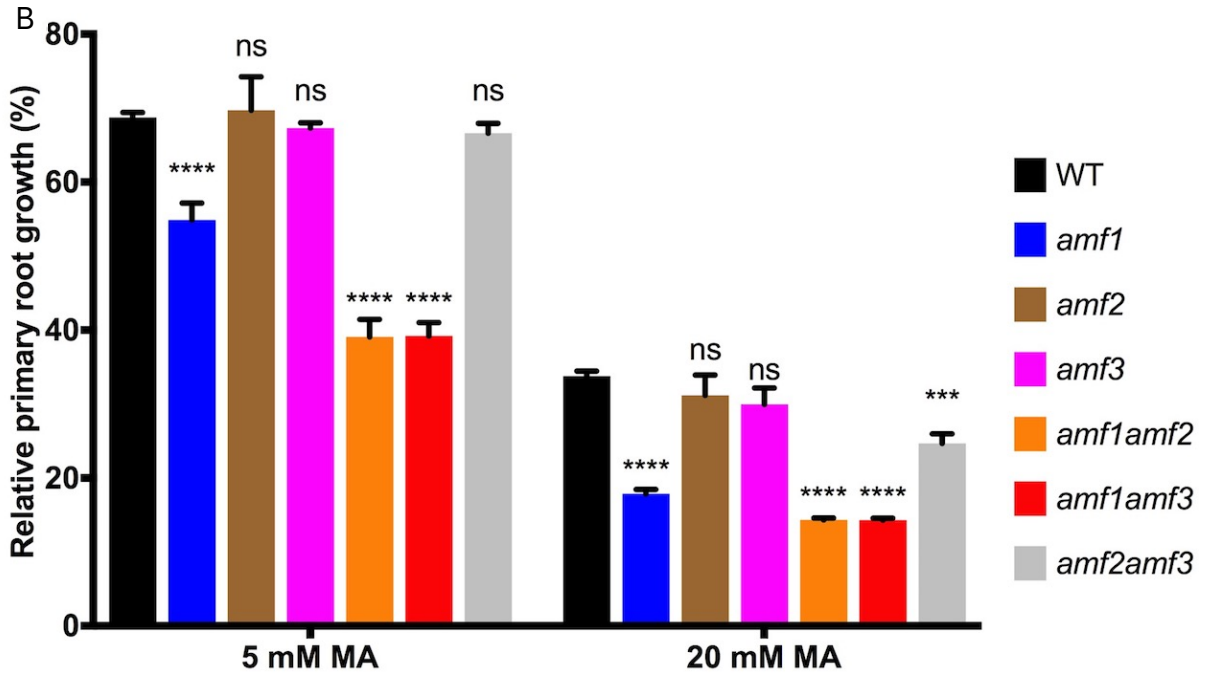

Figure 4.5. Mutants with *amf1* background displayed increased sensitivity to MA.

A. Representative pictures of 14-day-old WT and *amf* mutant seedlings grown under grown under low (0.05 mM) NO_3^- and adequate K^+ (3.75 mM) supplemented with increasing MA concentrations (0, 5 and 20 mM). Scale bar = 1 cm.

B. Primary root length (%) of 7-day-old seedlings of WT and *amf* mutants grown under adequate K^+ (3.75 mM) supplemented with either low NO_3^- (0.05 mM) as control or with 5 or 20 mM MA (treatments). % root growth is calculated from control and treatment grown seedlings. Data values represent the means ± SEM (n = 9-12 biological replicates). Asterix indicates significant differences compared to WT, *** P<0.001; **** P<0.0001 and uncorrected Fisher's LSD post-test; ns = not significant.

A

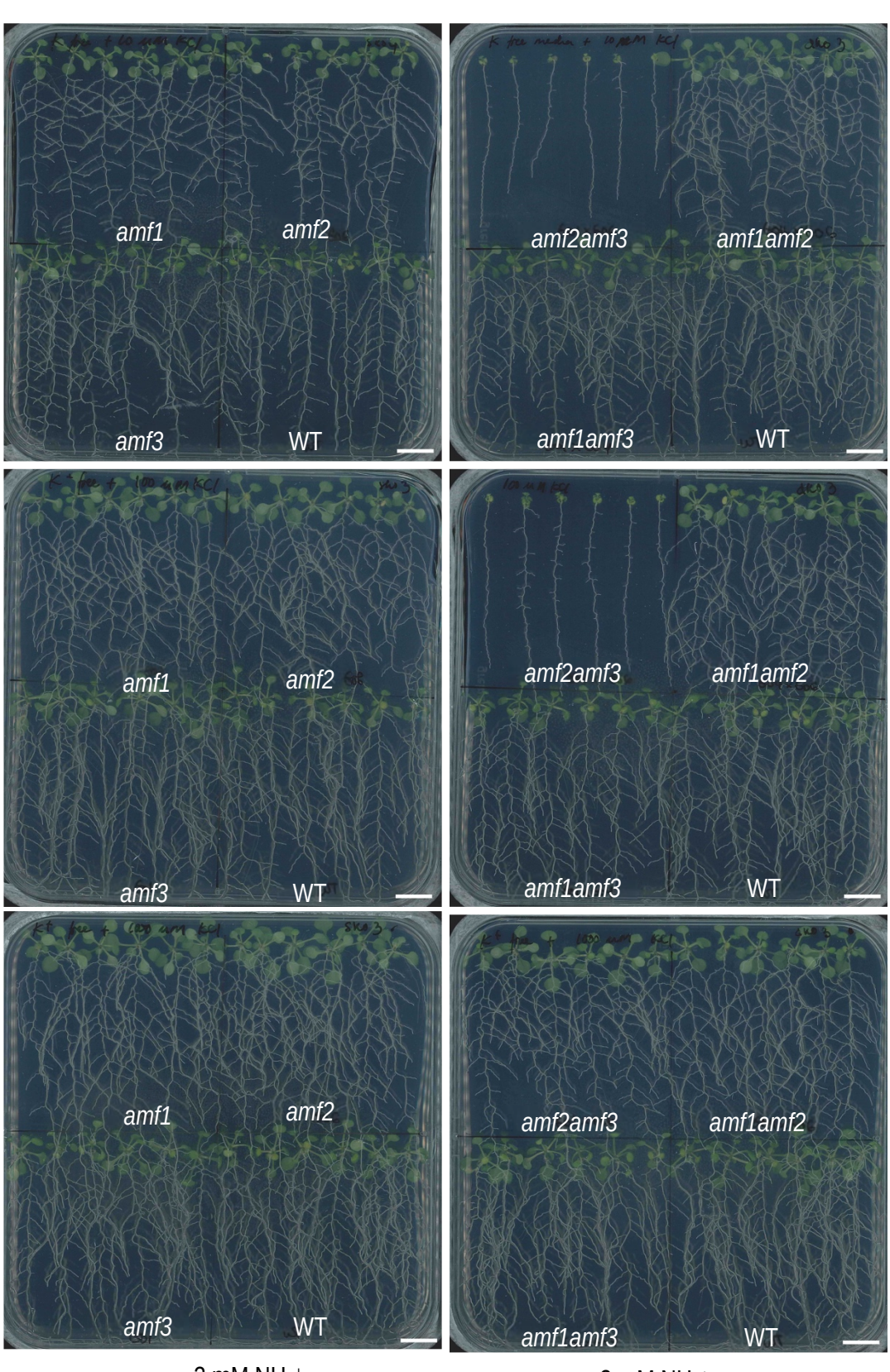
K+ (μM)
amf1
amf2
amf3
WT
amf2amf3
amf1amf2
amf1amf3
WT
10
100
1000
2 mM NH4+
2 mM NH4+

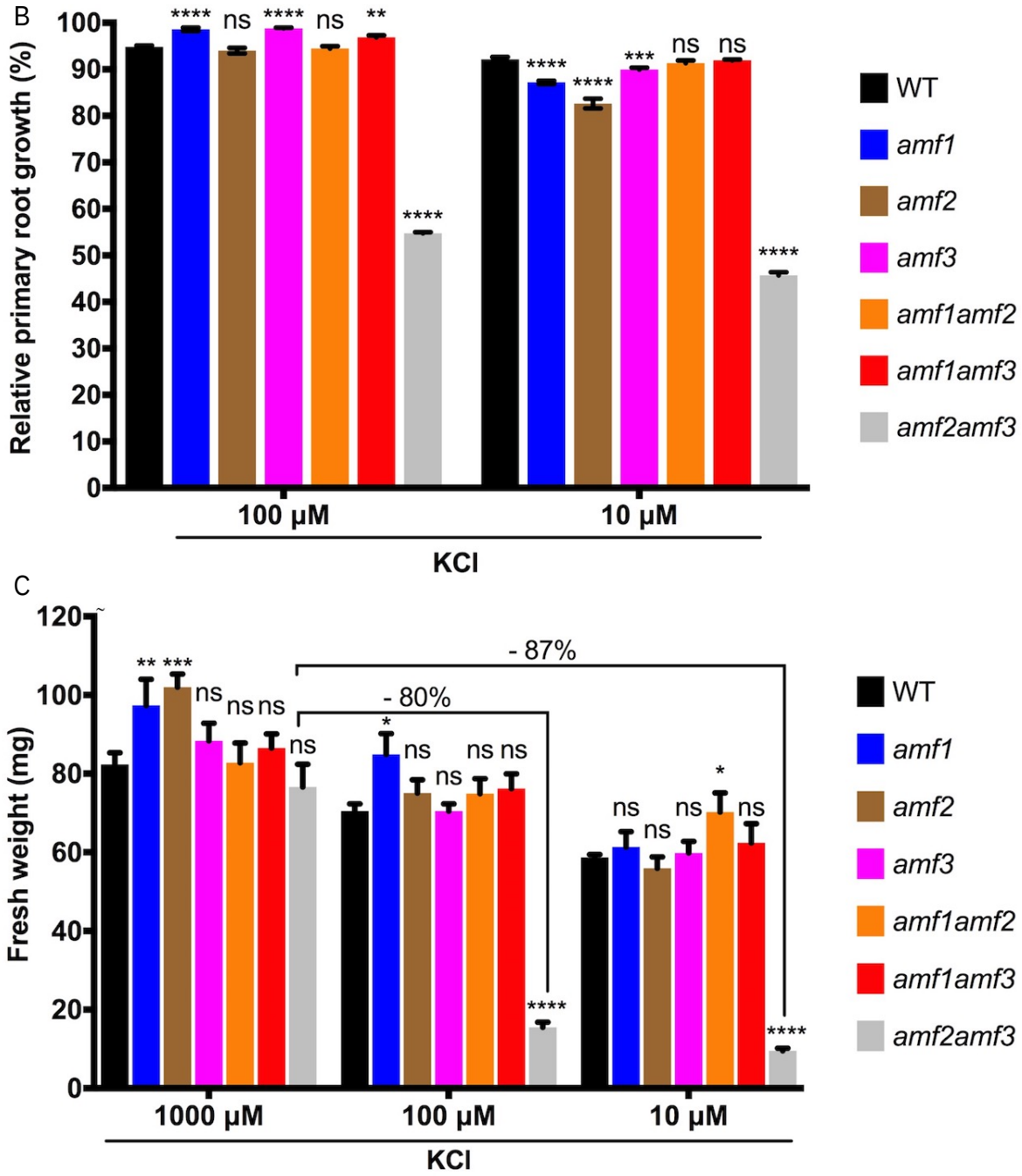

Figure 4.6. *amf2amf3* mutant plants displayed significant reductions in root growth and plant biomass at 2 mM NH_4^+ under low K^+ supply.

A. Representative pictures of 14 d WT and *amf* mutant lines grown on 2 mM NH_4^+ with 10, 100 or 1000 µM K^+ supplements in the presence of 7.5 mM NO_3^-. Scale bar = 1 cm.

B. Primary root length (%) of 7-day-old *amf* mutant seedlings grown on 2 mM NH_4^+ with 10 or 100 or 1000 µM K^+ supplements in the presence of 7.5 mM NO_3^-. Relative primary root growth (%) represents growth relative to growth on 1000 µM K^+. Data values represent the means ± SEM (n = 20-24). Asterix indicates significant difference compared to WT, * P<0.05; ** P=0.0076; *** P=0.0006; **** P<0.0001 and uncorrected Fisher's LSD post-test; ns = not significant.

C. Fresh weight of 14-day-old seedlings grown on 2 mM NH_4^+ with 10, 100 or 1000 µM K^+ supplements in the presence of 7.5 mM NO_3^-. Data values represent the mean ± SE (n= 4 biological replicates, pooled

from 5 seedlings per data point). Asterix indicates significant difference compared to WT, ** P=0.0017; *** P=0.0008; **** P<0.0001 and uncorrected Fisher's LSD post-test; ns = not significant. – N% denotes fresh weight reduction on low K^+ concentration relative to control condition (1000 µM K^+).

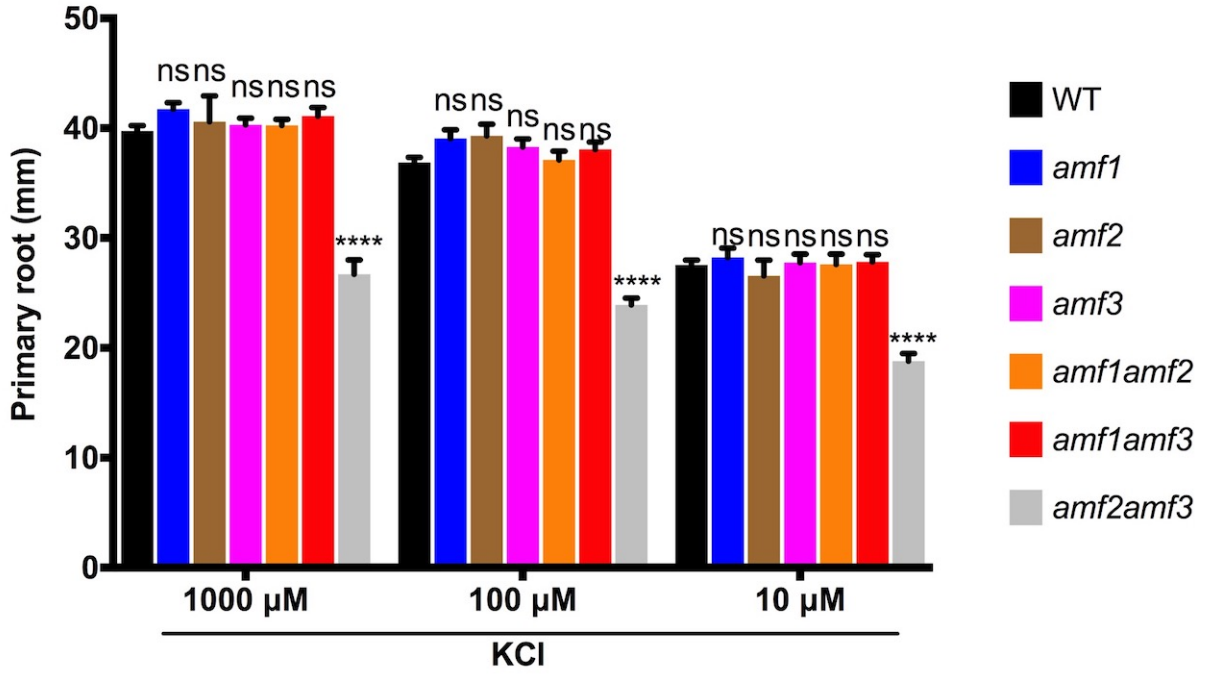

Figure 4.7. MA reduced primary root length of *amf2amf3* mutant at 1 mM K^+.

Primary root length of 7-day-old seedlings grown on media containing 5 mM MA with 10, 100 or 1000 µM K^+ supplements in the presence of 7.5 mM NO_3^-. Data values represent the mean ± SEM (n=12-20 plants). Asterix indicates significant difference compared to WT, **** P<0.0001 and uncorrected Fisher's LSD post-test; ns = not significant.

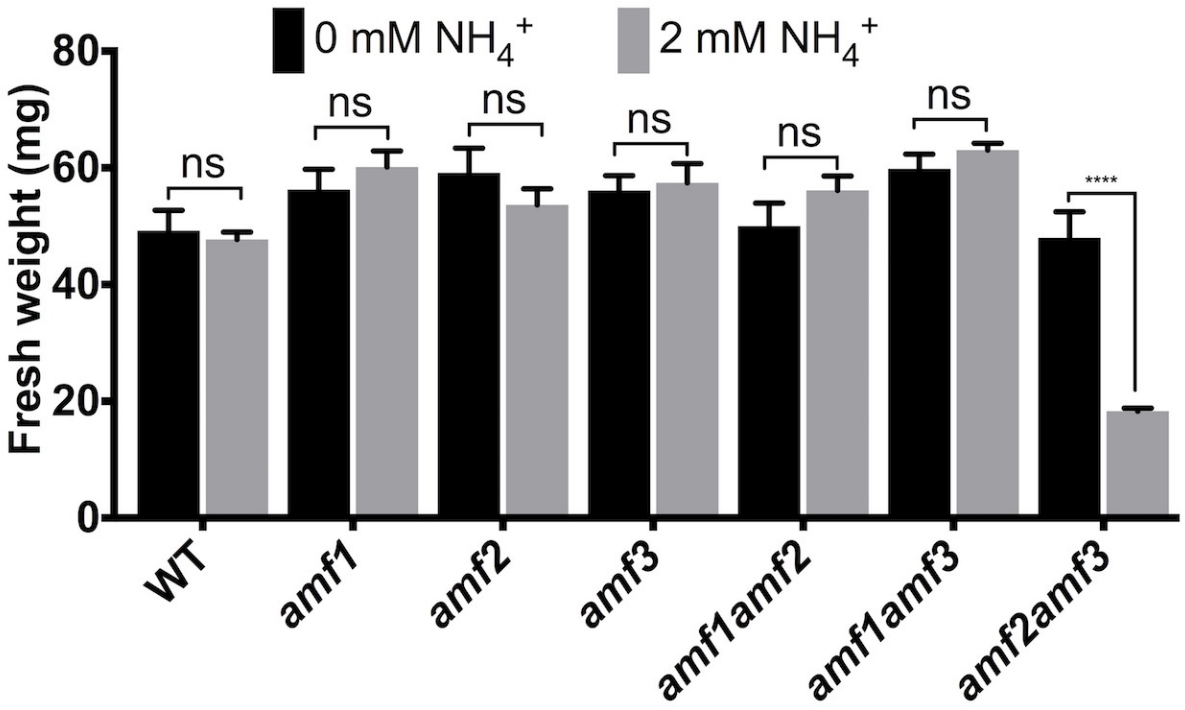

Figure 4.8. Reduction in biomass of *amf2amf3* seedlings following transfer from control media (1000 μM K^+ and 0 mM NH_4^+) onto treatment media (10 μM K^+ and ± 2 mM NH_4^+).

Arabidopsis WT and mutant seeds were germinated for four days on control media (1000 μM K^+ and 0 mM NH_4^+) prior to transplantation onto the treatment media (10 μM K^+) in the presence or absence of 2 mM NH_4^+. Both control and treatment media contained NO_3^- basal concentration 7.5 mM. Whole plant fresh weights were measured 10 d after transplantation. Data values represent the mean ± SEM; n = 4 biological replicates (5 seedlings pooled for each data point). Asterix indicates significant difference within the same genotype, **** P<0.0001 and uncorrected Fisher's LSD post-test; ns = not significant.

4.4 Discussion

In this chapter, the aim was to investigate the impact that a loss of AMF function may have on plant growth and function. As information regarding the definite function of the AMF family is limited, a phenotypic analysis of plant growth was conducted. In light of the phenotypes displayed in the yeast heterologous expression assays in Chapter 3, the impact of MA, NH_4^+ and K^+ on plant growth were also explored.

4.4.1 AtAMF1 linked to enhanced sensitivity to methylammonium under low NO_3^- concentrations

Plant growth was evaluated using hydroponic growing systems where 1 mM NH_4NO_3 was supplied over a 6-week period. All three *amf sko* lines showed a reduction in root dry weights, while *amf2* and *amf3* had shoot growth which was compromised relative to the wild-type. An analysis of ammonium uptake using ^{15}N-labelled 0.5 mM $(NH_4)_2SO_4$ showed that *amf1* had higher retention levels of ^{15}N label than the wild type, *amf2* and *amf3*. Traditionally, the loss of NH_4^+ transport proteins (AMTs) in Arabidopsis has resulted in a decrease of ammonium uptake across a range of external concentrations (Kaiser et al., 2002; Loque et al., 2006; Yuan et al., 2007; Lima et al., 2010; Giehl et al., 2017). This different response with AMF proteins, suggests a different type of function than that observed with AMT proteins which are more aligned with uptake activities. It is interesting, that the loss of *amf1* resulted in an increase in NH_4^+ uptake which either suggests a role in NH_4^+ efflux or redistribution to aerial tissues in the plant.

The reduction in long-term growth of the root systems of *amf1*, *amf2* and *amf3* plants was investigated further in the context of NH_4^+ sensitivity. This was done in light of the phenotypes observed in yeast cells that were described in Chapter 3. Ammonium sensitivity in Arabidopsis has been evaluated using the toxic analogue methylammonium (MA) where poor growth is associated with an accumulation of MA or tolerance by reduced uptake. One assay recently used involves the measurement of hypocotyl growth which is particularly sensitive to MA supply (Straub et al., 2017). When plants were supplied high levels of MA (20 mM) there were significant restrictions in hypocotyl growth in all of the *amf* lines tested except for *amf2* (Figure 4.4). This response to MA was investigated further using a plate-based assay that allowed for the analysis of root growth across a 14-day window. When grown on 20 mM MA, *amf1* and the dko lines *amf1amf2*, *amf1amf3* and *amf2amf3* showed a significant reduction in root growth (Figure 4.5). At reduced levels of MA (5 mM), the overall impact of MA was less but the trends were similar except for *amf2amf3* which didn't show a reduction in root growth. This increased sensitivity to MA on root growth was in contrast to that observed in AMT mutants, where multiple AMT KO's combined in one plant (AMT1;1, AMT1;2, AMT1;3 and AMT2;1). The quadruple KO mutant has an increased tolerance to high levels of MA supply (Yuan et al., 2007).

NH_4^+ uptake through shoot tissues can occur when presented directly to the tissue particularly when Arabidopsis seedlings are grown on solid plate media. Experiments were conducted using a split media system to determine if the primary cause of the poor root growth of the *amf* mutant lines was a

consequence of the direct exposure of MA on shoot or root tissues. Previous studies have demonstrated that direct contact of toxic concentrations of NH_4^+ on shoot tissues promotes root growth inhibition through auxin and ethylene regulatory pathways (Li et al., 2011; Li et al., 2013). Accordingly, split plate experiments demonstrated that all lines suffered mild primary root growth inhibition 3 d after transfer to split media in which only shoot tissues were directly exposed to MA (20 mM) (Supplemental Figure S4.4.A). However, direct contact of root tissues to high MA caused a more significant root growth inhibition (Supplemental Figure S4.4.B). Furthermore, this data consistently shows that the mutant lines with an *amf1* background are hypersensitive to high MA. Mutant *amf1*, *amf1amf2* and *amf1amf3* ceased to grow after three days on the split media in which only root tissues were exposed to high MA (Supplemental Figure S4.4.B). Collectively, these data indicate that the dysfunctional *amf1* might affect NH_4^+ influx regulation, leading to the potential hyperaccumulation of NH_4^+ in root tissues and associated toxicity symptoms.

Among the *amf* mutant lines identified here, the *amf1* background consistently displayed a hypersensitivity to MA. At 5 mM MA, *amf1*, *amf1amf2* and *amf1amf3* exhibited reduced primary root growth (45, 60 and 60%, respectively), while at 20 mM MA the mutants displayed even further reductions in primary root growth (82, 85 and 85%, respectively) relative to root growth under control conditions (0 mM MA) (Figure 4.5.B). In contrast, the WT control plants showed less growth repression from MA toxicity, even though primary root growth was reduced by 30 and 65% relative to control conditions at 5 and 20 mM MA, respectively (Figure 4.5.B). These findings suggest that AtAMF1 might be partly responsible for an NH_4^+ tolerance mechanism. Correspondingly, the short-term $^{15}NH_4$ uptake experiment with the *sko* mutant lines showed a significant increase of $^{15}NH_4$ influx into root tissues (Figure 4.3.C). Unfortunately, due to time constraints, it was not possible to conduct more extensive $^{15}NH_4$ uptake experiments on the *dko* mutant lines. Additionally, the *dko amf2amf3* displayed an increased sensitivity to MA with a 75% decrease in relative primary root growth at 20 mM MA relative to control condition (Figure 4.5.B). It is intriguing to see why the double mutation of AMF family members increased MA-induced toxicity as each member is potentially localised across different organelles (detailed in Chapter 2, Figure 2.11-14). However, it could be that each AMF interacts therefore effecting each other's functionalities.

The *amf1* mutant lines respond to toxic MA conditions through changes in root growth. Accordingly, adaptation by alteration of root system architecture (RSA) is a natural response of plants to adapt with nutrient availability in both deficient or excessive concentrations (Giehl et al., 2014). Most often, plants promote root growth under mild N-deficiency but display a decreased root growth under severe N-deficiency. Interestingly, plants also exhibit a reduced root growth in both primary and lateral roots under excessive supply of NH_4^+ (Li et al., 2011; Giehl and von Wirén, 2014). This response might be a strategy to limit the exposure to the excessive NH_4^+ as shorter primary and/or lateral roots will minimize root surface area, hence reduce the uptake of NH_4^+. However, based on these limited data it is not possible to identify the role of AMF1 in RSA adaptation in response to excessive NH_4^+.

4.4.2 AtAMF2 and AtAMF3 might be involved in NH_4^+ tolerance under low K^+ concentrations

Detrimental effects of NH_4^+ are enhanced with limited availability of K^+. Cao et al. (1993) have demonstrated that complete omission of K^+ from growing solutions containing NH_4^+ completely inhibited root growth of *Arabidopsis* seedlings even with the presence of NO_3^-. Alleviation of NH_4^+ toxicity by the supply of K^+ have been reported in other species including barley (Hoopen et al., 2010) and cucumber (Roosta and Schjoerring, 2008). Similarly, K^+-concentration-dependent-NH_4^+-toxicity has also been reported in yeast (Hess et al., 2006), which revealed that yeast only suffer NH_4^+ toxicity under low K^+ concentrations. Accordingly, a study by Martinelle and Häggström (1993) also suggested that increased concentrations of K^+ can be used to detoxify NH_3/NH_4^+ in animal cells. In chapter 3, the activity of AMF2 was clearly associated with an ability to rescue yeast cell growth on low K^+ concentrations when excess NH_4^+ was provided to the cells. It seems the relationship between K^+-concentration and NH_4^+ toxicity is a common condition across many organisms. Unfortunately, the molecular mechanism underlying this phenomenon remains unexplored.

To investigate whether *amf* mutant lines displayed similar phenotypes to those previously described, the mutant lines were grown on media containing different concentrations of K^+ in the presence of 7.5 mM NO_3^- and 2 mM NH_4^+ or 5 mM MA. Initial experiments showed that by growing plants on NH_4^+-free media supplemented with 1000 μM K^+ and 7.5 mM NO_3^-, all lines grew normally without any visible phenotype (Figure S4.5). In the following experiments the K^+ concentration was kept at either 10, 100 (both low K^+ conditions) or 1000 μM (control condition). With each K^+ concentration (100 and 10 μM), the *dko amf2amf3* mutant was the only line that experienced a substantial growth inhibition. At 7 d, primary root growth of *amf2amf3* was reduced by 55% and 45% at 10 and 100 μM K^+ relative to control (1000 μM K^+) conditions, respectively (Figure 4.6.C). Additionally, this line also exhibited significant fresh weight reductions of 87 and 80% at 10 and 100 μM K^+, respectively, relative to control conditions (Figure 4.6.C). When supplied 5 mM MA, *amf2amf3* primary root growth was suppressed across all the K^+ concentrations tested (Figure 4.7). Collectively, these results indicate the potential roles of AtAMF2 and AtAMF3 in mediating potential NH_4^+ toxicities as K^+ concentrations decrease. ıncreased NH_4^+ toxicity symptoms have been reported in *Arabidopsis* mutant lines that are defective in K^+ transport mechanisms. Hirsch et al. (1998) demonstrated that *atakt1* failed to grow on media containing 10 μM K^+ in the presence of 2 mM NH_4^+. Furthermore, the double mutant *athak5 akt1* displayed a significant reduction in seedling establishment in the presence of NH_4^+ (Pyo et al., 2010). These studies consistently demonstrated that with reduced K^+ influx by either a decreased external supply or dysfunctional K^+ transport systems, plants displayed enhanced NH_4^+ toxicity symptoms.

Previous studies have documented the impact of low K^+ and high NH_4^+ in post-germination seedling establishment (Cao et al., 1993; Pyo et al., 2010). Experiments were conducted here to investigate whether *amf* mutant lines also display comparable phenotypes. The results showed corresponding phenotypes to those of previous studies. Following transfer from NH_4^+-free media containing 1 mM K^+

onto media containing 10 μM K^+ in the presence of 2 mM NH_4^+, *amf2amf3* mutants showed significant reductions in fresh weight (60% relative to fresh weight on media without NH_4^+) (Figure 4.8). The growth arrest of *amf2amf3* was indeed caused by exposure to NH_4^+ at low K^+ concentrations and this finding indicates that a disruption of both *amf2* and *amf3* have a significant impact on seedling post-germination establishment.

The *amf1* mutant displayed toxicity symptoms to NH_4^+/MA only when grown with low NO_3^- irrespective of available K^+ (Figure 4.5 and Supplemental Figure S4.3). This is in contrast to the *amf2amf3* mutant line which was found sensitive to low K^+ concentrations and NH_4^+ (based on primary root growth reduction) at both adequate and low NO_3^- levels (Supplemental Figure S4.7.A and C, respectively). These results suggested that AtAMF2 and AtAMF3 phenotypes are NO_3^--concentration independent and most likely K^+-concentration dependent. Correspondingly, this is in agreement with a previous study by Cao et al. (1993) that demonstrated the inhibitory effect of NH_4^+ on primary root growth of *Arabidopsis* seedlings at low K^+ concentrations even in the presence of NO_3^-. Furthermore, it was observed here that all *dko* mutant lines exhibited significant reductions in lateral root numbers under adequate NO_3^- supply (Supplemental Figure S4.7.B). In contrast under low NO_3^-, only *amf2amf3* displayed reduced lateral root numbers (Supplemental Figure S4.7.D). These results are contrary to the initial hypothesis that at low NO_3^- and in the presence of NH_4^+, mutant lines with the *amf1* background would show a NH_4^+ hypersensitivity response. However, none of the *amf1* mutant lines displayed a significant reduction of both primary root growth or lateral root number (Supplemental Figure S4.7.C and D, respectively). It is possible that enhanced root growth (primary and lateral roots) in response to low NO_3^- helps to overcome the effect of NH_4^+ on root growth repression. Accordingly, Giehl and von Wirén (2014) explained that plants grown under limited N promote primary elongation as well as lateral root elongation and emergence in order increase root surface area and hence acquire nutrients more efficiently from the media or soil.

4.4.3 The AtAMF family is involved in NH_4^+ tolerance *in planta* – but the mechanism remains unclear

Ammonium toxicity in plants is a complex response as it systematically affects plant growth from the molecular, physiological and biochemical levels culminating in morphological changes. Interaction with other nutrients such as NO_3^- and K^+, adds another level of complexity to how plants manage high concentrations of NH_4^+. Regulation of NH_4^+ influx through finely controlled transport proteins, such as the AMT families, plays a crucial role in NH_4^+ toxicity tolerance. This has been demonstrated using multiple mutations in the Arabidopsis AMT1 and AMT2 family, where collective loss of *amt1;1*, *amt1;2*, *amt1;3*, and *amt2;1* improves plant growth on toxic concentrations of MA (Yuan et al., 2007; Straub et al., 2017). Other than regulating NH_4^+ influx, other physiological, biochemical and morphological adaptations to MA and NH_4^+ remain poorly understood.

The data presented here reveal the involvement of the AMF family in managing NH_4^+ toxicity. Studies presented in the thesis demonstrate that the loss of AMF1 (*amf1*) led to MA hypersensitivity when

grown on low NO_3^- concentrations, suggesting an involvement of the protein in the regulation of NH_4^+ influx through an unidentified pathway under low NO_3^- concentrations (i.e. deficient-N). Accordingly, N-deficiency has been shown to up-regulate the expression of AtAMT families (Gazzarrini et al., 1999; Rawat et al., 1999; Straub et al., 2017). Therefore, a mechanism may be required to control or moderate NH_4^+ influx when other systems (AMT's) are stimulated by N-deficient conditions. AMF1 might directly or indirectly participate in this unknown mechanism. Previous data has shown that AMF1 displayed localisation in the ER (Chapter 2.3.7). AMF1 might interact with other proteins in the ER, potentially with AMF2 and/or AMF3, to form multi-subunit transporter(s)? As observed, there was an enhanced hypersensitivity to MA at low NO_3^- in *amf1amf2* and *amf1amf3* plants (Figure 4.5.B). Moreover, based on its tissue specific localisation around vascular bundle tissues (potentially pericycle) (Chapter 2.3.6), AMF1 might participate in NH_4^+ translocation. However, to understand the definite functions of AtAMF1 in toxicity tolerance in Arabidopsis will require further studies.

There was also a strong connection between AMF2 and AMF3 with NH_4^+ toxicity in plants grown on low K^+ concentrations. Unlike AtAMF1, which appears to be NO_3^- dependent, AtAMF2 and AtAMF3 appear to regulate NH_4^+ toxicity in a K^+-concentration dependent manner. Correspondingly, overexpression of AtAMF2 in yeast CY162 defective in two main K^+ transporters (*trk1*Δ and *trk2*Δ), rescued the yeast grown under toxic NH_4^+ conditions (Chapter 3.3.3). Localisation of AtAMF2 in the tonoplast of the plant (Chapter 2.3.8) and yeast cells (Chapter 3.3.6) indicates potential roles in cellular NH_4^+ homeostasis by facilitating NH_4^+ transport across the tonoplast. Heterologous expression experiments in yeast suggest that AtAMF2 is participating in NH_4^+ efflux from the vacuole to slowly release NH_4^+ into cytoplasm for further assimilation processes (Chapter 3.4.3). AtAMF3 could be responsible for a similar efflux function in plant cells at the plasma membrane (Chapter 2.4.3). Limited evidence showed that overexpression of AtAMF3 slightly improved the growth of 31019b yeast cells grown at toxic MA concentrations at pH 7.0 (Chapter 3.3.2). This might be related to the ability of AtAMF3 to facilitate MA efflux that eventually improves MA detoxification processes in the yeast cells. The AtAMF3-facilitated efflux mechanism might also occur in plant cells. Interestingly, the potential localisation of AtAMF3 in the pericycle cells might indicate its involvement in NH_3/NH_4^+ loading to xylem. Regardless, the phenotypes of *amf2amf3* revealed in these studies demonstrated an obvious interaction between NH_4^+ toxicity and low K^+ concentration. The reason why *sko amf2* or *amf3* did not display NH_4^+ hypersensitivity remains unclear. At low K^+ concentration, it is possible that both *sko* mutants require a higher (>2 mM) NH_4^+ to induce a distinguishable phenotype. Alternatively, it could be suggested that AtAMF2 and AtAMF3 might be redundant to each other, hence disruption of one protein does not significantly affect the overall sensitivity to NH_4^+.

4.5 Supplementary materials of Chapter 4

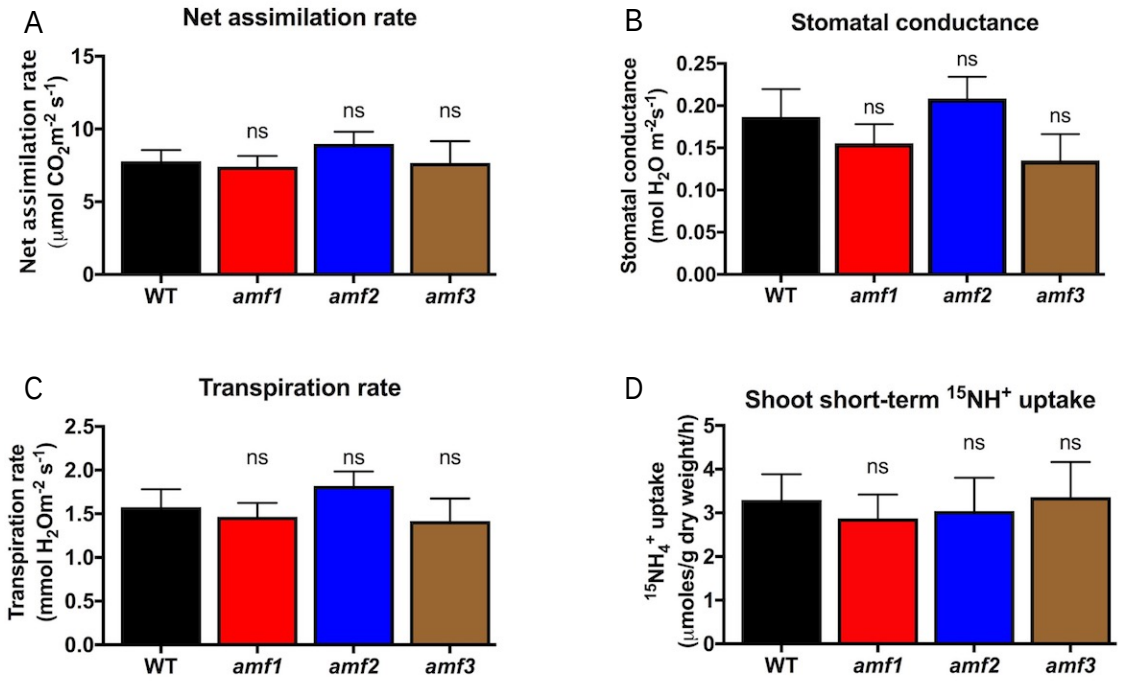

Supplemental Figure S4.1. Phenotypic analysis of WT and *sko* mutant plants grown under control conditions.

Two days prior to short-term $^{15}NH_4^+$ uptake experiments, Infrared Gas Analyzer (IRGA) was used to measure Net assimilation rate (A), stomatal conductance (B), transpiration rate (C) of the same plants used for the uptake experiments. ~3 mg of dried shoot samples was then used to measure the amount of $^{15}NH_4^+$ uptake (D). ns = not significant.

A. 1 mM NH_4NO_3

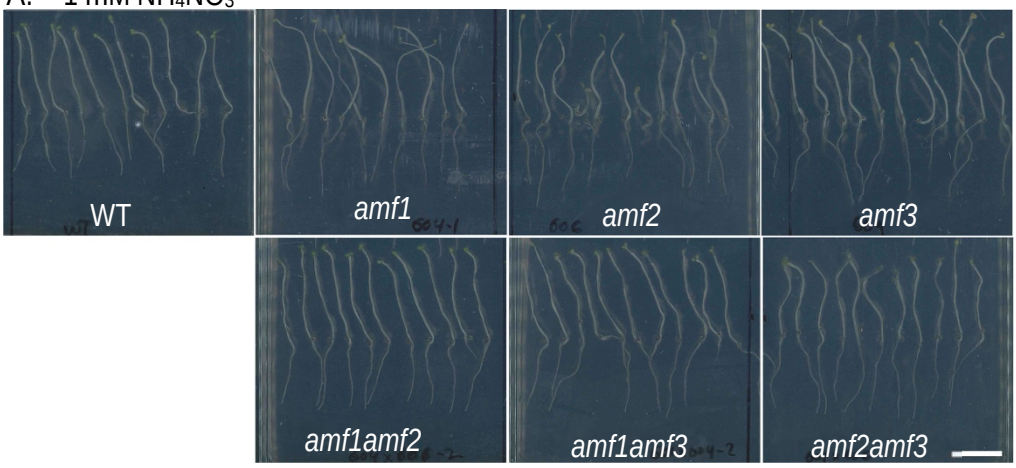

B. 20 mM NH_4Cl

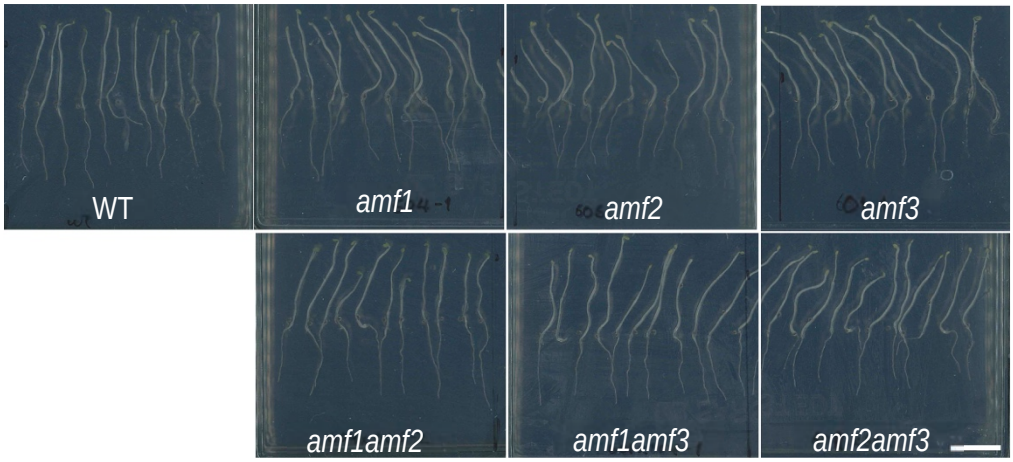

C. 20 mM MA

D

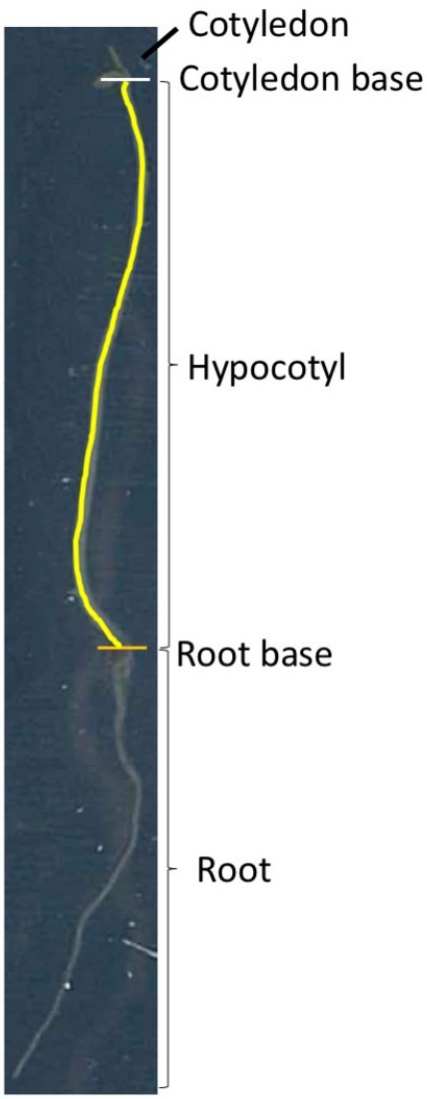

Supplemental Figure S4.2. Exposure to high MA reduced hypocotyl length

Representative pictures of 7-day-old seedlings grown in the dark under control conditions (1 mM NH_4NO_3) (A), and treatment conditions 20 mM NH_4Cl (B) and 20 mM MA (C). Scale bar = 1 cm.

D. Representative picture of hypocotyl length measurement of a 7-day-old seedling. Hypocotyl length was measured from cotyledon base to root base (yellow line).

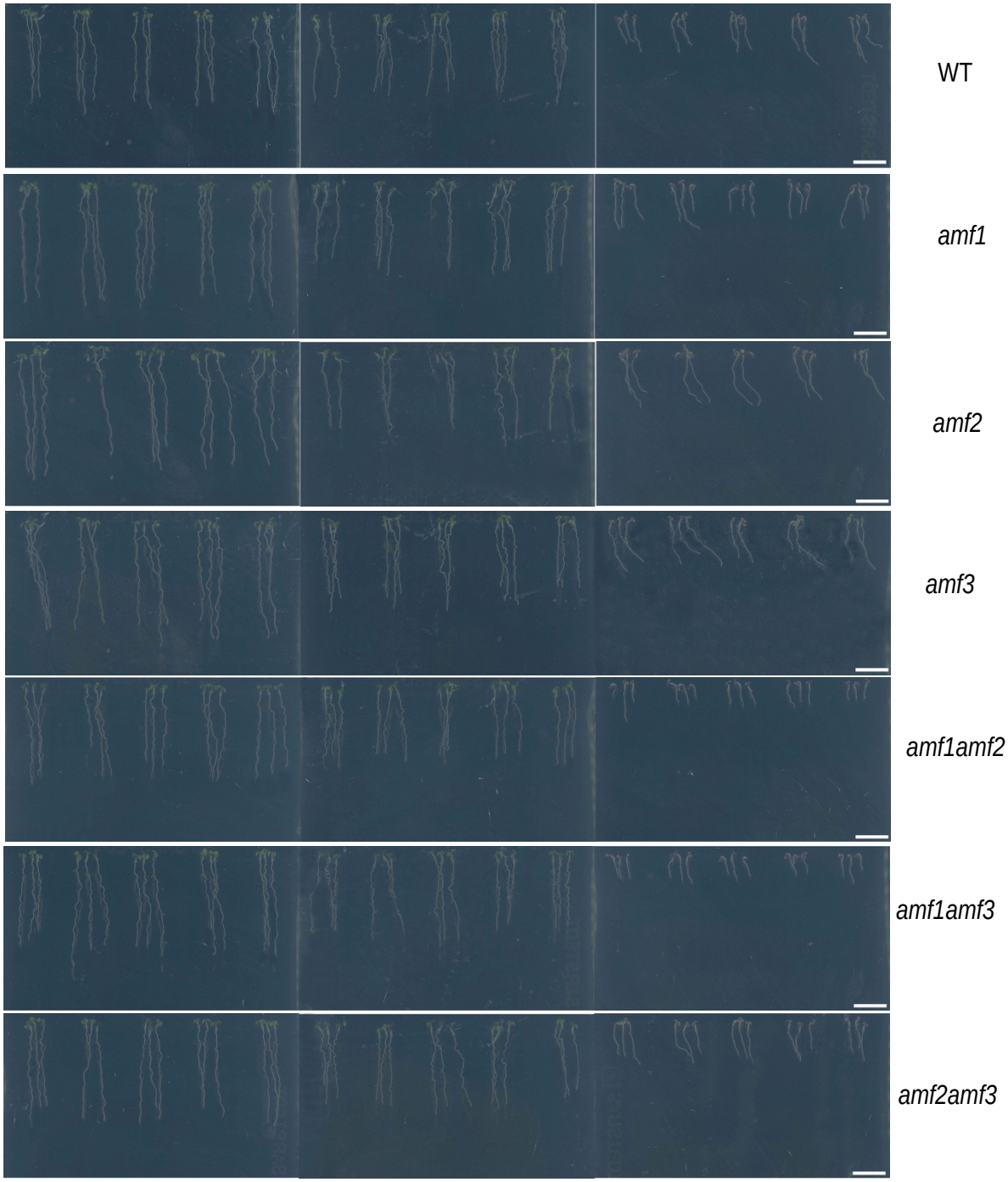

Supplemental Figure S4.3. Comparison of growth inhibition by high MA and NH_4 at low NO_3. Phenotype representation of 7-day-old WT and *amf* mutant seedlings grown on media containing low NO_3^- (0.05 mM) without (control) or with supplementation of 20 mM NH_4Cl or 20 mM MA in the presence of 3.75 mM K^+. Scale bar = 1 cm.

A

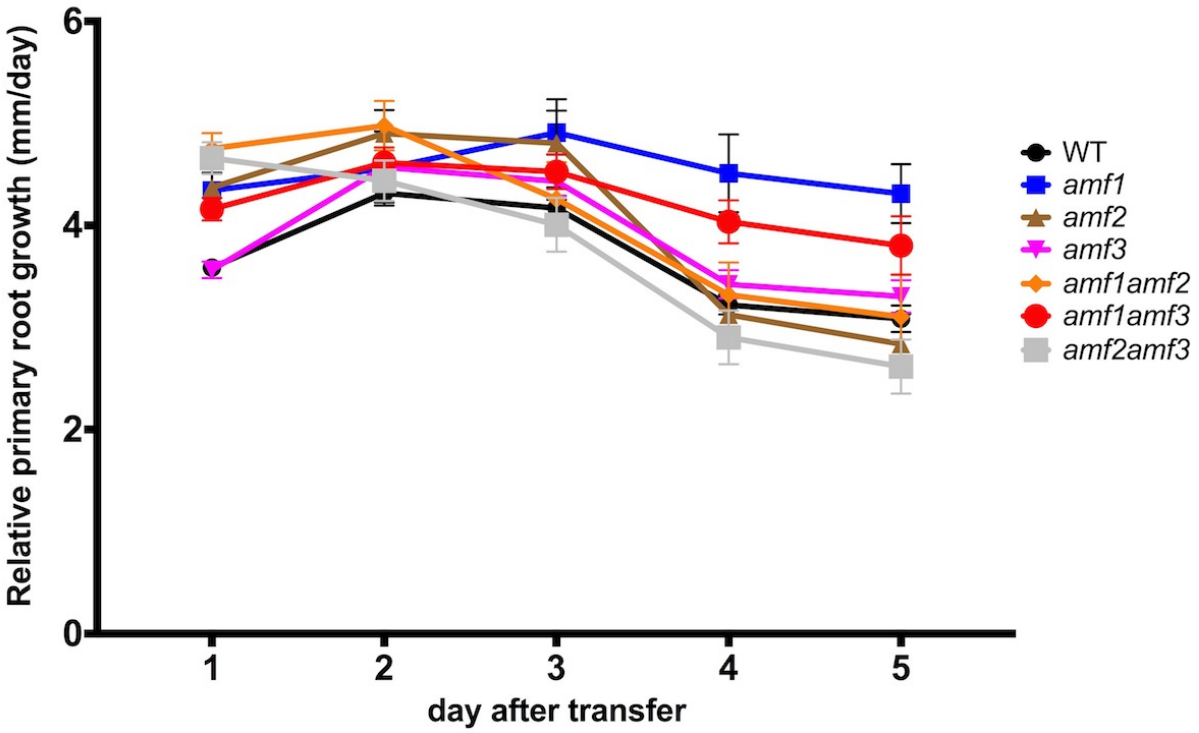
Relative primary root growth (mm/day)
6
4
2
0
1
2
3
4
5
day after transfer
WT
amf1
amf2
amf3
amf1amf2
amf1amf3
amf2amf3

B

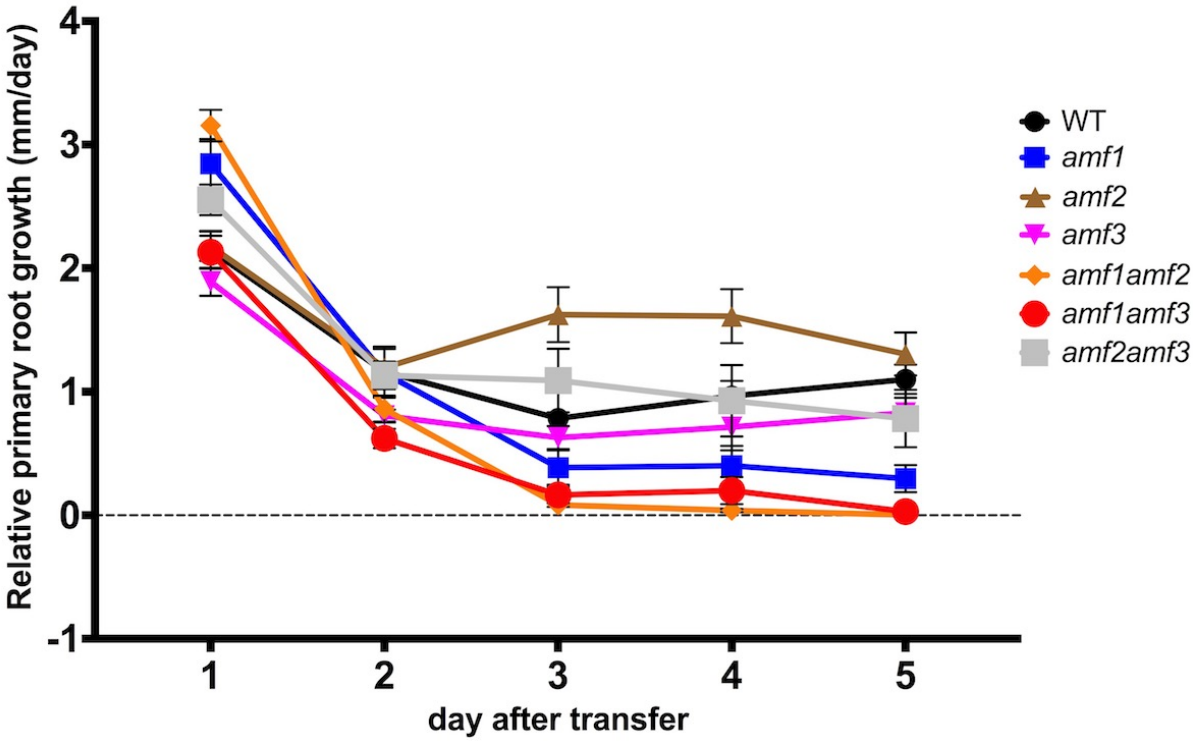
Relative primary root growth (mm/day)
4
3
2
1
0
-1
1
2
3
4
5
day after transfer
WT
amf1
amf2
amf3
amf1amf2
amf1amf3
amf2amf3

C. Shoot exposed to high MA

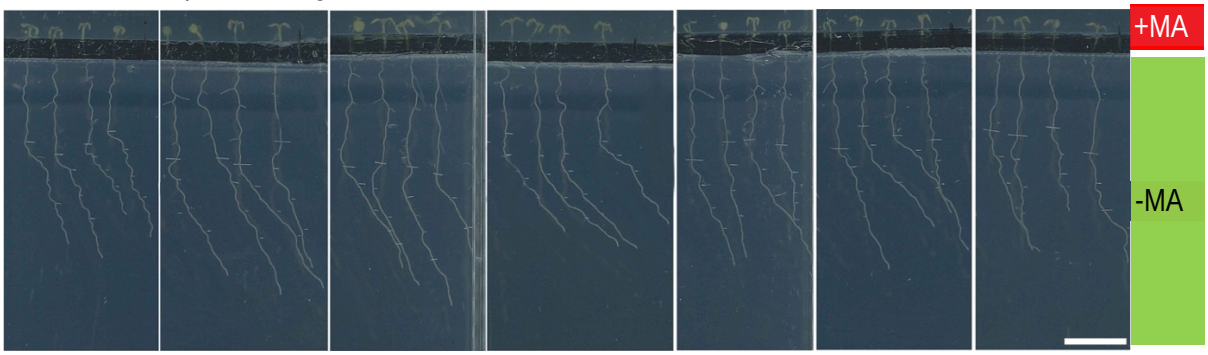

D. Root exposed to high MA

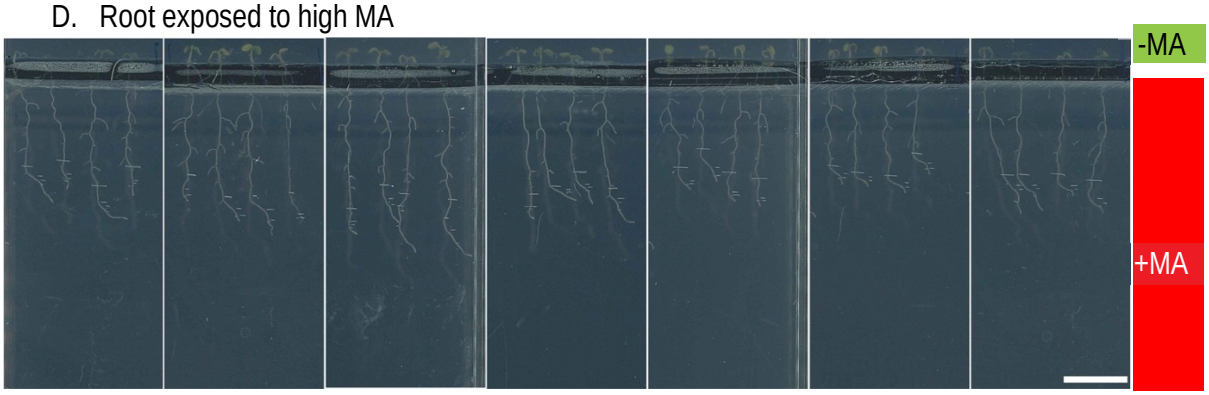

WT *amf1* *amf2* *amf3* *amf1amf2* *amf1amf3* *amf2amf3*

Supplemental Figure S4.4. MA exposure inhibited primary root growth at low NO_3^- concentration. 5-day-old seedlings germinated at 1 mM NH_4NO_3 were transferred to split media on plates containing low NO_3^- (0.05 mM) and 3.75 mM K^+. Primary root length was measured daily to calculate relative root growth with only shoot (A) or root (B) tissues exposed to high MA at low NO_3^-. Data values represent the mean ± SEM (n=11-12 biological replicates). Dash line indicates zero primary root growth.

Representative pictures of WT and *amf* seedlings five days after transplantation with only shoot (C) or root (D) tissues exposed to high MA. -MA: low NO_3^- media without MA; +MA: low NO_3^- media supplemented with 20 mM MA. Scale bar = 1 cm.

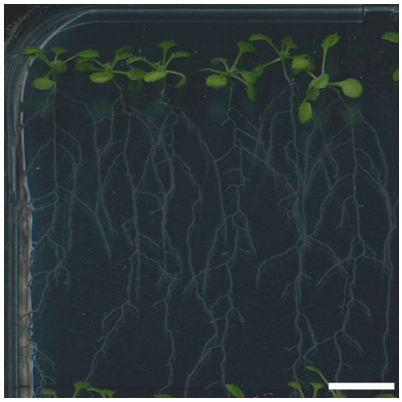

WT

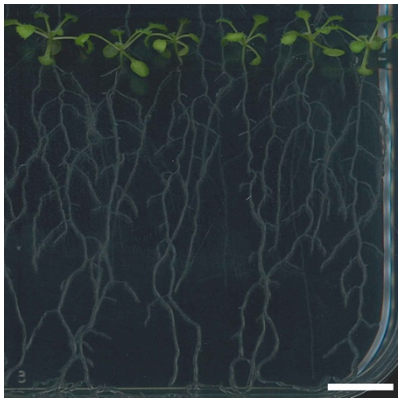

amf1

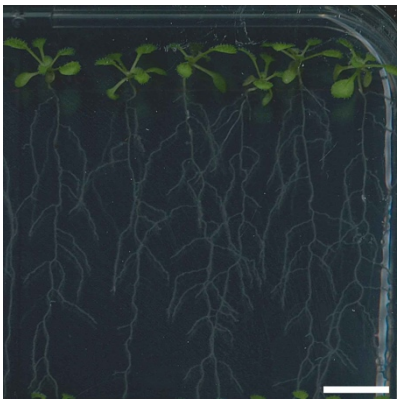

amf2

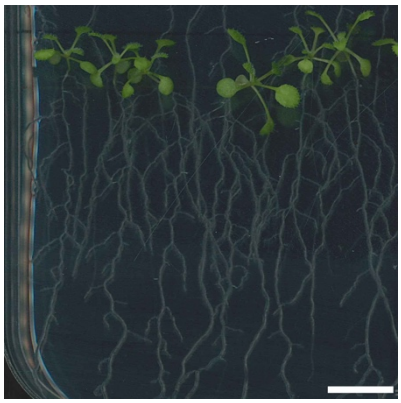

amf3

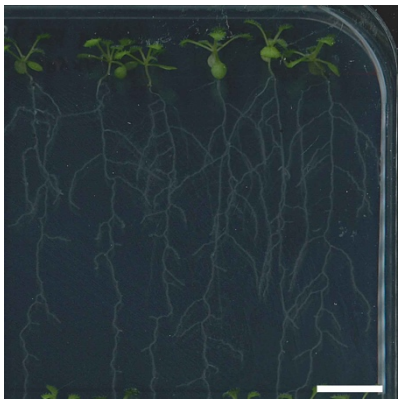

amf1amf2

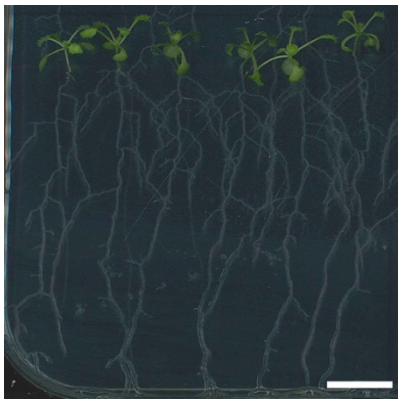

amf1amf3

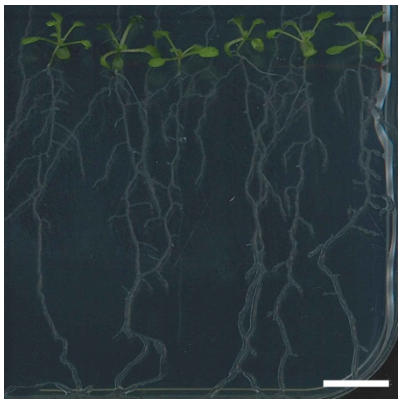

amf2amf3

Supplemental Figure S4.5. *amf* mutants grew similar to WT on NH_4^+-free media with 1 mM K^+ and 7.5 mM NO_3^-.

Representative pictures of 14-day-old WT and *amf* mutant lines seedlings. Scale bar = 1 cm.

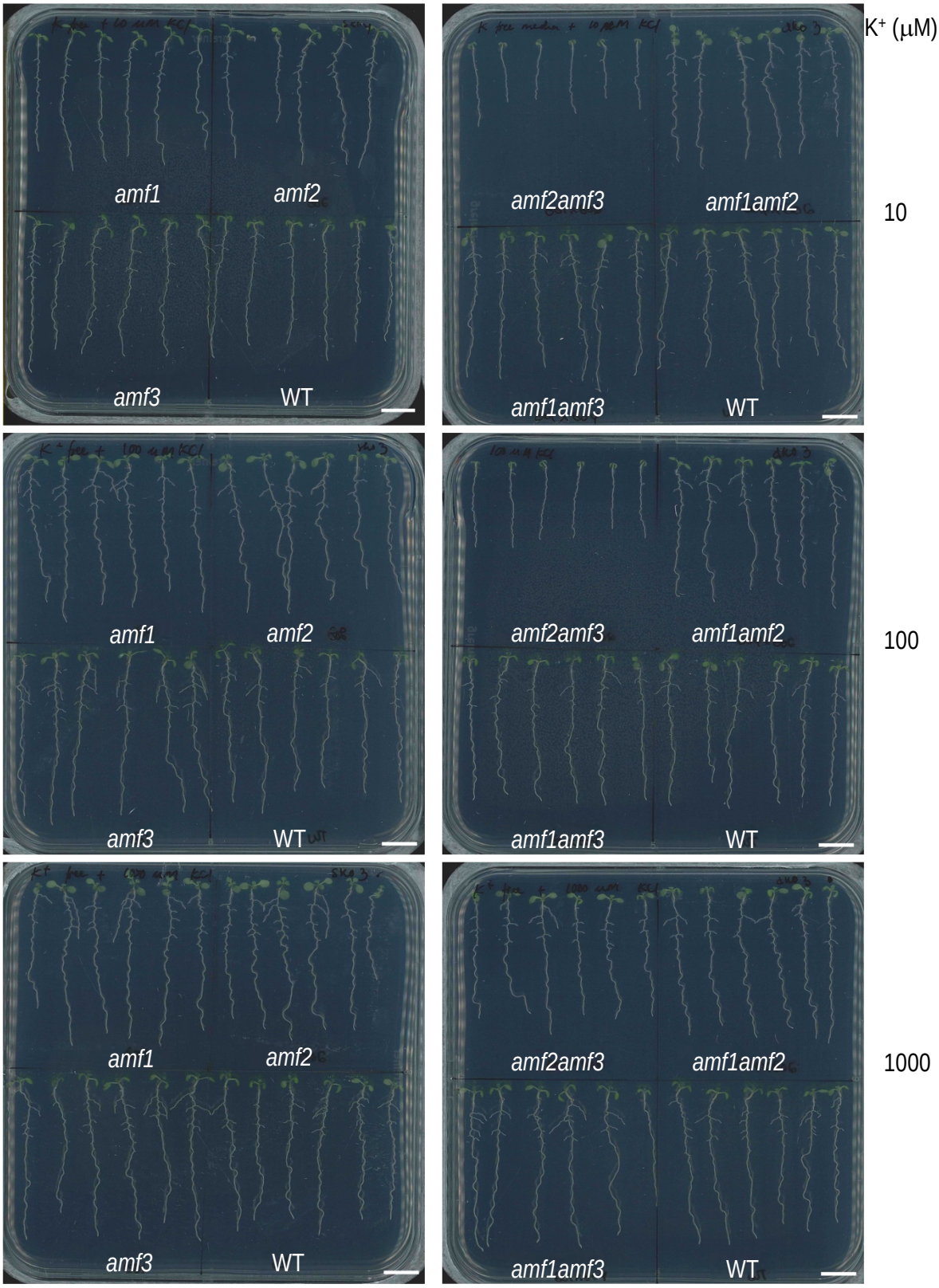

Supplemental Figure S4.6. *amf2amf3* mutant plants displayed delayed growth at low K^+ conditions (≤100 μM) in the presence of 2 mM NH_4^+ and 7.5 mM NO_3^-

Representative pictures of WT and *amf* mutant lines at 7 d after germination. Scale bar = 1 cm.

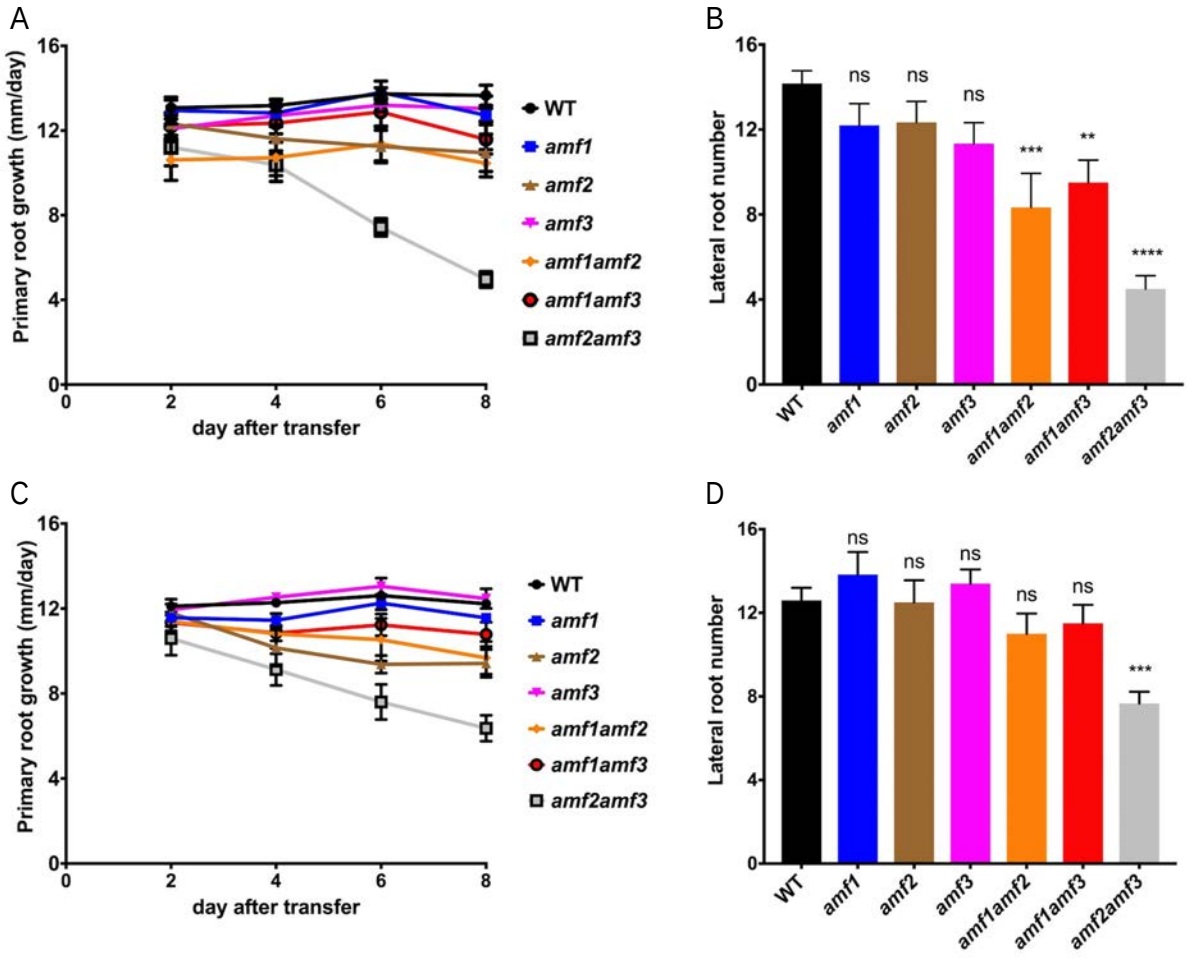

Supplemental Figure S4.7. Phenotype of WT and *amf* mutant seedlings at 10 μM K^+ grown with adequate NO_3^- (7.5 mM) (A) and low NO_3^- (0.05 mM) (B) in the presence of 2 mM NH_4^+

4-day-old seedlings germinated on NH_4-free media containing 1 mM K^+ were transplanted onto different treatment media. Primary root growth and lateral root number of plants grown under adequate NO_3^- (A and B, respectively) and under low NO_3^- (C and D). Primary root growth was measured every two days (C) using ImageJ software. Data values represent the means ± SEM (n=5-6 biological replicates). Asterix indicates significant difference compared to WT, ** P=0.0027; *** P<0.0005; *** P<0.0001 and uncorrected Fisher's LSD post-test; ns = not significant.

Supplemental Table S4.1. Primer pairs for homozygosity screening

Primer pair	Sequence (5'-3')	Purpose
AMF1-gene-F	GAATCTGTTGGAAACCTTCCC	AMF1 gene amplification
AMF1-gene-R	GAAGATGACAATACACCATCTTCG	
AMF2-gene-F	TAGGCAGATTCCCCTAAGAGG	AMF2 gene amplification
AMF2-gene-R	GGGCAGCAAGACTTACAAATG	
AMF3-gene-F	CCAAATCAAAACAGGAATCGG	AMF3 gene amplification
AMF3-gene-R	GGACAACCAGGTTCTTGGATC	
Sail_LB3	TAGCATCTGAATTTCATAACCAAT CTCGAT	*amf1* T-DNA amplification
AMF1-gene-R	GAAGATGACAATACACCATCTTCG	
Sail_LB3	TAGCATCTGAATTTCATAACCAAT CTCGAT	*amf2* T-DNA amplification
AMF2-gene-R	GGGCAGCAAGACTTACAAATG	
Sail_LB3	TAGCATCTGAATTTCATAACCAAT CTCGAT	*amf3* T-DNA amplification
AMF3-gene-R	GGACAACCAGGTTCTTGGATC	
AtAMF1-F	CACCATGGTGACCAAAGAAGAA	AMF1 transcript amplification
AtAMF1-R	TTATGAATATCCCTTGCAAAAGCAC	
AtAMF2-F	CACCATGGATGTTGACGGAGAA	AMF2 transcript amplification
AtAMF2-R	TCATGCTTCCTGGAGAAGAGGC	
AtAMF3-F	CACCATGACGAGAGTTGGCCA	AMF3 transcript amplification
AtAMF3-R	TTAGGCGAGAGTAGAGTTCTCTGTTTTGCT	

Supplemental Table S4.2. Composition of hydroponic media

Components	Concentration (mM)
$MgSO_4.7H_2O$	1.0000
KH_2PO_4	1.0000
Fe-Na-EDTA	0.1000
NH_4NO_3	1.0000
Trace Elements	
H_3BO_3	0.0500
$MnSO_4.H_2O$	0.0050
$ZnSO_4.7H_2O$	0.0010
$CuSO_4.5H_2O$	0.0010
$Na_2MoO_4.2H_2O$	0.0007
KCl	0.0500
K & Ca supplements	
K_2SO_4	0.2500
$CaCl_2.2H_2O$	0.2500

Supplemental Table S4.3. *In-vitro* media composition for low K^+ experiments.

Macronutrients		Vitamins	(mg L^{-1})
$NaNO_3$	2.5 mM	Glycine	2
$Ca(NO_3)_2$	2.5 mM	Myo-inositol	100
$NH_4H_2PO_4$	2 mM	Nicotinic acid	0.5
$MgSO_4$	2 mM	Pyridoxine-HCl	0.5
Fe-Na-EDTA	0.1 mM	Thiamine-HCl	0.1
Trace elements			
H_3BO_3	2.5 μM	MES	0.05%
$CaCl_2$	2.5 μM	Sucrose	1%
$MnSO_4$	2.0 μM	Agar	0.8%
$CuSO_4$	0.5 μM		
Na_2MoO_4	0.2 μM		
$CoCl_2$	0.01 μM		

5. General discussion and future directions

5.1 Summary of findings

The studies performed in this thesis identified a number of interesting insights into the potential function of the AMF family in Arabidopsis. Features of each AMF family member identified through studies in wild type plants (Col-0), multiple yeast strains and *amf ko* mutant plants are summarised in Table 5.1.

In wild type plants, the *AMF* family is preferentially expressed in shoot tissues, particularly in senescing leaves. This pattern contrasts to the high-affinity ammonium transporter family *AMT*, which are predominantly expressed at high levels in root tissues. This then suggests the function of the Arabidopsis AMF family is most likely distinctive to that of the AtAMTs in relation to NH_4^+ transport and cellular NH_4^+ regulation. *AtAMFs* were found to be expressed next to vascular tissues in pericycle cells and in vascular regions of emerging lateral roots. These results suggest a potential role in NH_4^+ translocation between cells as well as in cellular adaptation induced by the presence of NH_4^+. Furthermore, the AtAMF family exhibited a specified subcellular localisation in *Nicotiana benthamiana,* where AtAMF1 was localised in the ER while AtAMF2 and AtAMF3 was localised in the tonoplast and plasma membrane, respectively.

Functional activities of AtAMFs were partly described using heterologous expression in selected NH_4^+ and K^+ transport mutants of *Saccharomyces cerevisiae*. It was shown that overexpression of AtAMF2 induced MA toxicity in the NH_4^+ transport deficient strain, 31019b. Interestingly, this phenotype could be reversed with the addition of K^+. This data supports the idea that AMF activity allows for competition or interaction between NH_4^+/MA and K^+. Using a yeast strain defective in two main K^+ transporters, CY162 (*trk1⊿*; *trk2⊿*) revealed that K^+ transport deficiencies causes NH_4^+ hypersensitivity in CY162. Interestingly, overexpression of AtAMF2 rescued CY162 hypersensitivity to high NH_4^+. This data was at first sight contradictory to previous findings in this thesis, where overexpression of AtAMF2 in 31019b increased hypersensitivity to MA. Subcellular localisation revealed that AtAMF2 is localised to the tonoplast of CY162 and BY4741strains similar to its localisation in *Nicotiana benthamiana* cells. A proposed model (Figure 3.12) places AtAMF2 as a functional NH_4^+ efflux protein responsible for retrieving NH_4^+/MA from the vacuole back into the cytoplasm. Figure 3.12.B demonstrates how the MA-resistant 31019b yeast strain overexpressing AtAMF2 showed toxicity symptoms at high MA. PIPs facilitate uncharged MA transport through the plasma membrane and then undergoes sequestration into the vacuole facilitated by a TIP2-like protein, potentially by the tonoplast bound yeast aquaporin, AQY3 (Patel, 2013). The presence of AtAMF2 in the tonoplast releases vacuolar MA into the cytoplasm leading to MA toxicity. In contrast, when NH_4^+ is supplied to the CY162 strain, NH_4^+ retrieval facilitated by AtAMF2 provides NH_4^+ to support cell growth (Figure 3.12.D) or induce toxicity when supplied with MA (Figure 3.12.E). Accordingly, Hess et al. (2006) revealed that under low K^+ and high NH_4^+, yeast cells excrete amino acids as part of a proposed detoxification mechanism. This event potentially leads to an amino acid starvation state, poor growth and eventually cell death. The importance of essential amino acids

during NH_4^+/MA toxicity events was confirmed in this thesis. When supplied with proline as the sole amino acid, the NH_4^+ sensitive yeast strain CY162 failed to grow at high MA. However, when supplied with a select few essential amino acids, growth was improved. Supplementation of complete essential amino acids overcame MA toxicity. Interestingly, there were comparable functionalities of an AMF homolog cloned from maize (ZmAMF1) when expressed in yeast. Accordingly, transient expression in *Nicotiana benthamiana* epidermal cells also demonstrated its subcellular localisation in the tonoplast, the same as AtAMF2. These data indicate that this might be a conserved mechanism as AMF homologs are present across plants.

The potential roles of the AtAMF family in relation to NH_4^+ toxicity was further investigated by *in-planta* analysis of *amf* mutants. It was shown, that *dko* mutants exhibited enhanced sensitivity compared to *sko* mutant lines. This additional effect is intriguing, especially based on the alternative organelle arrangement of each protein. Most-likely, AtAMFs interact with each other to provide a collective NH_4^+ toxicity or homeostatic response in plants. The results also confirmed a close interrelation between NH_4^+ toxicity with external availability of NO_3^- and K^+. AtAMF1 was linked to NH_4^+ toxicity under low [NO_3^-], while AtAMF2 and AtAMF3 potentially participate in NH_4^+ toxicity under low [K^+] independent of [NO_3^-]. However, the definite mechanisms of the AtAMFs in relation to NH_4^+ toxicity tolerance still requires further study.

5.2 Proposed functions of the AtAMF family in plants

Based on the data collected so far, a model is presented to summarise the potential role(s) of the AtAMF family (Figure 5.1). This model details how AtAMF proteins in collaboration with the other transport protein families facilitate NH_4^+ transport in plant cells.

a) AtAMF1 did not behave as either an NH_4^+ or MA transporter in yeast cells. In plants, the loss of AtAMF1 influenced plant growth by reducing primary root growth when *sko amf1* mutant plants were grown on low NO_3^- media in the presence of methylammonium. This response increased when combined with deletions in AtAMF2 or AtAMF3 e.g. *dko amf1amf2* and *amf1amf3* mutant lines. Additionally, N-deficient conditions triggers the expression of nitrate transporters as well as high-affinity ammonium transporters in roots (Gazzarrini et al., 1999; Rawat et al., 1999; Kaiser et al., 2002; Yuan et al., 2007; Kiba and Krapp, 2016). It is proposed that under N deficiency, NO_3^- uptake requires an accompanying uptake of NH_4^+ to help maintain charge balance during uptake and assimilation, and CIPK23, a regulator of both NPF and AMT transporters has also been shown to participate in the regulation of this coupled transport process (Straub et al., 2017). Since AtAMF1's primary location is in the ER and didn't show any NH_4^+/MA transport activities in yeast, it is unlikely that AtAMF1 participates in plasma membrane NH_4^+ transport (influx or efflux). However, it may have a role in the ER to influence root-cell NH_4^+ management. Surprisingly, loss of AtAMF1 resulted in an increased rate of unidirectional NH_4^+ uptake into roots, suggesting either increased NH_4^+ uptake across the plasma membrane either from AMTs or other AMFs

or a change in root cells retaining NH_4^+ through decreased efflux or transfer to the shoot. Intriguingly, qPCR results and online database revealed that *AtAMF1* was expressed mostly in the leaf tissues. Additionally, based on promoter::GUS experiments, it was shown that AtAMF1 was localised around the vascular bundle. These data suggest that AtAMF1 might potentially involve in root-to-shoot NH_4^+ translocation mechanism(s). Furthermore, the mechanism could involve a signalling cascade directed from the ER initiated through cytosolic N availability as proposed in Figure 5.1. Further studies are required to define the transport activities of AtAMF1 using both a heterologous expression system (*Xenopus* oocytes) and plant mutants (AMT/AMF *ko* crosses) to link activity to MA sensitivity and enhance NH_4^+ uptake in Arabidopsis roots.

b) In the yeast K^+ transport mutant CY162, AtAMF2 was shown to rescue cell growth when exposed to toxic concentrations of NH_4^+. In contrast, using the NH_4^+ transport mutant 31019b, AtAMF2 activity increased MA sensitivity (cell death) at elevated pH. AtAMF2 was found to be targeted to the tonoplast in both yeast and plant cells (*Nicotiana benthamiana*). The ability to relieve NH_4^+ toxicity or induce MA sensitivity in yeast cells is hypothesised to be through a process where AtAMF2 transports either NH_4^+ or MA out of the vacuole into the cytoplasm, where it is either metabolised or concentrated, respectively. Correspondingly, *in planta*, the NH_4^+ efflux capabilities of AtAMF2 might be important for NH_4^+ recycling from the vacuole following substrate degradation. Indeed, qPCR and online database demonstrated an up-regulation of AtAMF2 expression in senescing leaves. Based on currently available data, it is suggested that AtAMF2 is a functional NH_4^+ effluxer retrieving NH_4^+ from the vacuole into the cytoplasm (Figure 5.1). Unfortunately, the transport mechanism of the protein, whether it functions as a uniporter, symporter or antiporter, needs more extensive studies.

In contrast to *amf1* mutant phenotypes, the *amf2* mutant plants failed to show any impact on plant growth when grown on low NO_3^- and MA. However, a cross between *amf2* and *amf1* (*amf1 amf2*) increased the sensitivity to MA over that of the *sko amf1* line, suggesting an accumulative role of *amf2* in the MA toxicity phenotype. When plants were grown on NH_4^+ containing media with decreasing concentrations of K^+, the *sko amf2* mutant line had a reduction in root growth at 10 µM K^+ but not at 100 µM. However, when crossed with the *amf3* KO (*amf2amf3*), root growth and plant fresh weight was drastically reduced when grown on NH_4^+ and low [K^+]. Significant impact of NH_4^+ on root growth of *amf2 amf3* mutant line might be linked to the AtAMF2 tissue localisation in the root tip and root primordia of lateral roots. Collectively, these data evidently demonstrate the importance of AMF2 in NH_4^+ toxicity under low K^+ availability.

c) The role of AtAMF3 is less clear. AtAMF3 was found localised to the plasma membrane in *Nicotiana benthamiana* leaf cells, similar to other AMF homologs, ScAMF1 and GmAMF3. Both ScAMF1 and GmAMF3 have been shown to facilitate MA influx in yeast and *Xenopus* oocytes (Chiasson et al.,

2014). In contrast, based on limited data gathered from heterologous expression in yeast (Figure 3.3.2), it seems that AtAMF3 might be involved in NH_4^+/MA efflux from the cytoplasm. Therefore, *in planta*, it is possible that AtAMF3 may transport NH_4^+ out of the cell across the plasma membrane to the apoplast. Moreover, the tissue localisation of AtAMF2 around the vascular bundle and pericycle cells might indicate it potential role in NH_4^+ loading to xylem for translocation (Figure 5.1). Unfortunately, at this time, the evidence supporting NH_4^+/MA efflux properties are limited with the exception that when AtAMF3 was expressed in 31019b cells and grown on high MA concentrations (100 mM) at neutral pH (7), cell growth improved over the empty vector controls (Figure 3.2). This result suggested an AMF3-enhanced tolerance to toxic MA, possibly through a yet unidentified CH_3NH_3 efflux capability. The *amf3* KO line showed no measurable sensitivity to MA (increased tolerance) when grown on low [NO_3^-] but hypocotyl growth was compromised at elevated MA (20 mM). Although *amf3* root growth decreased at low [K^+] in the presence of NH_4^+, this was not translated into reductions in overall plant biomass. As mentioned previously, a double mutation in *dko amf2 amf3* mutant plants displayed significant reductions in root growth and overall plant biomass. Root growth on NH_4^+ or MA containing plate media was inhibited in a [K^+] independent manner, while overall plant fresh weight decreased significantly at reduced [K^+] concentrations in the presence of NH_4^+. Previous studies have demonstrated that uncharged NH_3 is the main species effluxed across plasma membrane of yeast (Wood et al., 2006) and barley (Coskun et al., 2013a) a process, which usually occurs at more alkaline pH or when plants are grown with low [K^+]. Based on the evidence in-hand, the *in-planta* activity of AtAMF3 is more aligned with NH_3 efflux from the cytoplasm into the apoplast. It is unclear when this activity would be required outside of situations where NH_4^+ toxicity becomes a problem. The fate of effluxed NH_3 into the apoplast is unknown but could be delivered to the xylem or out of the root via passive diffusion. Molecular evidence for NH_4^+ efflux activity has been previously linked to AtAMT2 (Sohlenkamp et al., 2002; Neuhäuser et al., 2009) and in recent studies by Giehl et al. (2017) who demonstrated a significant decrease in NH_4^+ translocation (root to shoot) in *atamt2;1* mutant plants when supplied with high external NH_4^+. Unfortunately, empirical studies regarding the efflux capabilities of both AMT2;1 and AMF3 have yet to be determined, future research in this area is required.

5.3 Future directions

Although a number of discoveries were made in this thesis, the definite function of the AtAMF family in regard to NH_4^+ transport still remains poorly understood. Therefore, more studies need to be undertaken to fully unmask the transport and potential signal roles of these proteins. Further studies focusing in mutagenesis of conserved regions are required to identify amino acid residues crucially important for functional proteins. Detailed electrophysiological studies in oocytes, yeast or other systems are extremely critical to confirm the proposed function of the proteins. Moreover, more precise tissue specific localisation studies using a wider range of native promoter sizes are required to clarify the exact tissue specific localisation of the proteins and validate their proposed function. Different promoter sizes have been shown to cause discrepancies in AtAMT2 tissue specific localisations (Sohlenkamp et al., 2002; Neuhäuser et

al., 2009; Giehl et al., 2017). Additionally, *in-planta* pulse-chase studies using $^{15}NH_4$ is essential to investigate the involvement of the AtAMF family in NH_4^+ translocation mechanisms.

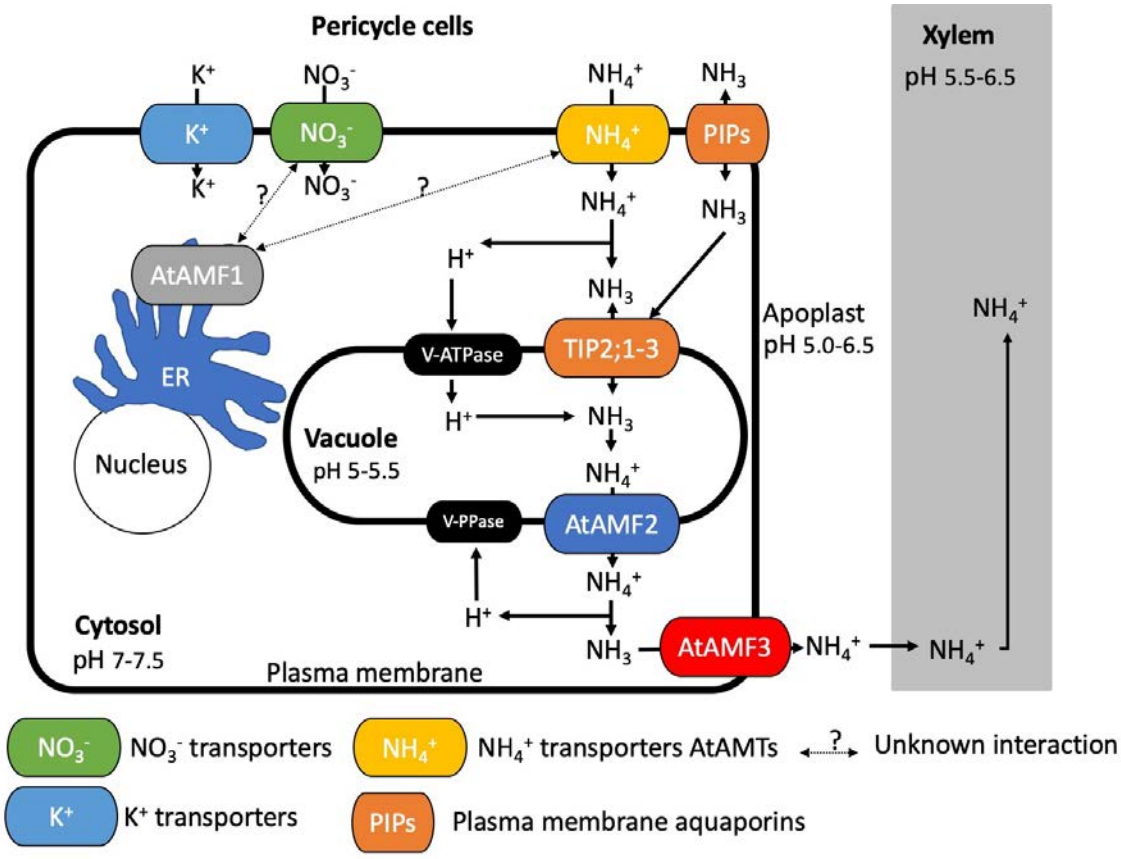

Figure 5.1 Proposed function of the AtAMF family *in planta* in regard to NH_4^+ transport.

This model proposes the interaction of AtAMF1 (directly or indirectly through unidentified mechanisms) with NO_3^- and/or NH_4^+ transporters in order to finely regulate N nutrient homeostasis in the cell cytoplasm. Additionally, this model also demonstrates a proposed direct involvement of AtAMF2 and AtAMF3 in NH_4^+ regulation mechanisms linked to NH_4^+ tolerance. NH_4^+ enters the pericycle cells via the symplastic route facilitated by the AMT1 proteins (Yuan et al., 2007) while the plasma membrane localised aquaporins (PIPs) facilitate the uncharged NH_3 fluxes into the cytoplasm. The ion is then de-protonated and the uncharged NH_3 is rapidly sequestrated by AtTIP2 proteins and acid-trapped inside the vacuole (Loqué et al., 2005) to avoid toxicity or stored as reserves for further assimilation when required. AtAMF2 acts to slowly release the trapped ion back into the cytoplasm, probably triggered by a signal generated by the NH_3/NH_4^+ concentration in the cytoplasm. The same signal may also negatively regulate the TIP2. A fine-tune regulation of both AMF2 and TIP2 by yet unidentified signalling pathway(s) is essential to maintain appropriate NH_3 concentration in the cytoplasm. Due to the slightly alkali environment in the cytoplasm, the released NH_4^+ undergoes de-protonation to NH_3. The uncharged species is either assimilated into amino acids under low N conditions/high N demand or alternatively is effluxed out of the cells by AtAMF3 when the [NH_3] in the cytoplasm is high and/or the vacuole is saturated with NH_4^+ e.g. under high NH_4^+ and low K^+. Evidence for this type of response was found in the double mutant *amf2amf3* that displayed severe NH_4^+ toxicity symptoms. As AtAMF3 is localised in pericycle cells, it facilitates the release of NH_3 into the apoplast. The uncharged NH_3 is protonated into NH_4^+ in the acidic environment of the apoplast and possibly be loaded into the xylem or alternatively lost out of the root.

Table 5.1. Summary of AtAMF family member features

Gene Expression	Tissue localisation	Subcellular localisation in plant cells	Phenotype in yeast strain			Yeast subcellular localisation		T-DNA mutant phenotypes
			Mutant 31019b	Mutant CY162	Wild type BY4741	Mutant CY162	Wild type BY4741	
AtAMF1								
Low level of expression amongst AtAMF members	Vascular bundles, pericycle cells	ER	Failed to rescue growth with NH_4^+ as sole N source	Failed to rescue growth under low K^+ and high NH_4^+	N/A	N/A	N/A	Increased sensitivity to MA under low nitrate
Expressed in young leaf tissues	Guard cells		Failed to induce toxicity phenotype on MA media	Failed to rescue growth with low K^+ (<0.1 mM)				Double knockout with *amf2* or *amf3* increased sensitivity to MA under low nitrate
Diurnal regulation, peak expression in the afternoon								
Responds to N-starvation and resupply								
AtAMF2								
High expression relative to other AtAMF members	Root cap	Tonoplast	Failed to rescue growth with NH_4^+ as sole N source	Rescued growth under low K^+ and high NH_4^+ with limited amino acid supply	Induced toxicity phenotype on MA media with limited amino acid supply	Tonoplast, cytoplasm and ER	Tonoplast	Double knockout with *amf3* (*amf2amf3*) induced hypersensitivity to NH_4^+ under low K^+.

Senescing leaf tissues	Pericycle cells under root primordia and lateral roots		Induced toxicity phenotype on MA media	Induced toxicity phenotype on MA media with limited amino				
Diurnal regulation, peak expression in the afternoon				Failed to rescue growth with low K^+ (<0.1 mM)				
Responds to N-starvation and resupply								
AtAMF3								
Expressed at higher levels than AtAMF1 but less than AtAMF2	Vascular bundle, pericycle cells	Plasma membrane	Failed to rescue growth with NH_4^+ as sole N source	Failed to rescue growth under low K^+ and high NH_4^+	N/A	N/A	N/A	Double knockout with *amf3* (*amf2amf3*) induced hypersensitivity to NH_4^+ under low K^+.
Senescing leaf tissues			Improved growth on media containing MA at neutral pH	Failed to rescue growth with low K^+ (<0.1 mM)				
Diurnal regulation, peak expression in the afternoon								
Responds to N-starvation and resupply								

6. References:

Alberti, S., Gitler Aaron, D., and Lindquist, S. (2007). A Suite of Gateway® Cloning Vectors for High-throughput Genetic Analysis in *Saccharomyces cerevisiae*. Yeast 24, 913-919.

Alonso, J.M., and Ecker, J.R. (2006). Moving Forward in Reverse: Genetic Technologies to Enable Genome-wide Phenomic Screens in *Arabidopsis*. Nature Reviews Genetics 7, 524.

Andrade, S.L., and Einsle, O. (2007). The Amt/Mep/Rh Family of Ammonium Transport Proteins. Molecular membrane biology 24, 357-365.

Ariz, I., Boeckstaens, M., Gouveia, C., Martins, A.P., Sanz-Luque, E., Fernández, E., Soveral, G., von Wirén, N., Marini, A.M., Aparicio-Tejo, P.M., and Cruz, C. (2018). Nitrogen isotope signature evidences ammonium deprotonation as a common transport mechanism for the AMT-Mep-Rh protein superfamily. Science Advances 4, eaar3599.

Arpat, A.B., Magliano, P., Wege, S., Rouached, H., Stefanovic, A., and Poirier, Y. (2012). Functional Expression of PHO1 to the Golgi and Trans-Golgi Network and its Role in Export of Inorganic Phosphate. The Plant Journal 71, 479-491.

Bagola, K., Mehnert, M., Jarosch, E., and Sommer, T. (2011). Protein Dislocation from the ER. Biochimica et Biophysica Acta (BBA) - Biomembranes 1808, 925-936.

Bai, L., Ma, X., Zhang, G., Song, S., Zhou, Y., Gao, L., Miao, Y., and Song, C.-P. (2014). A Receptor-Like Kinase Mediates Ammonium Homeostasis and Is Important for the Polar Growth of Root Hairs in *Arabidopsis*. The Plant cell 26, 1497-1511.

Balkos, K.D., Britto, D.T., and Kronzucker, H.J. (2010). Optimization of Ammonium Acquisition and Metabolism by Potassium in Rice (*Oryza sativa* L. cv. IR-72). Plant, cell & environment 33, 23-34.

Barker, A.V. (1999). Foliar Ammonium Accumulation as an Index of Stress in Plants. Communications in Soil Science and Plant Analysis 30, 167-174.

Barreto, L., Canadell, D., Valverde-Saubí, D., Casamayor, A., and Ariño, J. (2012). The Short-term Response of Yeast to Potassium Starvation. Environmental Microbiology 14, 3026-3042.

Bertl, A., and Kaldenhoff, R. (2007). Function of a Separate NH_3-pore in Aquaporin TIP2;2 from Wheat. FEBS Letters 581, 5413-5417.

Bloom, A.J. (2011). Energetics of Nitrogen Acquisition. In Annual Plant Reviews, Nitrogen Metabolism in Plants in the Post-genomic Era, C. Foyer and H. Zhang, eds (West Sussex, UK: Wiley-Blackwell.

Bloom, A.J., Sukrapanna, S.S., and Warner, R.L. (1992). Root Respiration Associated with Ammonium and Nitrate Absorption and Assimilation by Barley. Plant Physiology 99, 1294-1301.

Boll, M., Daniel, H., and Gasnier, B. (2004). The SLC36 Family: Proton-coupled Transporters for the Absorption of Selected Amino Acids from Extracellular and Intracellular Proteolysis. Pflügers Archiv 447, 776-779.

Bozdag, G.O., Uluisik, I., Gulculer, G.S., Karakaya, H.C., and Koc, A. (2011). Roles of ATR1 Paralogs YMR279c and YOR378w in Boron Stress Tolerance. Biochemical and Biophysical Research Communications 409, 748-751.

Britto Dev, T., Siddiqi, M.Y., Glass Anthony, D.M., and Kronzucker Herbert, J. (2002). Subcellular NH_4^+ Flux Analysis in Leaf Segments of Wheat (*Triticum aestivum*). New Phytologist 155, 373-380.

Britto, D.T., and Kronzucker, H.J. (2002). NH_4^+ Toxicity in Higher Plants: a Critical Review. Plant Physiology 159, 567-584.

Britto, D.T., Siddiqi, M.Y., Glass, A.D., and Kronzucker, H.J. (2001). Futile Transmembrane NH_4^+ Cycling: a Cellular Hypothesis to Explain Ammonium Toxicity in Plants. PNAS 98, 4255-4258.

Büttner, M. (2007). The Monosaccharide Transporter(-like) Gene Family in *Arabidopsis*. FEBS Letters 581, 2318-2324.

Byrt, C.S., Zhao, M., Kourghi, M., Bose, J., Henderson, S.W., Qiu, J., Gilliham, M., Schultz, C., Schwarz, M., Ramesh, S.A., Yool, A., and Tyerman, S. (2017). Non-selective Cation Channel Activity of Aquaporin AtPIP2;1 Regulated by Ca_2^+ and pH. Plant, cell & environment 40, 802-815.

Camargo, J.A., and Alonso, A. (2006). Ecological and Toxicological Effects of Inorganic Nitrogen Pollution in Aquatic Ecosystems: A global Assessment. Environment international 32, 831-849.

Cao, Y., Glass, A.D.M., and Crawford, N.M. (1993). Ammonium Inhibition of *Arabidopsis* Root Growth Can Be Reversed by Potassium and by Auxin Resistance Mutations *aux1*, *axr1*, and *axr2*. Plant Physiology 102, 983.

Chiasson, D.M., Loughlin, P.C., Mazurkiewicz, D., Mohammadidehcheshmeh, M., Fedorovac, E.E., McLeand, M.O.E., Glass, A.D.M., Smith, S.E., Bisseling, T., Tyerman, S.D., Day, D.A., and Kaiser, B.N. (2014). Soybean SAT1 (Symbiotic Ammonium Transporter 1) Encodes a bHLH Transcription Factor Involved in Nodule Growth and NH_4^+ Transport. PNAS2014:1312801111v1-201312801.

Clough, S.J., and Bent, A.F. (1998). Floral Dip: a Aimplified Method for *Agrobacterium*-mediated Transformation of *Arabidopsis thaliana*. The Plant Journal 16, 735-743.

Cohen, R., and Engelberg, D. (2007). Commonly used *Saccharomyces cerevisiae strains* (e.g. BY4741, W303) are Growth Sensitive on Synthetic Complete Medium due to Poor Leucine Uptake. FEMS Microbiology Letters 273, 239-243.

Coskun, D., Britto, D.T., and Kronzucker, H.J. (2017). The Nitrogen–Potassium Intersection: Membranes, Metabolism, and Mechanism. Plant, cell & environment 40, 2029-2041.

Coskun, D., Britto, D.T., Li, M., Becker, A., and Kronzucker, H.J. (2013a). Rapid Ammonia Gas Transport Accounts for Futile Transmembrane Cycling under NH_3/NH_4^+ Toxicity in Plant Roots. Plant Physiology 163, 1859.

Coskun, D., Britto, D.T., Li, M., Oh, S., and Kronzucker, H.J. (2013b). Capacity and Plasticity of Potassium Channels and High-Affinity Transporters in Roots of Barley and *Arabidopsis*. Plant Physiology 162, 496.

Cueto-Rojas, H.F., Milne, N., van Helmond, W., Pieterse, M.M., van Maris, A.J.A., Daran, J.-M., and Wahl, S.A. (2017). Membrane Potential Independent Transport of NH_3 in the Absence of Ammonium Permeases in *Saccharomyces cerevisiae*. BMC Systems Biology 11, 49.

Davenport, R.J., and Tester, M. (2000). Davenport RJ, Tester M. A Weakly Voltage-Dependent, Nonselective Cation Channel Mediates Toxic Sodium Influx in Wheat. Plant Physiology 122, 823-834.

Day, D.A., Poole, P.S., Tyerman, S.D., and Rosendahl, L. (2001). Ammonia and Amino Acid Transport Across Symbiotic Membranes in Nitrogen-fixing Legume Nodules. Cellular and Molecular Life Sciences CMLS 58, 61-71.

Demidchik, V., and Tester, M. (2002). Sodium Fluxes Through Non-selective Cation Channels in the Plasma Membrane of Protoplasts from *Arabidopsis* Roots. Plant Physiology 128, 379–387.

Dermaut, B., Norga, K.K., Kania, A., Verstreken, P., Pan, H., Zhou, Y., Callaerts, P., and Bellen, H.J. (2005). Aberrant Lysosomal Carbohydrate Storage Accompanies Endocytic Defects and Neurodegeneration in Drosophila benchwarmer. The Journal of Cell Biology 170, 127-139.

Dias, P.J., and Sá-Correia, I. (2013). The Drug:H^+ Antiporters of Family 2 (DHA2), Siderophore Transporters (ARN) and Glutathione:H^+ Antiporters (GEX) Have a Common Evolutionary Origin in Hemiascomycete Yeasts. BMC Genomics 14, 901-901.

Edwards, K., Johnstone, C., and Thompson, C. (1991). A Simple and Rapid Method for the Preparation of Plant Genomic DNA for PCR Analysis. Nucleic Acids Research 19, 1349.

Escobar, M.A., Geisler, D.A., and Rasmusson, A.G. (2006). Reorganization of the Alternative Pathways of the *Arabidopsis* Respiratory Chain by Nitrogen Supply: Opposing Effects of Ammonium and Nitrate. The Plant Journal 45, 775-788.

Esteban, R., Ariz, I., Cruz, C., and Moran, J.F. (2016). Review: Mechanisms of Ammonium Toxicity and the Quest for Tolerance. Plant Science 248, 92-101.

FAO. (2017). World Fertilizer Trends and Outlook to 2020 (Food and Agriculture Organisation of United Nations), pp. 1-38.

Frommer, W.B., and Ninnemann, O. (1995). Heterologous Expression of Genes in Bacterial, Fungal, Animal, and Plant Cells. Annual Review of Plant Physiology and Plant Molecular Biology 46, 419-444.

Gaber, R.F., Styles, C.A., and Fink, G.R. (1988). TRK1 Encodes a Plasma Membrane Protein Required for High-affinity Potassium Transport in *Saccharomyces cerevisiae*. Molecular and Cellular Biology 8, 2848.

Garnett, T., Conn, V., and Kaiser, B.N. (2009). Root Based Approaches to Improving Nitrogen Use Efficiency in Plants. Plant Cell Environment 32, 1272-1283.

Gazzarrini, S., Lejay, L., Gojon, A., Ninnemann, O., Frommer, W.B., and von Wirén, N. (1999). Three Functional Transporters for Constitutive, Diurnally Regulated, and Starvation-Induced Uptake of Ammonium into *Arabidopsis* Roots. The Plant cell 11, 937–947.

Gerendas, J., Zhu, Z., Bendixen, R., Ratcliffe, R.G., and Sattelmacher, B. (1997). Physiological and Biochemical Processes Related to Ammonium Toxicity in Higher Plants. Journal of Plant Nutrition and Soil Science 160, 239-251.

Gerendás, J., Zhu, Z., Bendixen, R., Ratcliffe, R.G., and Sattelmacher, B. (1997). Physiological and Biochemical Processes Related to Ammonium Toxicity in Higher Plants. Zeitschrift für Pflanzenernährung und Bodenkunde 160, 239-251.

Giehl, R.F.H., and von Wirén, N. (2014). Root Nutrient Foraging. Plant Physiology 166, 509.

Giehl, R.F.H., Gruber, B.D., and von Wirén, N. (2014). It's Time to Make Changes: Modulation of Root System Architecture by Nutrient Signals. Journal of Experimental Botany 65, 769-778.

Giehl, R.F.H., Laginha, A.M., Duan, F., Rentsch, D., Yuan, L., and von Wirén, N. (2017). A Critical Role of AMT2;1 in Root-to-Shoot Translocation of Ammonium in *Arabidopsis*. Molecular Plant 10, 1449-1460.

Gietz, R.D. (2014). Yeast Transformation by the LiAc/SS Carrier DNA/PEG Method. In Yeast Genetics: Methods and Protocols, J.S. Smith and D.J. Burke, eds (New York, NY: Springer New York), pp. 1-12.

Glass, A.D., Britto, D.T., Kaiser, B.N., Kronzucker, H.J., Kumar, A., Okamoto, M., Rawat, S.R., Siddiqi, M.Y., Silim, S.M., Vidmar, J.J., and Shoun, D. (2000). Nitrogen Transport in Plants, with an Emphasis on the Regulation of Fuxes to Match Plant Demand. Journal of Plant Nutrition and Soil Science 164, 199-207.

Glass, A.D., Britto, D.T., Kaiser, B.N., Kinghorn, J.R., Kronzucker, H.J., Kumar, A., Okamoto, M., Rawat, S., Siddiqi, M.Y., Unkles, S.E., and Vidmar, J.J. (2002). The Regulation of Nitrate and Ammonium Transport Systems in Plants. Journal of Experimental Botany 53, 855-864.

Grefen, C., Donald, N., Hashimoto, K., Kudla, J., Schumacher, K., and Blatt, M.R. (2010). A Ubiquitin-10 Promoter-based Vector Set for Fluorescent Protein Tagging Facilitates Temporal Stability and Native Protein Distribution in Transient and Stable Expression Studies. The Plant Journal 64, 355-365.

Hachiya, T., Watanabe, C.K., Fujimoto, M., Ishikawa, T., Takahara, K., Kawai-Yamada, M., Uchimiya, H., Uesono, Y., Terashima, I., and Noguchi, K. (2012). Nitrate Addition Alleviates Ammonium Toxicity Without Lessening Ammonium Accumulation, Organic Acid Depletion and Inorganic Cation Depletion in *Arabidopsis thaliana* Shoots. Plant and Cell Physiology 53, 577-591.

Hecht, K.A., O'Donnell, A.F., and Brodsky, J.L. (2014). The Proteolytic Landscape of the Yeast Vacuole. Cellular Logistics 4, e28023.

Hess, D.C., Lu, W., Rabinowitz, J.D., and Botstein, D. (2006). Ammonium Toxicity and Potassium Limitation in Yeast. PLOS Biology 4, e351.

Hirsch, R.E., Lewis, B.D., Spalding, E.P., and Sussman, M.R. (1998). A Role for the AKT1 Potassium Channel in Plant Nutrition. Science 280, 918.

Holm, L.M., Jahn, T.P., Møller, A.L.B., Schjoerring, J.K., Ferri, D., Klaerke, D.A., and Zeuthen, T. (2005). NH_3 and NH_4^+ Permeability in Aquaporin-expressing *Xenopus* oocytes. Pflügers Archiv 450, 415-428.

Hoopen, F.t., Cuin, T.A., Pedas, P., Hegelund, J.N., Shabala, S., Schjoerring, J.K., and Jahn, T.P. (2010). Competition Between Uptake of Ammonium and Potassium in Barley and *Arabidopsis* Roots: Molecular Mechanisms and Physiological Consequences. Journal of Experimental Botany 61, 2303-2315.

Howitt, S.M., and Udvardi, M.K. (2000). Structure, Function and Regulation of Ammonium Transporters in Plants. Biochimica et Biophysica Acta (BBA) - Biomembranes 1465, 152-170.

Jahn, T.P., Møller, A.L.B., Zeuthen, T., Holm, L.M., Klærke, D.A., Mohsin, B., Kühlbrandt, W., and Schjoerring, J.K. (2004). Aquaporin Homologues in Plants and Mammals Transport Ammonia. FEBS Letters 574, 31-36.

Jones, D.L., Owen, A.G., and Farrar, J.F. (2002). Simple Method to Enable the High Resolution Determination of Total Free Amino Acids in Soil Solutions and Soil Extracts. Soil Biology and Biochemistry 34, 1893-1902.

Kagenishi, T., Yokawa, K., and Baluška, F. (2016). MES Buffer Affects *Arabidopsis* Root Apex Zonation and Root Growth by Suppressing Superoxide Generation in Root Apex. Frontiers in plant science 7, 79.

Kaiser, B.N., Rawat, S.R., Siddiqi, M.Y., Masle, J., and Glass, A.D. (2002). Functional Analysis of an *Arabidopsis* T-DNA "knockout" of the High-affinity NH_4^+ Transporter AtAMT1;1. Plant Physiology 130, 1263-1275.

Kaiser, B.N., Finnegan, P.M., Tyerman, S.D., Whitehead, L.F., Bergersen, F.J., Day, D.A., and Udvardi, M.K. (1998). Characterization of an Ammonium Transport Protein from the Peribacteroid Membrane of Soybean Nodules. Science 281, 1202-1206.

Kaya, A., Karakaya, H.C., Fomenko, D.E., Gladyshev, V.N., and Koc, A. (2009). Identification of a Novel System for Boron Transport: Atr1 Is a Main Boron Exporter in Yeast. Mol. Cell. Biol. 29, 3665-3674.

Kiba, T., and Krapp, A. (2016). Plant Nitrogen Acquisition Under Low Availability: Regulation of Uptake and Root Architecture. Plant and Cell Physiology 57, 707-714.

Kim, K.-W., Franceschi, V.R., Davin, L.B., and Lewis, N.G. (2006). β-Glucuronidase as Reporter Gene. In Arabidopsis Protocols, J. Salinas and J.J. Sanchez-Serrano, eds (Totowa, NJ: Humana Press), pp. 263-273.

Kingsman, S.M., Kingsman, A.J., Dobson, M.J., Mellor, J., and Roberts, N.A. (1985). Heterologous Gene Expression in *Saccharomyces cerevisiae*. Biotechnology and Genetic Engineering Reviews 3, 377-416.

Kirscht, A., Kaptan, S.S., Bienert, G.P., Chaumont, F., Nissen, P., de Groot, B.L., Kjellbom, P., Gourdon, P., and Johanson, U. (2016). Crystal Structure of an Ammonia-Permeable Aquaporin. PLoS Biology 14, e1002411.

Klepikova, A.V., Kasianov, A.S., Gerasimov, E.S., Logacheva, M.D., and Penin, A.A. (2016). A high resolution map of the Arabidopsis thaliana developmental transcriptome based on RNA-seq profiling. The Plant Journal 88, 1058-1070.

Klionsky, D.J., Herman, P.K., and Emr, S.D. (1990). The Fungal Vacuole: Composition, Function, and Biogenesis. Microbiological Reviews 54, 266-292.

Ko, C.H., and Gaber, R.F. (1991). TRK1 and TRK2 Encode Structurally Related K^+ Transporters in *Saccharomyces cerevisiae*. Molecular and Cellular Biology 11, 4266-4273.

Ko, C.H., Buckley, A.M., and Gaber, R.F. (1990). TRK2 is Required for Low Affinity K^+ Transport in *Saccharomyces cerevisiae*. Genetics 125, 305.

Kronzucker, H.J., Szczerba, M.W., and Britto, D.T. (2003). Cytosolic Potassium Homeostasis Revisited: ^{42}K-tracer Analysis in *Hordeum vulgare* L. Reveals Set-point Variations in $[K^+]$. Planta 217, 540-546.

Kronzucker, H.J., Britto, D.T., Davenport, R.J., and Tester, M. (2001). Ammonium Toxicity and the Real Cost of Transport. Trends in Plant Science 6, 335-337.

Kumar, N., Singh, A.K., Kochhar, V.K., and Murty, A.S. (1986). Role of Guard Cell Chloroplasts in Stomatal Movement. Biochemie und Physiologie der Pflanzen 181, 421-424.

Lea, P.J., and Miflin, B.J. (2011). Nitrogen Assimilation and its Relevance to Crop Improvement. In Nitrogen Metabolism in Plants in the Post-Genomic Era, C.H. Foyer and H. Zhang, eds, pp. 1-40.

Lejay, L., Xavier Gansel, Cerezo, M., Tillard, P., Müller, C., Krapp, A., von Wirén, N., Daniel-Vedele, F., and Gojon, A. (2003). Regulation of Root Ion Transporters by Photosynthesis: Functional Importance and Relation with Hexokinase. The Plant Cell Online 15, 2218-2232.

Li, B., Li, G., Kronzucker, H.J., Baluška, F., and Shi, W. (2014). Ammonium Stress in *Arabidopsis*: Signaling, Genetic Loci, and Physiological Targets. Trends in Plant Science 19, 107-114.

Li, B., Li, Q., Xiong, L., Kronzucker, H.J., Krämer, U., and Shi, W. (2012). *Arabidopsis* Plastid AMOS1/EGY1 Integrates Abscisic Acid Signaling to Regulate Global Gene Expression Response to Ammonium Stress. Plant Physiology 160, 2040.

Li, B., Li, Q., Su, Y., Chen, H.A.O., Xiong, L., Mi, G., Kronzucker Herbert, J., and Shi, W. (2011). Shoot-supplied Ammonium Targets the Root Auxin Influx Carrier AUX1 and Inhibits Lateral Root Emergence in *Arabidopsis*. Plant, cell & environment 34, 933-946.

Li, G., Li, B., Dong, G., Feng, X., Kronzucker, H.J., and Shi, W. (2013). Ammonium-induced Shoot Ethylene Production is Associated with the Inhibition of Lateral Root Formation in *Arabidopsis*. Journal of Experimental Botany 64, 1413-1425.

Li, Q., Li, B.-H., Kronzucker, H.J., and Shi, W.-M. (2010). Root Growth Inhibition by NH_4^+ in *Arabidopsis* is Mediated by the Root tip and is Linked to NH_4^+ Efflux and GMPase Activity. Plant, cell & environment 33, 1529-1542.

Li, S.C., and Kane, P.M. (2009). The Yeast Lysosome-like Vacuole: Endpoint and Crossroads. Biochimica et biophysica acta 1793, 650-663.

Lima, J.E., Kojima, S., Takahashi, H., and von Wirén, N. (2010). Ammonium Triggers Lateral Root Branching in *Arabidopsis* in an Ammonium Transporter1;3-Dependent Manner. The Plant cell 22, 3621.

Lin, S.-H., Kuo, H.-F., Canivenc, G., Lin, C.-S., Lepetit, M., Hsu, P.-K., Tillard, P., Lin, H.-L., Wang, Y.-Y., Tsai, C.-B., Gojon, A., and Tsay, Y.-F. (2008). Mutation of the *Arabidopsis* NRT1.5 Nitrate Transporter Causes Defective Root-to-Shoot Nitrate Transport. The Plant cell 20, 2514-2528.

Liu, Y., Lai, N., Gao, K., Chen, F., Yuan, L., and Mi, G. (2013). Ammonium Inhibits Primary Root Growth by Reducing the Length of Meristem and Elongation Zone and Decreasing Elemental Expansion Rate in the Root Apex in *Arabidopsis thaliana*. PLOS ONE 8, e61031.

Loque, D., Yuan, L., Kojima, S., Gojon, A., Wirth, J., Gazzarrini, S., Ishiyama, K., Takahashi, H., and von Wiren, N. (2006). Additive Contribution of AMT1;1 and AMT1;3 to High-affinity Ammonium Uptake Across the Plasma Membrane of Nitrogen-deficient *Arabidopsis* roots. The Plant Journal 48, 522-534.

Loqué, D., Ludewig, U., Yuan, L., and von Wirén, N. (2005). Tonoplast Intrinsic Proteins AtTIP2;1 and AtTIP2;3 Facilitate NH_3 Transport into the Vacuole. Plant Physiology 137, 671.

Mani, R., St.Onge, R.P., Hartman, J.L., Giaever, G., and Roth, F.P. (2008). Defining Genetic Interaction. PNAS 105, 3461.

Marger, M.D., and Saier, M.H. (1993). A Major Superfamily of Transmembrane Facilitators that Catalyse Uniport, Symport and Antiport. Trends in Biochemical Sciences 18, 13-20.

Marini, A., Soussi-Boudekou, S., Vissers, S., and Andre, B. (1997). A Family of Ammonium Transporters in *Saccharomyces cerevisiae*. Molecular and Cellular Biology, 4282-4293.

Marini, A.-M., Springael, J.-Y., Frommer, W.B., and Bruno, A. (2000a). Cross-talk Between Ammonium Transporter in Yeast and Interference by the Soybean SAT1 Protein. Molecular Microbiology 35, 378-385.

Marini, A.-M., Matassi, G., Raynal, V., Andre, B., Cartron, J.-P., and Cherif-Zahar, B. (2000b). The Human Rhesus-associated RhAG Protein and a Kidney Homologue Promote Ammonium Transport in Yeast. Nature Genetics 26, 341-344.

Marini, A.M., Boeckstaens, M., Benjelloun, F., Chérif-Zahar, B., and André, B. (2006). Structural Involvement in Substrate Recognition of an Essential Aspartate Residue Conserved in Mep/Amt and Rh-type Ammonium Transporters. Current Genetics 49, 364-374.

Martinelle, K., and Häggström, L. (1993). Mechanisms of ammonia and ammonium ion toxicity in animal cells: Transport across cell membranes. J. Biotechnol. 30, 339-350.

Martinoia, E., Maeshima, M., and Neuhaus, H.E. (2007). Vacuolar Transporters and Their Essential Role in Plant Metabolism. Journal of Experimental Botany 58, 83-102.

Masclaux-Daubresse, C., Daniel-Vedele, F., Dechorgnat, J., Chardon, F., Gaufichon, L., and Suzuki, A. (2010). Nitrogen Uptake, Assimilation and Remobilization in Plants: Challenges for Sustainable and Productive Agriculture. Annals of botany 105, 1141-1157.

Mattsson, M., and Schjoerring, J.K. (2003). Senescence-induced Changes in Apoplastic and Bulk Tissue Ammonia Concentrations of Ryegrass Leaves. New Phytologist 160, 489-499.

Mayer, M., Schaaf, G., Mouro, I., Lopez, C., Colin, Y., Neumann, P., Cartron, J.P., and Ludewig, U. (2006). Different Transport Mechanisms in Plant and Human AMT/Rh-type Ammonium Transporters. Journal of General Physiology 127, 133-144.

Mazurkiewicz, D. (2008). Functional Analysis of a Novel Ammonium Transporter in Yeast. In School of Agriculture, Food and Wine (Adelaide: The University of Adelaide).

Mazurkiewicz, D. (2013). Characterisation of a Novel Family of Eukaryotic Ammonium Transport Proteins. In School of Agriculture, Food and Wine (Adelaide: The University of Adelaide), pp. 232.

Miller, A.J. (2010). Plant Nitrogen Nutrition and Transport. eLS.

Moroni, A., Bardella, L., and Thiel, G. (1998). The Impermeant Ion Methylammonium Blocks K^+ and NH_4^+ Currents through KAT1 Channel Differently: Evidence for Ion Interaction in Channel Permeation. The Journal of Membrane Biology 163, 25–35.

Nakano, Y., Fujitani, K., Kurihara, J., Ragan, J., Usui-Aoki, K., Shimoda, L., Lukacsovich, T., Suzuki, K., Sezaki, M., Sano, Y., Ueda, R., Awano, W., Kaneda, M., Umeda, M., and Yamamoto, D.

(2001). Mutations in the novel membrane protein spinster interfere with programmed cell death and cause neural degeneration in *Drosophila melanogaster*. Mol. Cell. Biol., 3775–3788.

Navarrete, C., Petrezsélyová, S., Barreto, L., Martínez José, L., Zahrádka, J., Ariño, J., Sychrová, H., and Ramos, J. (2010). Lack of Main K^+ Uptake Systems in *Saccharomyces cerevisiae* Cells Affects Yeast Performance in both Potassium-sufficient and Potassium-limiting Conditions. FEMS Yeast Research 10, 508-517.

Nehls, S., Snapp, E.L., Cole, N.B., Zaal, K.J.M., Kenworthy, A.K., Roberts, T.H., Ellenberg, J., Presley, J.F., Siggia, E., and Lippincott-Schwartz, J. (2000). Dynamics and Retention of Misfolded Proteins in Native ER Membranes. Nature Cell Biology 2, 288.

Nelson, B.K., Cai, X., and Nebenführ, A. (2007). A Multicolored Set of *In-vivo* Organelle Markers for Co-localization Studies in *Arabidopsis* and Other Plants. The Plant Journal 51, 1126-1136.

Neuhäuser, B., Dynowski, M., and Ludewig, U. (2009). Channel-like NH_3 Flux by Ammonium Transporter AtAMT2. FEBS Letters 583, 2833-2838.

Nielsen, K.H., and Schjoerring, J.K. (1998). Regulation of Apoplastic NH_4^+ Concentration in Leaves of Oilseed Rape. Plant Physiology 118, 1361.

Niemietz, C.M., and Tyerman, S.D. (2000). Channel-mediated Permeation of Ammonia Gas Through the Peribacteroid Membrane of Soybean Nodules. FEBS Letters 465, 110-114.

Obermeyer, G., and Tyerman, S.D. (2005). NH_4^+ Currents across the Peribacteroid Membrane of Soybean. Macroscopic and Microscopic Properties, Inhibition by Mg_2^+, and Temperature Dependence Indicate a SubpicoSiemens Channel Finely Regulated by Divalent Cations. Plant Physiology 139, 1015-1029.

Osborne, N., K Brand-Arzamendi, Ober, E.A., Jin, S.W., Verkade, H., Holtzman, N.G., Yelon, D., and Stainier, D.Y.R. (2008). The spinster homolog, two of hearts, is required for sphingosine 1-hosphate signaling in zebrafish. Curr. Biol. 18.

Özcan, S., and Johnston, M. (1999). Function and Regulation of Yeast Hexose Transporters. Microbiology and Molecular Biology Reviews 63, 554-569.

Patel, D. (2013). Characterization of Vacuole Aquaporin Function and its Implication in Membrane Fission. In Deparment of Biology (Montreal, Canada: Concordia University).

Pearson, J., and Stewart, G.R. (1993). The Deposition of Atmospheric Ammonia and its Effects on Plants. New Phytologist 125, 283-305.

Peña, A., Pardo, J.P., and Ramírez, J. (1987). Early Metabolic Effects and Mechanism of Ammonium Transport in Yeast. Archives of Biochemistry and Biophysics 253, 431-438.

Provart Nicholas, J., Alonso, J., Assmann Sarah, M., Bergmann, D., Brady Siobhan, M., Brkljacic, J., Browse, J., Chapple, C., Colot, V., Cutler, S., Dangl, J., Ehrhardt, D., Friesner Joanna, D., Frommer Wolf, B., Grotewold, E., Meyerowitz, E., Nemhauser, J., Nordborg, M., Pikaard, C., Shanklin, J., Somerville, C., Stitt, M., Torii Keiko, U., Waese, J., Wagner, D., and McCourt, P. (2015). 50 Years of *Arabidopsis* Research: Highlights and Future Directions. New Phytologist 209, 921-944.

Pyo, Y.J., Gierth, M., Schroeder, J.I., and Cho, M.H. (2010). High-Affinity K^+ Transport in *Arabidopsis*: AtHAK5 and AKT1 Are Vital for Seedling Establishment and Postgermination Growth under Low-Potassium Conditions. Plant Physiology 153, 863.

Ramos, F., and Wiame, J.-M. (1979). Synthesis and Activation of Asparagine in Asparagine Auxotrophs of *Saccharomyces cerevisiae*. European Journal of Biochemistry 94, 409-417.

Rawat, S.R., Silim, S.N., Kronzucker, H.J., Siddiqi, M.Y., and Glass, A.D.M. (1999). *AtAMT1 G*ene Expression and NH_4^+ Uptake in Roots of *Arabidopsis thaliana*: Evidence for Regulation by Root Glutamine Levels. The Plant Journal 19, 143-152.

Regenberg, B., Villalba, J.M., Lanfermeijer, F.C., and Palmgren, M.G. (1995). C-terminal Deletion Analysis of Plant Plasma Membrane H^+-ATPase: Yeast as a Model System for Solute Transport across the Plant Plasma Membrane. The Plant cell 7, 1655-1666.

Rentsch, D., Laloi, M., Rouhara, I., Schmelzer, E., Delrot, S., and Frommer Wolf, B. (1995). NTR1 Encodes a High Affinity Oligopeptide Transporter in *Arabidopsis*. FEBS Letters 370, 264-268.

Rodríguez-Navarro, A., and Ramos, J. (1984). Dual System for Potassium Transport in *Saccharomyces cerevisiae*. Journal of Bacteriology 159, 940-945.

Rong, Y., McPhee, C.K., Deng, S., Huang, L., Chen, L., Liu, M., Tracy, K., Baehrecke, E.H., Yu, L., and Lenardo, M.J. (2011). Spinster is Required for Autophagic Lysosome Reformation and mTOR Reactivation Following Starvation. PNAS 108, 7826-7831.

Roosta, H.R., and Schjoerring, J.K. (2008). Effects of Nitrate and Potassium on Ammonium Toxicity in Cucumber Plants. Journal of Plant Nutrition 31, 1270-1283.

Rothstein, R.J. (1983). One-step Gene Disruption in Yeast. In Methods in Enzymology (Academic Press), pp. 202-211.

Rubio, F., Schwarz, M., Gassmann, W., and Schroeder, J.I. (1999). Genetic Selection of Mutations in the High Affinity K^+ Transporter HKT1 That Define Functions of a Loop Site for Reduced Na^+ Permeability and Increased Na^+ Tolerance. Journal of Biological Chemistry 274, 6839-6847.

Sahrawy, M., Avila, C., Chueca, A., Canovas, F.M., and Lopez-Gorge, J. (2004). Increased Sucrose Level and Altered Nitrogen Metabolism in *Arabidopsis thaliana* Transgenic Plants Expressing Antisense Chloroplastic Fructose-1,6-bisphosphatase. Journal of experimental botany 55, 2495-2503.

Santos, J., Sousa, M.J., and Leão, C. (2012). Ammonium Is Toxic for Aging Yeast Cells, Inducing Death and Shortening of the Chronological Lifespan. PLOS ONE 7, e37090.

Schachtman, D.P., and Schroeder, J.I. (1994). Structure and Transport Mechanism of a High-affinity Potassium Uptake Transporter from Higher Plants. Nature 370, 655.

Scharwies, J.D. (2017). The Role of Aquaporins in Plant Responses to Drought. In School of Agriculture, Food and Wine (Adelaide: The University of Adelaide).

Scheiner-Bobis, G. (2018). Gene Expression in Yeast. eLS.

Schjoerring, J.K., Husted, S., Mäck, G., and Mattsson, M. (2002). The Regulation of Ammonium Translocation in Plants. Journal of Experimental Botany 53, 883-890.

Shelden, M.C., Dong, B., de Bruxelles, G.L., Trevaskis, B., Whelan, J., Ryan, P.R., Howitt, S.M., and Udvardi, M.K. (2001). *Arabidopsis* Ammonium Transporters, AtAMT1;1 and AtAMT1;2, Have Different Biochemical Properties and Functional Roles. Plant and Soil 231, 151-160.

Snapp, E. (2005). Design and Use of Fluorescent Fusion Proteins in Cell Biology. Current protocols in cell biology / editorial board, Juan S. Bonifacino ... [et al.] CHAPTER, Unit-21.24.

Sohlenkamp, C., Shelden, M., Howitt, S., and Udvardi, M. (2000). Characterization of *Arabidopsis* AtAMT2, a Novel Ammonium Transporter in Plants. FEBS Letters 467, 273-278.

Sohlenkamp, C., Wood, C.C., Roeb, G.W., and Udvardi, M.K. (2002). Characterization of *Arabidopsis* AtAMT2, a High-affinity Ammonium Transporter of the Plasma Membrane. Plant Physiology 130, 1788-1796.

Spalding, E.P., Hirsch, R.E., Lewis, D.R., Qi, Z., Sussman, M.R., and Lewis, B.D. (1999). Potassium Uptake Supporting Plant Growth in the Absence of AKT1 Channel Activity. The Journal of general physiology 113, 909.

Straub, T., Ludewig, U., and Neuhäuser, B. (2017). The Kinase CIPK23 Inhibits Ammonium Transport in *Arabidopsis thaliana*. The Plant cell 29, 409-422.

Sundin, B.A., Chiu, C.-H., Riffle, M., Davis, T.N., and Muller, E.G.D. (2004). Localization of Proteins that are Coordinately Expressed with Cln2 During the Cell Cycle. Yeast 21, 793-800.

Szczerba, M.W., Britto, D.T., Balkos, K.D., and Kronzucker, H.J. (2008). Alleviation of Rapid, Futile Ammonium Cycling at the Plasma Membrane by Potassium Reveals K^+-sensitive and -insensitive Components of NH_4^+ Transport. Journal of Experimental Botany 59, 303-313.

Takata, K., Matsuzaki, T., and Tajika, Y. (2004). Aquaporins: Water Channel Proteins of the Cell Membrane. Progress in Histochemistry and Cytochemistry 39, 1-83.

Ton, V.-K., and Rao, R. (2004). Functional Expression of Heterologous Proteins in Yeast: Insights into Ca_2^+ Signaling and Ca_2^+-transporting ATPases. American Journal of Physiology-Cell Physiology 287, C580-C589.

Touraine, B. (2004). Nitrate Uptake by Roots-transporters and Root Development. . In Nitrogen acquisition and assimilation in higher plants, S. Amancio and I. Stulen, eds (Dordrecht, The Netherlands: Kluwer Academics Publisher.

Tyerman, S.D., Whitehead, L.F., and Day, D.A. (1995). A Channel-like Transporter for NH_4^+ on the Symbiotic Interface of N_2-fixing Plants. Nature 378, 629 - 632.

Udvardi, M.K., and Day, D.A. (1997). Metabolite Transport Across Symbiotic Membranes of Legum Nodules. Annual Review of Plant Physiology and Plant Molecular Biology 48, 493-523.

Uozumi, N., Gassmann, W., Cao, Y., and Schroeder, J.I. (1995). Identification of Strong Modifications in Cation Selectivity in an *Arabidopsis* Inward Rectifying Potassium Channel by Mutant Selection in Yeast. The Journal of biological chemistry 270, 24276-24281.

USDA-ERS. (2013). U.S. Consumption of Nitrogen, Phosphate, and Potash, 1960-2011. In Fertilizer Use and Price (USDA).

van der Eerden, L.J.M. (1982). Toxicity of Ammonia to Plants. Agriculture and Environment 7, 223-235.

Vida, T.A., and Emr, S.D. (1995). A New Vital Stain for Visualizing Vacuolar Membrane Dynamics and Endocytosis in Yeast. The Journal of Cell Biology 128, 779.

von Wiren, N., Gojon, A., Chaillou, S., and Raper, D. (2001). Mechanism and Regulation of Ammonium Uptake at Higher Plants. In Plant Nitrogen, P.J. Lea and J.-F. Morot-Gaudry, eds (Germany: Springer-Verlag

Wang, R., Tischner, R., Gutiérrez, R.A., Hoffman, M., Xing, X., Chen, M., Coruzzi, G., and Crawford, N.M. (2004). Genomic Analysis of the Nitrate Response Using a Nitrate Reductase-Null Mutant of *Arabidopsis*. Plant Physiology 136, 2512.

Wege, S., Khan, G.A., Jung, J.-Y., Vogiatzaki, E., Pradervand, S., Aller, I., Meyer, A.J., and Poirier, Y. (2016). The EXS Domain of PHO1 Participates in the Response of Shoots to Phosphate Deficiency via a Root-to-Shoot Signal. Plant Physiology 170, 385.

Weigel, D., and Glazebrook, J. (2006). Transformation of Agrobacterium Using the Freeze-Thaw Method. Cold Spring Harbor Protocols 2006, pdb.prot4666.

Weiner, I.D., and Hamm, L.L. (2007). Molecular Mechanisms of Renal Ammonia Transport. Annual Review of Physiology 69, 317-340.

Westhoff, C.M., Siegel, D.L., Burd, C.G., and Foskett, J.K. (2004). Mechanism of Genetic Complementation of Ammonium Transport in Yeast by Human Erythrocyte Rh-associated Glycoprotein. Journal of Biological Chemistry 279, 17443-17448.

White, P.J. (1996). The Permeation of Ammonium through a Voltage-independent K^+ Channel in the Plasma Membrane of Rye Roots. The Journal of Membrane Biology 152, 89–99.

Wilson-O'Brien, A.L., Patron, N., and Rogers, S. (2010). Evolutionary Ancestry and Novel Functions of the Mammalian Glucose Transporter (GLUT) Family. BMC Evolutionary Biology 10, 152.

Wood, C.C., Porée, F., Dreyer, I., Koehler, G.J., and Udvardi, M.K. (2006). Mechanisms of Ammonium Transport, Accumulation, and Retention in Ooyctes and Yeast Cells Expressing *Arabidopsis* AtAMT1;1. FEBS Letters 580, 3931-3936.

Wu, B., and Beitz, E. (2007). Aquaporins with Selectivity for Unconventional Permeants. Cellular and Molecular Life Sciences 64, 2413-2421.

Xu, G., Fan, X., and Miller, A.J. (2012). Plant Nitrogen Assimilation and Use Efficiency. Annual review of plant biology 63, 153-182.

Yamaya, T., and Oaks, A. (2004). Metabolic Regulation of Ammonium Uptake and Assimilation. In Nitrogen acquisition and assimilation in higher plants, S. Amancio and I. Stulen, eds (Dordrecht, The Netherlands: Kluwer Academics Publisher.

Yan, N. (2013). Structural Advances for the Major Facilitator Superfamily (MFS) Transporters. Trends in Biochemical Sciences 38, 151-159.

Yang, Z., Huang, J., Geng, J., Nair, U., and Klionsky, D.J. (2006). Atg22 Recycles Amino Acids to Link the Degradative and Recycling Functions of Autophagy. Molecular Biology of the Cell 17, 5094-5104.

Yool, A.J., and Campbell, E.M. (2012). Structure, Function and Translational Relevance of Aquaporin Dual Water and Ion Channels. Molecular Aspects of Medicine 33, 553-561.

Young, R.M., Marty, S., Nakano, Y., Wang, H., Yamamoto, D., Lin, S., and Allende Miguel, L. (2002). Zebrafish Yolk-specific Not Really Started (nrs) Gene is a Vertebrate Homolog of the *Drosophila* Spinster Gene and is Essential for Embryogenesis. Developmental Dynamics 223, 298-305.

Yuan, L., Graff, L., Loque, D., Kojima, S., Tsuchiya, Y.N., Takahashi, H., and von Wiren, N. (2009). AtAMT1;4, a Pollen-specific High-affinity Ammonium Transporter of the Plasma Membrane in *Arabidopsis*. Plant Cell Physiology 50, 13-25.

Yuan, L., Loque, D., Kojima, S., Rauch, S., Ishiyama, K., Inoue, E., Takahashi, H., and von Wiren, N. (2007). The Organization of High-affinity Ammonium Uptake in *Arabidopsis* Roots Depends on the Spatial Arrangement and Biochemical Properties of AMT1-type Transporters. The Plant cell 19, 2636-2652.

Yuva-Aydemir, Y., Bauke, A., and Klambt, C. (2011). Spinster controls Dpp signaling during glial migration in the *Drosophila* Eye. The Journal of Neuroscience 31, 7005–7015.

Zhang, C., Hicks, G.R., and Raikhel, N.V. (2014). Plant Vacuole Morphology and Vacuolar Trafficking. Frontiers in plant science 5, 476.

Zhao, M., Tan, H.-T., Scharwies, J., Levin, K., Evans, J.R., and Tyerman, S.D. (2016). Association between Water and Carbon Dioxide Transport in Leaf Plasma Membranes: Assessing the Role of Aquaporins. Plant, cell & environment 40, 789-801.

Zheng, X., He, K.A.I., Kleist, T., Chen, F., and Luan, S. (2015). Anion Channel SLAH3 Functions in Nitrate-dependent Alleviation of Ammonium Toxicity in *Arabidopsis*. Plant, cell & environment 38, 474-486.

Zheng, Y., Drechsler, N., Rausch, C., and Kunze, R. (2016). The *Arabidopsis* Nitrate Transporter NPF7.3/NRT1.5 is Involved in Lateral Root Development Under Potassium Deprivation. Plant Signaling & Behavior 11, e1176819.

Zhou, Y., Bai, L., and Song, C.-P. (2015). Ammonium Homeostasis and Signaling in Plant Cells. Science Bulletin 60, 741-747.

Zou, N., Li, B., Dong, G., Kronzucker, H.J., and Shi, W. (2012). Ammonium-induced Loss of Root Gravitropism is Related to Auxin Distribution and TRH1 Function, and is Uncoupled from the Inhibition of Root Elongation in *Arabidopsis*. Journal of Experimental Botany 63, 3777-3788.

Zou, N., Li, B., Chen, H., Su, Y., Kronzucker, H.J., Xiong, L., Baluška, F., and Shi, W. (2013). GSA-1/ARG1 Protects Root Gravitropism in *Arabidopsis* under Ammonium Stress. New Phytologist 200, 97-111.